híradástechnika

VOLUME L.

1999/12

50th ANNIVERSARY

journal on
communications
computers
convergence
contents
companies

JOURNAL ON C^5

A PUBLICATION OF THE SCIENTIFIC SOCIETY FOR TELECOMMUNICATIONS, HUNGARY

Szerkesztőség / Editorial office
HÍRADÁSTECHNIKA
1061 Budapest, Paulay E. u. 56. II.14/A.
Telefon:(361) 341-6421, (361) 470-0713
Fax: (361) 341-6421, (361) 470-0713
Előfizetés / Orders to
Híradástechnikai Tudományos Egyesület
1055 Budapest, Kossuth tér 6-8.
Tel./Fax: (361) 353-1027
*** 2000. január 30-ig 50% kedvezmény.**

2000-es ELŐFIZETÉSI DÍJAK (12 szám + 1 CD)
Hazai közületi előfizetők részére
1 évre 20000 Ft +12% ÁFA = Btto 22400 Ft
Hazai egyéni előfizetők részére*
1 évre 4000 Ft +12% ÁFA = Btto 4480 Ft
HTE tag előfizetők részére
1 évre 2000 Ft +12% ÁFA = Btto 2240 Ft
Subscription rates for foreign subscribers in 2000
(12 issues + 1 CD) 100 USD, single copies 10 USD
Transfer should be made to the Scientific Society for Telecommunications
H-1055 Budapest, Kossuth tér 6-8.

HÍRADÁSTECHNIKA, JOURNAL ON C^5 is published monthly, in English and in Hungarian by Regiszter Kft.
H-1164 Budapest, Csókakő u. 27. Phone: (361) 400-2166, 400-2167, Fax: 400-2168.
Type-setting by HTE. Printed by Regiszter Kft.

HU ISSN 0018-2028

Special Issue on WLAN and ISM applications of MICROSTRIP ANTENNAS

Associate Editor : F. Völgyi

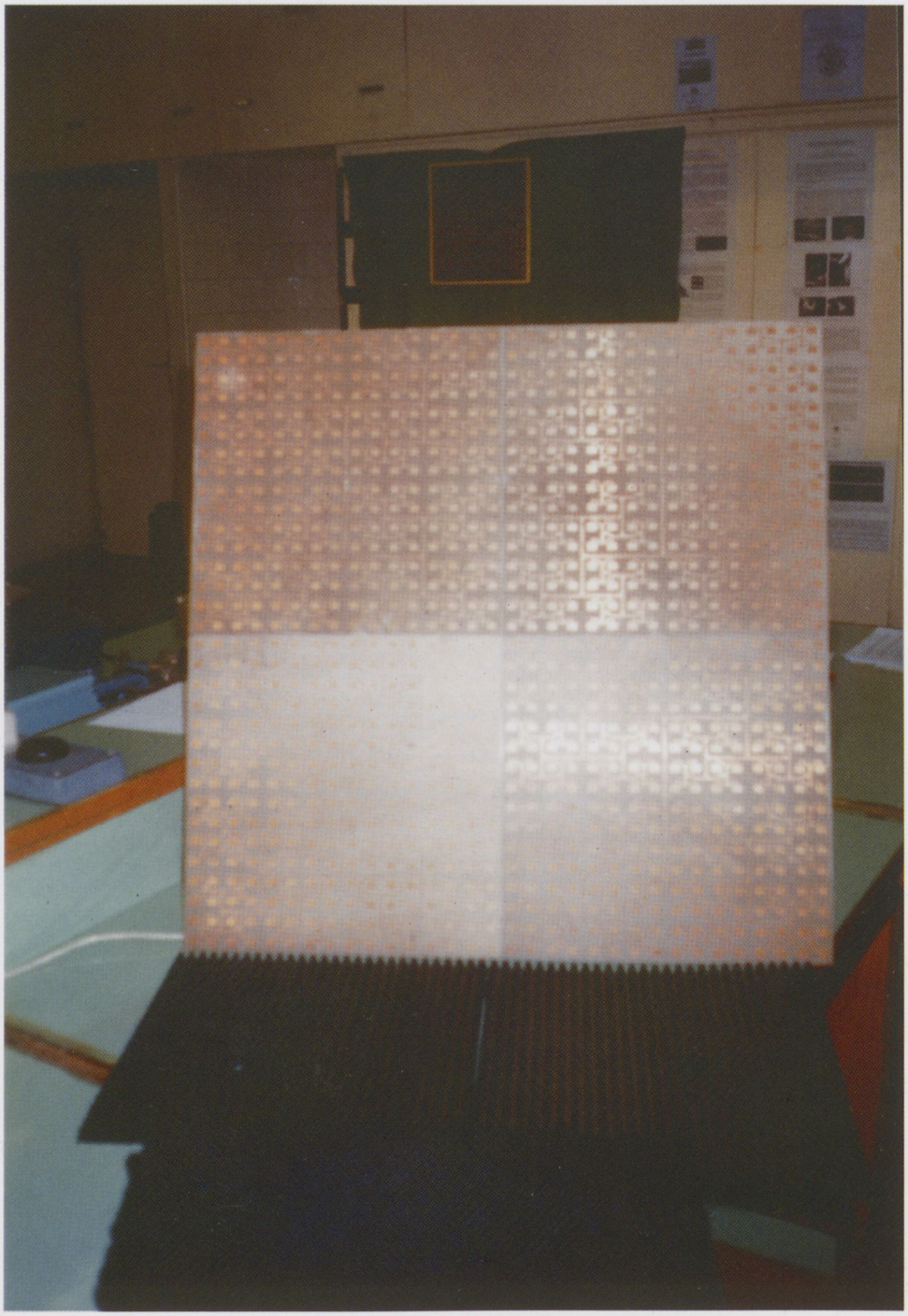

Fig. 9. Photograph of our experimental MSA-array with 1024-elements for TV-satellite signal reception.

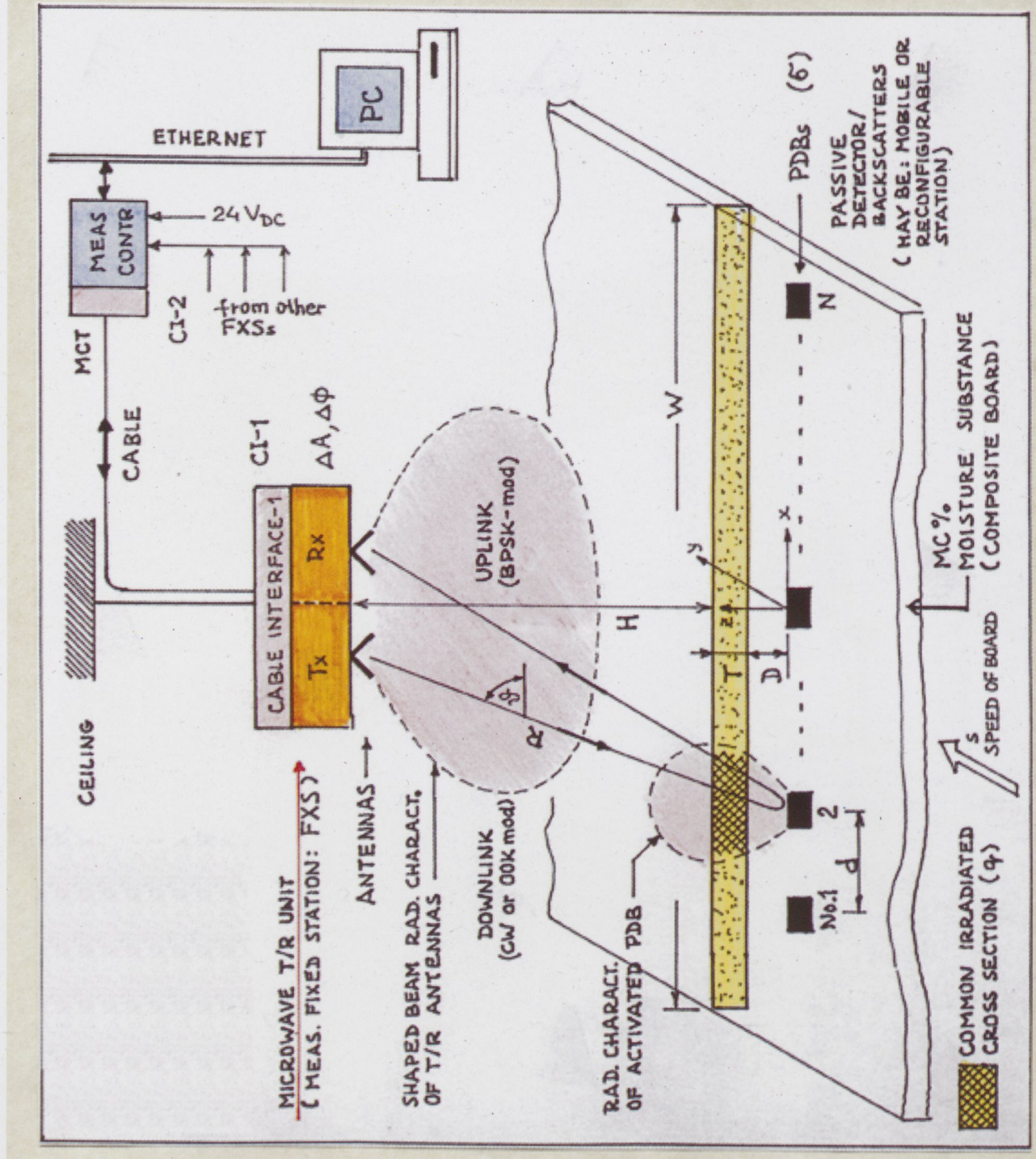

Fig. 1. Scheme of the basic measurement setup

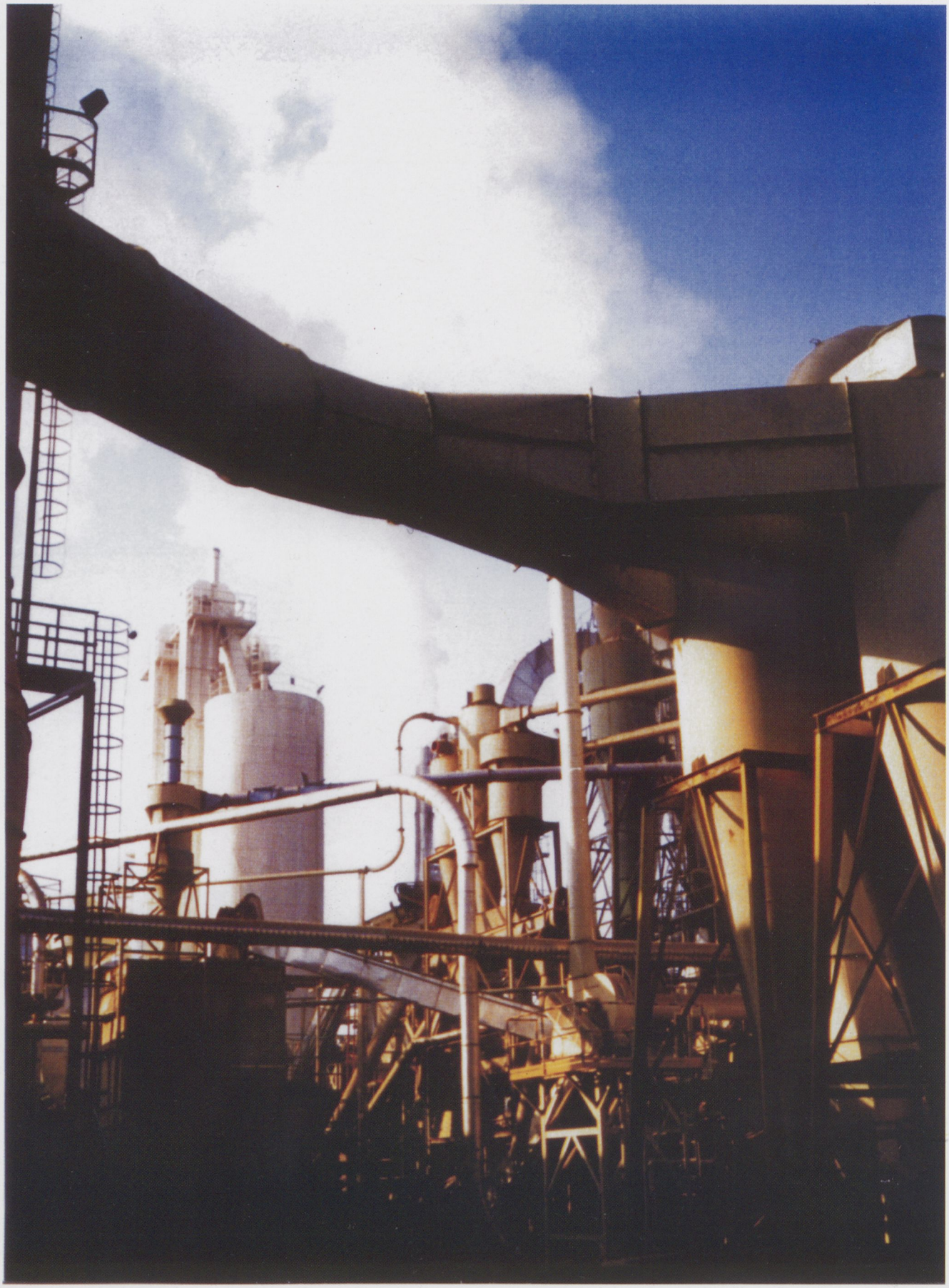

Fig. 2. The hot air dryers of a particleboard plant (INTERSPAN, Vasarosnameny, Hungary).

HÍRADÁSTECHNIKA

Vol. L. No. 12, DECEMBER, 1999
HU ISSN 0018-2028

JOURNAL ON C[5]

Associate editor: Ferenc Völgyi

Abstract: In this special issue on WLAN & ISM Applications of Microstrip Antennas 11 papers are presented. Section **Communications** is represented by 3 contributions on High-Gain Microstrip Antenna Arrays, on Flying Decibels – Extremely Lightweight Microstrip Antennas and on Microstrip Antennas with Polarization Diversity and Frequency Agility. Section **Computers** is comprised of 1 contribution on A Microwave Monitoring System used for Prediction of the Quality of Particleboards, which paper deals with a sophisticated measurement system using industrial computer. **Convergence** is formed by 4 contributions written on Specifying the Quality of Eggs using Microwave Sensors, on MSSA-exciter using as a Whispering Gallery Mode Transducer, on Microwave Drying using a Microstrip Antenna Array Applicator and on Versatile Microwave Moisture Sensors. All these represent the agricultural, scientific and industrial applications of microwaves using microstrip antennas and sensors. **Contents & Distribution of Multimedia** contains 2 contributions on Microstrip Antennas used for WLAN Systems and on Simple Methods for Testing the Temperature Dependence of Microstrip Antenna Arrays. Section **Companies** is now dealing with a single contribution on the RF-Absorbers for GTEM-Cell Applications, introducing the cooperation between TKI Innovation Company and Technical University of Budapest, Department of Microwave Telecommunications. In this issue all submitted papers are scientifically evaluated by senior reviewers. Most of the papers have been accepted by the reviewers as scientific contributions. They are marked on their first pages by the sign of $\mathcal{L}$ giving the evidence of the scientific applications result.

GENERAL ACKNOWLEDGMENTS

The author of this special issue Ferenc **Völgyi** is extremely grateful for the help (moral support, sponsoring him, or leading joint researches) that he received from many persons all over the world, namely in:

- Brazil: Dr. Karl **Kögl** (Sao Roque, SP), Prof. Alvaro Augusto Almeida **De Salles** (CETUC-PUC, Rio de Janeiro), Dr. Celio Antonio **Finardi** (CPqD/TELEBRAS, Campinas, Sao Paulo);
- Bulgaria: Georgi **Cenkov** (chief radar engineer, formerly at Balkan Airlines, Sofia), Prof. Nikola Ivanov **Dodov** (Microwave D&S Lab., Sofia);
- Czeh Republic: Prof. Jan **Zehentner** (Czeh Technical University, Prague);
- Finland: Prof. Veikko **Porra**, Dr. Ari **Sihvola** and Prof. Martti **Waltonen** at Helsinki University of Technology;
- France: Prof. Jean Charles **Bolomey** (Paris XI University and CNRS Supelec), Prof. Jean-Pierre **Daniel** (University of Rennes), Prof. Tuami **Lasri** (IEMN, University, Lille);
- Germany: Dr. Klaus **Kupfer** (MFPA/ Weimar), Dr. Georg Schöne (L&S Hochfrequenztechnik, Lichtenau/ Ulm), Prof. Werner **Wiesbeck** and Alexander **Brandelik** (University of Karlsruhe);
- Greece: Dr. **Dimitra**, I. **Kaklamani** (NTUA/ Athens);
- Holland: Dr. Antoine **Roederer** (Head of EM-Division, European Space Agency, Noordwijk ZH);
- India: Prof. C. **Natarajan** and Dr. K. S. **Rao** (Indian Institute of Technology, Bombay), Dr. R. K. **Tewary** (DEAL/Dehra Dun);
- Israel: Dr. Noam **Livneh**, Eli **Gimmon** and Beni **Engel** (HeliComm, Yoqneam Illit), Dr. Asher **Madjar** (RAFAEL, Haifa);
- Italy: Piergentili **Adriano** (Fara Sabina/ RI), Prof. Roberto De **Leo** (Univ. Ancona), Prof. Vittorio **Rizzoli** (University of Bologna);
- Japan: S. **Mizoguchi** (President) and Shunji **Matsuoka** (Vice President) at Tateyama Kagaku Ind. Co., Toyama, Prof. Seichi Okamura (Shizuoka Univ.), Prof. Tadashi **Takano** (University of Tokyo), and Dr. Tsuneo **Morita** (Nomura Res. Inst. in Budapest, HU);
- Poland: Prof. Edward J. **Sedek** (PIT Res. Inst., Warsaw);
- Spain: Prof. Magdalena **Salazar Palma** (Polytechnic University of Madrid);
- Switzerland: Prof. F. **Gardiol** (University of Lausanne), Dr. Gabriel **Meyer** (ETH Centrum – IKT, Zurich);
- Turkey: eng. Nusret **Tunay** (Kusadasi), Prof. Kemal **Özmehmet** and Ahmet **Özkurt** (Dokuz Eylül University, Buca – Izmir), Prof. Alexey A. **Vertiy** (Director of the Turkish–Ukrainien Joint Research Lab., Gedze-Kocaeli),
- United Arab Emirates: Eur. eng. Dr. Adil **El Safi** and eng. Mohamed **Osman** (Abu Dhabi);
- United Kingdom: David J. **Daniels** (Manager of R&D at ERA Technology), Dr. J. C. **Williams**;
- United States of America:
- California: Dr. Stephen F. **Adam** (President at Adam Microwave Consulting, Inc., Los Altos), Dr. Les **Besser** (President at Besser Associates, Los Altos), Julius **Bottka** (R&D Proj. Manager at HP Co., Santa Rosa), Dr. Steve **Böröcz** (Cosmetic and Plastic Surgery, Walnut Creek), Prof. Tatsuo **Itoh** (UCLA, Los Angeles), Gabe **Sanchez** (AEMI, San Diego), Tom **Szilagyi** (Wavespan Co., Mountain View);
- Colorado: Prof. Reza **Zoughi** (Colorado State Univ., Fort Collins);
- Georgia: István **Nógrádi** (sr.res.eng. GeorgiaTech, Atlanta/Smyrna), Dr. Andrzej W. **Kraszewski**, Dr. Kurt **Lawrence** and Dr. Stuart O. **Nelson** (USDA-ARS, Athens), Dr. Barry J. **Cown** (President, SATIMO, Inc., Ackworth);
- Massachusetts: Thomas P. **Cheatham** and Alexander **Herman** (HeliOss Comm. Inc., Waltham), Dr. István **Novák** (Sun Microsystems, Burlington), Dr. Richard J. **Temkin** and Dr. Kenneth **Kreischer** (Plasma Fusion Center, MIT, Cambridge);
- Pennsylvania: Csaba **Besskó** (sr.eng. Westinghouse Electric Co., Pittsburgh), Robert J. S. **Haris** (Pres. & CEO, Real Time Devices, Inc., State College), Prof. Peter **Herczfeld** (Drexel University, Philadelphia), Dr. Jeff **Polan** (VP of R&D, OBIT/FR, Inc., Horsham), Dr. Attila A. **Sooky** (Academic Coordinator, Univ. of Pittsburgh);
- Texas: Prof. Cam **Nguyen** (Texas A&M University, College Station),
- Virginia: Prof. Géza **Ifjú** (Virginia Tech, Blacksburg);

and in Hungary:
Prof. János **Beke** (vice dean) and Dr. Endre **Judák** (sr.res.eng. at GATE Agricultural University, Gödölló), Dr. Ferenc **Divós** (Wood NDT Lab., West-Hungarian University, Sopron), Sándor **Domokos** (HP Hungary Ltd, Budapest), Tibor **Eszik**, József **Orbán**, and Tamás **Umann** (LRI, Air Traffic and Airport Administration), Botond **Farkas** (Westel-450 Co., Budapest), Tibor **Hajder** and Dr. Miklós **Kenderessy** (KHVM, Ministry of Transport, Telecommunications and Water Management), Dr. Karolyn **Kazi**, Zoltán **Mirk**, Dr. János **Solymosi** and Gönder **Tunay** (Bonn – Hungary Ltd, Budapest), Dr. Csaba **Kántor** (MATÁV PKI/FI), Dr. Miklós **Kelemen** (director) and István **Rácz** (chief technologist at INTER-SPAN Particleboard Company, Vásárosnamény), Ildikó **Magyar** (Manager, Telecom-Fort Ltd), Ferenc **Mernyei** (sr.res.eng., Austria – Micro Ltd), Prof. Csaba **Szabó** (Manager, BCN – Hungary, Budapest), Dr. Pál **Szabó** (Antenna Hungária), Dr. Béla **Szentpáli** (KFKI Res. Inst.), Tamás **Tóth** (Manager, Totaltel Co).

The author is grateful to Prof. Imre **Mojzes** (Government Commissioner for Y2K Compliance), Attila **Denk** and Dr. András **Somogyi** (formerly at ORION Co.) and

Sándor **Tatár** (TKI Innovation Company for Telecommunication) for making together some innovations and patents.

He would also like to express his thanks and appreciation to Prof. László **Pap**, the dean of the Faculty of Electrical Engineering and Informatics, and to Prof. László **Zombory**, the head of Dept. of Microwave Telecommunications, for their support of the research and development.

The author thanks members of the Faculty of Electrical Engineering and Informatics, namely: Dr. Gyula **Csopaki**, Dr. László **Gál**, Dr. János **Pinkola**, Dr. Gábor **Ripka**, Dr. Endre **Tóth**, Dr. István **Vajda**, and Prof. Gyula **Veszely** for their support and help with the R&D of many systems.

He would like to express his appreciation of discussions over the years with his colleagues at the Department of Microwave Telecommunications: Prof. Tibor **Berceli**, Dr. István **Bozsóki**, Dr. Antal **Bánfalvy**, Dr. Éva **Gödör**, Dr. Ferenc **Lénárt**, Dr. Gábor **Mátay**, Béla **Szekeres**, Dr. Rudolf **Seller**, and at the Kandó Kálmán Technical Highschool: Prof. György **Lukács**.

Getting on for sixty, he is most grateful to teachers and professors for their conscientious education: Ferenc **Kennedy** and Károly **Remes** teachers of physics at Primary School of Siófok and at Kandó Kálmán Technical College, Budapest, Prof. Károly **Simonyi**, Prof. Károly **Géher** and Prof. Árpád **Csurgay** at the Technical University of Budapest.

He would also like to express his appreciation of discussions (other than technical) over many years with his devoted "old friends": Prof. Tamás **Mészáros** (Vice Rector, Economical University of Budapest), Prof. József **Roóz** (Director General, Highschool of Finance and Accountancy, Budapest), Attila **Besskó** (yacht owner in Antigua, Caribbean Sea), István **Haffner** (el.eng., yacht owner at Lake Balaton), Péter **Juhász** (chem.eng., yacht manufacturer), Dr. Árpád **Perlaky** (psychologist, ANTSz) and Attila **Selmeczy** (journalist at Elvis Presley Club), János **Székely** (assoc.prof. at KKMF), Gyula **Wirth** (chief eng. at Radio Station, Siófok) and Gyula **Zsivótzky** (hammer-thrower, olympic champion).

He would like to thank his daughters **Sylvia** and **Katharine** for their patient, and his wife **Martha**, for her support and encouragement during the time it took to write this special issue.

Last but not least, mention must be made of the efforts of Dr. Ernő **Simonyi**, the editor in chief of this journal. Precise editing work made by Katalin **Lesnyik** is also highly appreciated.

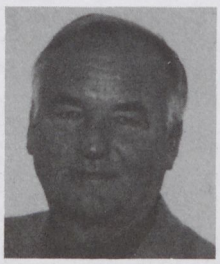

Völgyi Ferenc 1941. február 15-én született Balatonújhelyen (ma Siófok II). 1955-ben végezte el az általános iskolát Siófokon, 1959-ben pedig a középiskolát a Kandó Kálmán Híradásipari Technikumban Budapesten, mindkettőt kitűnő eredménnyel. A Budapesti Műszaki Egyetem Villamosmérnöki Kara Híradástechnika Szakán folytatta tanulmányait. Kitüntetéses oklevéllel végzett 1964-ben, később ugyancsak kitüntetéses mikrohullámú szakmérnöki diplomát is szerzett. Völgyi Ferenc a BME Mikrohullámú Híradástechnika Tanszékének oktatója 1964 óta, egyetemi adjunktus. Számos tantárgy tematikájának kidolgozója és önálló előadója. Kezdettől fogva részt vesz a Külföldi Hallgatók Mérnökképző Központja angol nyelvű szakmai oktatásában, valamint 1998 óta a Kandó Kálmán Híradásipari Műszaki Főiskolán is tanít. Aktív szerepet vállalt tudományos műhelyek létrehozásában, diplomatervezők és PhD-hallgatók színvonalas képzésében, melynek eredményességét mutatja, hogy az utóbbi 5 évben hét esetben nyerték el hallgatói a Híradástechnikai és Informatikai Tudományos Egyesület (HTE) diplomaterv pályázata, az Ipar a Korszerű Mérnökképzésért Alapítvány, illetve nemzetközi fórumok (Nemzetközi Rádiótechnikai Unió, Yokohama Konferencia) legmagasabb díjait.

Tudományos munkái kezdetben a passzív és aktív mikrohullámú áramkörök, parametrikus erősítők, mm-hullámú oszcillátorok és nyomtatott (microstrip) antennák felé irányultak. Jelenleg az aktív nyomtatott antennák, integrált antennák- és áramkörök, magas hőmérsékletű szupravezetők mikrohullámú alkalmazásai, mikrohullámú szenzorok és felszín alatti radarok, mikrohullámok ipari, mezőgazdasági és tudományos alkalmazásai tartoznak fő érdeklődési körébe. Több országban folytatott kutatómunkát, tudományos eredményeit számos ország egyetemein és konferenciáin ismertette, ezek: Amerikai Egyesült Államok (California, Colorado, Georgia, Pennsylvania, Virginia), Brazília, Bulgária, Csehszlovákia, Egyesült Arab Emírségek, Finnország, Franciaország, Görögország, India, Izrael, Japán, Németország, Lengyelország, Olaszország, Spanyolország, Svájc és Törökország. Színvonalas előadásaiért és szakirodalmi tevékenységéért több nemzetközi és hazai elismerésben részesült (Dehra Dun – India, Izmir – Törökország, Pollák–Virág díj, Orion-nívódíj, HTE ezüst jelvény).

Völgyi Ferenc adjunktus több mint 50 kutatási téma vezetője illetve főmunkatársaként több vállalattal állt hosszabb-rövidebb ideig munkakapcsolatban, nevezetesen: Finommechanikai Vállalat Budapest, Magyar Tudományos Akadémia Műszaki Fizikai Kutató Intézete, Stog GmbH Munich, L&S Hochfrequenztechnik GmbH Lichtenau-Ulm/Germany, Boston Communication Networks USA, Real Time Devices Inc. State College PA, USA, Tateyama Kagaku Industrial Co. Toyama Japan, Microval Bt. Budapest.

Tagja a hazai Híradástechnikai és Informatikai Tudományos Egyesületnek és a Méréstechnikai és Automatizálási Tudományos Egyesületnek, valamint az USA-beli IEEE-nek (senior member, MTT, AP, IM, COM). Tudományos konferenciákon szekcióelnöki szerepet vállalt Indiában, USA-ban és hazánkban. A 2000-ben indított új IEEE-folyóirat (Subsurface Sensing Technologies and Applications) szerkesztőbizottsági tagja és az SSTA-konferencia egyik szervezője ezév júliusában San Diego-ban.

Völgyi Ferenc több mint 50 szakcikk, valamint 4 könyv egyes fejezeteinek szerzője, kutatási beszámolói 2-3 ezer oldalt tesznek ki. Több újítása és knowhow-ja van, két elfogadott és két bejelentett szabadalommal rendelkezik. Több tudományos népszerűsítő rövidfilmben és tv-műsorban ismertette a nyomtatott antennákat. 1962-75 között a Budapesti Közgazdaság-tudományi Egyetem Népi Együttesében táncolt. Nős, felesége Márta, 1975-ben és 1980-ban született leányaik Szilvia és Katalin. Kedvenc kikapcsolódásai: néptánc és zene, utazás, tengeri és balatoni vitorlázás.

HIGH-GAIN MICROSTRIP ANTENNA ARRAYS*

FERENC VÖLGYI

TECHNICAL UNIVERSITY OF BUDAPEST
DEPT. OF MICROWAVE TELECOMMUNICATIONS
H-1111 BUDAPEST, GOLDMANN TÉR 3, HUNGARY
PHONE: 36 1 463 1559; FAX: 36 1 463 3289; T-VOLGYI@NOV.MHT.BME.HU

A fixed beam (broadside) two-dimensional microstrip array of 16×16 resonant rectangular radiating elements at the frequency of 8.15 GHz with a gain of 29.5 dB is presented. A modular approach is utilized in which a given antenna is used as a building block for a higher gain antenna. A high efficiency is achieved by optimising the layout and the impedance levels of subarray feeding of the conventional uniformly illuminated monolithic array.

1. INTRODUCTION

Microstrip antenna (MSA) arrays draw increasing interest due to their flat profile, low weight, ease of fabrication and low cost [1]. In this paper, the design of a 8.15 GHz microstrip array is described. This antenna is planned to be integrated in a short-range communication system replacing conventional dish.

The main design goal was to achieve maximum gain in a given size. There are several possible ways *to increase gain*:

- by increasing the number of elements in a two--dimensional MSA array [2], [3],
- decreasing the loss of the feeding network [4],
- using radiating elements with higher gain [5],
- using more complex structures (e.g., multilayer construction [6]).

M. A. Weiss [2] developed 1024-element mm-wave arrays. To assure an acceptable array design, a 3x scaled version of the final 32×32 element array was fabricated and tested at 13.8 GHz. The array produced 31.0 dBi gain and was fed entirely with a microstrip corporate feed network [2].The gain was not maximum, because of the line losses and of the Taylor-amplitude tapering.

J. Ashkenazy et al [3] developed MSA-arrays with modular approach. The gain of the 64-element antenna was 24.3 dB at 9 GHz. Since the increase of gain was only 4 dB as compared to the previous version employing 16 elements, the further increase of antenna elements did not seem useful. They proposed a method, which can be used to build higher gain antennas to connect 64-element subarrays with power splitters and semirigid coax lines (which have almost no radiation loss).

A. Nesic et al [4] developed an excellent planar array of antiresonant printed dipoles with a new feeding network. The gain of the 10×10 element array was 28 dB at 17 GHz. The fabrication of this antenna is more complicated then usual.

A. A. Oliner [5] proposed the increase of length of the Menzel-type travelling-wave MSA to $4.8\lambda_0$ based on his calculations referring to the loss of microstrips due to higher-order mode leakage. This would provide a power radiation of about 90 %. The construction of similar arrays with such elements seems to be also feasible.

At the Technical University of Budapest, Department of Microwave Telecommunications (TUB/DMT) a 128-element, X-band MSA-array was constructed (in 1975) and built with *multilayer technique* on Polyguide substrate (for details, see [6]). Even though the parameters were acceptable, the cost and complexity of manufacturing made it unfavorable for our present task. Instead, the modular, monolithic construction of [3] was chosen because of its easy manufacturability. The *technical parameters* of the antenna *were improved*:

a) by optimal, variable microstrip layout of the building blocks,
b) by repleacing the corporate-feed lines symmetrically in between the radiating elements,
c) by optimizing the line impedances based on the compromise between minimum line-loss and minimum line-radiation,
d) by using fine-tuning microstrip susceptances placed symmetrically on the corporate feed lines, symmetrically to the feed (input) point.

2. DESIGN OF RADIATING ELEMENT

From the operational point of view, it is essential to start the design with the optimum-radiating element. In most situations rectangular patch element are well usable (see *Fig. 2*), where the length L of the element determines the resonant frequency and width W, with the given thickness h of substrate allow us to adjust radiating parameters within a wide range.

There are numerous models for the design and analysis of rectangular MSA (see e.g., [7]). Based on these, computer programmes were developed and different antennas were designed [6]. It was a general experience that the measured resonant frequency was $1.5-2.5$ % lower and the bandwidth was $30-40$ % higher than calculated. In case of ceramic substrates the difference was even higher. It was astonishing that the calculated frequency shift versus the temperature and dimension ambiguities was several times greater than the bandwidth for our 35 GHz GaAs MMIC-MSA design. We thought it was impossible.

The rearranged computer programmes (which show very good agreement with the measured results) are based on the following models:

1. Electric Surface Current Model, which gives the main antenna parameters for lossless case [8],
2. model for resonator losses,
3. model for calculating the resonant frequency with losses [9].

* This is a version of the paper presented by F. Völgyi in Rome, Italy at the 17th EuMC [10].

Fig. 1 shows some of the results of calculations for Duroid-5880 substrate ($h = 1.575$ mm) at the frequency of 8.15 GHz. BW denotes the bandwidth ($VSWR = r \leq 2$), R is the radiation resistance, G is the gain of the antenna, $\Theta_H(3)$ is the 3 dB beamwidth of main lobe in the H-plane.

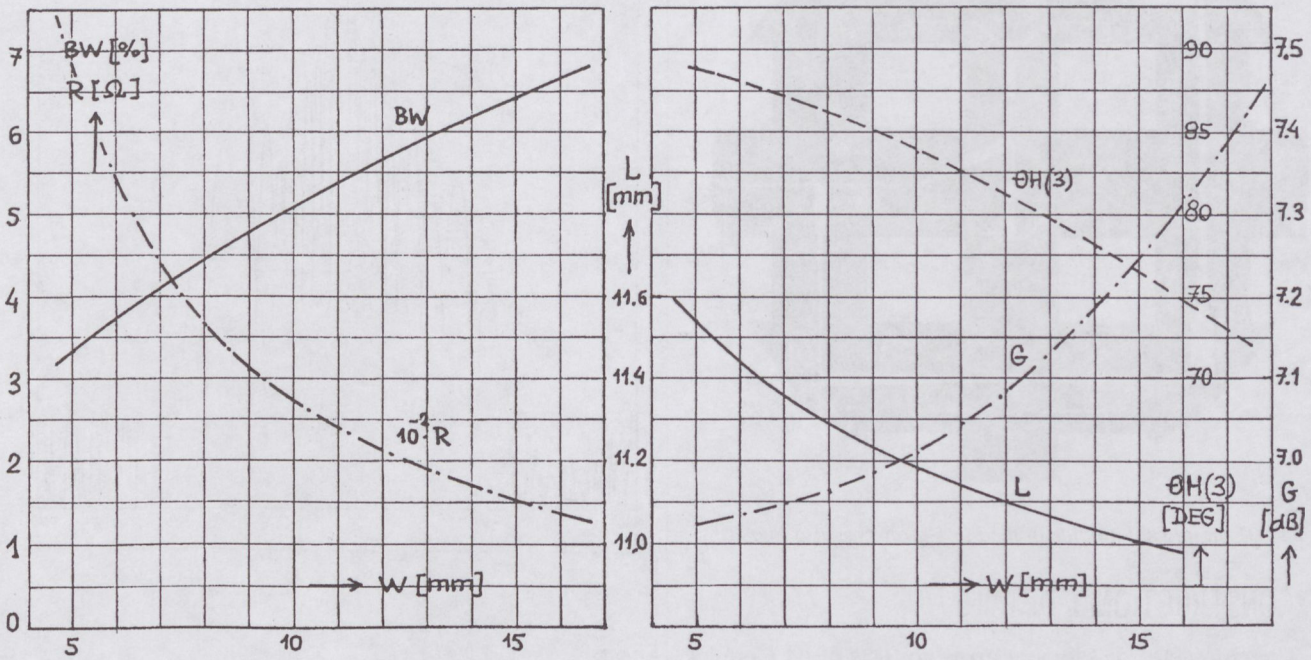

Fig. 1. Characteristics of a rectangular patch element at the frequency of 8.15 GHz.

3. SUBARRAY (MODULE) AND ARRAY-DESIGN

The building blocks with 2×2 radiating elements of a MSA-array can be seen in *Fig. 2*, where the lines are shown without matching components. The radiators are rectangular patch elements. The spacing between the elements is around $(0.7 - 0.9)\lambda_0$, which provides maximum gain in case of connecting several modules.

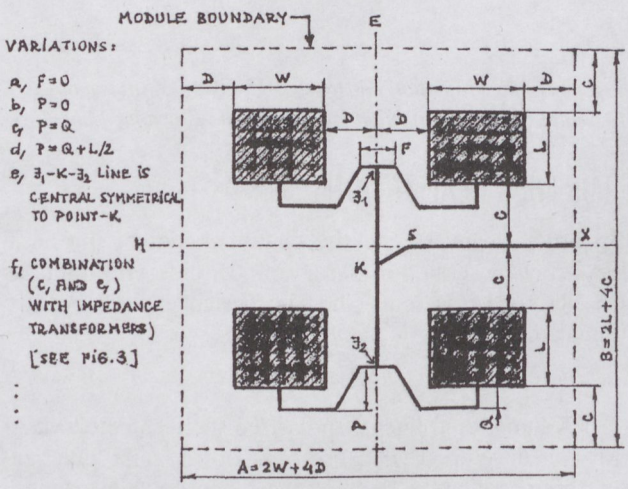

Fig. 2. A module of the MSA-array (sketch of feeding, without transformers).

Features of the $A \times B$ sized *module*, are:

a) the input point X is placed in the middle of side B,
b) most of the distributing lines are placed symmetrically in between the module (H and E symmetry planes),
c) the length of feeding lines as measured from the X-input are the same for every module.

The construction of modules guarantees that in case of connecting more modules, the connecting lines are running on the borderlines which in turn minimizes the stray coupling (see *Fig. 3*). It is also possible to generate further versions (*Fig. 2a...f*) in order to meet impedance or other requirements. The input impedance for radiating elements was chose to be 170Ω by taking into account the tolerances of microstrip lines, as well. The matching transformers have 120Ω, 101Ω and 143 impedances. The input impedance of the module is 170Ω, too.

It is then possible to build an *antenna array* consisting of $M = 2^n$, $n = 0, 1, 2, 3 \ldots$ blocks, where the number of radiators is $N = 4M = 2^{n+2}$. In case of our project $N = 256$, $M = 64$ and $n = 6$ were, respectively. To achieve maximum gain, all elements were fed with the same amplitude and phase.

Computer programmes were written for analysis and design of MSA-arrays, microstrip- and other lines and discontinuities. In this work students were involved. The calculations gave a gain of 7.2 dB, an efficiency of 87 % and a bandwidth ($r \leq 2$) of 515 MHz for a single rectangular radiating element. The measurement results showed good correspondence with the calculated values. The optimization shown in paragraph 1.c resulted in a line impedance of mainly 120Ω for the connecting lines, the complete power splitter had a total loss of about 0.7 dB (plus the radiation loss in the corporate-feed lines, which is negligible).

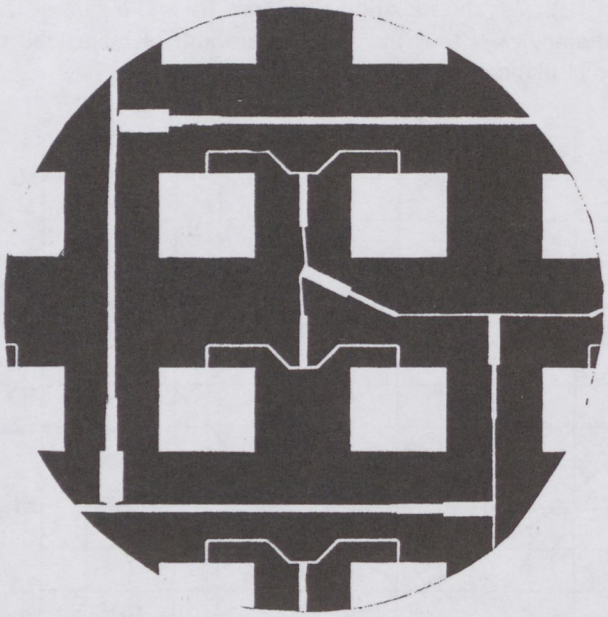

Fig. 3. An internal module of the MSA-array (see also Fig. 2f).

4. CONSTRUCTIONAL DETAILS

The complete 256-element array consists of 64 modules (*Fig. 3*). Its production is simple, since only a single layer is used and the antenna is fed by a single 50Ω coaxial SMA connector. The substrate used was Duroid-5880 ($\varepsilon_r = 2.22, \tan = 9{\cdot}10^{-4}$; 35 μm copper cladding). The low ε_r is needed in order to have sufficient gain and bandwidth for the rectangular radiating element. The substrate thickness used was h= 1.575 mm, which choice is a compromise between the desire to have maximum bandwidth and the need to keep the surface wave radiation low.

The arrays were reproduced from an appropriate full size mask. A lower dimension array of "cut-and-strip" master pattern was produced and that antenna array was measured. Masks for any (closer) frequency made by an appropriate scaling at the photographic stage. The complete 256-element array was a composition of two pieces of 410×205 mm^2 Duroid laminates, which were stuck to the smooth surface of the arial positioning structure using "Araldite". The MSA array has an epoxi-glass radome.

5. ARRAY PERFORMANCE

The radiation pattern of the array in H-plane is shown in *Fig. 4*. The beamwidth is 4.9°, and a sidelobe level of nearly 14 dB is found. The cross-polarization level is better than -40 dB, the front-to-back ratio is higher than 40 dB. In the E-plane, the beamwidth is 4.9°, sidelobe level is nearly 13 dB. The width of the mainlobe in the H- and E-plane 11.4° and 11.0° are, respectively. The center frequency and gain of the linearly polarized array 8.15 GHz and 29.5 dB are, respectively. For a $VSWR \leq 2$, the bandwidth is nearly 500 MHz (6 %).The efficiency is $\sim$ 60 %, the overall size: 41×41 cm. *Fig. 5* shows the frequency characteristics of the MSA-array.

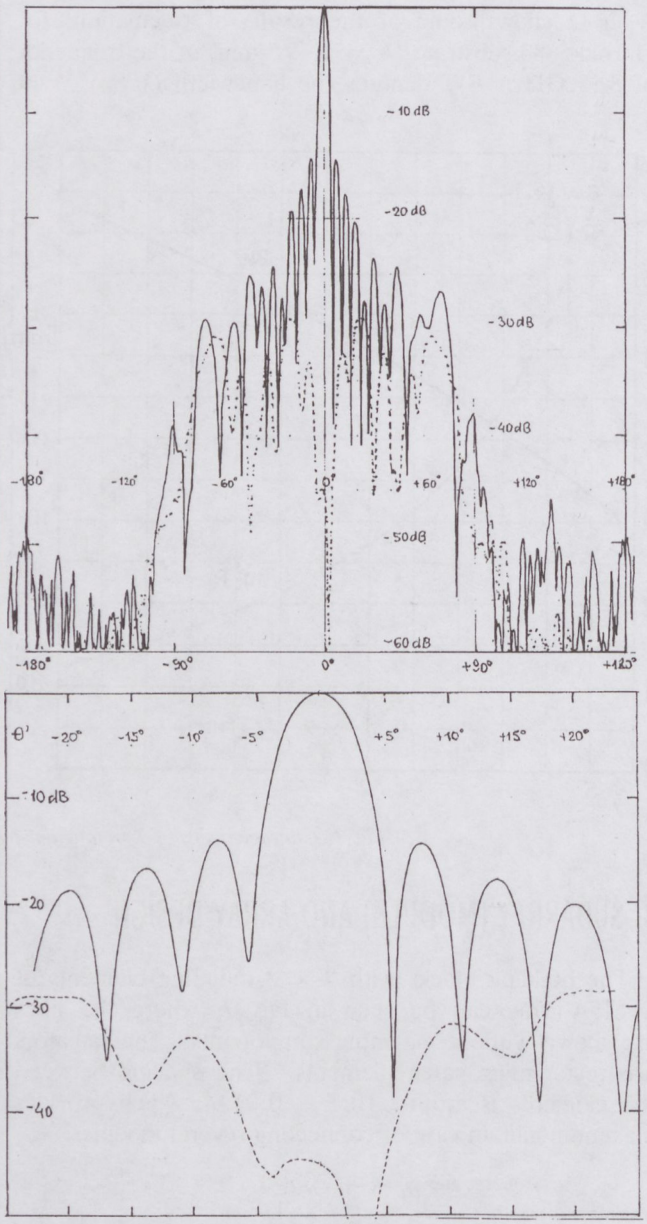

Fig. 4. H-plane radiation pattern at 8.15 GHz (Θ' on expanded scale). Cross-polarization level is shown using dotted line.

6. FURTHER REALIZATIONS

In order to investigate the characteristics of the basic MSA-array (described in paragraph 3), different antennas were designed and realized. The design experiences are summarized below.

6.1. Scatterometer MSA

An X-band, dual linearly polarized scatterometer MSA-array was developed. Because of the orthogonal polarization, square radiating elements were chosen with independent dual-side feed. For thin substrates ($h \sim 0.8$ mm) the radiation resistance is too high, requiring extremely narrow strips in the microstrip transmission line feeds. Therefore, even if it is not dictated by bandwidth considerations, a thickness of $h = 1.59$ mm may be required. This however suffers from the disadvantage of surface waves. Three different structures were designed and compared.

a) Monolithic structures as given on p. 262 of [7] by A. G. Derneryd with the difference that each element is fed from the four sides with an appropriate phase.
b) Two-layer structure. For vertical polarization this is the basic MSA-array described in paragraph 3, for horizontal polarization the microstrip distribution network is placed behind the radiating elements rotated by 90 degrees and the radiators are fed by coaxial feedthrough.
c) Three-layer structure similar to the two-layer structure, but the power splitter network is made on stripline.

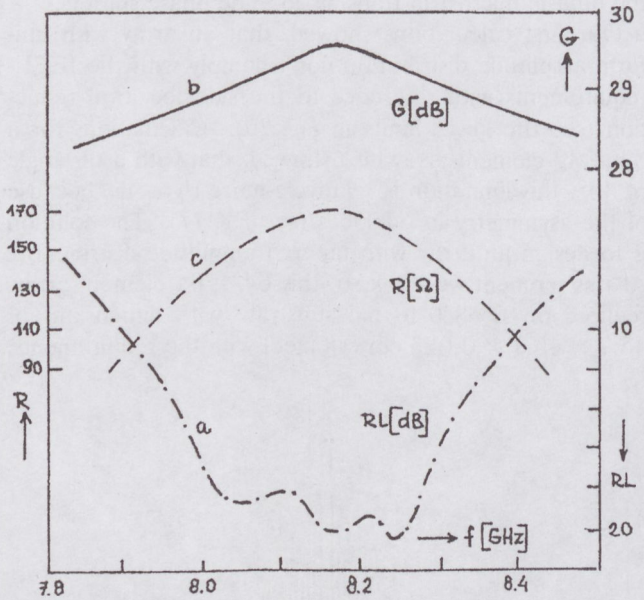

Fig. 5. Frequency characteristics of the MSA-array: a/ ..... (RL) input return loss; b/ _ _ _ _ _ (G) gain; c/ —— (R) real part of the input impedance (for a single element).

6.2. Composite-MSA on ceramic substrate

The radiating elements of this 12 GHz array were realized on ceramic with power splitter made on soft substrate. It is known [7], that ceramic substrates are not the best choice for realizing MSAs: the bandwidth is narrow, efficiency and gain are low, line losses are high, effects of surface waves are high. In some cases (active antennas, phased arrays, etc.) however such antennas are required. To gain experience, 4×4 element MSA-modules were designed and realized on Alumina ceramic substrate (50.8×50.8 mm^2, $h = 0.635$ mm).To reduce line losses, the connections of modules were realized on soft substrate (which can be replaced by rectangular waveguides) behind the ceramic substrate. Calculated results (for a single element):
$f = 11.8$ GHz, $W = 5.476$ mm, $G = 4.86$ dB, $\Theta_H(3) = 86°$, $R = 316\Omega$;
$L = 3.822$ mm, $BW = 1.73$ % $\Theta_E(3) = 156°$, $\varepsilon_r = 9.8$.

Due to the second-order characteristic with a local maximum of the real part of frequency dependent input impedance, a special microstrip feeding network was designed to increase the bandwidth. It provided matching at two frequencies, below and above the resonance of radiating element. The solution worked well in practice, the measured bandwidth of a 4×4 module was 680 MHz (5.8 %) for $VSWR \leq 2$, which was in good agreement with the simulation results.

6.3. ISM-band antennas for spread-spectrum communications

We have developed different configurations (with 8×8, 8×16 and 16×16 elements) of 5.8 GHz-band MSA-arrays for short range spread-spectrum communications. The layout of the 8×16 element array is shown in *Fig. 6.* The dimensions are: $45.7 \times 30.5 \times 0.16$ cm, the mass of the array is 0.54 kg. Measured parameters are: the gain $G = 27.5$ dB, aperture efficiency $\eta = 86$ %, bandwidth ($RL = 10$ dB) is 292 MHz (5.0 %) as shown in *Fig. 7*, cross polarization level in E-plane is 39.4 dB, in the H-plane is between 32−40 dB. The 3 dB beamwidth in the H-plane is 6.28°, sidelobe level is $SLL = -12$ dB, forward-back ratio $F/B = 36$ dB as shown in *Fig. 8.* Calculated results from measurements are: the figure of merit $FM = G \cdot \Theta_{E3}\Theta_{H3} = 22000$, specific gain is 15.3 dB/GHz^2 kg. These antennas are used in California.

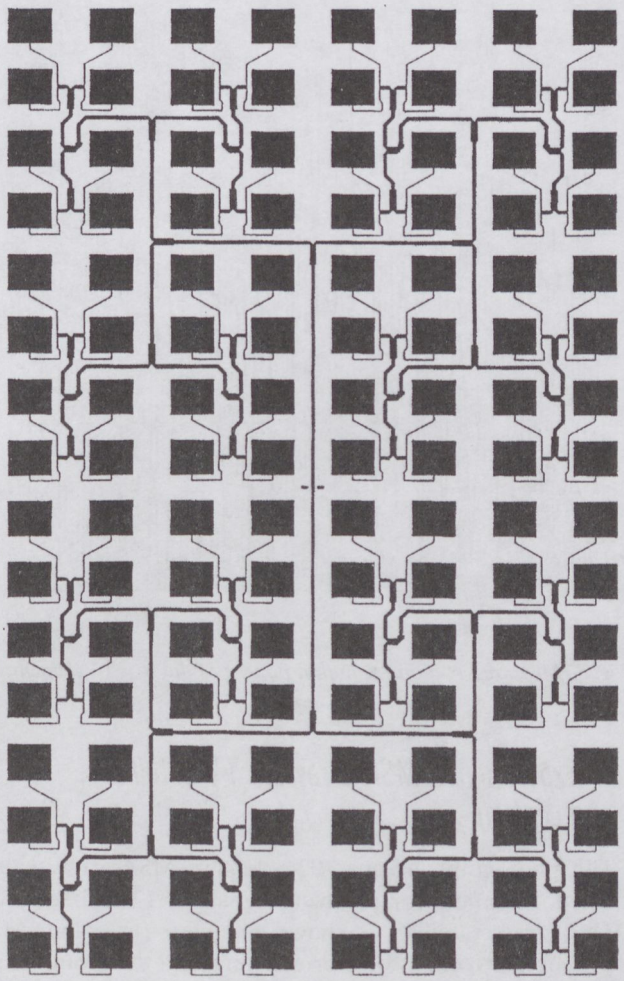

Fig. 6. Layout of the 8×16 *element MSA-array for 5.8 GHz*

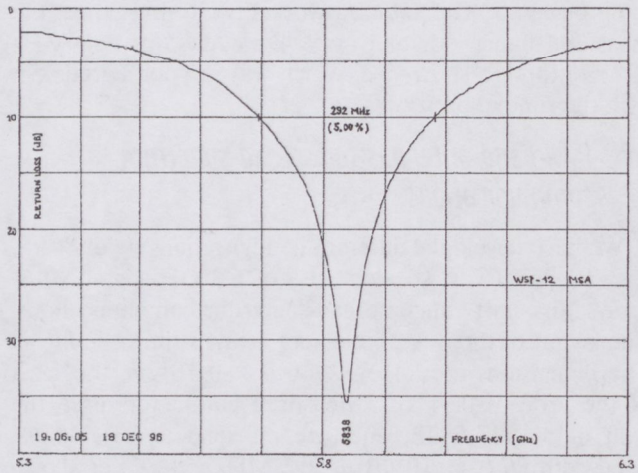

Fig. 7. Measured input return loss versus frequency characteristic of the 8 × 16 element MSA-array.

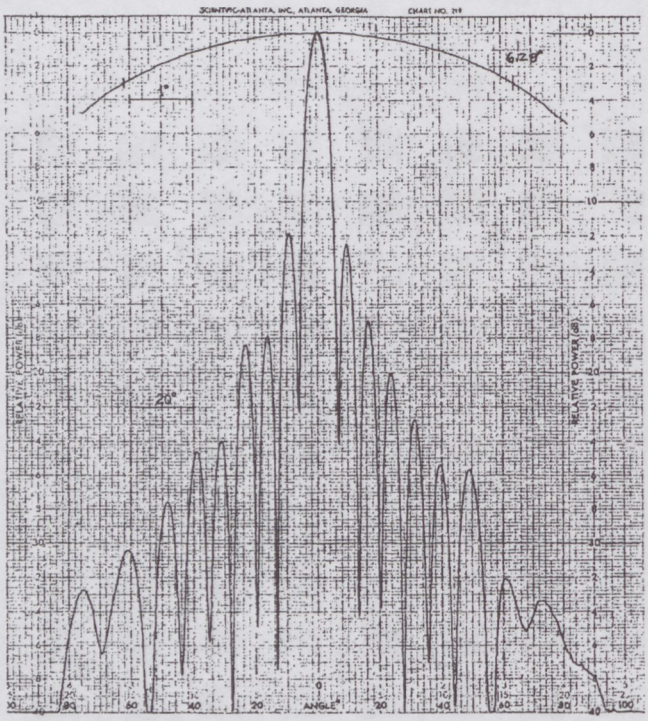

Fig. 8. Measured H-plane radiation pattern of the 8 × 16 element MSA-array.

6.4. Experimental MSA-array for TV-satellite reception

The photograph of our 1024-element MSA-array with linear polarization, for receiving signals of 12 GHz direct TV-broadcast satellites is shown in *Fig. 9* (in colours*). The structure consists of four quarters, and the inputs are combined using semi-rigid cables and a hybrid. Dimensions of the array: $0.7 \times 0.7 \times 0.005$ m are, respectively. The antenna is shown in the Microwave Laboratory (V2-building, No. 604) of the TUB/DMT. The extrapolated gain (from the measurements of the quarter of this antenna) is $G = 39$ dB, aperture efficiency $\eta = 72$ %. The variation of gain is -0.4 dB at temperature rise of 28°C.

6.5. A 4096-element MSA-array for 38 GHz-band

One of our newest tasks (from USA) was to design a 4096 (64×64) element MSA-array for 38 GHz wideband point-to-point communications of 500 channels television. To cut expenses of the deployment of antennas, the main requirement was the possibility of pasting those on the windows of the skyscrapers. We thought so, that the tilting of main-beam in horizontal and vertical planes will do by the built-in microstrip transmission line phase shifters.

Our first calculations showed, that an array with uniform amplitude distribution don't comply with the IEEE-requirements with reference to the sidelobe level reduction (see the lower limits in *Fig. 10*). Calculations for a 32×32 element array also showed, that with a tilt angle of 30°, this limitation is relatively more rigorous, because of the asymmetry in sidelobes (see *Fig. 11*). The solution is to design an array with tapered amplitude distribution. At this moment we think so, this 64×64 element array, realized on D-5880-10 mil substrate with dimensions of $45.7 \times 45.7 \times 0.025$ cm will meet with the requirements.

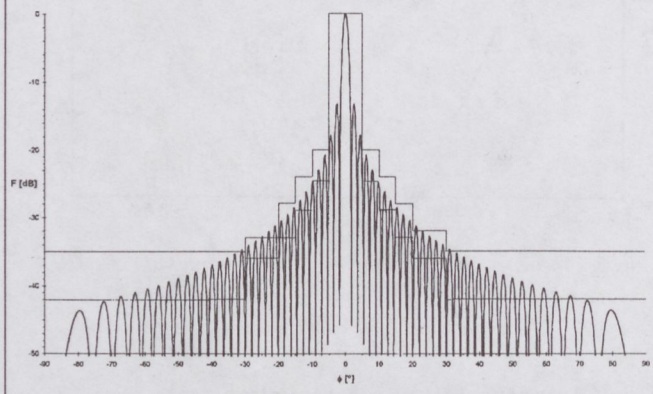

Fig. 10. Calculated E-plane radiation pattern of the 64 × 64 element MSA-array with uniform amplitude distribution. The lower tolerance-lines show the IEEE-recommendation for side-lobe reduction.

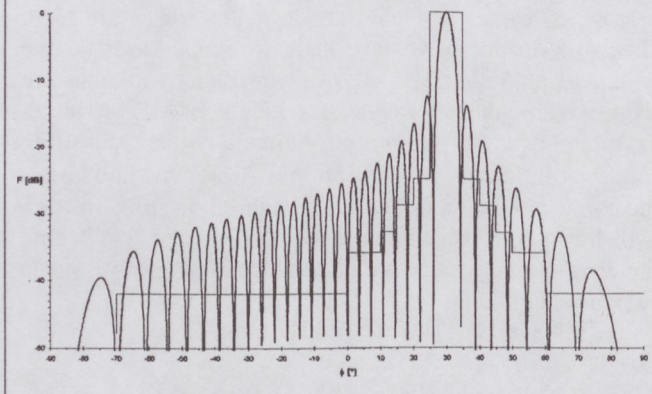

Fig. 11. Calculated H-plane radiation pattern of a 32 × 32 element MSA-array with uniform amplitude distribution, using phase shifters to tilt the main-beam angle by 30°.

*** Coloured picture cited is shown separately in the colour pages of this issue.**

7. CONCLUSIONS

A high-gain, high-efficiency, ease to manufacture antenna construction is introduced in the conventional monolithic array. The manufacturing cost of the MSA-array is only a fraction of that of the paraboloid antenna previously used in the communication system. In the project, students were also involved. The modular design concept can be well exploited in the education and in the laboratory practice of students.

8. ACKNOWLEDGMENTS

I thank Dr. I. Bozsóki and Prof. Dr. T. Berceli for their scientific support, asst. prof. F. Mernyei for making some calculations and Dr. I. Novák for his useful critical comments. Last but not least special thank goes to the ORION Radio and Electrical Works which company provided the financial fund for the experiments of the 256-element MSA-array.

REFERENCES

[1] R. L. Mailloux et al: "Microstrip Array Technology" IEEE/AP-29, No. 1, January 1981, pp. 25-37.
[2] M. A. Weiss: "Microstrip Antennas for Millimeter Waves" IEEE/AP-29, No. 1, January 1981, pp. 171-174.
[3] J. Ashkenazy et al: "A Modular Approach for the Design of Microstrip Array Antennas" IEEE/AP-31, No. 1, January 1983, pp. 190-193.
[4] A. Nesic et al: "Highly Efficient Two-Dimensional Printed Antenna Array with a New Feeding Network" 14th European Microwave Conference (EuMC), 1984, pp. 697-701.
[5] A. A. Oliner: "Leakage from Higher Order Modes on Microstrip" U.R.S.I. Int. Symp. on Electromagnetic Theory, August 25-29, 1986, Budapest, Hungary, Part A, pp. 25-27.
[6] F. Völgyi: "High-Gain Microstrip Antennas" (in Hungarian), Híradástechnika XXXVI, 1985, No. 6, pp. 266-281 (A Pollák-Virág Awarded Paper).
[7] I. J. Bahl and P. Bhartia: "Microstrip Antennas" Artech House, Inc., 1980.
[8] P. Perlmutter et al: "Electric Surface Current Model for the Analysis of Microstrip Antennas with Applications to Rectangular Elements" IEEE/AP-33, No. 3, March 1985, pp. 301-311.
[9] Y. T. Lo et al: "Theory and Experiment on Microstrip Antennas" IEEE/AP-27, No. 2, March 1979, pp. 137-145.
[10] F. Völgyi: "High Efficiency Microstrip Antenna Array" Proc. of the 17th EuMC, 7-11 September 1987, Rome, Italy, pp.747-752.

NAGYNYERESÉGŰ NYOMTATOTT ANTENNÁK

Két pont közötti mikrohullámú összeköttetéshez éles-irányítású, nagynyereségű antennák szükségesek. A planár-struktúrájú nyomtatott antennák (MSA) ezen célokra kiválóak. A nagynyereségű nyomtatott antennákra vonatkozó szakirodalmi hívatkozások után a cikk egy 16×16 elemű, 8.15 GHz frekvenciájú, 29.5 dB nyereségu oldalsugárzó MSA tervezését és konstrukciós kialakítását mutatja be. Az antenna kialakításánál modulszerű elrendezést használ, ahol egy 2×2 elemű felületi antenna sokszorozásával lehet a teljes antennarendszert felépíteni. A nagy nyereség eléréséhez jó hatásfokú elemi sugárzók, optimális impedanciájú és elrendezésű mikrosztrip teljesítményosztók kellenek. A pontos tervezést a BME Mikrohullámú Híradástechnika Tanszékén készített, többszörösen módosított és a realizált antennák méréseivel ellenőrzött számítógép program támogatja. A cikk hátralévő részében további antenna realizációkat ismertet a szerző, nevezetesen: egy mikrohullámú szóródásmérőhöz készített kettős-polarizációju, X-sávú antennát, egy 5×5 cm^2-es kerámia lapkán kialakított 16-elemes antennát, egy 5.8 GHz-es kommunikációs antennát, egy 1024-elemes 12 GHz-es műhold vevő antennát és egy ablakra ragasztható 4096-elemű 38 GHz-es felületi antenna tervét. A hírközlési célokra készített 8.15 GHz-es nyomtatott antenna költségei a töredékét teszik ki a mikrohullámú rendszerben eredetileg használt csőtápvonalas primer sugárzos paraboloid antennáénak, így nagy sikkerrel gyártották az akkori ORION Gyárban, Budapesten. Az 5.8 GHz-es antenna realizációk és a 38 GHz-es antenna tervek USA-beli felhasználásra készültek.

Ferenc Völgyi was born in Siófok, at the Balaton Lake, Hungary. He received a diploma in electrical engineering (with honors) and the specialized microwave engineer degree (honors) in 1964 and 1972 respectively, both from the Technical University, Budapest, Hungary. He then became an Assistant Professor, then a Senior Assistant of the Department of Microwave Telecommunications at the Technical University of Budapest. His teaching and research activities have been devoted to several topics, including the design of passive and active microwave circuits, parametric amplifiers, mm-wave oscillators and microstrip antennas. He got the Pollak—Virág award in 1986, for the paper of "High-Gain Microstrip Antenna Arrays" (in Hungarian) from the HTE/Scientific Society for Telecommunications, Hungary and he obtained one of the "best solution" awards in 1986, for development of a 256-element Microstrip Antenna Array, from Orion Co. He has held positions or made important developments at Precision Mechanics Enterprise Budapest, at Research Institute for Techn. Physics of the Hungarian Academy of Sciences, Stog GmbH Munich, L&S Hochfrequenztechnik GmbH Lichtenau-Ulm, Germany, Boston Communication Networks USA, Real Time Devices Inc. State College PA-USA, Tateyama Kagaku Co. Toyama City Japan, and Microval Ltd. Hungary. He was the leader or cooperator of more than 50 R&D projects. He is a member of the HTE and MATE (Scientific Society of Measurement and Automation, Hungary).

He served as session chairman of the SSTA'99 Int. Conf., Denver, Colorado, USA, the 20th EuMC, Budapest, Hungary and ICOMM'90 Dehradun, India, where he received the silver Jubilee Memorial Plaque from D.E.A.L./Dehradun. Ferenc Völgyi has authored or co-authored more than 50 journal articles, conference papers and presentations, has written chapters three text-books in the field of microwave theory and techniques, and holds four relevant patents. He gave lectures and presentations at Universities and Conference cities of: Brazil, Bulgaria, Czechoslovakia, Finland, France, Germany, Greece, Hungary, India, Israel, Italy, Japan, Poland, Spain, Switzerland, Turkey, United Arab Emirates and United States of America (California, Colorado, Georgia, Pennsylvania, Virginia). His current research activities include active microstrip antennas and arrays, integrated microwave and millimeter-wave circuits, WLAN and EMC-test systems, high-temperature superconductivity, microwave sensors and radars, industrial, agricultural and scientific applications of microwaves, Ferenc Völgyi serves the Program Committee and the Editorial Board for the International Conference and Journal of "Subsurface Sensor Technologies and Applications" (SSTA). He is a senior member of IEEE (MTT, AP, IM, and COM). Mr. Völgyi is married, his wife is Martha, they have two daughters Sylvia and Katharine. His hobbies are: folkdance, voyage and sailing.

FLYING DECIBELS – EXTREMELY LIGHTWEIGHT MICROSTRIP ANTENNAS*

FERENC VÖLGYI

TECHNICAL UNIVERSITY OF BUDAPEST
DEPT. OF MICROWAVE TELECOMMUNICATIONS
H-1111 BUDAPEST, GOLDMANN TÉR 3, HUNGARY
PHONE: 36 1 463 1559; FAX: 36 1 463 3289; T-VOLGYI@NOV.MHT.BME.HU

Extremely Lightweight Microstrip Antennas (ELW/MSA) designed on the base of modern constructional principles and produced with the usage of new productional technology overfulfil the conventional antennas. After introducing a new concept (specific gain) the paper qualitatively characterizes the "lightness" and the technological quality of microstrip (and other type) antennas. To illustrate the new concept an extremely lightweight microstrip antenna is discussed. This flat antenna with less than -27 dB side lobe level, mountable on airplanes had to be prepared for a 1.4 GHz radiometer, developed at our department.

1. INTRODUCTION

Recently I have examined a $0.94\times0.70\times1.06$ m sized, 24 kg pyramidal horn antenna, having 20 dB gain at 1.45 GHz. I have found it large-sized and very heavy. Later we have designed and produced a microstrip antenna for a 1.4 GHz passive radiometer to be installed on the PC-6 Turbo Porter aircraft (Pilatus Aircraft Ltd., Switzerland). The size of the MSA is $0.66\times0.66\times0.013$ m, its mass is 1.45 kg, the gain of it is 20.5 dB. How can we evaluate these data? The answer will be discussed in this paper.

Microstrip antennas have now reached an age of maturity. Their fundamental action is well understood and the basic radiating elements have been exhaustively treated [1]. There are more than three thousand technical papers discussing the theoretical investigation, and design of MSA-s as well as the calculation of their parameters [2]. Some of them deal with tolerance of production or the temperature dependence of the antennas [3]. There are special applications of MSA-s, too [4].

The gain of the antenna often has major importance and we want to achieve the maximum gain within certain size limitation [5]. The weight (mass) of the antennas is also an important parameter, in several applications (for instance in aerospace) the low profile is an important characteristic, too. These parameters are in connection with the technology of modern production. Because of the lack of a numeric characteristic based on the antenna gain and taking into account the modernity of applied technology, up to now we can't compare antennas operating on different frequencies, having different construction and weight. This paper introduces such a new characteristic.

2. SUGGESTED NEW PARAMETER

In several applications the construction of the antenna is not mainly determined by the mechanical loads (ice- or widload). In these cases the fastening assembly is simpler and the plane- or conform MSA-arrays can be mounted directly to the surface of the aircraft, or can be stuck on the outer side of a portable equipment. The minimal weight is an important requirement.

The gain of the antenna is:

$$G = 4\pi A_e/\lambda^2 = 4\pi\eta A f^2/c^2 \qquad (1)$$

where λ is the wavelength, A_e is the effective aperture area, c is the velocity of light, f is the frequency, η is the aperture efficiency, A is the true aperture area.

Supposing a planar antenna with mass M, volume V, surface area A, an imaginary equivalent thickness d, an imaginary specific bulk density γ (which is supposed to be homogeneous), we get the following equations:

$$M = \gamma V = \gamma A d; \quad A = M/\gamma d \qquad (2)$$

Substituting the value of A into eq. (1) and dividing it by $f^2 M$, we get the proposed parameter, which we call *specific gain*:

$$\mathbf{G}_s = \mathbf{G}/f^2 M = 4\pi\eta/\gamma d c^2 \qquad (3)$$

or in logarithmic scale:

$$G_s = 10\log(\mathbf{G}/f^2 M)\ [\text{dB GHz}^{-2}\text{kg}^{-1}] \qquad (4)$$

The specific gain G_s can be considered from eq. (4) as the gain in dB-s of an 1 kg antenna operating at 1 GHz. The *conditions to achieve high* G_s according to eq. (3) are:

- high efficiency (good antenna elements, low loss distributing network, etc.),
- usage of light materials (carbon fibre, Kevlar, Hexcell, Honeycomb-structure sandwich materials, polyester dough moulding compound [6] etc.), that is introducing of modern technology,
- forming thin planar arrays, using thin substrates.

As come of all the above, state of the art antenna design is well included the specific gain parameter.

The question arising from eq. (4): what to consider as the mass of the antenna? In my opinion it is the mass of essential elements of the antenna, excluding the mounting assembly. For instance in the case of parabolic antennas, it includes the mass of the reflector and the mass of the primary feed with its mounting structure; in the case of MSA-arrays the mass of substrates and the mass of the feeding network (microstrip or stripline power dividers, semi-rigid cables, hybrids, etc.).

My further comments on modern antenna construction and on specific gain are:

* This is a version of papers presented by F. Völgyi on ICOMM'90 in Dehra Dun, India [17], [18].

- He who doesn't produce a given construction in the lightest possible form, doesn't only waste energy and material but causes pollution as well. Better features not be achieved by extending the built-in material but rather by giving way to good ideas.
- We should make an effort to deprive the antenna of being a separate unit and be the integrated part of the equipment it belongs to. In that case the total mass should be minimized.
- The principles mentioned above can not be applied to only the MSA-s, but the heavy weight pyramidal horn antenna – mentioned in the introduction – could also be substituted by a horn made by modern technology, and the parabolic antennas can also be produced in a similar way as the "paragrid antennas" [7] or the "segmented diamond antennas" [6].
- An additional cost optimum could also be examined, but the economists calculate it anyway. On the other hand high specific gain usually results in the reduction of costs.
- Eq. (4) should be used at high gain arrays first of all, mainly at systems mounted on aircrafts or at portable ones.
- Calculation of G_s could also be interesting for basic antenna elements. As eq. (3) suggests it would be better to construct a sandwich structure of thin substrates with electro-magnetically coupled parasitic elements instead of the thick substrate (which even decreases the efficiency [8]) used for increasing the bandwidth.

G_s in the mirror of numbers. I have summarized the specific gain and characteristic features of some known antennas in *Table 1.* In spite of the fact that all categorizations are artificial in a way (and there are always exceptions), the classification of antennas on the basis of specific gain according to *Table 2* could also be possible.

Table 1

Ser. No.	Specific Gain G_s $dB \cdot GHz^{-2} \cdot kg^{-1}$	Antenna type	Gain G [dB]	Freq. f [GHz]	Mass M [kg]	Characteristics (Remarks)	Designer or Manufacturer	Ref. No.
1	-3,3	AR-6 (JFS-32R)	28,0	9,445	15,0	1,8 m long, slot antennas (for ship radar)	JFS-Electronic (Schweiz)	[9]
2	+5,4	EMH 12-121.A	40,8	12,1	23,5	1,2 m diam. parabolic	Hirschmann (BRD)	[10]
3	7,2	PG-4/450	13,1	0,45	19,0	1,2 m "Paragrid" antennas	Radio Masts Ltd (England)	[7]
4	13,0	PG-10/1500	33,0	1,5	45,0	3,05 m "Paragrid" antennas	Radio Masts Ltd	[7]
5	9,4	RPV-MSA	10,0	0,955	1,27	Fuselage integr. MSA	Yee and Furlong	[11]
6	9,8	"Printed Antennae"	21,5	10,6	0,13	16×8 el. MSA	EMI-Varian Ltd	[12]
7	11,9	Modular-MSA	29,5	9,3	0,60	256 el., 40×40 cm^2	Levine et al.	[13]
8	13,3	MSA-256	29,5	8,1	0,63	256 el., 41×41 cm^2	F. Völgyi	[5]
9	16,0	ELW/MSA-16	20,5	1,4	1,45	66×66×1,3 cm^3, 16 el.	Völgyi–Mernyei	[17]
10	13,5	SEASAT-A	34,9	1,275	103	10,7×2,2 m^2 MSA	Ball Aerosp. S/D	[14]

Table 2

Ser. No.	Suggested Antenna Category	Specific Gain, G_s $[dB \cdot GHz^{-2} \cdot kg^{-1}]$	Examples	Ref. No.
1	Conventional microwave antennas (heavy weight construction)	< 5	Conventional radar antennas Parabolic antennas Pyramidal horns waveguide slot arrays, etc.	
2	Modern (lightweight) microwave antennas (new: materials, structures)	5 – 10 (13)	"Paragrid" antennas Flat-late arrays "Segmented diamond" antennas Carbon fibre slot antennas, etc.	[7] [6] [6]
3	Microstrip antennas (MSA)	10 – 15	Single (thick) layer MSA-array Modular MSA-array	 [13], [5]
4	Extremely lightweight microstrip antennas (ELW-MSA)	> 15	Multi-(thin)layer MSA-array Honeycomb-structure MSA MSA with extra low loss feeder	

3. AN EXAMPLE FOR ELW/MSA-ARRAY

Fig. 1 shows the cross-sectional view of an extremely lightweight microstrip antenna array mentioned in the introduction. This 16-element antenna is built up of four 2×2 element modules, which are connected to the corporate hybrid by a semirigid cable. A stripline power splitter can be found behind each module, which supplies the radiating elements of the modules by their four coaxial fedthroughs. The rigidity of the structure is guaranteed by a 10 mm thick Divinicell polyfoam (with suspended back metallization) material together with the thin substrates and the bonding technology. Because we use a minimum-sized microwave substrate only in the most necessary cases, the antenna is relatively cheap, lightweight and the power splitter has an extremely low loss. The further parameters of the antenna can be found in the 9th row of *Table 1.*

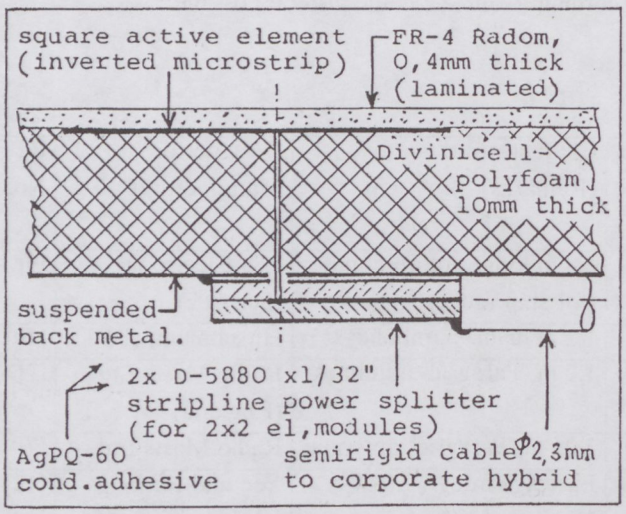

Fig. 1. Cross-sectional view of an ELW/MSA [18].

4. PLANAR ARRAY FOR AIRBORNE RADIOMETER APPLICATIONS

This antenna is made up of a 4×4 element microstrip antenna array. In the construction of the radiating elements our main aim was the achievement of lightweight and flatness. We worked out the necessary low sidelobe level by the application of the adequate amplitude distribution.

4.1. Construction of the radiating elements

The parameters of microstrip antennas mainly depend on the characteristics of the selected substrate material. Since our goal was to construct a 4×4 elements antenna for 1.4 GHz, the choice of low loss substrate (RT-Duroid, Di-Clad) would have proved to be very expensive -owing to the large size of the sheet. In order to get the necessary bandwidth (> 6.5 %) a thick substrate ($h = 10$ mm) is needed, however we did not have disposal the generally used honeycomb [16]. Our solution can be seen on *Fig. 2.* In this case the dielectric is a 10 mm thick air layer. The supporting surface of the resonant elements is a traditional fiberglass FR-4 type substrate, which serve as RADOM at the same time (inverted microstrip). The ground plane is guaranteed by the metallization of another FR-4 substrate. The coaxial feedings of the radiating elements are carried out by metal feed probes placed inside the cylindrical teflon (PTFE) distance pieces. They are connected to the microstrip power splitter circuit placed on the back side of the antenna. The strength of this "sandwich" structure is ensured by the PVC distance pieces, placed in the minimums of the electromagnetic field. We applied the low-loss substrates only at places where the power splitting lines run. This way we managed to work out a cheap and very light product. The parameters of the radiating elements are the following:

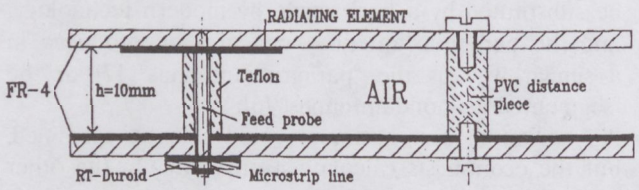

Fig. 2. Cross-sectional view of a planar antenna array for 1.4 GHz airborne radiometer [17].

frequency: 1.4 GHz
size: 86.3×86.3 mm
thickness: 10 mm (with air dielectric layer)
bandwidth: 96 MHz (6.9 %, VSWR<2)
gain: 9.2 dB
input imp.: 50 Ohms

To design the radiating elements we used our CAD program made earlier for IBM-PC [5].

4.2. Determing the necessary amplitude distribution

Using the well-known formula:

$$F(\phi) = F_s(\phi) \sum_{k=1}^{n} I_k e^{-jk\frac{2\pi}{c}d\cos(\phi)} \qquad (5)$$

as our starting point for the 1-dimension case, the application of 4 elements with a 1:2:2:4 amplitude distribution, $d = 1/6$ m distance between the elements and $f = 1.4$ GHz resonant frequency results in a -27 dB side-lobe level, which meets the requirements. This way we got the amplitude distribution for the 4×4 array shown on *Fig. 3* (while the phase distribution is constant).

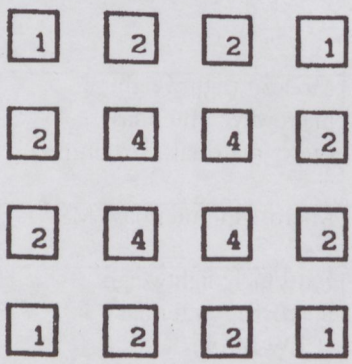

Fig. 3. Relative amplitudes of the -27 dB sidelobe level MSA-array.

4.3. The power splitting circuit

As can be seen on *Fig. 3* the antenna has two symmetry planes, so the splitting circuit can be divided into two different parts:

1. a splitter, dividing the power into 4 equal parts,
2. 4 identical circuits, each realizing a 1:2:2:4 distribution.

The first circuit consists of 3 hybrid rings. Inside the rings is a matched load with a radial line connected to it, realizing a short circuit (*Fig. 4a*). The other circuits consist of 3 identical power splitters, each realizing a 1:2 division ratio (*Fig. 5a*).

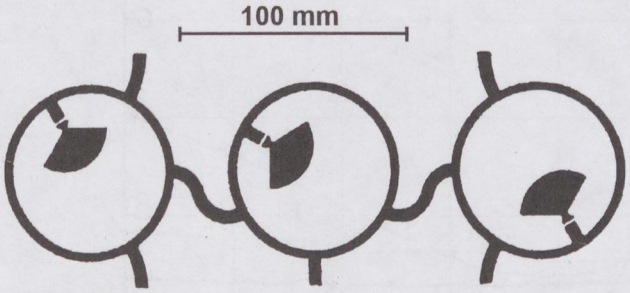

Fig. 4a. Hybrid rings dividing the power into 4 equal parts.

As can well be seen, the end points of these circuits are fitted on the coaxial input of each antenna elements. In order to achieve uniform phase distribution, the electrical lengths of the lines had to be equal. The two types of splitters were connected to each other via semirigid cables.The measured insertion losses of the splitters can be seen on *Fig. 4b* and on *Fig. 5b*. As it is apparent from the diagrams, the bandwidth of the splitters is greater than that of the radiating elements [3], and the total loss is less than 0.25 dB.

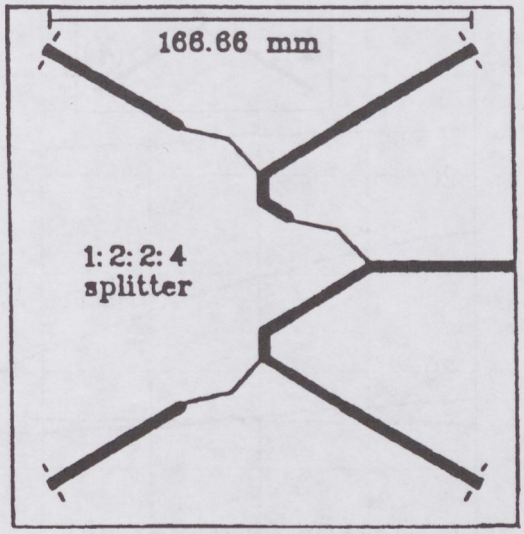

Fig. 5a. The reactive, 1:2:2:4 splitter.

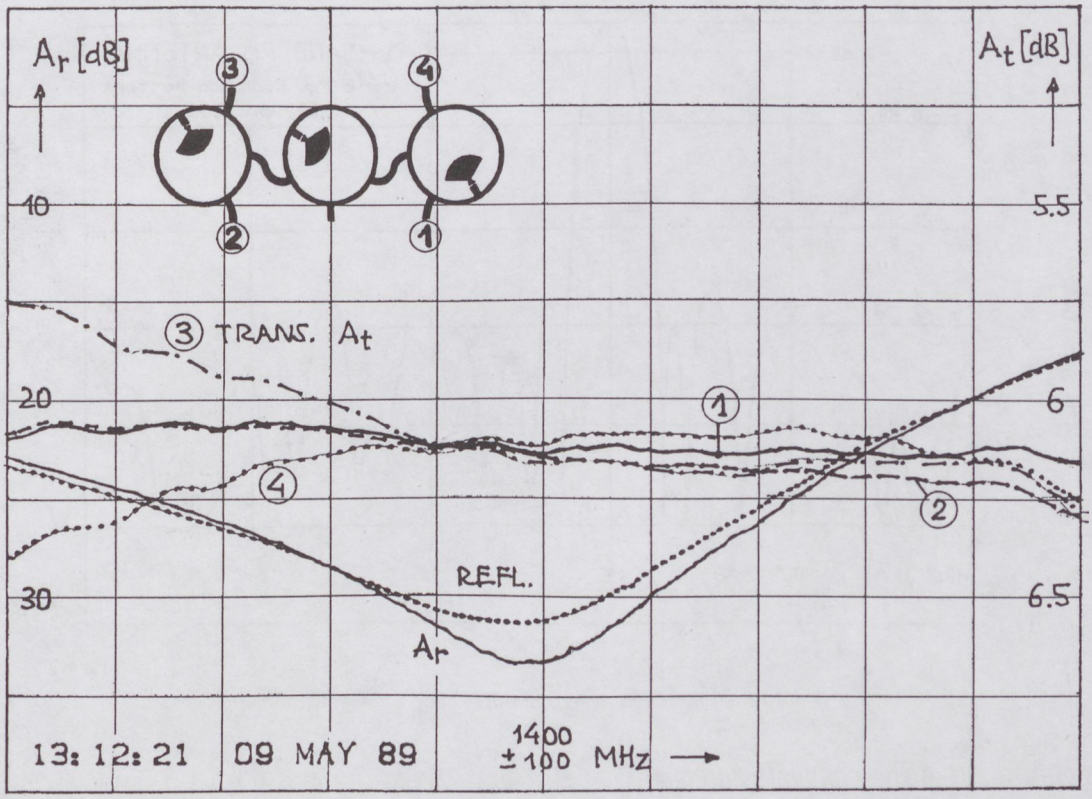

Fig. 4b. Measured input return losses and insertion losses of the splitter shown in Fig. 4a.

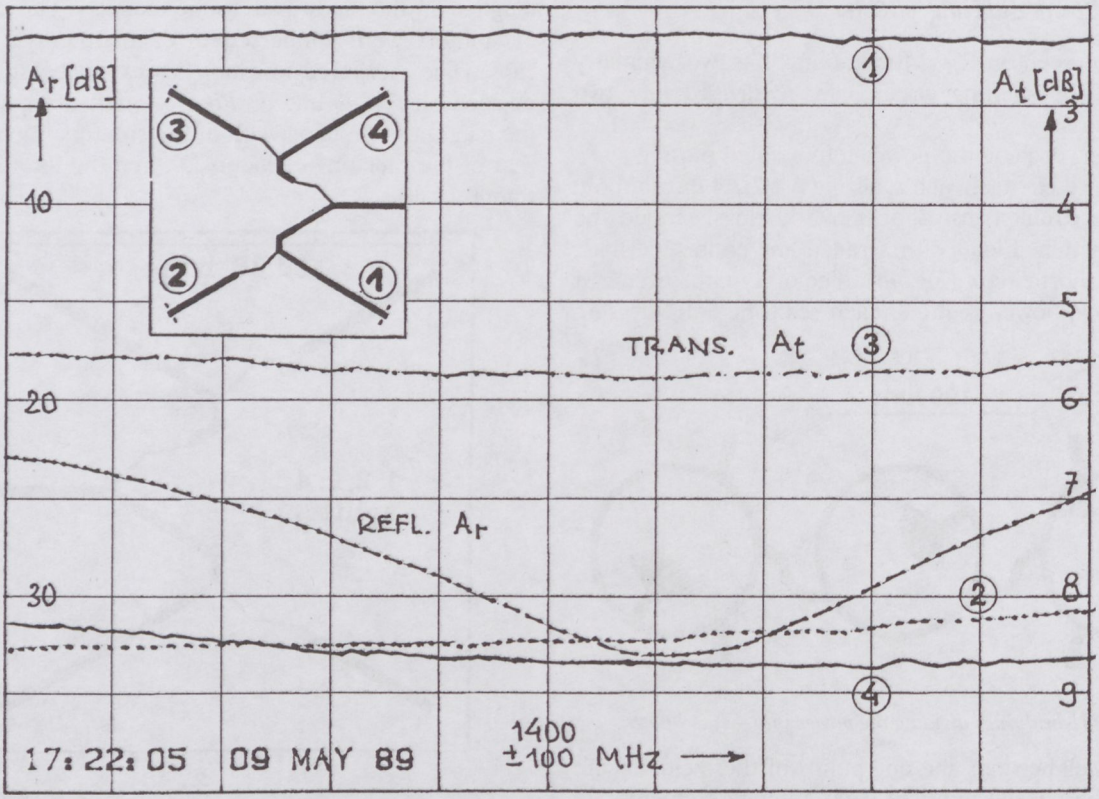

Fig. 5b. Measured input return losses and insertion losses of the splitter shown in Fig. 5a.

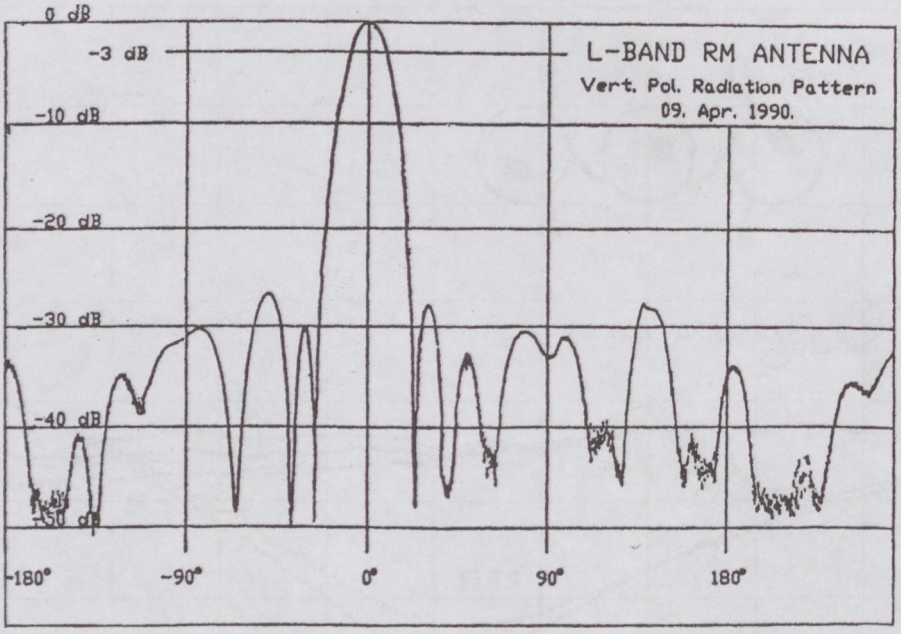

Fig. 6. Measured radiation pattern of the L-band radiometer antenna.

4.4. Characterization of the complete antenna

The measured radiation pattern is shown on *Fig. 6.* The minimum and maximum points and the sidelobe levels are in good agreement with the calculations. The characteristic features [18] of the complete antenna are the following:

size:	$66 \times 66 \times 1.5$ cm
mass:	3 kg
3 dB beamwidth:	10 degrees
side lobe level:	< -27 dB
gain:	20 dB
specific gain:	12.3 dB GHz^{-2} kg^{-1}

5. CONCLUSIONS

The suggested new parameter (specific gain) described here is not only suitable to compair the extremely light and ordinary MSA-s, but it reflects the results of the modern antenna design as well. To make the decibels fly – that is to create high gain extremely light MSA arrays – new ideas and a series of technological solutions are needed. The described ELW-MSA is only one example among the possible solutions.

The application of air layer as dielectric proved to be a novel solution at the airborne radiometer antenna. It enabled the production of cheap and definitely lightweight antennas. Due to the low side lobe level, the antenna has proved to be really satisfactory for the radiometer.

6. ACKNOWLEDGMENT

The author wish to acknowledge Ferenc Mernyei for many informative discussions and for contributing to experiments, acquiring the data of the planar airborne radiometer antenna.

REFERENCES

[1] James, J. R,.: "Printed Antennas" SBMO Int. Microwave Symp. 1987 Rio de Janeiro, Brazil, pp. 597-606.
[2] Völgyi, F.: "Microstrip Antenna – Bibliography" (manuscript) 1998.
[3] Mernyei, F. and Völgyi, F.:"A Simple Method for Testing the Temperature Dependence of Microstrip Antenna Arrays" 20th EuMC, Budapest, Hungary, Sept., 1990, pp. 365-370
[4] Völgyi, F.: "Versatile microwave moisture sensor" in Conf. Rec. SBMO'89, Sao Paulo, Brazil, 1989, Vol. II, pp. 456-462.
[5] Völgyi, F.: "High Efficiency Microstrip Antenna Array" 1987, 17th European Microwave Conference, Rome, Italy, Proc. pp. 747-752.
[6] Watson, B. K.: "Product Range, RF-Products" ERA Technology Ltd., England, 1987.
[7] "Paragrid Antennas" Catalogue, Radio Masts Ltd., England, 1980.
[8] Roudot, B., Mosig, J. R,. and Gardiol, F. E.: "Surface Wave Fields and Efficiency of Microstrip Antennas" 18th EuMC, Stockholm, Sweden, 1988, pp. 1055-1062.
[9] Radar JFS 32R, Service Handbook, JFS Electronic (Schweiz), 1977.
[10] Hirschmann TML-AM Richtfunksystem, Systembeschreibung (Microwave Links and Headends for CATV).
[11] Yee, J. S. and Furlong, W. J.: "An extremely Lightweight Fuselage – Integrated Phased Array for Airborne Applications" Proc. Workshop on Printed Circuit Antennas Technology, New Mexico State Univ., Las Cruces, October 1979, pp. 15.1-15.12.
[12] "Printed Antennae" Catalogue, EMI- Varian Ltd., England, 1973.
[13] Levine, E. et al: "High Gain Modular Microstrip Antennas" 16th EuMC, Dublin, Ireland, Proc. pp. 655-660.
[14] Murphy, L. R.: "SEASAT and SIR-A Microstrip Antennas" Proc. Workshop on Printed Circuit Antennas Technology, New Mexico State Univ., Las Cruces, October 1979, pp. 18.1-18.20.
[15] Ijjas, G.: "An Airborne Microwave Radiometer System for Soil Moisture Mapping" 20th EuMC, Budapest, Hungary, September, 1990, Paper P.4.1.
[16] Huang, J.: "Wideband Microstrip Antenna – Feeding Array" JET Propulsion Lab., Invention Report, NPO-17548/7057, March 1990.
[17] Mernyei, F. and Völgyi, F.: "Planar Antenna Array for Airborne Radiometer Applications" ICOMM'90 Int. Conf. on Millimeter Wave and Microwave, Dehradun, India, 1990, Proc. pp. 393-396.
[18] Völgyi, F.: "Flying Decibels ű Extremely Lightweight Microstrip Antennas" ICOMM'90 Int. Conf. on Millimeter Wave and Microwave, Dehradun, India, 1990, Proc. pp. 343-348.

SZÁRNYALÓ DECIBELEK – EXTRÉM KÖNNYŰ NYOMTATOTT ANTENNÁK

VÖLGYI FERENC

BUDAPESTI MŰSZAKI EGYETEM
MIKROHULLÁMÚ HÍRADÁSTECHNIKA TANSZÉK
TEL.: 36 1 463 1559; FAX: 36 1 463 3289; T-VOLGYI@NOV.MHT.BME.HU

Különlegesen könnyű nyomtatott antennákra van szükség műholdakon és repülőgépeken való alkalmazásoknál. Ezen antennák kialakításánál a legújabb konstrukciós elveket, elkészítésük során pedig az új gyártási technológiákat használva végeredményben a hagyományos antennákat túlszárnyaló megoldásokat kapunk.

Egy a szerző által javasolt új antenna paraméter (fajlagos nyereség) bevezetésével összehasonlíthatóvá válnak "könnyűség" szempontjából a különböző konstrukciójú, eltérő frekvenciákon működő más-más tömegű antennák. Az eszmefuttatásból az is kiderül, hogy nagy fajlagos antenna-nyereség eléréséhez jó hatásfokú elemi antennákra, kisveszteségű elosztó hálózatra, vékony planár struktúrára, minimális mennyiségű és könnyű szerkezeti anyagokra van szükség, melyek összeépítésénél gyümölcsöző a ragasztásos technológia használata.

A cikkben különböző antennák specifikus nyereség szempontjából való táblázatos összehasonlítását is megtaláljuk, melyet két konkrét példa követ. Az első egy ragasztásos technológiával készített, kemény habanyagon kialakított, vékony laminátumokat felhasználó extrém-könnyű antenna. A másik antenna távtartókkal készített "légdielektrikumú" konstrukció, változó amplitúdó eloszlás miatti nagy melléknyaláb elnyomással, repülőgépre szerelt rádiométer alkalmazáshoz. Ezen antenna tervezési részletei, teljesítményosztóinak felépítése és mérése, valamint a teljes antenna specifikációja és mért iránykarakterisztikája található a cikkben.

Az írás mottója lehetne: "nem anyaggal, hanem ésszel", vagyis nem a beépített anyag mennyiségének növelésével, hanem új ötletek és modern konstrukciós elvek alkalmazásával kell a nagynyereségű antennákat kialakítani.

MICROSTRIP ANTENNAS WITH POLARIZATION DIVERSITY AND FREQUENCY AGILITY*

FERENC VÖLGYI

TECHNICAL UNIVERSITY OF BUDAPEST
DEPT. OF MICROWAVE TELECOMMUNICATIONS
H-1111, BUDAPEST, GOLDMANN TÉR 3, HUNGARY
PHONE: 36 1 463 1559; FAX: 36 1 463 3289; T-VOLGYI@NOV.MHTI.BME.HU

A dual-linear polarized microstrip antenna (DPMSA), which consists of two isolated 4×8 element uniformly illuminated arrays, built on a single-layer substrate in orthogonal position, having highly isolated two inputs for the operational frequencies (which are shifted some percent), and a varactor tuned frequency agile microstrip antenna (FAMSA), using only a single varactor diode in each radiating rectangular patch element and the array has only a single DC-bias point and contains identical varactor diodes, are introduced.

1. BACKGROUND

The main military electronic systems (Electronic Warfare: EW Systems) are: Radars, Radio-meters, Seekers, Missile Tracking Systems, Electronic Counter Measures: ECMs, Secured Communications, Remotely Piloted Vehicles: RPVs, Drones fitted with pre-programmed Flight Control Systems, Tactical Radar Threat Generators: TRTGs, Satellite Communications, etc. The EW covers jamming, chaff dispersing, emitter detection, identification and location. Applications could range from VHF communications up to the radar frequency bands.

Many kinds of sophisticated antennas are used in this field. High gain and efficiency, beam scanning possibly with multi-beams, polarization diversity, frequency agility, size and weight constraints, low cost, low sidelobes for security and antijamming, large bandwidth (instantaneous or operational) for frequency hopping, etc. are the main antenna characteristics, as mentioned at James and Henderson [1].

These types of antennas used in scatterometer radar systems (see at Petersson [2]), are in successful operation in space environment, too. At L-band mobile satellite communications, innovative antennas (both portable and vehicular units) for terrestrial mobiles were introduced by Shafai [3].

2. INTRODUCTION

To minimise weight and aperture area, a printed circuit microstrip antenna array (Doppler navigator antenna) had been designed by Gibson [4]. Microstrip patch elements are the new generation or antennas due to their small size, lightweight at Völgyi [5], at Mernyei and Völgyi [6], low profile, and easy configuration into high efficiency arrays, as introduced by Völgyi [7]. In our earlier design of S-band microstrip phased array antenna (see at Nizar N.M. Suleiman [8]), varactor diodes were used as switched elements of the 4-bit digital phase shifters. Planar varactor diodes were used in the integral dipole-phaseshifter elements of an electronically steerable, X-band reflect array (using 779 microstrip dipoles) introduced by Patel and Thraves [9].

2.1. Frequency agility

The relatively narrow bandwidth and the excitation of surface waves are the major disadvantages of the microstrip patch. Using varactor diodes as active loads, it is possible to increase the operational frequency bandwidth of MSA (Microstrip Antenna) as given at Bhartia and Bahl [10]. Recently this method is actively studied by Waterhouse [11], for increasing the scanning range of MSA-arrays.

By using frequency agile radiating patch elements, thin conformal communication of radar antenna can be fabricated with the ability to track the computer controlled tuning of the transmitter or receiver. This system provides added flexibility in avoiding interfering signals. A varactor tuned circular microstrip patch antenna was introduced by Purchine et al. [12]. The varactor diode was biased by microprocessor-controlled digital-to-analog converter circuitry that simulates the microprocessor of the receiver.

2.2. Polarization diversity

Polarization switching of an antenna is needed in EW and Electromagnetic Remote Sensing, where polarization information is important since an electromagnetic scatterer acts like a polarization transformer. In one of our earlier designs, two isolated 8×16 rectangular element microstrip arrays were used as dual-polarized antenna of an X-band scatterometer as given at Mihály and Bozsóki [13].

There are more sophisticated polarimetric MSAs, too (see at Itoh [14]). For military satellite communications, a multilayer – sandwich construction MSA was introduced by Owens and Smith [15]. Circularly polarized conformal printed antennas are used for small missile tracking systems at Newham [16]. Very low interaction on the radiating near-field was observed by Völgyi [17], with the X-band circularly polarized MSAs used in microwave moisture sensors.

2.3. High power MSA

Power applications of MSAs, seem to be a contradiction. With a unique construction, Völgyi [18] introduced an

* This is an extend of the paper presented by F. Völgyi at MILCON'95 in Abu Dhabi, UAE [25].

MSA-array applicator, which can radiate a CW-power of 1 kW, and it is possible to use it as a transmit antenna, e.g. for FM-CW radar applications.

3. OUR DESIGNS (Modular Approach, Construction)

3.1. Dual polarized microstrip antenna

"The simple is the best" – frequently! The upper S-band dual polarized microstrip antenna (DPMSA) consists of two isolated 4×8 element uniformly illuminated array built on a single-layer (monolithic) substrate, in orthogonal position (*Fig. 1*). To gain higher isolation between two inputs, the resonant frequencies are shifted by 5 % (f_{01} and f_{02} in *Fig. 2*). A modular approach is utilized in which a given antenna is used as a building block for a higher gain antenna (Völgyi and Mernyei [19]).

At the design stage of DPMSA, we used our computer program (mentioned by Völgyi [7]), which is based on the Electric Surface Current Model. For calculations of the frequency dependent input impedance of rectangular microstrip antenna element, we modified the expressions of Bhattacharjee et al. [20]. Calculated H-plane radiation characteristics for single element and for a module are given in *Fig. 3*.

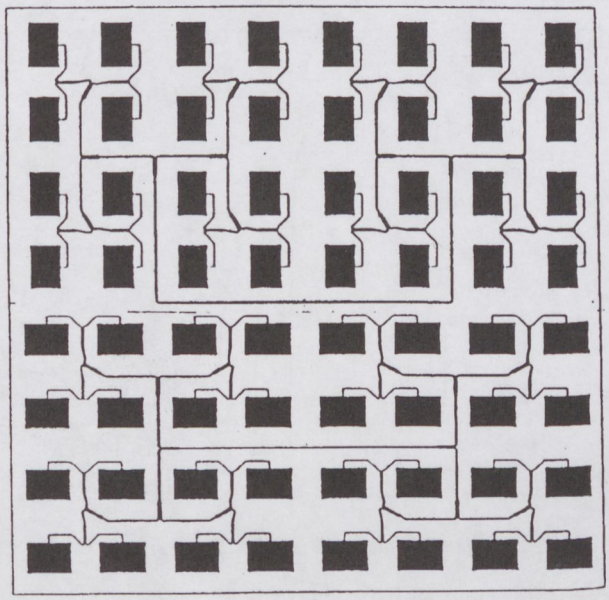

Fig. 1. Upper S-band dual polarized microstrip antenna (DPMSA). Dimensions: $40 \times 40 \times 0.16$ cm^3, substrate material: D-5880. Gain of the array is 24.5 dB, isolation between two inputs is better than 45 dB, half power beamwidth 8.8° and 17.6° are, respectively. Relative difference of the center frequencies is 5 %.

3.2. Frequency agile microstrip antenna

The frequency agile microstrip antenna (FAMSA) uses the 2×2 element building block (module) of DPMSA, and only a single varactor diode is used, and directly soldered into one of the radiating edges of each rectangular patch (*Fig. 4*). The FAMSA module contains identical varactors and has only a single DC-bias point, which is low-pass filtered from microwave input.

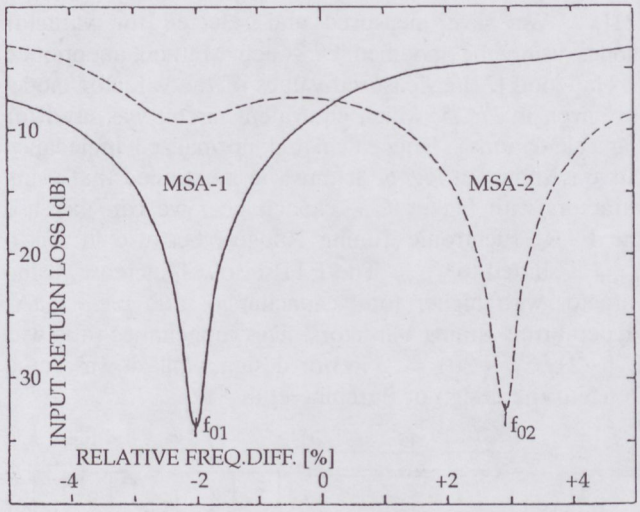

Fig. 2. Measured input return loss versus relative frequency difference of the polarization diversity MSA having 2x (4x8) elements.

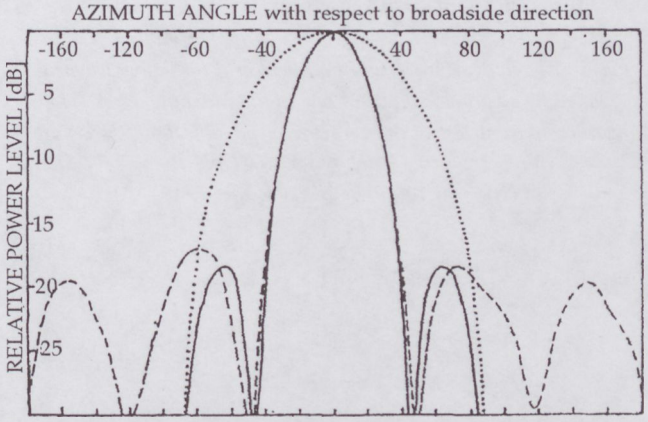

Fig. 3. Calculated H-plane radiation characteristics for single element (... line) and four element passive array at the frequency of f_{max}. Measured values, for varactor tuned MSA are also shown (dotted line).

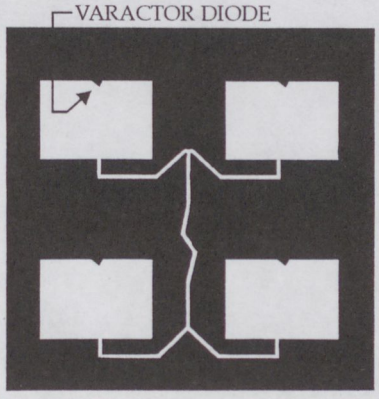

Fig. 4. Frequency Agile Microstrip Antenna (FAMSA). Outer dimensions of the 4-element module: 10x10x0.08 cm^3, substrate material: 3M-Cuclad-217. Tuneability: 10 %, gain at fmax is 12.7 dB, half power beamwidth nearly 36° and 46° are, respectively. Instantaneous bandwidth is 1.5 %.

At the experimental work of FAMSA our practice in the field of Parametric Amplifiers was very useful (Völgyi

[21]). We have measured and selected the varactor diodes using the modified DeLoach Method, mentioned at Hapgood [22]. Measured values of the varactor model are given in *Fig. 5*, which equivalent circuit was used for the calculations. The calculated normalized impedance curve is shown in *Fig. 6*. It must be mentioned that using varactors with higher C_{j0} capacitance, we can increase the ETR (Electronic Tuning Range), because in *Fig. 6* $f_{\min}$ is shifted to f_{low}. The ETR also will increase, using varactor with higher total capacitance ratio e.g. GaAs Hyperabrupt Tuning Varactors. This capacitance ratio was $C_t(-2)/C_t(-20) \sim 2$ in our design, while it was equal to 6.5 at the design of Purchine et al. [12].

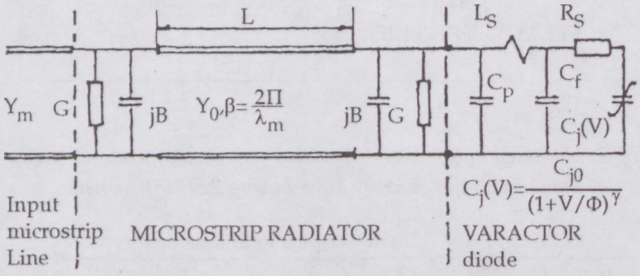

Fig. 5. The equivalent circuit of a Microstrip Radiating Element, loaded by a varactor diode at one of the radiating edges. The measured parameters of the varactor (Type MA-46600-J155) are: $C_p = 0.13\ pF$, $L_s = 0.16\ nH$, $C_f = 0.01\ pF$, $R_s = 2.73\ Ohm$, $C_{j0} = 0.79\ pF$, $\Phi = 1.1\ V$, $\gamma = 0.481$.

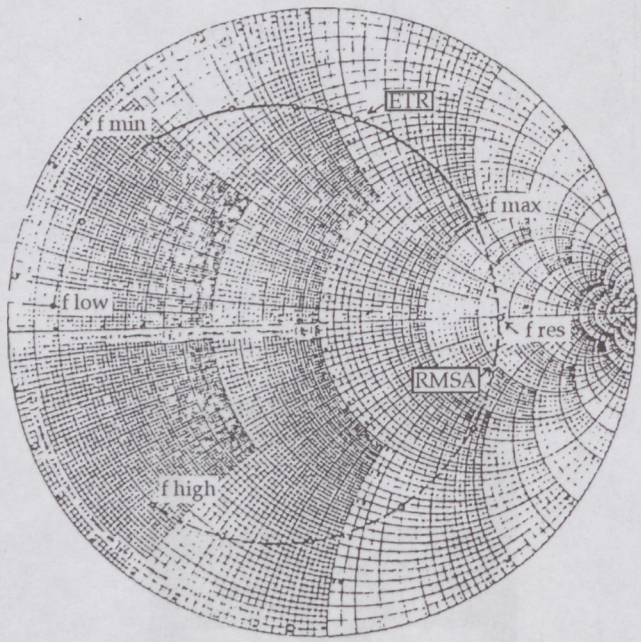

Fig. 6. Calculated normalized impedances. RMSA: Rectangular Microstrip Antenna, normalized input impedance against frequency at the center of one of the radiating edges. The resonant frequency of the passive RMSA is: f_{res}. *ETR: Electronic Tuning Range for frequency agile RMSA. Antenna impedance at the place of varactor.*

3.3. Large signal effects

Using varactor diodes to create the frequency agility of MSAs, large signal effect can modify the tuning characteristics because of the diodes rectify signals slightly if the voltage swing forward-biases the diode for part of the RF circle. This additional bias-shift caused by rectification increases, as the applied bias approaches 0 Volt.

At the high reverse voltage end of the tuning range, high signal levels cause a gradual reduction in tuning slope as the peak junction voltage approaches punch-trough. Because the FAMSA uses nonlinear capacitances, large signal levels will be accompanied by harmonics. Taking into account these effects, the main application of FAMSA is as a receiving antenna, when small signal levels are guaranteed.

3.4. Effect of tolerances

Analyzing the effect of tolerances of the junction capacitance at zero Volt (dC_{j0}) of varactor diodes for the directivity, 3 dB beamwidth,, sidelobe level, scan angle of a 8×8 element quadratic MSA-array, a lot of calculations have been made. Using the equivalent circuit of a microstrip radiating element (*Fig. 5*) standard capacitance matching (±10 %) was supposed, and individual capacitance value was given for each radiating element inside the 64 element array, using the drawn numbers of a pseudo random code generator. After some program running, calculated results are given in Table 1. This table completely shows the usefulness of cheap varactors with loose capacitance matching. Calculated H-plane pattern is shown in *Fig. 7*.

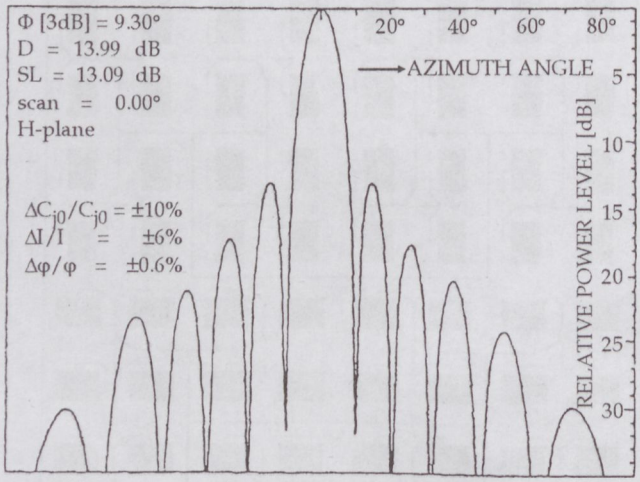

Fig. 7. Calculated H-plane pattern for the given capacitance matching

Table 1. Calculated performances of FAMSA-array versus capacitance matching of the used varactor diodes

Capacitance matching	$\Delta C_{j0}/C_{j0} = \pm10\%$
Relative error in the magnitude of input currents	$\Delta I/I = \pm6\%$
Relative phase error of input currents	$\Delta\phi/\phi = \pm0.7\%$
Directivity of the MSA array	$D = 27.7 \pm 0,13$ dB
Side lobe level	$SL = 13.2 \pm 0.6$ dB
Scan angle (negligible)	$\Theta s = 0°$

Assuming much higher tolerances, one of the calculated results is given in *Fig. 8.* calculated radiation patterns for ideal case are shown in *Fig. 9* and *Fig. 10.*

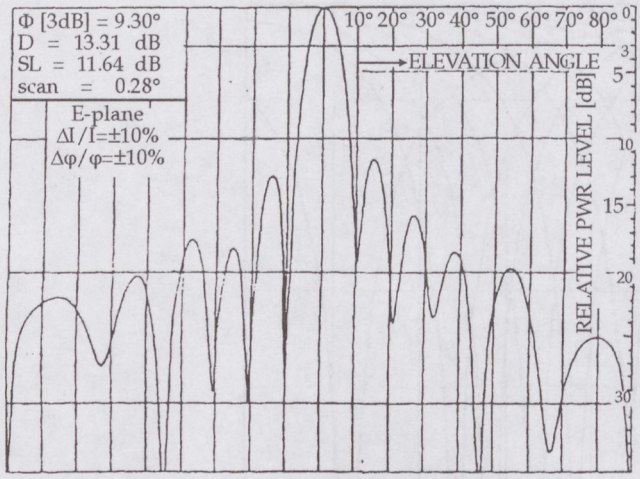

Fig. 8. Calculated E-plane pattern for a higher tolerance of capacitance matching

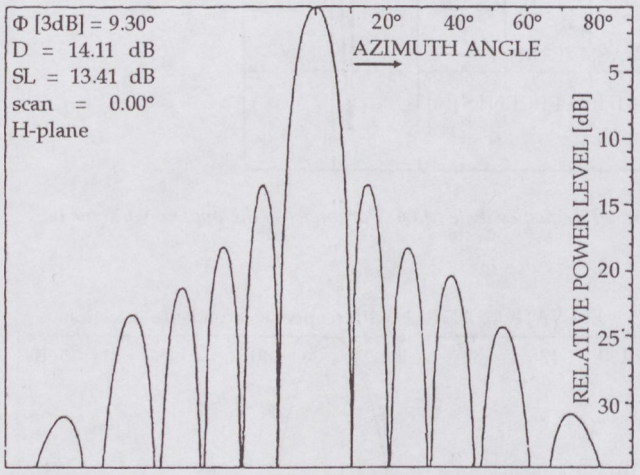

Fig. 9. Calculated H-plane pattern for ideal case (identical varactors)

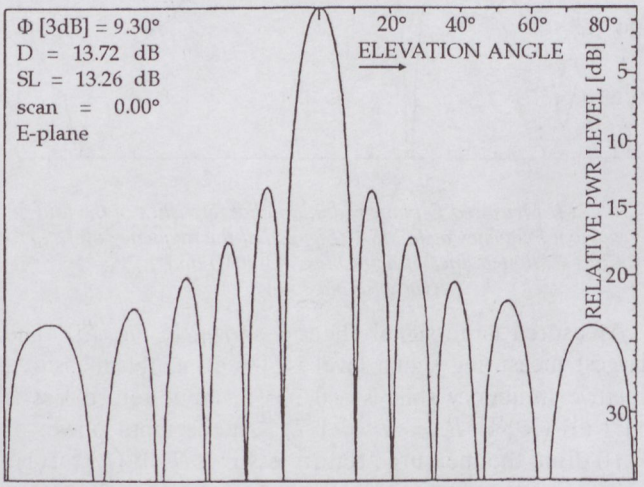

Fig. 10. Calculated E-plane pattern for ideal case (identical varactors)

3.5. Gain versus frequency estimation

Originally, the rectangular MSA was designed to the frequency of f_{max} (see *Fig. 6*), where the calculated gain of the single element is $G_e = 7.1$ dB, and at the frequency of fmin the gain is 6.6 dB. Using varactor diodes at the FAMSA-array, efficiency will degrade. This efficiency degradation is caused by the power dissipated in the series resistor of the varactor, and by the mismatch loss. As a consequence, this degradation will be harder at the lower end of the electronic tuning range (more details are given at Mustapha A. Agha [23]).

4. EXPERIMENTAL RESULTS

Measured H-plane characteristics of the DPMSA are shown in *Fig. 11* and *Fig. 13*, while the input return loss versus relative frequency difference is given in *Fig. 2*. Using our temperature test method (Mernyei and Völgyi [24]), the relative frequency shift of f_{01} and f_{02} was found 0.5 % in the temperature range of -40 C° ... $+$ 60 C°.

Changing the DC-bias voltage of varactors at the FAMSA-module, the resonant frequency is shifted (*Fig. 12*). It is to be noted that optimal matching is possible near the center frequency (bias voltage: -0.5 V) changing the impedance level of microstrip lines between radiating patches. Measured H-and E-plane radiation patterns of FAMSA are shown in *Fig. 3* and *Fig. 14*. The beamwidth decreases with increasing frequency as shown in *Fig. 14*.

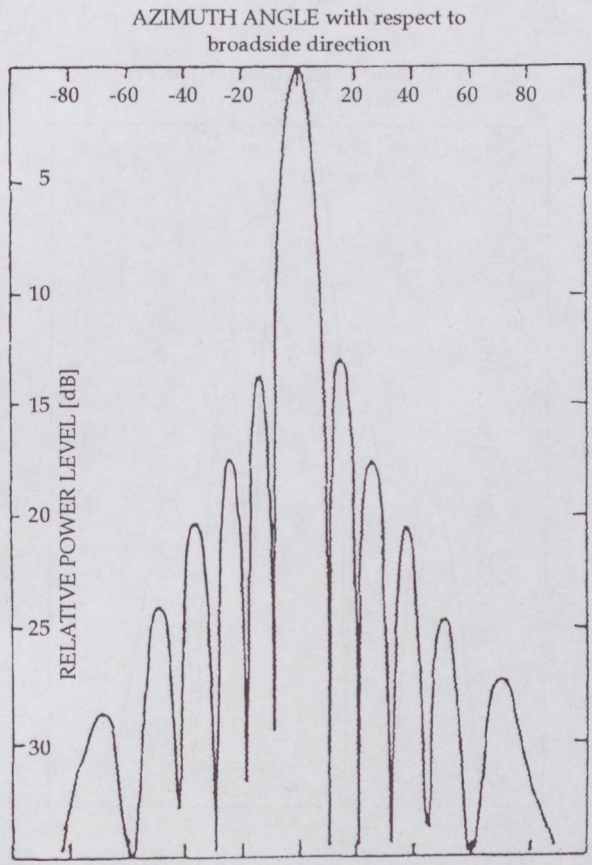

Fig. 11. Measured H-plane radiation characteristics at the frequency of f_{01} (lower antenna on Fig. 1.)

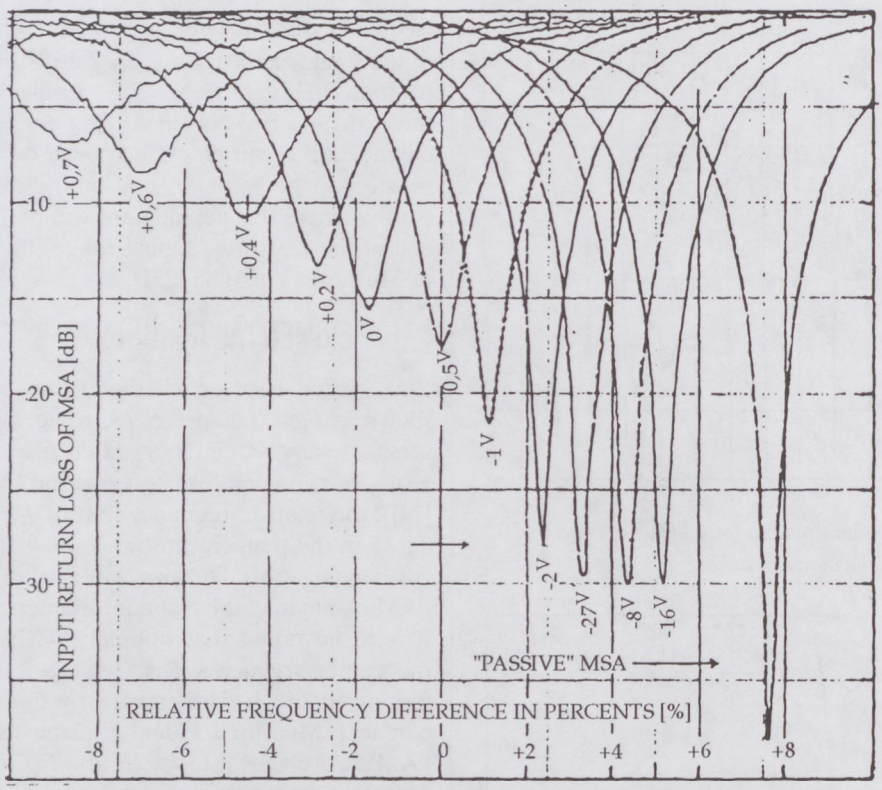

Fig. 12. Measured input return loss versus relative frequency of the 4-element frequency agile MSA. Parameter is the applied varactor bias voltage.

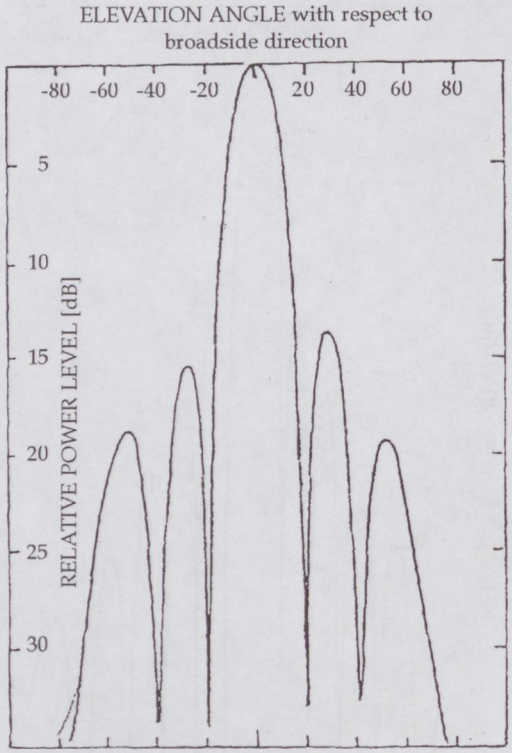

Fig. 13. Measured H-plane radiation characteristics at the frequency of f_{02} (upper antenna on Fig. 1.)

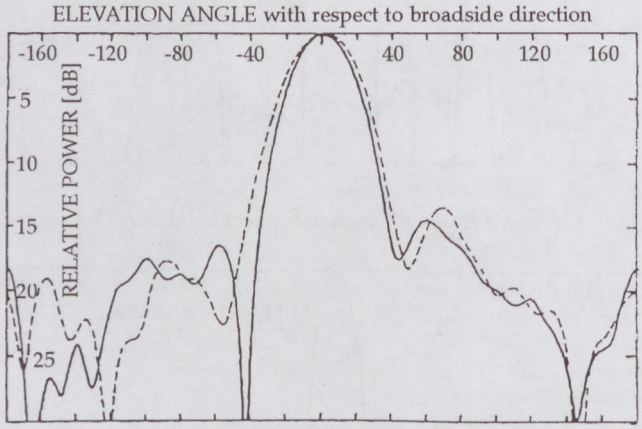

Fig. 14. Measured E-plane radiation characteristics of the four element frequency agile MSA (Fig. 2.), at the frequency of $f_{\min}$ (dotted line, varactor bias: $+0.4$ V) and $f_{\max}$ (varactor bias: -16 V).

Measured large signal effect is shown in *Fig. 15.* The largest measuring signal level is $+3$ dBm, the measured relative frequency shift is -0.75 %, input return loss is 11.2 dB ($VSWR = r = 1.7$). At the input power of -10 dBm, the measured return loss is 15.7 dB ($r = 1.4$).

The measured gain versus relative frequency difference of the 4-element FAMSA-array is shown in *Fig. 16.*

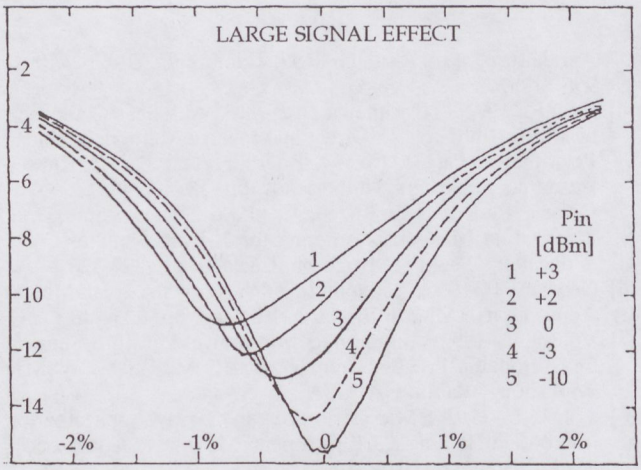

Fig. 15. Measured large signal effect for the FAMSA-array

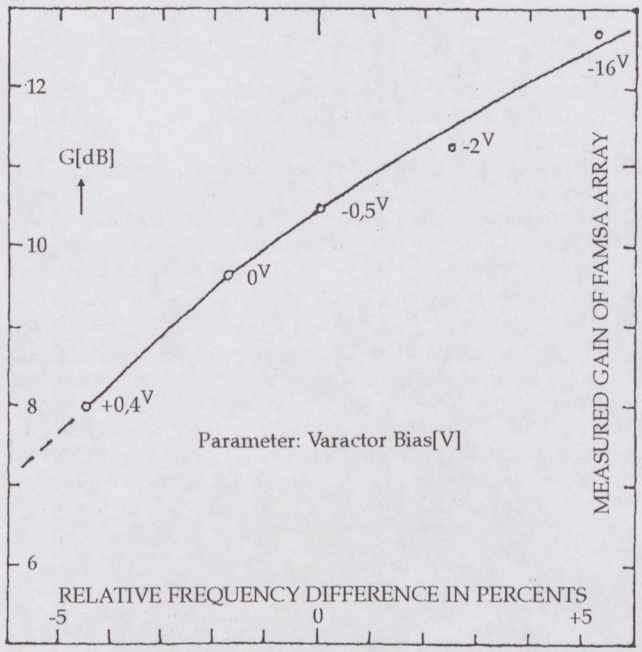

Fig. 16. Measured gain versus relative frequency difference characteristic of the 4-element FAMSA-array

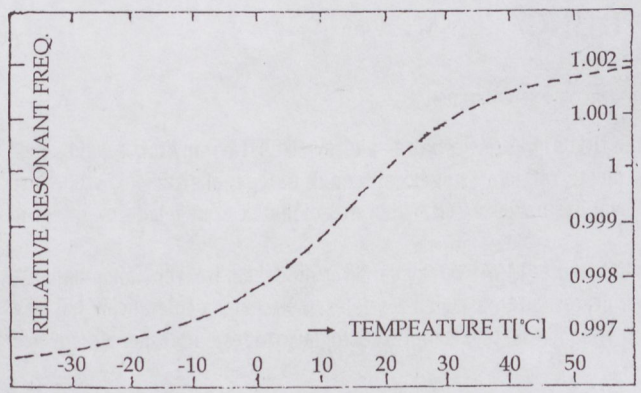

Fig. 17. Measured change in resonant frequency versus temperature of the passive MSA-array (without varactors)

4.1. Temperature dependence

Preliminary considerations:

1) At the temperature test of our passive MSA-array (without varactors) the change in resonant frequency versus temperature we have got (from *Fig. 17*): +117 ppm/C° at the temperature range of −14 . . . +46°C, and +55 ppm/C° at the temperature range of −40 . . .+60°C. The nonlinearity of the curve is due to the nonlinear permittivity-temperature function, which is a typical behaviour of PTFE (Teflon) substrates near 20°C.
2) Making a special varactor diode measuring coaxial holder (with characteristic impedance of 10 Ohms) we measured the capacitance change versus ambient temperature for different types of varactors. The measured temperature coefficients were typically between +130 and +250 ppm/C°, at the reverse bias of 1 Volt. Using these varactors in the FAMSA-array, the resonant frequency versus capacitance change will be: −0.5 dC/C, that means: −65 . . . − 125 ppm/C°, compensating mostly the frequency shift of the passive array.

5. CONCLUSIONS

The first part of this work has outlined the development of a dual (linear) polarized MSA-array used in a two-way microwave communications system at two frequencies (relative difference is only 5 %) using orthogonal polarization. Better than 45 dB decoupling was measured between MSA inputs. This design seems to be an optimal solution: using very simple construction of the isolated monolithic arrays, and eliminating diplexers.

The four-element frequency agile test-array (varactor tuned MSA) has shown an Electronic Tuning Range (relative resonant frequency shift with bias voltage) of 10 % using rectangular radiating elements having a relative instantaneous bandwidth of only 1.5 %. We expect so the price of this antenna has a minimum, because of: thin substrate and only a single varactor diode was used in each radiating element and the total array has only single DC-bias point and contains identical varactors. This solution may be applied to GaAs-MMIC realization.

In these experiments students were also involved. The modular design concept can be well exploited in the education and in the laboratory practice of students.

6. ACKNOWLEDGEMENTS

The author wishes to acknowledge his colleague: Mr. Mernyei F., who contributed to the design of the DPMSA-array. The author also would like to thank Dr. Novák, I., for technical discussions, and to the next fellow and graduate students: Porcsin, T., for making the calculations of capacitance match tolerances of FAMSA-array, to Mustapha A. Agha, Nizar Ali Barakeh and Isam M. Osman A. El Amin (in Abu Dhabi) for their invaluable assistance in the laboratory measurements at the Technical University of Budapest.

REFERENCES

[1] James, J. R. and Henderson, A., 1982: "A critical review of planar millimeter wave antennas for military applications", MM'82 Military Microwave Conference, London, UK, pp. 487-492.

[2] Petersson, R. N. O., 1992: "Antennas for Space Scatterometers and SAR's", MM'92, Brighton, UK, pp. 249-252.

[3] Shafai, L., 1992: "Antenna Candidates for Mobile Satellite Communication", MM'92, Brighton, UK, pp. 255-260.

[4] Gibson, P. J., 1986: "A large common aperture 4-beam printed antenna at Ka-band", MM'86, Brighton, England, pp. 152-157.

[5] Völgyi, F., 1990: "Flying Decibels – Extremely Lightweight Microstrip Antennas", ICOMM'90 Int. Conf. on Millimeter Wave and Microwave, Defense Electronic Applications Laboratory, Dehradun, India, pp. 343-348.

[6] Mernyei, F. and Völgyi, F. 1990: "Planar Antenna Array for Airborne Radiometer Applications" ICOMM'90 Int. Conf. on Millimeter Wave and Microwave, Defense Electronic Applications Laboratory, Dehradun, India, pp. 393-396.

[7] Völgyi, F., 1987: "High Efficiency Microstrip Antenna Array", 17th European Microwave Conference, Rome, Italy, pp. 747-752.

[8] Nizar N. M. Suleiman, 1990: "Design of microstrip phased array antennas" (Final Project for M. Sc. degree, Supervisor: Völgyi, F.), Tech. Univ. of Budapest, Dept. of Microwave Telecomm.

[9] Patel, M. and Thraves, J., 1994: "Design and development of a low cost, electrically steerable, X-band reflect array using planar dipoles", M'94 Microwaves Conf., London, UK, pp. 174-179.

[10] Bhartia, P. and Bahl, I. J., 1962, Microwave Journal, 25 pp. 67-70.

[11] Waterhouse, R. B., 1993, IEEE Microwave and Guided Wave Letters, 3, 12, pp. 450-452.

[12] Purchine, M. P. et al., 1993: "A Tuneable L-band Circular Microstrip Patch Antenna", Microwave Journal, October 1993, pp. 80-88.

[13] Mihály, S. and Bozsóki, I., 1988: "X-band Scatterometry in Agriculture", Proc. of IGARSS, Edinburgh, UK, pp. 991-996.

[14] Itoh, K., 1992: "Polarimetric Integrated Antennas Composed of Microstrip Patches", Direct and Inverse Methods in Radar Polarimetry, Part 2, (W. M. Boerner et al. eds.), Kluwer Academic Publishers, Netherlands, pp. 1335-1348.

[15] Owens, R. P. and Smith, A. C., 1986: "Dual Band, Dual Polarization Microstrip Antenna for X-band Satellite Communications", MM'86, Brighton, England, pp. 323-328.

[16] Newham, P., 1986: "Monolithic Patch Array for Small Missile Applications", MM'86 Brighton, England, pp. 335-340.

[17] Völgyi, F., 1993: "Integrated Microwave Moisture Sensors for Automatic Process Control", IEEE MTT-S'93, WSMJ-Workshop, Atlanta, GA, USA, pp. 39-44.

[18] Völgyi, F., 1993: "Microstrip Antenna Array Applicator for Microwave Heating",23rd European Microwave Conference, Madrid, Spain, pp. 412-415.

[19] Völgyi, F. and Mernyei, F.,1987: "Dual Polarized Tx/Rx Microstrip Antenna", Know-How Documentation (in Hungarian), Tech. Univ. of Budapest, Dept. of Microwave Telecomm.

[20] Bhattacharjee, A. K. et al., 1993, IEE Proceedings, Vol. 135, Pt. H, No. 5, pp. 351-352.

[21] Völgyi, F., 1975: "Parametric Amplifiers on Plastic Substrates", XX. International Coll., TH-Ilmenau, Germany, pp. 119-122.

[22] Hapgood, D. W., 1981, Microwave Journal, November 1981, pp. 83-90.

[23] Mustapha A. Agha, 1994: "Design of a frequency agile microstrip antenna array", (Final Project for B. Sc. degree, Supervisor: Völgyi, F.), Tech. Univ. of Budapest, Dept. of Microwave Telecomm.

[24] Mernyei, F. and Völgyi, F., 1990: "Simple Methods for Testing the Temperature Dependence of Microstrip Antenna Array" 20th European Microwave Conference, Budapest, Hungary, pp. 365-370.

[25] Völgyi, F., 1995: "Upper S-band Microstrip Antennas with Polarization Diversity and Frequency Agility" MILCON'95 Int. Defence Conference, Abu Dhabi, United Arab Emirates, Proc. pp. 200-207.

POLARIZÁCIÓ- ÉS GYORS FREKVENCIAVÁLTÁSRA ALKALMAS NYOMTATOTT ANTENNÁK

VÖLGYI FERENC

BUDAPESTI MŰSZAKI EGYETEM
MIKROHULLÁMÚ HÍRADÁSTECHNIKA TANSZÉK
TEL.: 36 1 463 1559; FAX: 36 1 463 3289; T-VOLGYI@NOV.MHT.BME.HU

Különösen az elektronikus hadviselés rendszereinél (radarok, rakétairányítók, a titkos hírközlés eszközei, pilóta nélküli, távirányított repülőgépek, zavarszórók stb.) jelentős előny az, ha a nagyfrekvenciák kisugárzására, illetve vételére szolgáló antennák az egypolarizációjú, szélessávú működéssel ellentétben mindig az éppen aktuális frekvencián és polarizációval üzemelnek. Célszerűen megoldhatók ezen feladatok integrált nyomtatott antennákkal (MSA).

Két független bemenettel rendelkező, kettős lineáris polarizációjú, 2×32 elemes MSA, és egy varaktor diódákkal frekvenciában hangolt, 4-elemes nyomtatott antenna konstrukciójának és áramköri modelljének bemutatása után a szerző részletesen vizsgálja a toleranciák hatását, a nagyjelű működést, a hőfokfüggést és a nyereség frekvenciafüggését. Ezen vizsgálatokat a kísérletekkel foglalkozó rész mérési eredményeivel támasztja alá.

Érdekes, és a gyakorlatban jól használható eredmény az, hogy a dielektromos hordozó és a hangoló varaktorok ellentétes hőmérsékletfüggése miatt a rezonancia frekvencia megváltozásában részleges kompenzáció lehetséges. Későbbi vizsgálataink azt is megmutatták, hogy nagy elemszámú felületi antennáknál a Monte-Carlo módszerrel kisorsolt kapacitású (± 10 % tolerancián belüli) diódákat használva, az iránykarakterisztika eltérései elhanyagolhatók, sőt az antennarendszer adott számú dióda meghibásodását (rövidzár vagy szakadás) gyakorlatilag „nem veszi észre".

A MICROWAVE MONITORING SYSTEM USED FOR PREDICTION OF THE QUALITY OF PARTICLEBOARDS*

FERENC VÖLGYI

TECHNICAL UNIVERSITY OF BUDAPEST
DEPT. OF MICROWAVE TELECOMMUNICATIONS
H-1111, BUDAPEST, GOLDMANN TÉR 3, HUNGARY
PHONE: 36 1 463 1559; FAX: 36 1 463 3289; T-VOLGYI@NOV.MHT.BME.HU

After introducing some possibilities of microwave moisture measurements, a non-destructive testing method of particleboards is shown, which is based on a microwave free-space (double transmission) reflection type two-parameter complex vector measurement. Using this basic idea, a 5.8 GHz monitoring system (*Fig. 1* in colours*) was developed, which is used for moisture content measurement and quality forecast of particleboards continuously, before mechanical testing would be accomplished. Recalling some basic equations, the calculation of dry wood basic weight, complex permittivity values, absolute moisture content and mechanical properties of composite boards, also are shown. Low cost MMICs, self-designed microstrip antennas and passive detector/backscatterers are used in the instrumentation for the realization of the concept, mentioned above. This paper summarises the phases of this development, giving some useful ideas about the instrument itself. Laboratory experiments and the results of on-line real-time industrial measurements are presented.
Keywords: particleboard, quality control, microwave aquametry, modulated backscatterer, microwave sensor.

1. INTRODUCTION

1.1. Microwave Aquametry

It is essential to insert control points into modern automated manufacturing processes to ensure homogeneous product quality. Particleboard manufacturing also needs a reliable control method that is able to monitor large-size composite boards continuously. Economic benefits from real-time, on-line determination of bulk moisture content (MC) in agricultural commodities, processed foods, manufactured wood products, minerals, polymers and many other products are exceptional. Such information is useful for determining the value of raw materials, for front-end processing, for in-process control and for output quality control [1]. Microwave moisture measurements exhibit the advantages of a nondestructive measurement with high accuracy, small influence of ionic conductivity, and automatic process control within severe environmental industrial conditions. Disturbances, such as bulk density, material grain size, and ionic conductivity, can be reduced by suitable data processing and choice of measuring frequency. The application of this technique for civil engineering was introduced by Kupfer [2]. Density independent moisture measurement methods are summarized by Kupfer [9].

The paper [3] reports the experience gained from the use of arrays of microwave sensors in different areas of applications: paper, wood, plaster composite, technical textiles, rock and glass wool, etc. The modulated scattering technique (MST) was introduced to provide an interesting technical solution, when significant speed and spatial resolution are required. Typically, an MST sensor consists of two parts: the retina, which is an array of small dipoles loaded by PIN diodes, and the collector, which collects the modulated perturbation resulting from the modulation of a given diode. An X-band linear sensor was mentioned which consists of an array of 128 probes spaced by 8 mm, and extending over about 1 meter.

The development of *microwave methods for composition analysis* from its early stages to the present state is covered by Kent [4]. For the most part this has meant the determination of water content, but it is shown that later work has attempted to measure or eliminate other variables such as temperature, density, other compositional variables or even different kinds of treatment. It was shown that for particulate materials there is a strong dependence of the dielectric properties on bulk density. This is understood if one considers each particle as a non-interacting absorber, then it is obvious that increasing the number of these absorbers per unit volume will increase the power absorbed proportionally. We have used these ideas in calculations.

Single-frequency and *frequency swept two-parameter* (e.g. attenuation A and phase Φ) measurements are well known in microwave bands. Proper processing of a suitable two- parameter measurement can led to density-independent moisture measurement, but also to *moisture independent density measurement* [5]. The commonly used functions are $A/\Phi = \varepsilon' - 1)$ or $\sqrt{\varepsilon''}(\sqrt{\varepsilon'}+1)/(\varepsilon'-1)$. Our experiments also showed the usefulness of these types of equations.

There are applications where the detection and quantification of *transverse moisture gradients* is necessary. Multiple electrodes can be used for detection of commonly encountered moisture gradient, near-surface regain and steep drying of timber, as described by Jazayeri and Ahmet [6]. Most modern moisture meters use digitally controlled instrumentation and *digital signal processing* afterwards. Daschner et al. [7] discussed various digital

* This is an extend of the paper presented by F. Völgyi at SSTA Conf. in Denver, Colorado, USA, in July 20, 1999. A version of this article also appeared at [22].

signal processing algorithms with respect to measurement speed, accuracy, speed of data processing, numerical stability, and hardware effort with a resonator-based 2.45 GHz moisture meter.

Lasri et al. [8] presented a low cost, 2.45 GHz moisture measurement system, using *free space technique*, which was applied for the control of sand and cellular concrete. The modeling of the reflection coefficient of the metal-backed material associated with the theory of dielectric mixtures allows the determination of the MC of the sample under test. In the *realization of our instrument* [10], some of the above mentioned ideas were used, in alternative ways: the free-space technique [11], digital signal processing [13], modulated scattering technique [14], composition analysis [15], application of microstrip antennas [17], microwave aquametry [18], multi-frequency measurements [19] etc.

1.2. Particleboard Technology

Particleboards are manufactured by heat pressing ($\sim$ 20 kp/cm^2, $\sim$ 2 min, $\sim$ 200°C), wood particles of various kinds and size (*Figs. 2* and *3* in colours*), mixed with webbing resin glue (e.g. urea-formaldehyde). The compression due to pressure is $\sim$ 20 %, the moisture content after pressing is $\sim$ 4 %, and the content of air remaining in the board is $\sim$ 5 %. The most frequently occurring 19 mm thick board contains $\sim$ 9 % glue (see *Table 1*). The tensile and bending strength (Modulus of Elasticity: MOE) decrease approximately with the square of increasing moisture content. In contrast, an increase of the resin glue by 5 % (referred to the nominal value) yields a strength increase of 10−15 %. The Modulus of Rupture (MOR) increases proportionally to glue content.

The kind of wood has a decisive impact on the strength (see *Table 2*). With equal board volume weight, at first glance surprisingly, the 1:3 rated strength order is beech, acacia, birch, pine, and poplar. By increasing the surface density (in addition to the volume density), the strength can be significantly increased. According to our measurements, the microwave parameters have a relationship first of all with these densities.

Table 1. Components of particleboard

Substance	ρ (g/cm^3)	ε'	ε''	tgδ	m/m %	v/v %	Eq. (8)	Eq. (9)
Wood particles	0.6361	1.668	0.0406	0.024	88	89.92	0.924	271.6
Glue: Urea-formaldehyde	1.29	4.5	0.056	0.012	9	4.53	2.751	3906
Water	1	70	21.7	0.310	3	1.96	0.670	10.1
Air	0	1	0	0	0	3.59	−−	−−
Mixture	0.65	2.1137	0.1213	0.0574	100	100	0.840	94.5

Table 2. Components of wood particle mixture

Type of wood	ρ (g/cm^3)	ε'	ε''	tgδ	m/m %	v/v %	Eq. (8)	Eq. (9)
Poplar	0.38	1.45	0.026	0.018	35	41.0	0.818	299.6
Pine/fir	0.45	1.80	0.050	0.028	50	49.5	0.968	256.0
Beech	0.68	1.95	0.059	0.030	11	7.2	1.027	259.3
Acacia	0.77	2.10	0.067	0.032	4	2.3	1.084	269.5
Mixture of wood particles	0.4453	1.668	0.0406	0.024	100	100	0.924	271.6

1.3. Quality Problems in Production

Recent international standards (e.g., ISO-9002) require the continuous control of manufacturing environment and quality of products. Until recently the mechanical properties (MOE, MOR) and physical properties (MC, swelling) of particleboards (PB) (see *Fig. 4* in colours*) were assessed by destructive standardised experiments on specimens taken from the boards every hour. Visual control is also applied, as shown in *Fig. 5* (in colours*). There is no information about the quality of the boards between two successive measurements. A continuous production line, in spite of the severe control of the constituents and the process, might produce substantial amounts of lower grade particleboards within that hour. These boards are downgraded or rechipped again, causing a significant deficit to the company annually. The solution is the continuous quality monitoring of the boards by a nondestructive method. We have developed a microwave monitoring system (see *Fig. 1* in colours* and *Fig. 6*), which is used for moisture measurement, and quality forecast of particleboards continuously, before mechanical testings are applied periodically.

1.4. Phases of this Development

Using our basic idea ([10], patent pending), first of all we have created a basic measurement setup shown in *Fig. 1* for the purpose of laboratory experiments. More details are given in [11]. Because the measured attenuation (ΔA) and phase shift ($\Delta\Phi$) mainly depends on the moisture content of PB, this setup is excellent for microwave aquametry [12].

In the next phase an industrial version of our equipment was realized and tested. Some cases high power RF-dryers are used in PB-production, the application of spread spectrum technique [13] was profitable. Measurements were accomplished to select the appropriate BPSK-code for the modulated backscatterers [14].

Using a simple dielectric mixing model some calculations and diagrams were presented [15] about the effect of glue-overdose and quality degrading air-inclusions formed during pressing of the board. The developed microwave monitoring system is also applicable for plastic-sheets and RF-absorbers [16].

2. MEASUREMENT SET-UP

2.1. Basic Set-up

The basic measurement set-up using a new application of WLAN-concept is shown in *Fig. 1* (Hungarian patent pending [10]). This is a *free-space, reflection/double transmission system*, in which the attenuation (ΔA) and phase ($\Delta\Phi$) is measured by the receiver.

The *microwave transmitter* (TX), which is working in one of the industrial-scientific-medical (ISM) frequency bands, radiates continuous wave (CW) during the measurement. After passing through the measured moist substance, this wave is reflected by one of the passive detector/backscatters (PDBs). At the Microwave Receiver (RX) the signal is converted to IF stage and then sampled by the DSP unit, which makes the code correlation and from the correlated signal the two parameters (attenuation – ΔA; phase shift – $\Delta\Phi$) can be measured, and from the measured data the relative complex permittivity ($\varepsilon^* = \varepsilon' - j\varepsilon''$), moisture content (MC), wet and dry densities, etc. can be calculated.

The *PDBs, having individual codes*, are interrogated (Downlink) successively (in time share mode) by the transmitter using on-off keying (OOK) modulation. The matched detector of PDB demodulates the signal and transfers the data the to the digital circuits of PDB. The radar cross section (RCS or σ) of the PDB is changed by a frequency shift keying (FSK) encoder and switch driver (10.7 MHz) so that the backscattered (Uplink) signal from the PDB is *binary-phase-shift-keying (BPSK) modulated* and ultimately detected by the receiver antenna of the fixed station (FXS). The PDBs can be cheap units, having minimal size and number of components; and can be reconfigured for a different setup (number of measurement points). The distance (D) between the matchbox-like PDBs may be small, without perturbing each other, because only one is activated in a given time-slot, the others are passive and matched. The measure of the irradiated common volume (V), from which the information is gained, depends on the distance (D) and depends on the radiation pattern of PDB.

In some simpler configurations the FSK encoders and switch drivers are eliminated. The PDBs answer in a time division multiplexing mode to the interrogating waves, and produce a modulated backscattered signal with an extended spectrum. In the receiver, the unique code, which originates from the backscatter units, is decoded and therefore a high signal-to-clutter ratio can be achieved.

Both the TX, RX antennas and PDB units are self-developed. More information of the se can be found in [11]. *Circularly polarized microstrip antennas* are used in the system, eliminating the disturbing effects of the reflected waves from the air-slab interface. The circular polarization of a wave reflected from an odd-bounce reflector surface is opposite from that of the incident wave (for example, RHCP incident wave yields LHCP reflected wave and vice versa), thereby the odd-bounce reflected waves will not appear at the receiver in *Fig. 1*, and the reflected wave from the bottom side of the slab will not appear at the PDB. The *Tx/Rx antennas have shaped-beam radiation patterns*. At the measurement of traveling board, sufficient to irradiate only the array of PDBs, using a fan-beam. Broad-beams are used in the case of stopping slabs, when many PDBs are taken on the area under slabs.

The *personal computer (PC)* of the measurement system is in a common network (Ethernet) with other computers, and the data communication between fix stations and PC is transferred by the measurement control (MCT) unit in *Fig. 1*.

The calibration of the computer controlled complex permittivity monitoring system is executed without moist substance, or using standard slabs with different moisture content and quality.

2.2. Block Diagram

The block diagram in *Fig. 6* shows the experimental system for laboratory measurements, for the sake of simplicity, with only one PDB [13]. The above mentioned RF, IF and digital stages can be clearly seen on it. The first IF stage operates on 280 MHz, which will be upconverted to the second IF stage at 2.45 GHz and finally to the RF stage, 5.8 GHz (the first and second IF frequencies correspond to a commercial spread-spectrum chipset). Digital sampling is done at the output of the I/Q receiver, on both channels. Digitized data are then processed by the host computer, which also controls the measurement (code for PDBs, output switching, etc.). After signal processing, measurement parameters can be read from the screen (e.g., in complex vector format) or saved continuously or manually in files for later data processing. In the industrial setup however, the signal processing/controlling and the display functions will be separated: the mini-computer doing signal preprocessing and controlling will be housed in the instrument box shown at the top of the measurement setup, while the display computer with a user-friendly interface is placed a few ten of meters away from the measurement site. Of course calibration is needed for the whole system, which can be done using known samples and a setup without the measured board.

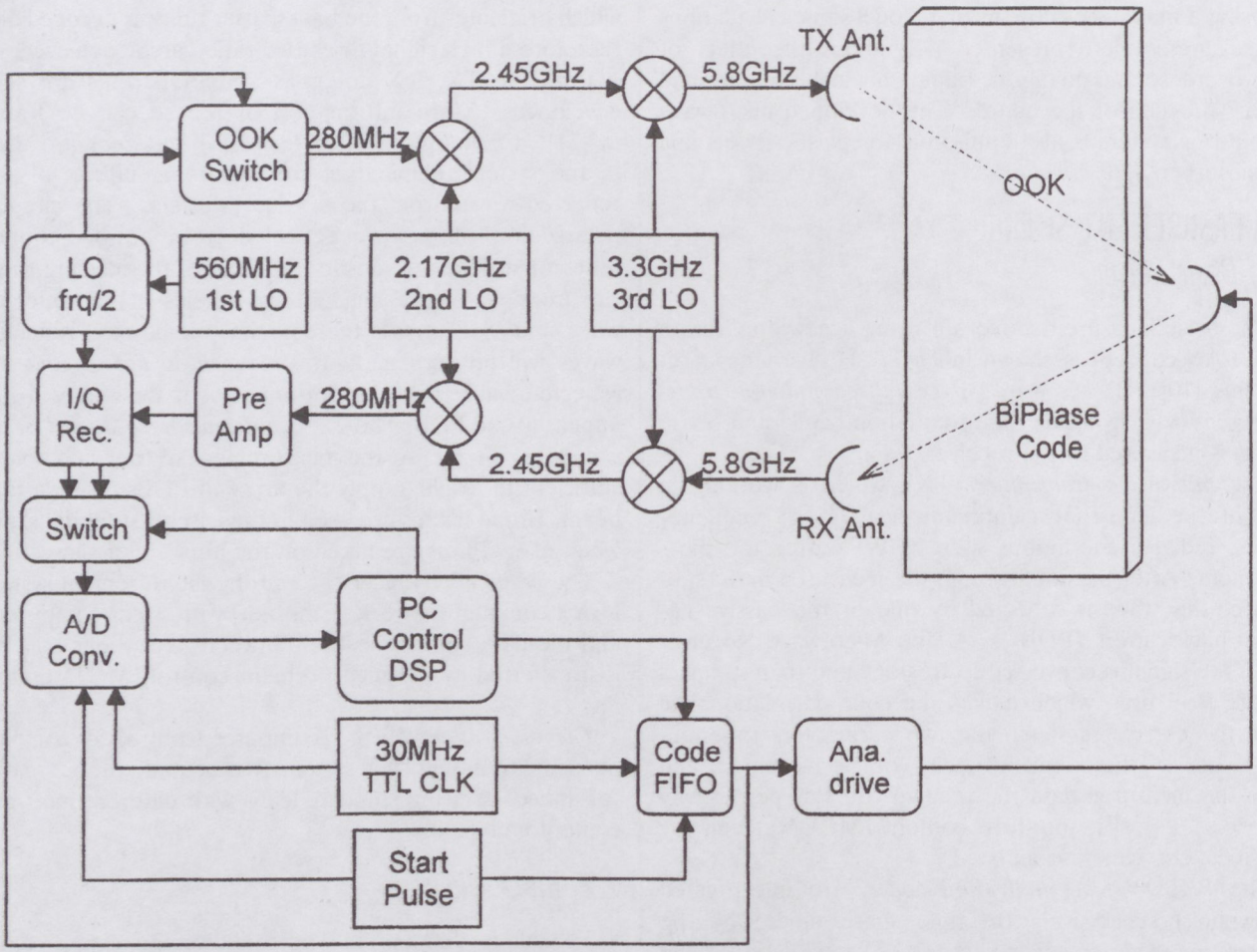

Fig. 6. Block diagram of microwave monitoring system.

3. CALCULATIONS

3.1. Complex Permittivity

The following equations were applied to calculate the ratio of substances in the mixture:
mass ratio:

$$m_i = \frac{v_i \rho_i}{\sum_i v_i \rho_i} \tag{1}$$

volumetric ratio:

$$v_i = \frac{m_i \rho_i}{\sum_i m_i \rho_i} = (m_i/\rho_i)\rho_r \tag{2}$$

densities:

$$\rho_i = \frac{m_i}{v_i}\rho_r \tag{3}$$

$$\rho_r = \frac{1}{\sum_i m_i/\rho_i} = \sum_i v_i \rho_i \tag{4}$$

where m_i, v_i, and ρ_i are the relative mass, relative volume, and fractional density of the i^{th} component, respectively, and ρ_r is the density, resulting for the mixture.

The Index of Refraction Mixing Model (IRMM) was used (see [12] pp. 123-140.), because this gives the best approximation at low moisture range:

$$\varepsilon_{\text{eff}}^{\frac{1}{2}} = \sum_{i=1}^{n} v_i \varepsilon_i^{\frac{1}{2}}. \tag{5}$$

The attenuation and phase shift of a particleboard of a thickness of T (= 19 mm in this example)

$$\Delta A = 273 \frac{2T}{\lambda_0} \frac{\varepsilon''}{\sqrt{\varepsilon'}} \text{ [dB]}, \tag{6}$$

$$\Delta\phi = (\sqrt{\varepsilon'} - 1)\frac{2T}{\lambda_0} \cdot 360°. \tag{7}$$

With hadbook data for 5.8 GHz, specified particleboard components (50 % pine, 35 % poplar, 15 % beech)at customary technology parameters, assuming 2 % air volume ratio, and 5 % volume ratio of water, we have calculated 3.3 dB for the attenuation of microwaves, which practically does not depend on the amount of glue. The desirable measurement accuracy is $\sim$ 0.2 dB. The phase change is cca. 180°. The measurement accuracy necessary for indication of glue is $\sim 2°$.

The two so-called density-independent functions were also calculated:

$$\frac{\sqrt[3]{\varepsilon'} - 1}{\sqrt{\varepsilon''}}, \tag{8}$$

$$\left(\frac{\varepsilon' - 1}{\varepsilon''}\right)^2, \tag{9}$$

which correlate well with the mechanical properties (Modulus of Elasticity) of the material (so these functions will be referred to [15] hence as MOE1 and MOE2). *Tables 1* and *2* also contain the densities, complex dielectric constants and the volume ratios obtained. The mass ratios were given by the particleboard manufacturer. All calculations were made by a self-designed program [21] under MATLAB (MathWorks, Inc.). *Figs. 7–9* present the effect of changing in MC, amount of glue and air volumetric ratio.

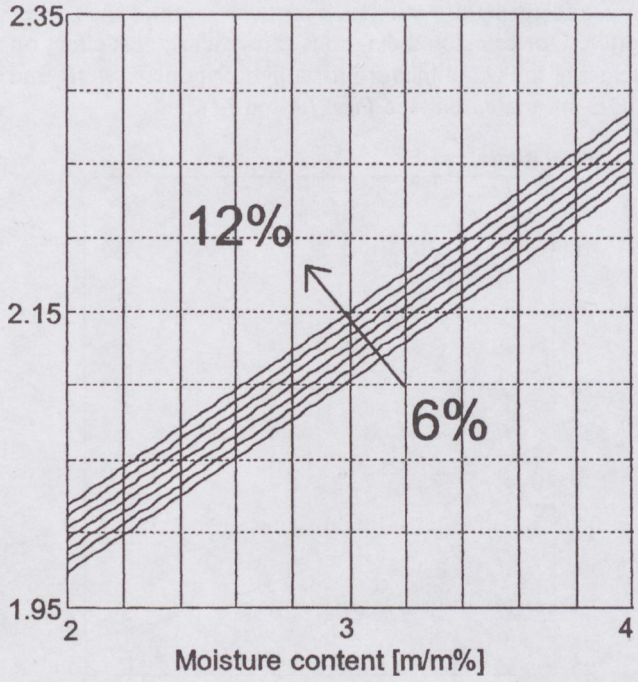

Fig. 7. ε' versus MC. Amount of glue changes between 6 % and 12 % in 1 % steps.

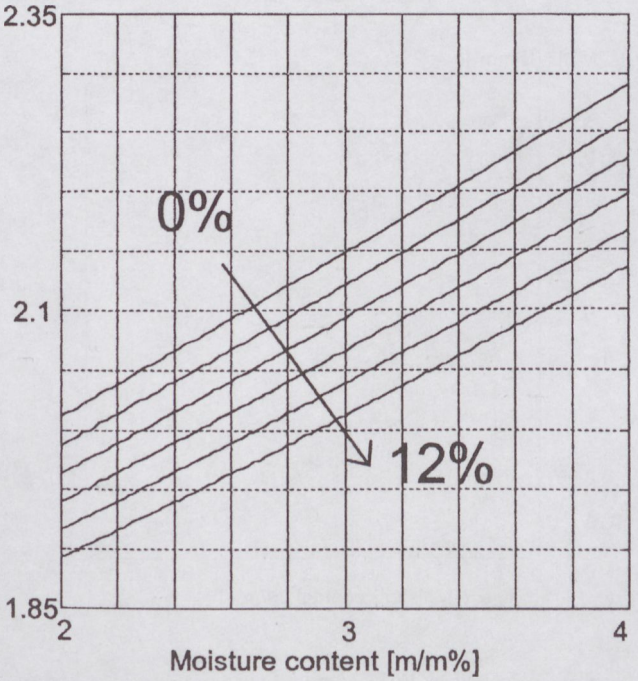

Fig. 8. ε' versus MC. Volumetric ratio of air changes 0 % and 12 % in 2 % steps.

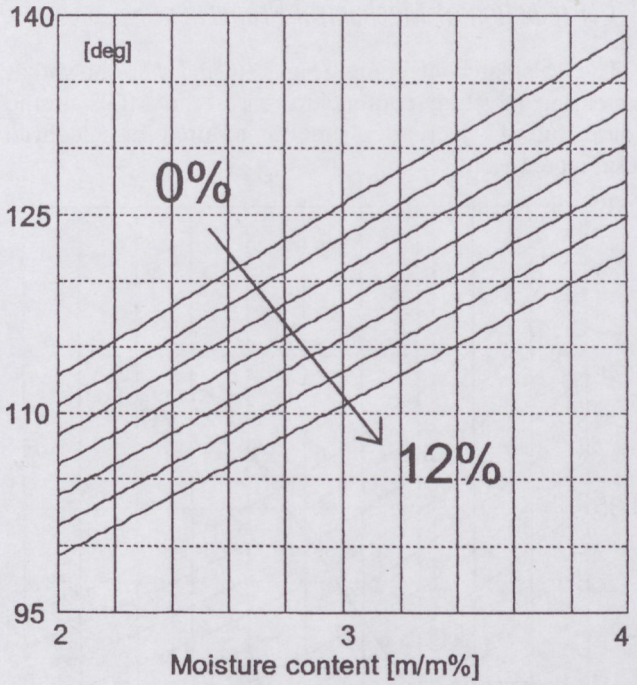

Fig. 9. $\Delta\Phi$ versus MC. Volumetric ratio of air changes 0 % and 12 % in 2 % steps.

During pressing the density of wood particles will pack by 20–40 %. Taking 30 %, the density of the mixture of wood particles increases by a factor of 1/0.7. This value is included in *Table 1*.

3.2. Moisture Content

As was mentioned in [1] (and earlier work of by King), both the insertion loss (ΔA) and phase ($\Delta\Phi$) are highly linear with the mass of the wood and of the moisture through which the electromagnetic waves must propagate:

$$\Delta A = a_1 m_d + a_2 m_w \tag{10}$$

$$\Delta\Phi = a_3 m_d + a_4 m_w, \tag{11}$$

where a_{1-4} are calibration constants, m_d is the dry wood basis weight [g/cm^2] and m_w is the basis weight of the contained water. From measured values, the absolute (dry basis) fractional moisture content MC, and m_d, m_w are:

$$MC = \frac{m_w}{m_d} = \frac{a_3\Delta A - a_1\Delta\Phi}{a_2\Delta\Phi - a_4\Delta A} \tag{12}$$

$$m_d = \frac{a_4\Delta A - a_2\Delta\Phi}{a_1 a_4 - a_2 a_3} \tag{13}$$

$$m_w = \frac{a_3\Delta A - a_1\Delta\Phi}{a_2 a_3 - a_1 a_4}. \tag{14}$$

In good agreement with our experiments, for $m_d = 1.169$ g/cm^2 and $m_w = 0.047$ g/cm^2; $a_1 = 1.1$, $a_2 = 25$, $a_3 = 93$, $a_4 = 500$ were used in our calculations, giving $MC = 4$ %, $\Delta A = 2.5$ dB, and $\Delta A = 132°$. Because of the noticeable breakpoint in ΔA at about $MC = 6$ %, two piecewise linear models are used in practice. From the measured temperature (t) dependencies of ΔA and $\Delta\Phi$, the calibration constants a1 and a3 are linear with t, whereas a2 and a4 have definite quadratic behaviours, in the temperature range of $25°\text{C} < t < 100°\text{C}$.

3.3. Prediction of Mechanical Properties

The calculated diagrams (*Figs. 10* and *11*) show that increasing moisture content decreases the MOE of the board, but the increasing amount of urea-formaldehyde resin increases it.

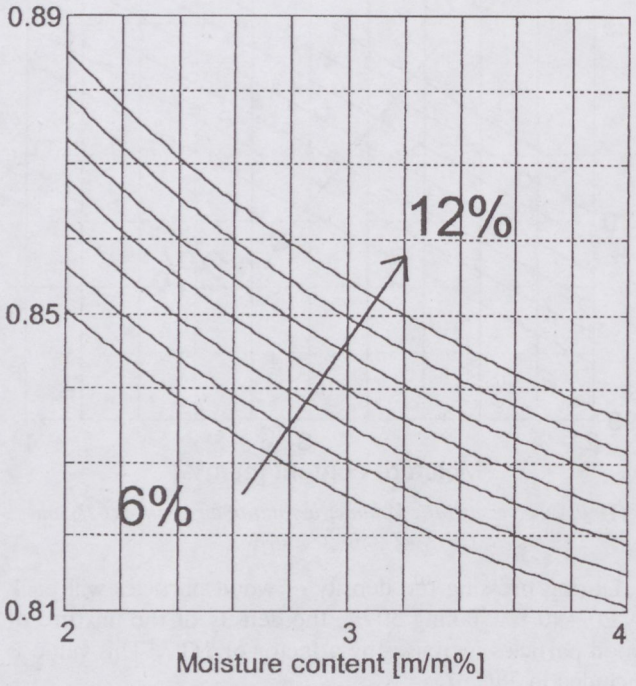

Fig. 10. $\sqrt[3]{\varepsilon'} - 1/\sqrt{\varepsilon''}$ *versus MC. Amount of glue changes between 6 % and 12 % in 1 % steps.*

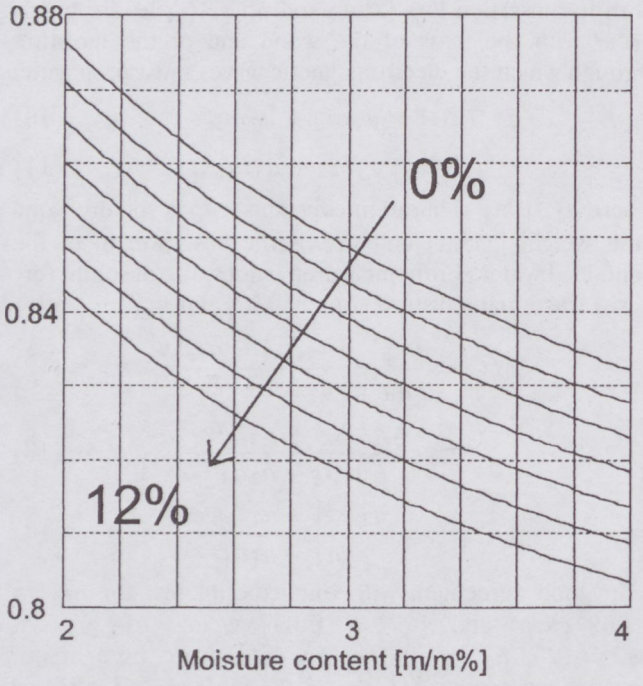

Fig. 11. $\sqrt[3]{\varepsilon'} - 1/\sqrt{\varepsilon''}$ *versus MC. Volumetric ratio of air changes 0 % and 12 % in 2 % steps.*

In industrial applications it could be important to detect fluctuations of amount of glue in the mixture. The parameters above shown seem to be suitable (except ε'' and ΔA) for this purpose. Air inclusions can also be detected well by all parameters except $(\varepsilon' - 1)/\varepsilon''$ (curves of different air volumetric ratios separate well on these diagrams). Monitoring of air volumetric ratio is also useful because boards with air inclusions may crack or explode after pressing.

3.4. Effect of Wood Mixture

For a given board density, woods of lower density give boards of higher strength, because a given weight contains more particles of a lighter wood using a higher amount of glue, and during pressure such particles contact each other better. Our calculated diagrams show clearly this effect on changing the wood mixture for a lighter poplar, MOR and MOE are increased (see *Figs. 12* and *13*).

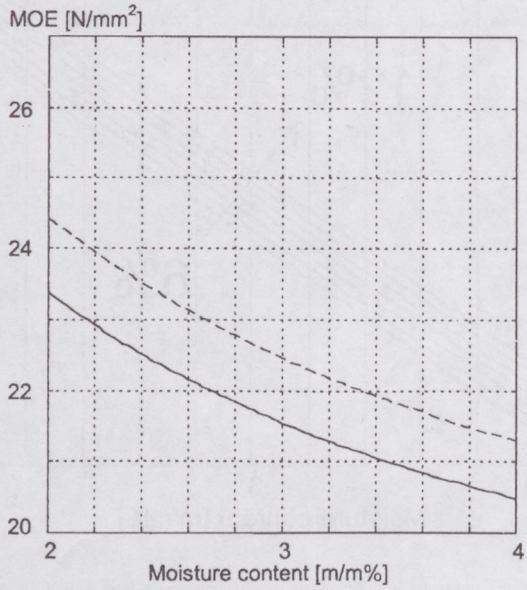

Fig. 12. Calculated MOE for standard mixture of woods and for poplar (dashed line).

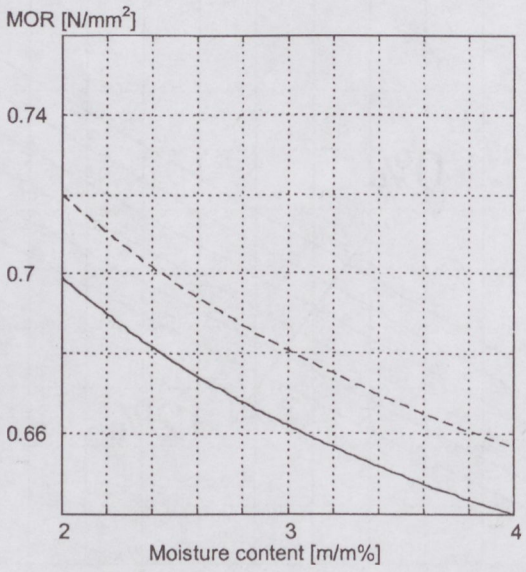

Fig. 13. Calculated MOR for standard mixture of woods and for poplar (dashed line).

3.5. Electromagnetic model and BPSK modulation

Set off the radar equation, using the designations of *Fig. 1*, the free-space attenuation is:

$$A_f = \frac{P_t}{P_r} = \frac{(4\pi)^3 R^4}{\lambda_0^2 \sigma G^2 \Gamma^2 M} \tag{15}$$

$$R = \frac{H + T + D}{\sin \vartheta}, \tag{16}$$

where P_t is the transmitted power, P_r is the received power, λ_0 is the free-space wavelength, σ is the radar cross section of the PDB, G is the gain of Tx and Rx antennas, Γ is the reflection coefficient of RF-diode circuit in PDB, M is the BPSK modulation rate. Using eq. (15), the calculated received power is $P_r = -62.2$ dBm, supposing: $H = 2$ m, $T = 2$ cm, $D = 10$ cm, $\vartheta = 60°$, $P_t = 100$ mW, $\lambda = 5.17$ cm, $\sigma = -20$ dBm^2, $G = 12$ dB, $M = -10$ dB. The received power is suitably high for good-quality signal processing.

The PDB is a non-ideal BPSK modulator, which has amplitude and phase error.

In its ON and OFF states the reflection coefficients are:

$$\Gamma_1 = |\Gamma_1| \cdot e^{j\varphi_1};\ \Gamma_2 = |\Gamma_2| \cdot e^{j\varphi_2}. \tag{17}$$

Introducing the amplitude and phase errors:

$$\Delta\Gamma = |\Gamma_1|/|\Gamma_2|; |\Gamma_1| > |\Gamma_2| \qquad \Delta\varphi = \varphi_1 - \varphi_2 + 180°. \tag{18}$$

The bit error rate for Uplink communication is:

$$\mathrm{BER} = \frac{1}{4}\left[\mathrm{erfc}\left(\sqrt{\frac{E}{N_0}}\right) + \mathrm{erfc}\left(\sqrt{\frac{E}{N_0}} \cdot \frac{1}{\Delta\Gamma \cos \Delta\varphi}\right)\right]. \tag{19}$$

It was shown that in order to maintain the signal-to-noise ratio (E/N_0) of 10.5 dB to 11 dB (then: BER $\sim 10^{-6}$) the amplitude error that can be tolerated is approximately 0.5 dB and the phase error that can be tolerated is 10°.

4. EXPERIMENTAL RESULTS

4.1. Preliminary Measurements

Before starting our development, we measured the single transmission attenuation of the 5.8 GHz signal for different values of pressure at Interspan (Vasarosnameny, Hungary). The results is shown in *Fig. 14* for a PB having dimensions of: $2.7 \times 16.5 \times 0.019$ m. Better homogeneity is obtained at higher pressure ((1) in *Figs. 14* and *15*).

4.2. Laboratory Experiments

First we created a basic measurement set-up for the purpose of laboratory experiments. The effects of incident angle of microwaves, moisture content, edge effect of PB, etc., were tested. *Fig. 16* shows the set-up for an oblique incident angle, where α and y parameters were changed [21]. The measured phase shift versus y is shown in *Fig. 17.*

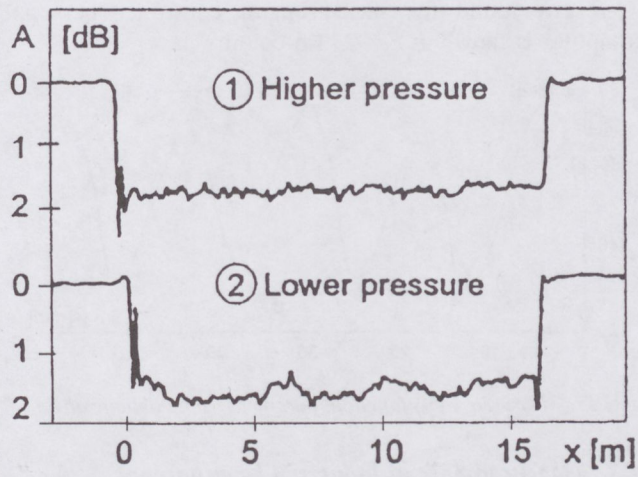

Fig. 14. Measured single transmission attenuation at two values of pressure versus position.

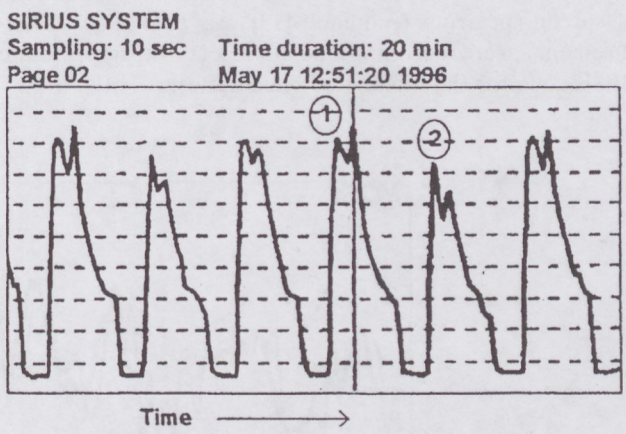

Fig. 15. Pressure-time diagram for continuous production of PBs ($p_1 = 350$ bar; $p_2 = 300$ bar).

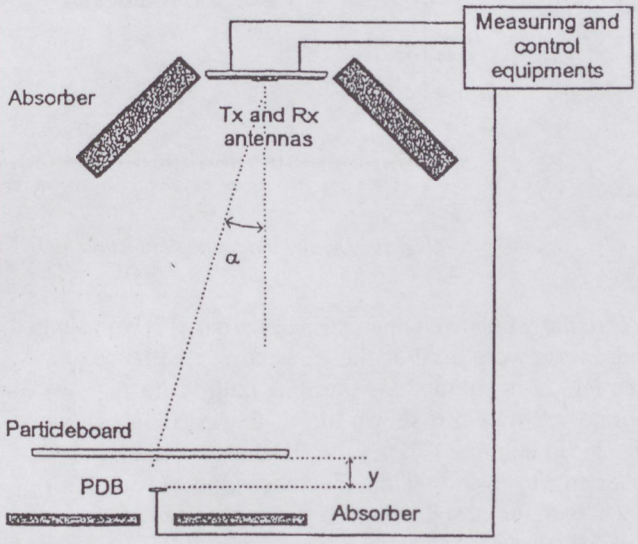

Fig. 16. Measurement setup for laboratory experiments.

After these experiments, we rearranged our set-up in a factory-like form. This is shown in *Fig. 22* (in colours*) where half of the backscatterer array is taken below. The low-frequency part of the set-up (IF and digital stages,

IQ-receiver) and the measurement controller personal computer is shown in *Fig. 23* (in colours*).

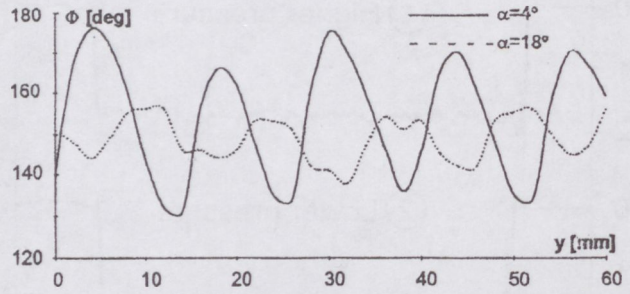

Fig. 17. Measured $\Phi(y)$ function; parameter is the oblique angle α

4.3. Measurements in Industrial Environment

In the next phase, an industrial version of our equipment was realized and tested. In some cases high power RF dryers are used in PB production, and the application of spread spectrum technique [13] was profitable. Measurements were accomplished to select the appropriate BPSK-code for the modulated backscatterers [14].

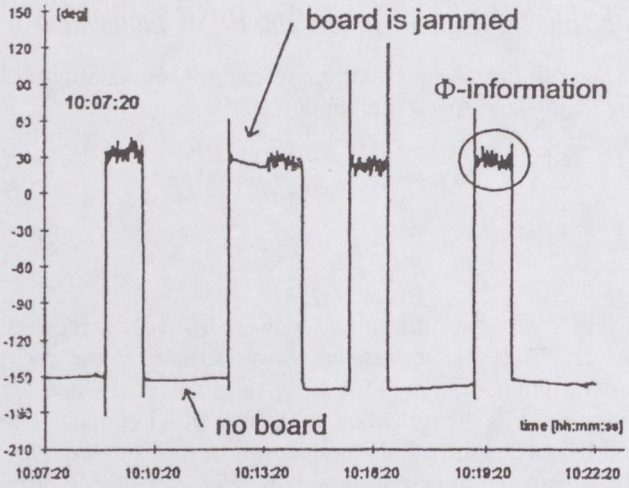

Fig. 18. Continuous phase measurement. Time duration is 15 min.

The result of continuous $\Phi(t)$ measurement is shown in *Fig. 18*. At the time of 10:13:20 the board was jammed in milling machine. This figure shows, that our instrument is applicable for the monitoring of PB production. *Fig. 19* shows the MOE1 versus longitudinal position function of a board.

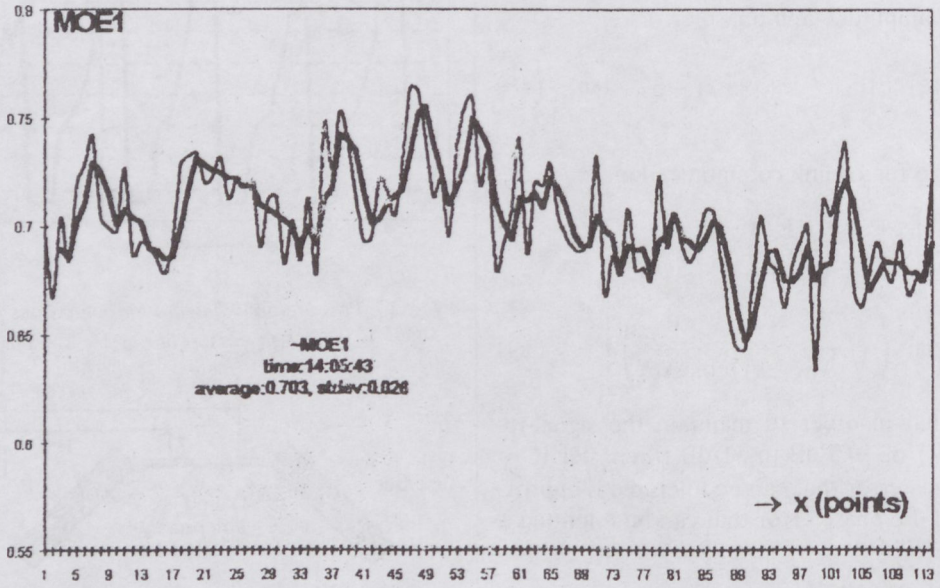

Fig. 19. Density-independent function MOE1 versus longitudinal position x for board No. 40.

Circularly polarized microstrip antennas [17] with shaped beam form were used at the transmitter and receiver side (see *Fig. 24* in colours*). Mounting [20] of our microwave monitoring system is shown in *Fig. 25* (in colours*), while *Fig. 26* (in colours*) shows the PDB array, taken between roller conveyor and milling machine. One can see a lot of places with metal reflection, so the application of circularly polarized waves was unavoidable. *Fig. 27* (in colours*) shows the particleboard and one end of the encapsulated PDB array.

4.4. Measurement of Microwave Circuits

The measurement results of the microstrip antenna array (shown in *Fig. 20*) are: the resonant frequency is 5.8 GHz, bandwidth is 130 MHz, the 3 dB beamwidth in array direction is 22°, perpendicularly to the array the beamwidth is 82°, the gain of the array is 12.5 dB.

The measurement results for the PDB (see *Fig. 21*) are: gain of the dual patch is 9.8 dB, the 3 dB beamwidth 82° and 44° are, respectively, the return loss of OOK detector is 15 dB, tangential signal sensitivity is -54 dBm, the reflection loss of the BPSK modulator is 1.8 dB, amplitude error is 0.3 dB, phase error is 4.3°, monostatic radar cross section (RCS) is -17 dBm^2.

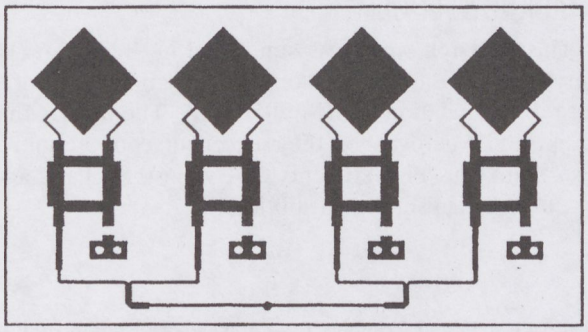

Fig. 20. Circularly polarized TX (and RX) antenna with 90° hybrids and the microstrip power splitter.

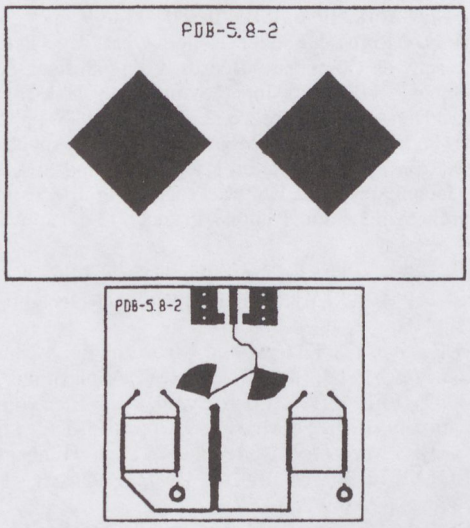

Fig. 21. Radiating-face and backside of a PDB. The 90° hybrids, $\lambda/4$ matching transformer and LPF are shown (without Schottky-diode).

4.5. Improvement of Accuracy

For standard wood particle mixtures (mentioned at the Introduction) the glue-overdose and air-inclusion plots were shown in *Figs. 10* and *11*, respectively. Industrial experience shows that the effect of the measurement site having a lot of reflective metals (*Figs. 25–27* in colours*) is negligible, because we used circular polarization at microstrip antennas. The effect of sawdust in *Fig. 27* is also negligible.

Preliminary measurements showed that the correlation between measured MOE and the result calculated from measured microwave parameters is acceptable (*Fig. 28*). The distance between PDBs and MUT gives the greatest effect among the errors. The relative amplitude error is significant (see *Fig. 29*). This error was minimized as a result of our further enhancements using three frequencies ($f_1 = 5.78$ GHz, $f_0 = 5.80$ GHz, and $f_2 = 5.82$ GHz). *Fig. 30* (in colours*) shows the measured relative amplitude and phase variation of a particleboard, while the measured absolute moisture content variation is shown in *Fig. 31* (in colours*).

*** Coloured pictures cited are shown separately in the colour pages of this issue.**

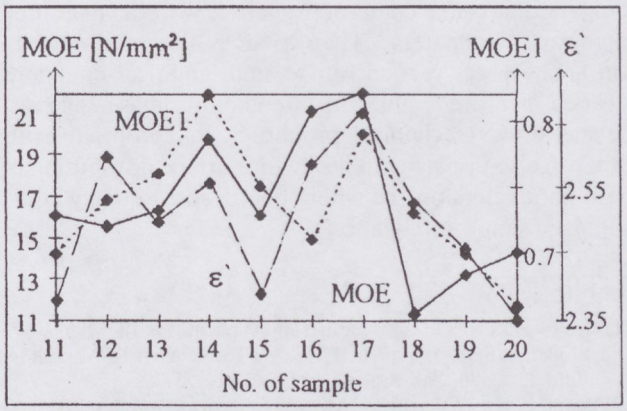

Fig. 28. Measured MOE, ε' and calculated MOE1 versus sample number.

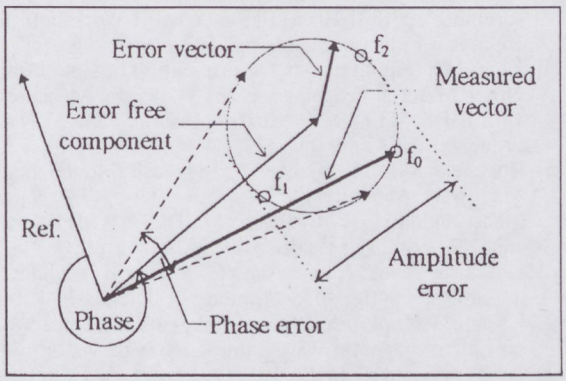

Fig. 29. Graphical error analysis.

4.6. Extended applications

Using our Composite Board Measuring instrument, we monitored the oblique angle performances of our new cell structure absorber [16] and a standard one. *Table 3* shows the characteristics of these absorbers.

Table 3. Measured performances of RF-absorbers

Type	Double shielding effectiveness 2SE [dB]			
	$\alpha = 90°$	±15°	±20°	±30°
CSA-100 Cell structure absorber 900x900x100 mm³	26	27.5	32	35
ECCOSORB AN-79 600x600x110 mm³ 6-layers	38	37	33	32

5. CONCLUSIONS

Complex permittivity monitoring of particleboards gives us information about moisture content, abnormal density or glue overdose or presence of air inclusions in the board at the moment of its occurrence. Using dielectric mixing models the effect of changes of moisture content, fluctuations in amounts of other ingredients were predicted. Industrial tests showed that the developed measurement system is suitable for on-line, real-time quality monitoring of large boards (3×17 m). In this phase the system is installed in industrial environment to collect more measurement data. In addition we performed experiments to

compare the real mechanical properties with the measured microwave parameters. Then a computer aided correlation analysis was carried out to find empirical equations between measured values of attenuation, phase shift and the measured mechanical properties. Appropriate software can also display graphically the surface distribution of these parameters on the whole board, so its quality could be judged simply at a glance.

6. ACKNOWLEDGEMENTS

This research work was supported by Interspan (Hungary), Zoltán Bay Foundation, Hungarian Ministry of Culture and Education (MKM 795/1996). The author thanks Quini and Microval for their excellent cooperation. He also thanks his PhD students G. Gyimesi, P. Olasz, and L. Nyúl for their useful contribution.

REFERENCES

[1] King, R. J.: "On-line Industrial Applications of Microwave Moisture Sensors", 17th IEEE MTTS-S, WMFB-Workshop, June 17, 1996, San Francisco, USA, pp. 75-78.

[2] Kupfer, K.: "Microwave Moisture Sensors and Their Application in Civil Engineering", 17th IEEE MTTS-S, WMFB-Workshop, June 17, 1996, San Francisco, USA, pp. 105-108.

[3] Cottard, G. Berthaud, P. and Bolomey, J. Ch.: "Microwave Linear Sensors for On-line Moisture Detection and Measurement", 17th IEEE MTTS-S, WMFB-Workshop, June 17, 1996, San Francisco, USA, pp. 127-128.

[4] Kent, M.: "Simultaneous Determination of Composition and Other Material Properties Using Dielectric Measurements", 17th IEEE MTTS-S, WMFB-Workshop, June 17, 1996, San Francisco, USA, pp. 131-134.

[5] Knochel, R. and Menke, F.: "Density Independence of Microwave Moisture Determination Using Two Para-meter Measurements", 17th IEEE MTTS-S, WMFB-Workshop, June 17, 1996, San Francisco, USA, pp. 138-142.

[6] Sina Jazayeri and Kemal Ahmet: "Moisture Gradient Studies in Timber by the Measurement of Dielectric Parameters Using a Multiple Electrode Arrangement", Third Workshop on Electromagnetic Wave Interaction with Water and Moist Substances, April 11-13, 1999, Athens, GA, USA Collection of Papers, pp. 148-152.

[7] Daschner, F., Knochel, R. and Kent, M.: "Resonator-Based Microwave Moisture Meter with Optimized Digital signal Processing", Third Workshop on Electromagnetic Wave Interaction with Water and Moist Substances, April 11-13, 1999, Athens, A, USA Collection of Papers, pp. 173-177.

[8] Lasri, T., Glay, D., Mamouni, A. and Leroy, Y.: "Free Space Moisture Measurement of Cellular Concrete", Third Workshop on Electromagnetic Wave Interaction with Water and Moist Substances, April 11-13, 1999, Athens, A, USA Collection of Papers, pp. 184-188.

[9] Kupfer, K.: "Methods and Devices for Density-Independent Moisture Measurement", Third Workshop on Electromagnetic Wave Interaction with Water and Moist Substances, April 11-13, 1999, Athens, A, USA Collection of Papers, pp. 11-19.

[10] Völgyi F., Mojzes I., Kelemen M., Rácz I., Seller R., Sonkoly A., Divos F. and Zombori B.: "Method and Equipment for Specifying the Parameters of Substances, Applied Mainly for Moving, Multilayer Materials" (in Hungarian: "Eljárás és berendezés anyagrendszerek paramétereinek mérésére, előnyösen mozgó, többrétegű anyagokon történő alkalmazására"), Announcement for Patent, MSzH-P 9601630

[11] Völgyi F. and Zombori B.: "A New Application of WLAN Concept: Complex Permittivity Monitoring of Large-Sized Composite Boards", 17th IEEE MTTS-S, WMFB-Workshop, June 17, 1996, San Francisco, USA, pp. 119-122.

[12] Kraszewski, A. W. (editor): "Microwave Aquametry", IEEE Press, New York, 1996, ISBN 0-7803-1146-9.

[13] Völgyi F., Mojzes I., Seller R and Olasz P.: "Permittivity Monitoring of Composite Boards Using Spread Spectrum Techniques", URSI'98, Int. Symp. on Electromagnetic Theory, Thessaloniki, Greece, 25-28 May 1998, pp. 97-99.

[14] Völgyi F., Olasz P. and Mojzes I.: "New Application of WLAN Concept: Modulated Backscatter and Spread Spectrum Techniques", PIERS'98, Progress in Electromagnetic Research Symposium, Nantes, France, 13-17 July 1998, p. 565.

[15] Nyúl L. and Völgyi F.: "Contactless Testing of Particleboards", APMC'98, Yokohama, Japan, 8-11 December 1998, pp. 213-216.

[16] Völgyi F., Nyúl L., Tatár S. and Mrovcza A: "A New Radio Frequency Absorber for GTEM Cell Applications", EMC Zurich'99, 13th Int. Zurich Symp. on Electromagnetic Compatibility, 16-18 February 1999, pp. 675-678.

[17] Völgyi, F.: "Microstrip Antenna R&D in Hungary", 10th MICROCOLL, March 21-24, 1999, Budapest, Hungary Proceedings pp. 249-252.

[18] Völgyi, F.: "Microwave Measurements for Specifying the Freshness of Eggs", Third Workshop on Electro-magnetic Wave Interaction with Water and Moist Substances, April 11-13, 1999, Athens, GA, USA pp. 52-56.

[19] Völgyi, F.: "Quality Forecast of Particleboards Using a Microwave Monitoring System", Third Workshop on Electromagnetic Wave Interaction with Water and Moist Substances, April 11-13, 1999, Athens, GA, USA Collection of Papers, pp. 102-106.

[20] Tunay, G.: "Industrial Applications of Microwaves: On-Line Monitoring of Particleboards", Diploma Thesis (MSc), TUB/DMT, 1999., Supervisor: Völgyi, F.

[21] Nyúl L.: "Electromagnetic Field Interaction with Substances" (in Hungarian), Diploma Thesis, Technical University of Budapest, Department of Microwave Telecommunications, 1998., Supervisor: Völgyi, F.

[22] Völgyi, F.: "Monitoring of Particleboard Production using Microwave Sensors", Ch.10 in book "Sensors Update", (editor: Wolfgang Göpel), Wiley-VCH Verlag GmbH, Weinheim, GE, 2000, Vol. 7, pp. 249-274.

MIKROHULLÁMÚ MEGFIGYELŐ RENDSZER FAFORGÁCSLAPOK MINŐSÍTÉSÉRE

Ma a világon csaknem ezer, nagymértékben automatizált üzemben gyártják a bútoripar alapanyagát szolgáltató faforgácslapokat mintegy 100 millió m^3 mennyiségben. Ismeretes, hogy különféle dielektromos anyagok (faforgácslapok, építőipari anyagok, mezőgazdasági szemes termények stb.) komplex permittivitásának mikrohullámú méréséből következtetni lehet ezen anyagok nedvességtartalmára, sűrűségére, minőségére. A cikk tárgya egy általunk kifejlesztett, folyamatszabályozási célokra használt mérőberendezés, mely faipari roncsolásmentes vizsgálatok folyamatos végzésére szolgál üzemi körülmények között. Az ismertetésre kerülő 5,8 GHz-es mérőrendszer a világon elsőként alkalmazza méréstechnikai célokra azon élenjáró műszaki megoldásokat, melyek eddig csak a digitális hírközlésben, illetve a radartechnikában voltak használatosak (WLAN-elv, kódmodulált visszaverők technikája, szórt spektrumú mérőjel, nyomtatott antennák). A mérőrendszer blokksémáját, a szoftver alapjául szolgáló térelméleti és ún. dielektromos keverékmodellt, néhány speciális mikrohullámú áramkör ismertetését, a tervezést megelőző laboratóriumi és üzemi kísérletek, valamint a Vásárosnaményi Faforgácslapgyárban (INTERSPAN Kft.) lefolytatott próbaüzem eredményeinek bemutatását célozza ez a cikk. A fejlesztés fázisainak bemutatását számos színes fotó teszi szemléletessé.

SPECIFYING THE QUALITY OF EGGS USING MICROWAVE SENSORS*

FERENC VÖLGYI

TECHNICAL UNIVERSITY OF BUDAPEST
DEPT. OF MICROWAVE TELECOMMUNICATIONS
H-1111, BUDAPEST, GOLDMANN TÉR 3, HUNGARY
PHONE: 36 1 463 1559; FAX: 36 1 463 3289; T-VOLGYI@NOV.MHT.BME.HU

This paper introduces a microwave measurement setup using three microstrip antennas integrated with a microwave oscillator and Schottky-diode detectors used as bistatic microwave sensors. We have measured the microwave attenuation (water content) and the bistatic radar cross section (dimensions) of eggs having different time of storage (see *Fig. 1*). The measured attenuation for fresh egg is $A = 8 - 10$ dB at the frequency of 14.2 GHz, the variation with time is: dA [dB] $= -0.033T$ (days), thus nearly -1 dB/30 days. Our next program is to create a microwave equipment for automatic selection of old eggs having bad quality. The basic arrangement and the results of our measurement are discussed.

KEYWORDS: egg, microwave aquametry, microstrip antenna, bistatic sensor, radar cross section.

1. INTRODUCTION

In food industries and at production of cosmetics it is important to know the freshness of eggs used as basic components. The aim of the first part of this work is: finding out the characteristic changes of eggs during the storage period, tracking the measurable chemical and physico-chemical parameters along the ageing [1]. At the second part of this development we have made a microwave setup of sensors (shown in *Fig. 1*) for the measurement of attenuation and bistatic radar cross section (RCS) of eggs, characterizing their freshness. Actually this setup is similar to a "surface penetrating radar" (SPR for short) used in reflection, and transillumination (transmission) mode [2].

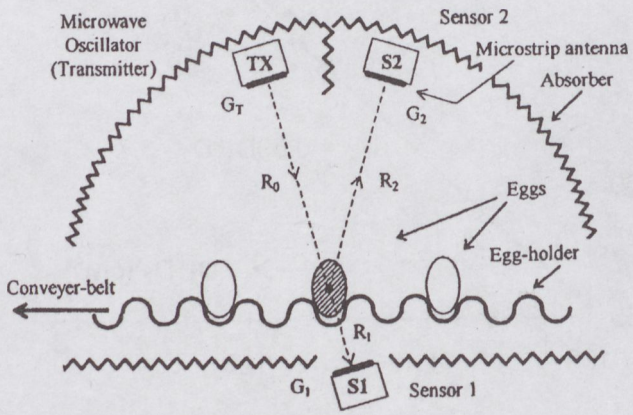

Fig. 1. Microwave measuring-tunnel for specifying the freshness of eggs

1.1. Surface-penetrating radars

There is a steadily increasing number of applications and organizations working on surface-penetrating radar [3]. The most important of these applications are: detection of nonmetallic mines, mapping of buried plants, internal inspection of non-metallic pipes, peatland investigations, exploration of coal [4], rock salt, oil shales and gypsums, limestones, granites, detecting skiers trapped in an avalanche, locating of voids, inconsistencies and buried metalwork in a wide variety of structures, fault detection of road and pavement, remote sensing of the Earth by radars from satellites, nondestructive testing of materials, etc.

We have made the first experiments using SPR-like instruments (sensors) for specifying the freshness of eggs [1], [5], [6]. Previously we have introduced some microwave sensors, which are used for moisture measurements [7], in automatic process control [8], [9], in agriculture [10], [11] and in particleboard production [12], [13]. The setup for the last mentioned application was also used for the measurement of our new cell-structure RF-absorber [14]. The radiating elements are the self-designed microstrip antennas [15] (MSAs), elements and arrays, sometimes scanning antennas [16]. One of these serves for scientific applications [17].

1.2. Characterization of egg [1]

The final aim of this work is to construct and to test an equipment that is able to determine the egg's freshness without cracking it. This equipment will measure the microwave attenuation and RCS of eggs, so these measured parameters will be assigned directly to the properties indicating the state of freshness. Since whole egg is examined, this subsection will deal with its characterization, highlighting those relevant details that influence considerably the microwave properties.

The whole fresh egg contains – as shown in Table 1 – considerable amount of water, while the solids, amounting to more than 30 %, are composed of 1/3 part lipids (fat-like substances), 1/3 part minerals (metallic salts) and 1/3 part protein. However, analyzing the composition of the egg-shell, egg-white and egg-yolk separately, significant differences can be found. So it can be stated that the egg-white contains about double the amount of water compared to egg-yolk, while lipids can be found only in the egg-yolk. Small-proportioned carbo-hydrate is typically bound to proteins (complex), but also can be detected as free glucose. Values shown in the table are obtained by examining two-days-old samples stored at 8°C, by simple averaging of 5 parallel measurements [1].

* Revised and shortened version of [20].

Table 1. Components of egg

	whole egg	egg-white	egg-yolk	egg-shell
water (%)	65.4	87.8	48.5	1.6
solids (%)	34.6	12.2	51.5	98.4
protein (%)	12.3	10.6	16.6	3.3
fat (%)	10.5	trace	32.6	trace
carbo-hidrates (%)	0.9	1.0	1.1	–
minerals (%)	10.9	0.6	1.1	95.1

The egg is an extremely complex colloid system being in thermodynamically unstable state. Because of trending to stability (energy minimum) it alters remarkably without any external influence during ageing.

1.3. Ageing properties

The aim of the work is to find out the characteristic changes of eggs during the storage period, tracking the measurable chemical and physico-chemical parameters along the ageing. The examined chemical and physical parameters are [1]: protein content, free amino acid content, ammonia content, PH value and content of dry substance, specific weight, mass and viscosity.

The water loss along the ageing, the escape of gas produced by enzymatic decomposing processes, in other words the complex dehydration process can be well characterized. As the volume of the egg remains unchanged, it is sufficient to know the function of change of mass versus storage period. The measured mass data [5] in the *Fig. 2* are simple arithmetic means of fifty samples stored at 21°C. The measurement error is 0.1 %. Using these data the functions

$$M = M_0 \cdot e^{-0{,}0038T}; \quad (R^2 = 0.997), \qquad (1)$$

or in a good approximation:

$$M \cong M_0 - 0.27 \cdot T; \quad T \leq 30 \text{ days} \qquad (2)$$

can be obtained where M stays for the actual mass, T for the storage time in days, M_0 for the mass of fresh eggs and R_2 for the reliability of the matching. It is to be noted that for the samples which already during the initial phase showed rising behaviour in destillated water of 18°C (that is, the deterioration processes were more intensive) the above relation between the change of mass and storage period is not valid because the regression straight is steeper.

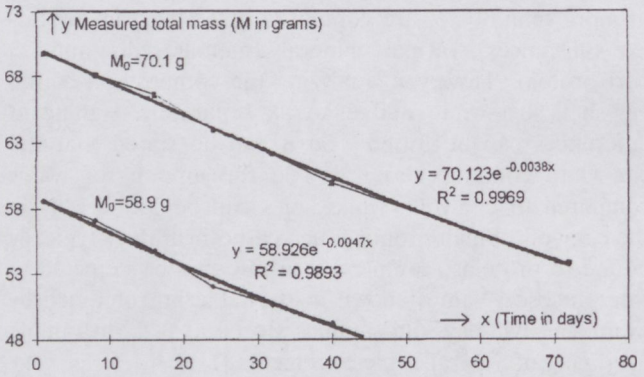

Fig. 2. Measured mass data

1.4. Microwave features

From microwave point of view, the change of specific weight and change of mass, caused by the water loss along the ageing, is most important. Because the egg-white contains 87.8 % water, the task: "specifying the freshness of eggs" is the problem of microwave aquametry [8]. Since the water content of egg decreases with age by nearly 20 % in 30 days [5], detection of water content of egg is a good measure of its freshness. The measured variation of microwave attenuation versus age of an egg is shown in *Fig. 3*. The other information about egg is the dimension (*Fig. 4*), which can be characterized by the radar cross section [18] (calculated curve is shown in *Fig. 6*).

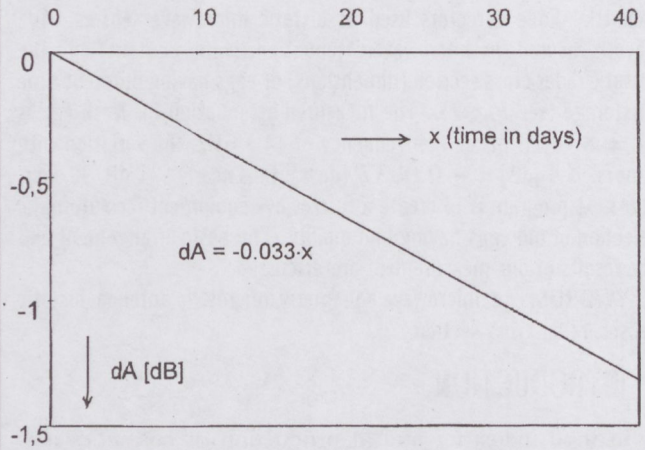

Fig. 3. Measured variation of microwave attenuation versus age of an egg

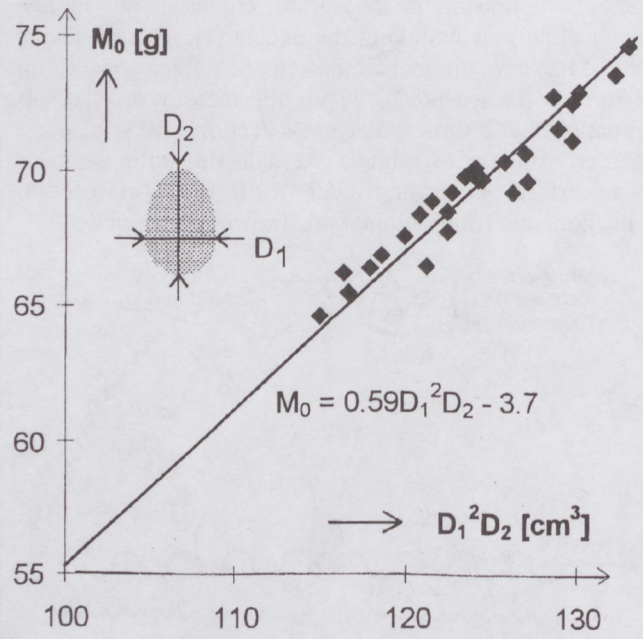

Fig. 4. Measured "fresh-mass" versus dimensions of eggs

2. THEORY

2.1 Microwave attenuation

The egg being a lossy dielectric material with equivalent thickness of L_{eq} [cm] attenuates the TEM wave as follows

(see [8] p. 244 eq. (15-3)):

$$A = 0.91\sqrt{\varepsilon'} \cdot \mathrm{tg}\delta \cdot f \cdot L_{\mathrm{eq}} \quad [\mathrm{dB}], \tag{3}$$

where f is the frequency in GHz, ε' is the real part of the complex relative permittivity of water:

$$\varepsilon^{\star} = \varepsilon' - j\varepsilon"|_{f=14.2\ \mathrm{GHz}} \cong 46 - j30. \tag{4}$$

The power dissipation is indicated by the loss factor $\varepsilon"$ which is proportional to the tangent of the loss angle δ:

$$\mathrm{tg}\delta = \varepsilon"/\varepsilon'|_{f=14.2\ \mathrm{GHz}} = 0.652. \tag{5}$$

The Eq. (3) comes from the well-known equations:

$$A = \alpha L;$$

$$\alpha\ [\mathrm{Np}] = \frac{2\pi}{\lambda}\varepsilon' \mathrm{tg}\delta;$$

$$\lambda\ [\mathrm{cm}] = \frac{30}{f\ [\mathrm{GHz}] \cdot \delta};$$

$$\alpha\ [\mathrm{dB}] = k \cdot \sqrt{\varepsilon'} \cdot \mathrm{tg}\delta \cdot f;$$

where

$$k = \frac{2\pi}{30} \cdot 10\lg(e) \cong 0.91; \quad e = 2.718.$$

Our measurements show, that:

$$L_{\mathrm{eq}} \cong K\frac{w}{q(\vartheta)}\ [\mathrm{cm}]; \tag{6}$$

where $K \cong 0.076\ [\mathrm{cm}^3/\mathrm{g}]$, w is the water content of egg in grams, q is the cross-section [in cm^2] of ϑ the egg at the incident angle of ϑ, which is measured from the axis at egg's top. The K-constant represents such effects as form-factor, forward scattering, geometry of measurement, etc., having its value experimentally determined.

The attenuation, expressed by markings from *Fig. 1* which shows the basic setup, is:

$$A_T\ [\mathrm{dB}] = 20\lg\frac{4\pi(R_0 + R_1)}{\lambda} - G_T - G_1 + A, \tag{7}$$

where A is the attenuation due to egg, G_T is the gain of the transmitter antenna in dBs, G_1 is the gain of the first receiver antenna in dBs, λ is the wavelength in cms. The approximate mass of fresh egg, expressed as function of its dimensions, as average of many measurements:

$$M_0\ [\mathrm{g}] = 0.59 \cdot (D_1^2 \cdot D_2) - 3.7\,. \tag{8}$$

The so-called dehydration (or water-lossing) function:

$$w\ [\mathrm{g}] = 0.654 \cdot M_0 - 0.27 \cdot T. \tag{9}$$

Herewith finally the change of attenuation in dBs, for eggs examined currently:

$$\Delta A = -0.033 \cdot T, \tag{10}$$

which yields – 0.23 dB/week or – 1 dB/30 days.

2.2. Radar Cross Section

The radar cross section of the egg target:

$$\mathrm{RCS} = \sigma(\vartheta) = \frac{\pi}{4} \cdot D_1(\vartheta) \cdot D_2(\vartheta) \cdot \eta, \tag{11}$$

where D_1 is the smaller diameter of egg, as a function of angle ϑ (see *Fig. 5*), D_2 is the larger diameter of egg, η is the efficiency, relative to a metallic backscatterer. For target dimensions large compared to the wavelength after [18] p. 65:

$$\eta = \left(\frac{1 - \sqrt{\varepsilon'}}{1 + \sqrt{\varepsilon'}}\right)^2 |_{\varepsilon'=46} \cong 0.552 \div -2.6\ \mathrm{dB}. \tag{12}$$

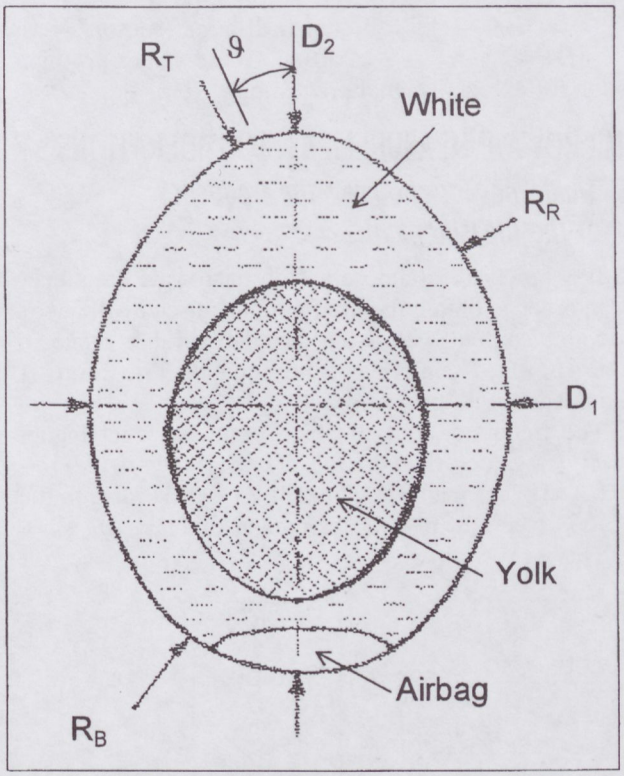

Fig. 5. Cross-section view of a hen's egg

The calculated RCS versus angle of incident of an egg is shown in Fig. 9.

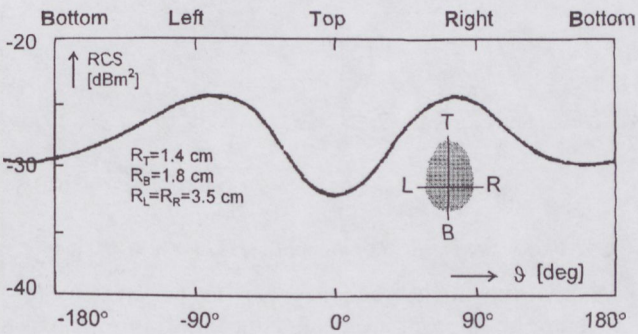

Fig. 6. Calculated RCS versus angle of incidence

For egg target the reflection attenuation measured in the receiver 2:

$$A_R\ [\mathrm{dB}] = 20 \cdot \lg(4\pi R_0 R_2) - \sigma\ [\mathrm{dB}]\mathrm{cm}^2 - G_2 - G_T, \tag{13}$$

where G_2n is the gain of the receiver antenna, R_2 is the distance marked in *Fig. 1.*

Making a simple calculation supposing: $D_1 = 4.44$ cm, $D_2 = 5.77$ cm, $R_0 = R_2 = 30$ cm, $R_1 = 10$ cm, $T = 0$ (fresh egg), $G_T = G_2 = 19$ dB, $G_1 = 13$ dB, transmitted power: $P_T = 1$ mW÷0 dBm, using eq. (8) the fresh-mass is $M_0 = 61.6$ g, from eq. (9) the

water content: $w = 40.3$ g, using eq. (6) the equivalent thickness: $L_{eq} = 0.194$ cm with $q(\vartheta = 15°) = 15.7$ cm^2. From eq. (3) the microwave attenuation of egg is $A = 9$ dB, using eq. (7) the system attenuation is $A_T = 24.5$ dB, from eq. (13) the reflection-attenuation is $A_R = 28.2$ dB with RCS $= 5.3$ dBcm^2 (-34.7 dBm^2) from eq. (11). The received power level at sensor S_1 is: $P_1 = P_T - A_T = -24.5$ dBm; at sensor S_2 is: $P_2 = P_T - A_R = -28.2$ dBm. These values are high enough for excellent signal processing.

3. MICROWAVE MEASUREMENT CONSIDERATIONS

3.1. Guidelines for choosing the frequency of the measurement

1. It is practical to choose a high microwave frequency in order to obtain the attenuation caused by the egg's water content within the well measurable range of $6-10$ dB. This is clear from equation (3), where A increases with frequency.
2. The frequency must be high enough to get higher D_1/λ values than in the Rayleigh-region ($D_1 \cong 0.1\lambda$) or resonance region ($D_1 \cong \lambda$) according to the RCS (see [18] p. 163), assuming ordinary egg sizes. This is shown in *Fig. 7.*

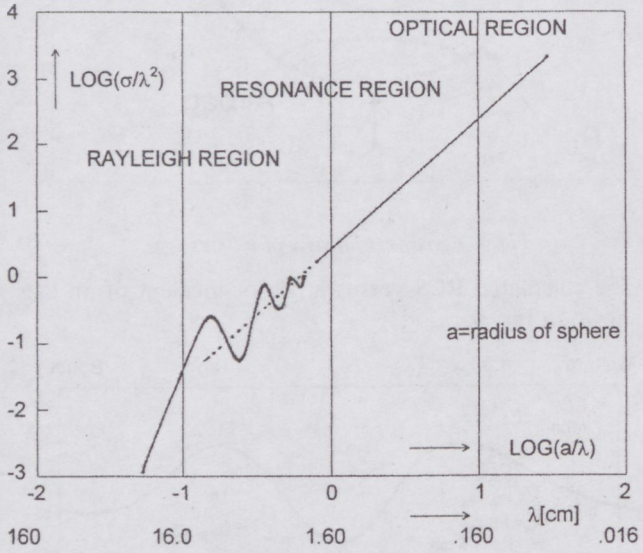

Fig. 7. Backscattering RCS of the sphere [18] for $a = 1.6$ cm

3. A relatively high frequency has to be chosen, to achieve an appropriate beam concentration with reasonable antenna dimensions.
4. It is important to mention that increasing the frequency the costs of the equipment under development rise significantly.

Considering the above, the chosen frequency is $f = 14.2$ GHz.

3.2. Guidelines for selecting the antennas

We have choosen printed (microstrip) antennas for the reason of small dimensions and simple manufacturing. One of our antennas is shown with slightly reduced dimensions in *Fig. 8.* Typical features are the followings: center frequency is 14.2 GHz, return loss at center frequency is 25 dB, bandwidth for return loss lower than 10 dB is 550 MHz. A fourth- or sixteenth part of this linearly polarized 8x8 elements antenna seems to be an optimal choice for our present examinations.

The on-axis power density of a uniform square aperture is shown in *Fig. 9* (which made after [16]). On the basis of these considerations the distance from the antennas to the egg as radar target can be chosen. It is noteworthy that in our previous examinations (see [8], p. 236, *Figs. 11, 15*) a very advantageous power density distribution has been achieved by circularly polarized microstrip antennas, even for small target ranges, which could be important from the aspect of reducing the dimensions of the equipment to be designed.

The main parameters of the realized microstrip antennas are given in Table 2, where R_m denotes the begin of the far field.

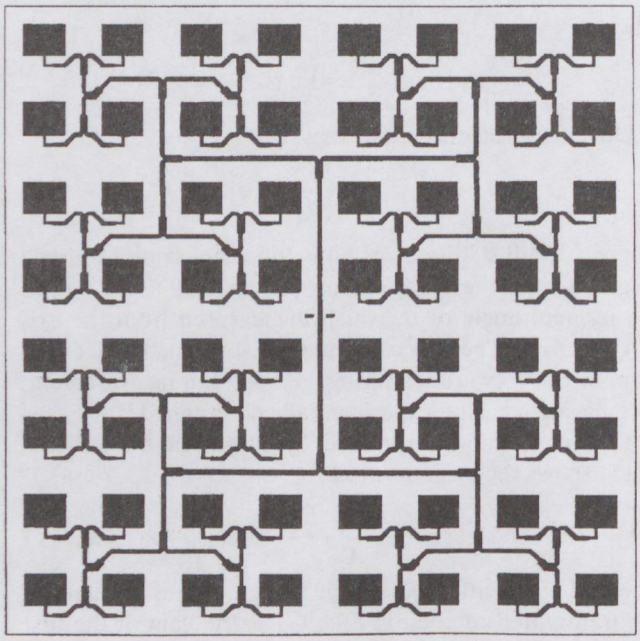

Fig. 8. A 8x8 elements microstrip antenna array

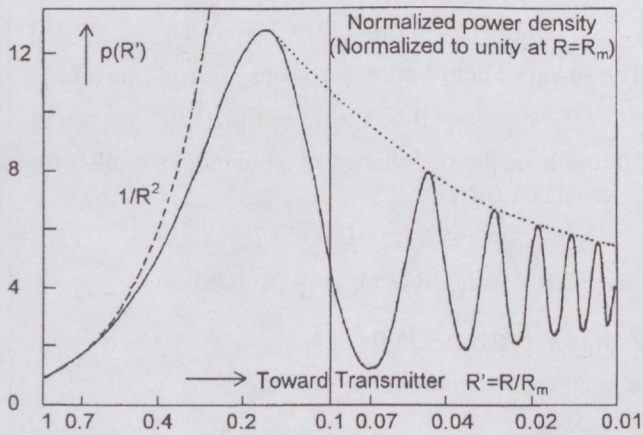

Fig. 9. On-axis power density [16] — uniform square aperture

Table 2. Specifications of our microstrip antenna arrays used for egg-measurement, as well as the typical measurement distances

MSA Type	Side dim.	Diagonal dim.	Far-field region	Measurement distances [cm]		Beamwidth	Gain
Number of elements	d [cm]	$D=\sqrt{2}d$ [cm]	$R_m=2D^2/\lambda$ [cm]	Near field max. $0.2R_m$	Two beams $0.07R_m$	BW [deg]	G [dB]
2x2	2.5	3.54	11.8	2.4	0.8	32	13.0
4x4	5.6	7.9	59.3	11.9	4.2	16	19.0
8x8	12	17.0	272.6	54.5	19.1	8	24.8

In the case of rectangular aperture the axial power density increases as far as $0.2R_m$ (which is advantageous from the aspect of the egg's positioning), but there is a minimum at $0.07R_m$ because the antenna beam splits in two, which is to avoid.

3.3. Further considerations for the geometry of the measurement setup

The basic measurement setup (shown in *Fig. 1*) has been realized to minimize the coupling between the transmitter and the receiver antenna, which measures the reflection when the reflecting egg is not present. It is at this point to mention that we got only a few dB-s smaller reflection for eggs than the measured values obtained with metallic reflectors, since the $(\varepsilon')^{0.5}$ refraction index of water in egg is high. Eggs were placed into each second position in the egg-holder, this way we ensured that only the measured egg was present in the antenna beam, moreover it filled out the -1 dB range.

4. EXPERIMENTAL RESULTS

4.1. RCS measurement of eggs

A typical result of measured RCS for an egg versus angle of incidence is shown in *Fig. 10.* The values are well reproducible from the top and side directions but there are large differences at the bottom direction, as it can be seen more remarkable at *Fig. 11.*

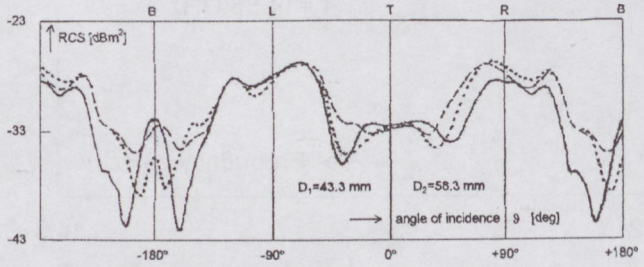

Fig. 10. Measured RCS of an egg versus angle of incidence. Various kinds of curves are shown depending on the geometrical positioning. The bistatic angle and frequency are 30° and 14.2 GHz, respectively.

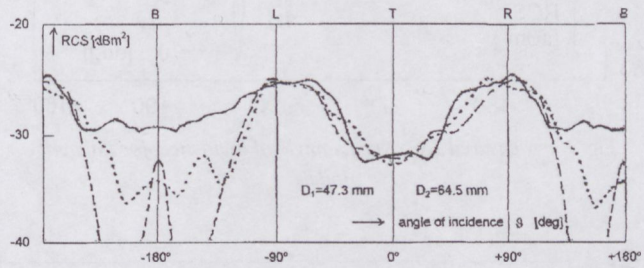

Fig. 11. Measured RCS of an egg versus angle of incidence. Various kinds of curves are shown depending on the geometrical positioning. After homogenization (by shaking) of egg the result is indicated by continuous line.

The considerable variation at egg's bottom direction is caused by the "airbag". This is also shown in *Fig. 12* for different polarizations. Selecting miscellaneous egg's models (metallized, normal, empty egg) the RCS-measurement results are shown in *Fig. 13.* The curve measured at "metallized egg" is not smooth enough, because the metallization was made merely by packing the egg in a thin foil of aluminium. *Fig. 14* shows the measured relative power level versus frequency at the sensor S2, for different eggs. At a fixed position of eggs the measured largest deviation in RCS was nearly 1 dB, between eggs having the smallest and largest D_1 dimension. Using the information of *Fig. 15*, we can calculate an equivalent distance for airbag from the measured frequencies of minima (f_1 and f_2), which is shorter than 0.78 cm in egg.

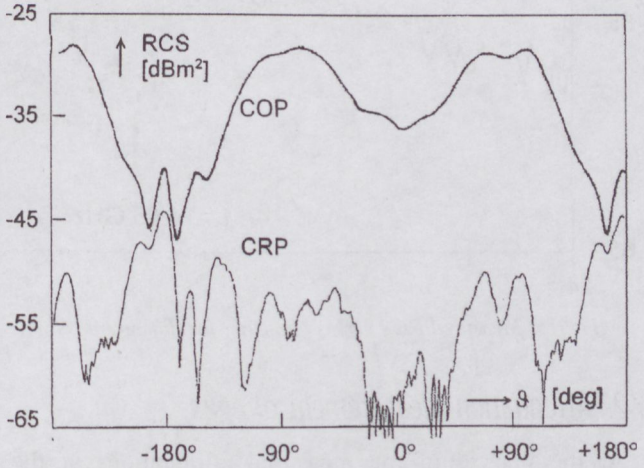

Fig. 12. Measured copolarized (COP) and crosspolarized (CRP) radar cross sections for egg

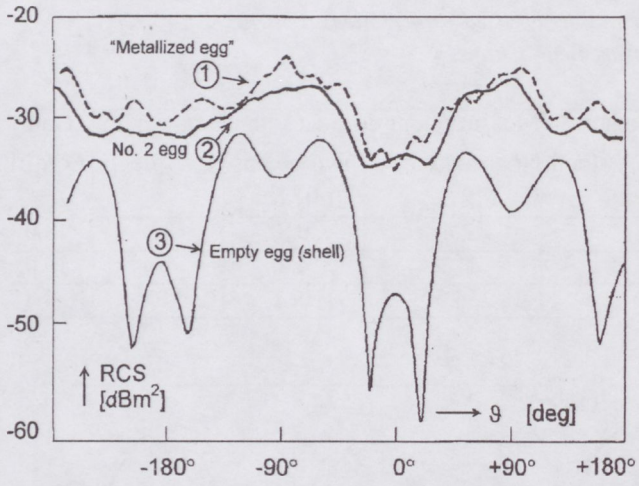

Fig. 13. Measured RCS versus angle of incidence, for different models

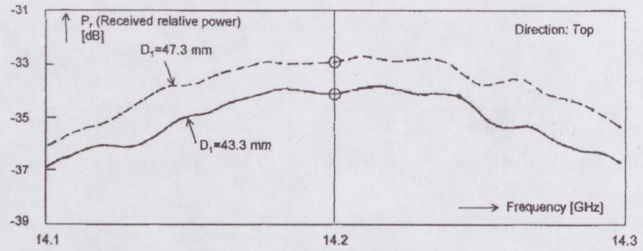

Fig. 14. Measured relative power level at the sensor S2, for different eggs. The measured values directly give RCS at the frequency of 14.2 GHz

The calculated and measured RCS from the top of vertically positioned eggs are between $-31 \ldots -34$ dBm^2, depending on the D_1 (and R_T) dimensions. The correlation between calculated and measured values are good enough.

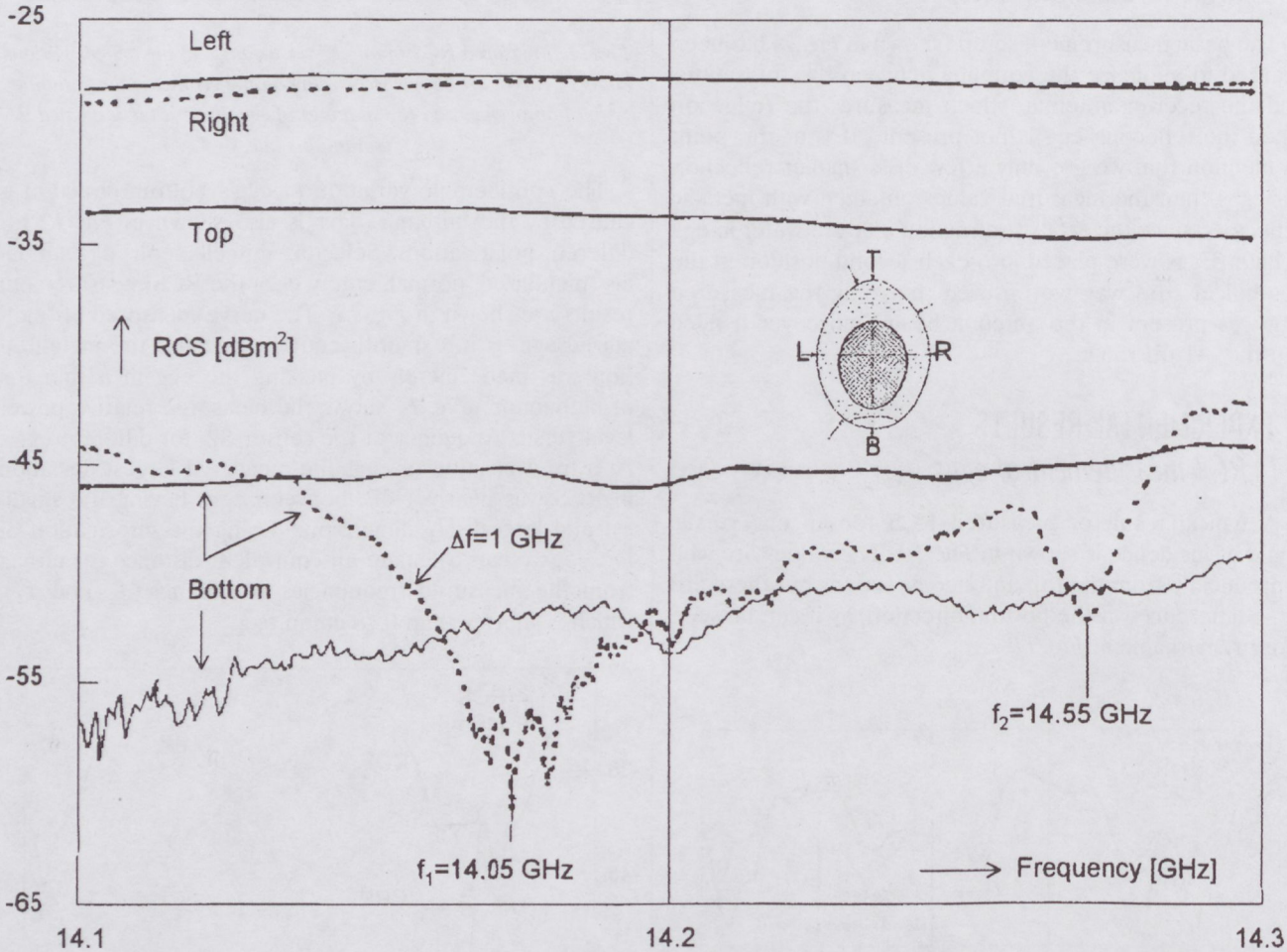

Fig. 15. Measured RCS versus frequency for different position. Two characteristic minima can be observed in the bottom direction (shown at ($\Delta f = 1$ GHz curve)

4.2. Attenuation measurement of eggs

At the first setup the measured attenuations at the frequency of 14.2 GHz were: empty egg (shell) ≈ 0.5 dB, No. 62 (lightest egg): 7.0 dB, No. 116 (heaviest egg): 8.6 dB. For different angles of incidence, the measured attenuation versus frequency curves are shown in *Fig. 16.*

The *Fig. 17* shows the curves of the measured attenuation versus frequency with zoomed dB-scale. Measured values for different eggs at 14.2 GHz are: No. 62 (16 days old, cracked, $M = 41.5$ g): 6.70 dB. Eggs of same size but different ages: No. 27 (27 days old, 60.1 g): 7.28 dB, No. 41 (16 days old, 64.4 g): 7.66 dB, No. 97 (2 days old, 68.4 g): 8.05 dB. Largest and heaviest egg: No. 116 (2 days old, 74.7 g): 8.34 dB. These results are self-explanatory and show the egg's freshness.

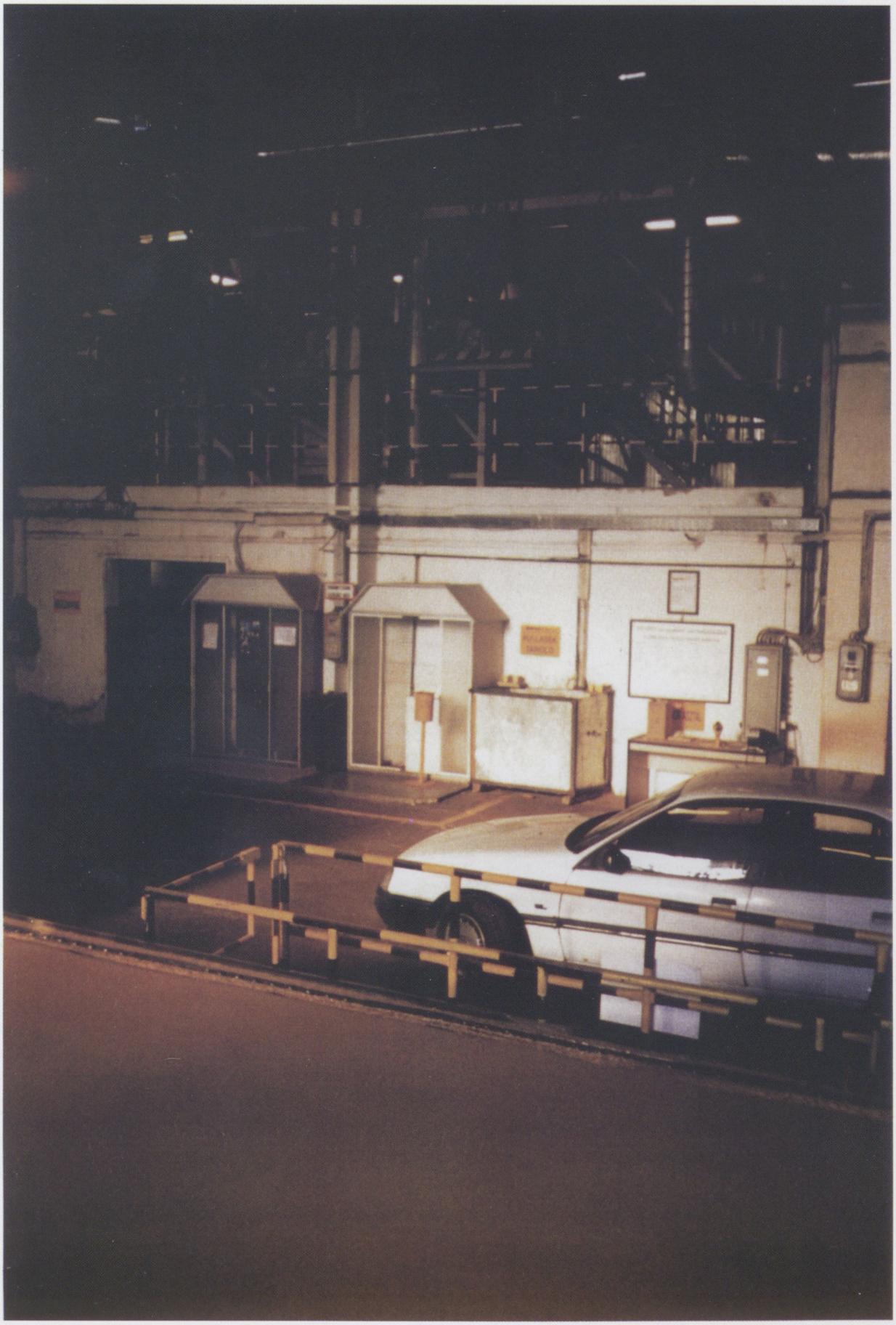

Fig. 3. The mat (mixture of wood particles and glue, see lower part of the figure) is transported from forming heads to the loader and press.

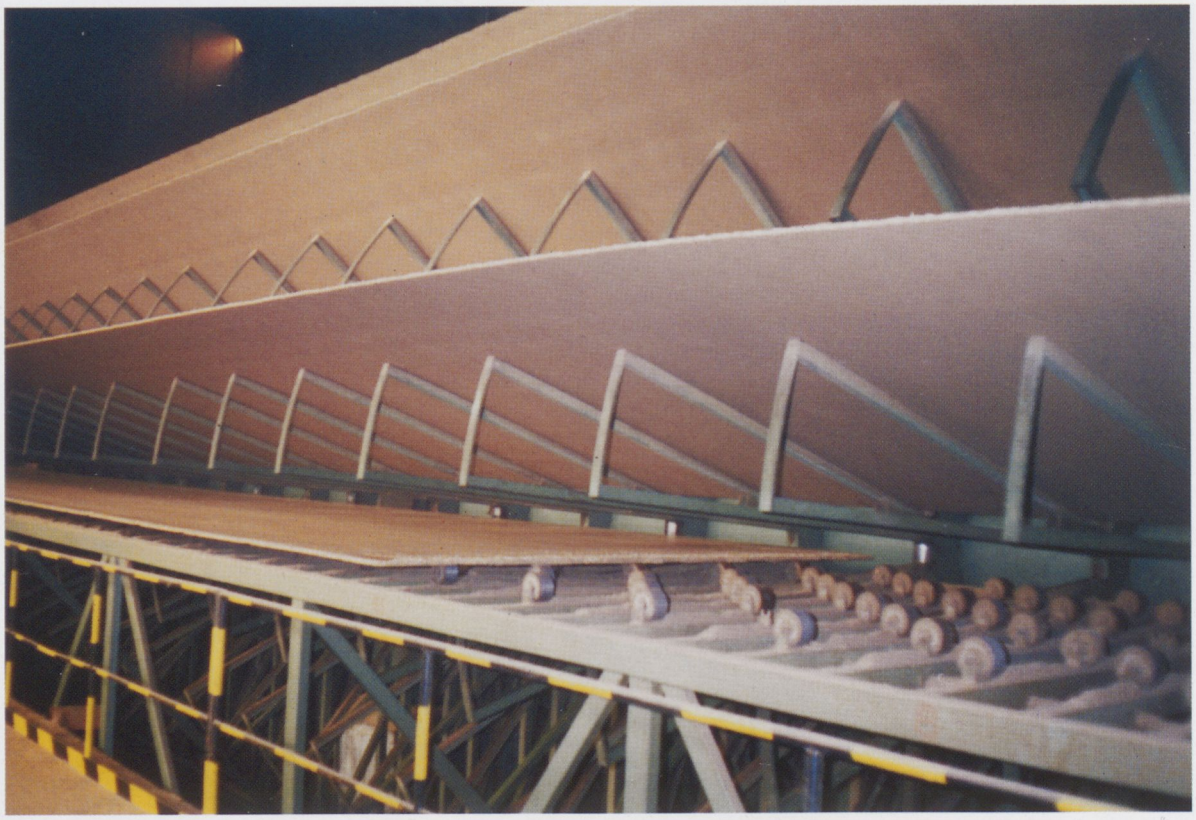

Fig. 4. Particleboards (each 2.07 x 16.5 m) in the rotating equalizer.

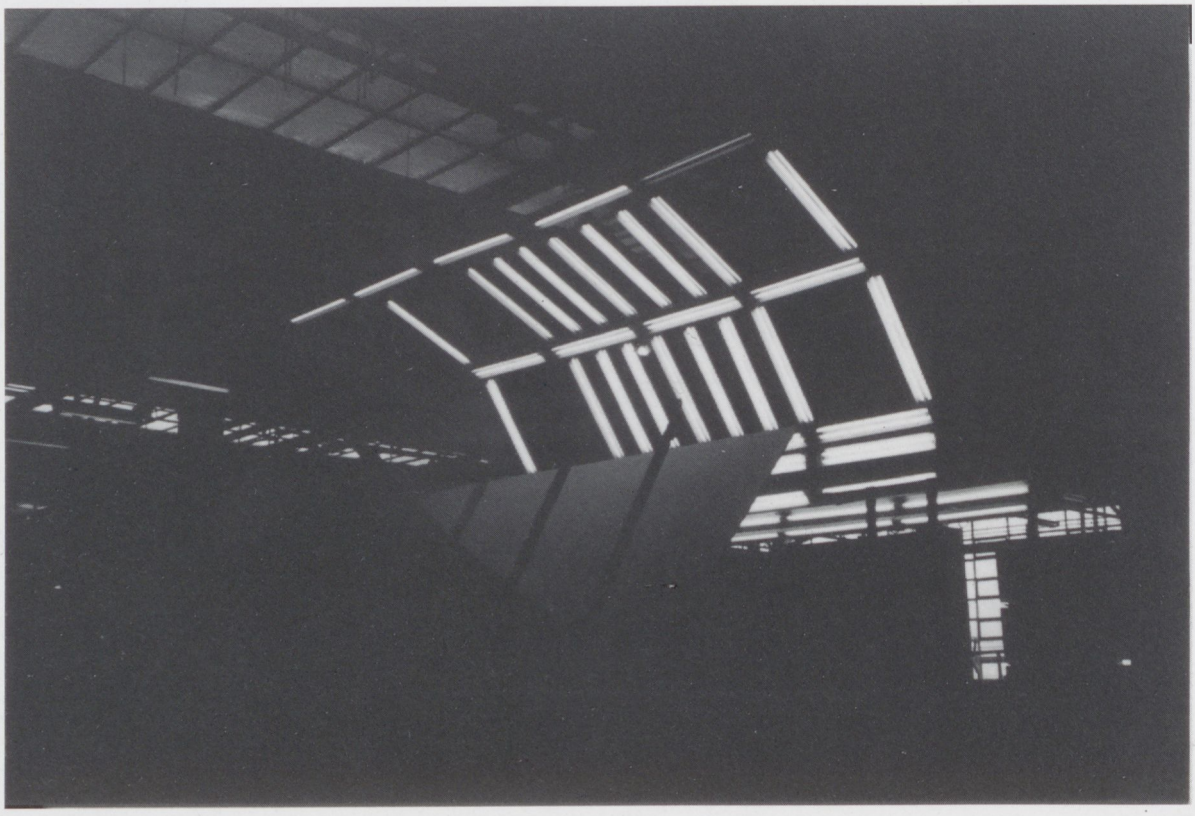

Fig. 5. Quality control of particleboards using ultraviolet light sources.

Fig. 22. Experiments in the laboratory (RX,TX and PDB-array).

Fig. 23. IQ-receiver (flat black box) and PC.

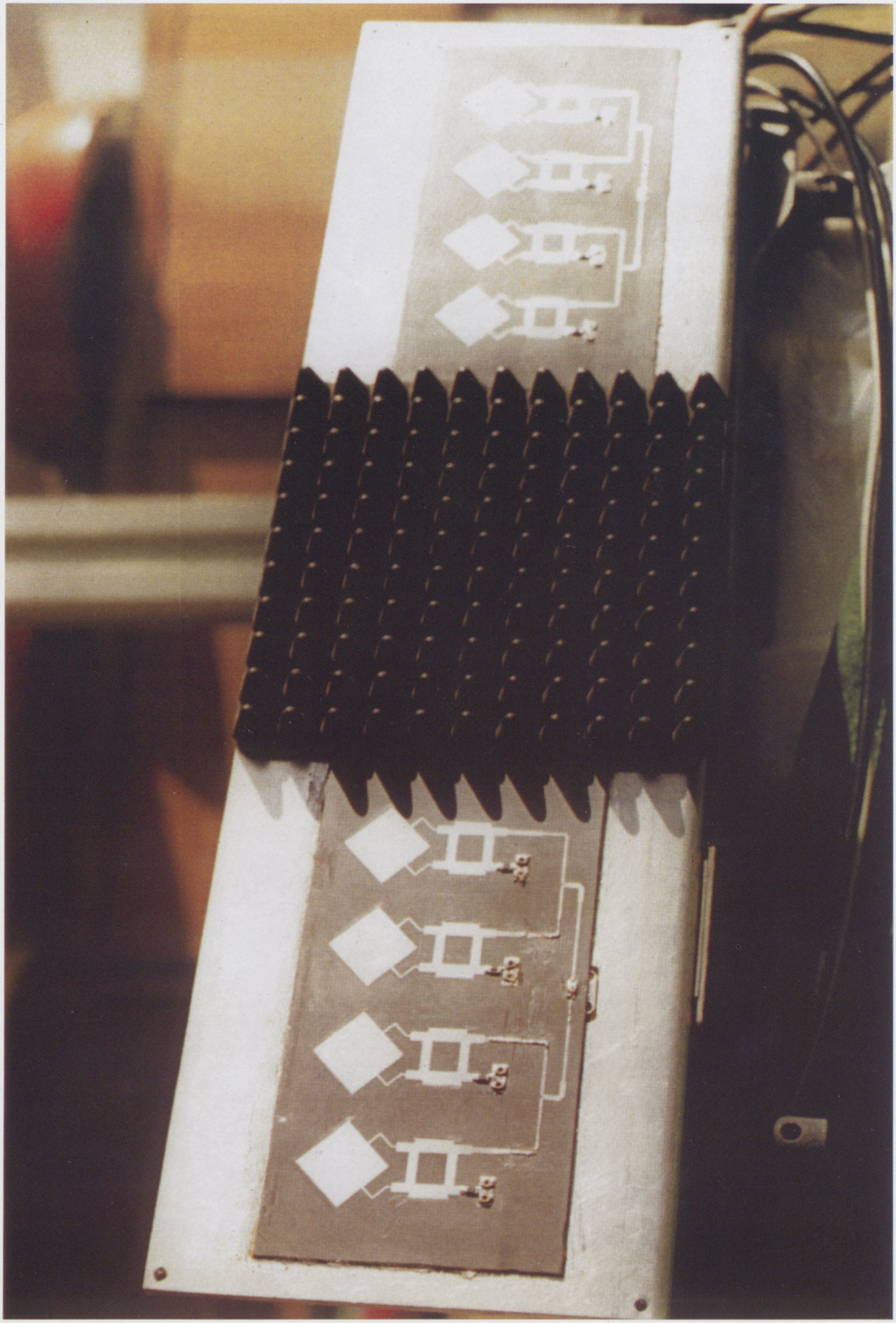

Fig. 24. Microwave transceiver using circularly polarized microstrip antennas

Fig. 25. Mounting of the microwave monitoring system at the particleboard plant.

Fig. 26. PDB array between roller conveyor and milling machine.

Fig. 27. PB and encapsulated PDB array.

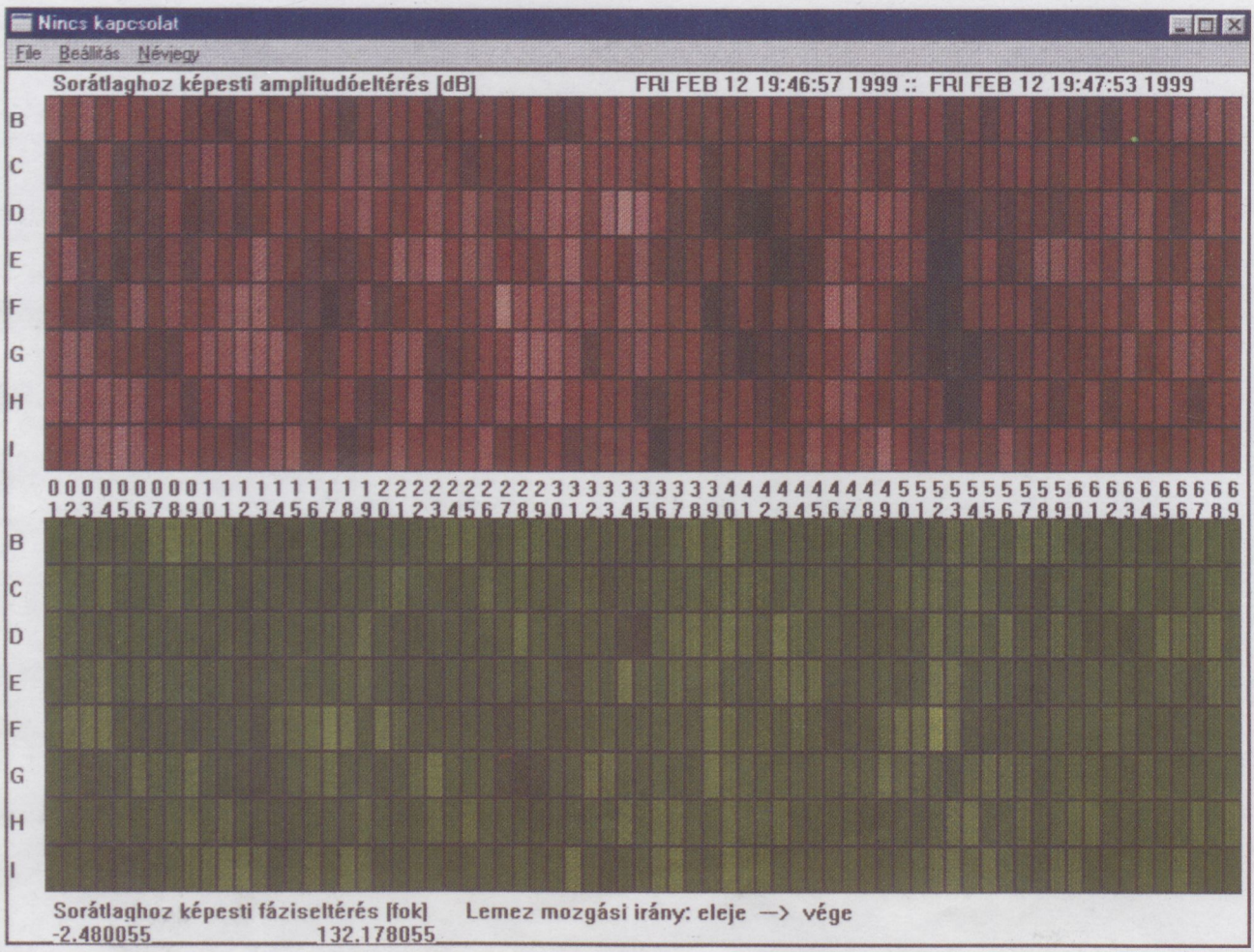

Fig. 30. Measured amplitude and phase variation of a composite board having dimensions of (0.017)x 2.07x 16.5 m.Contrast ranges (from white to black) are 2.48 ± 1 dB and 132.2± 30°, respectively. Horizontally compressed pictures, frequency is 5.8 GHz, time duration is 56 sec. Backscatterers are marked using letters B,C...I.

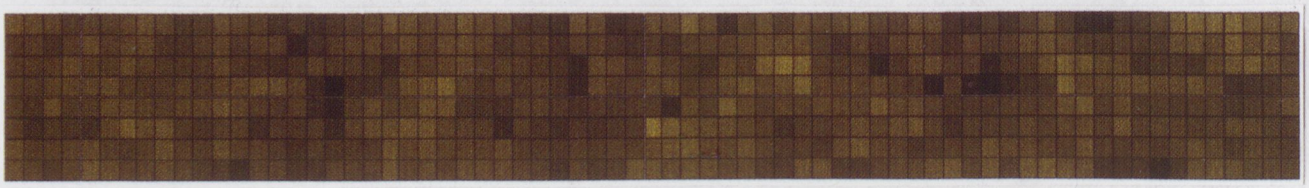

Fig. 31. Measured MC-variation of a PB of dimensions 2.07 x 16.5 m. The mean value of MC is 4% and the standard deviation is 0.48%.

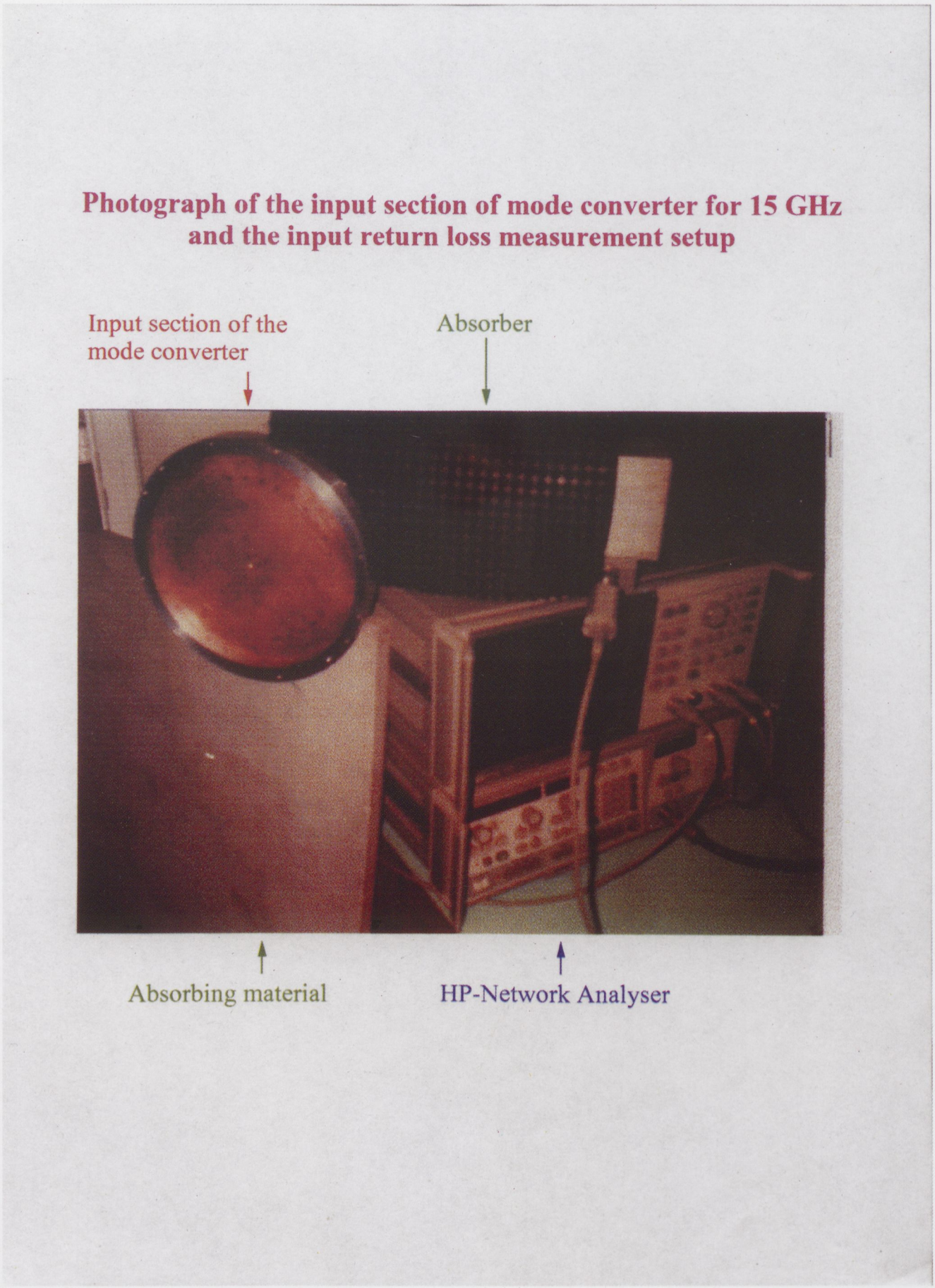

Fig. 20. Input return loss measurement setup.

Photograph of the 15 GHz-model of coaxial TEM to circular $TE_{16,2}$ mode converter using microstrip-slot antenna exciter

Input section, consisting of:
- housing with SMA conn.
- MSSA-exciter
- space keeper ring

Space-keeper ring
with the dimensions of
∅ 250 / ∅ 222 x 13 mm

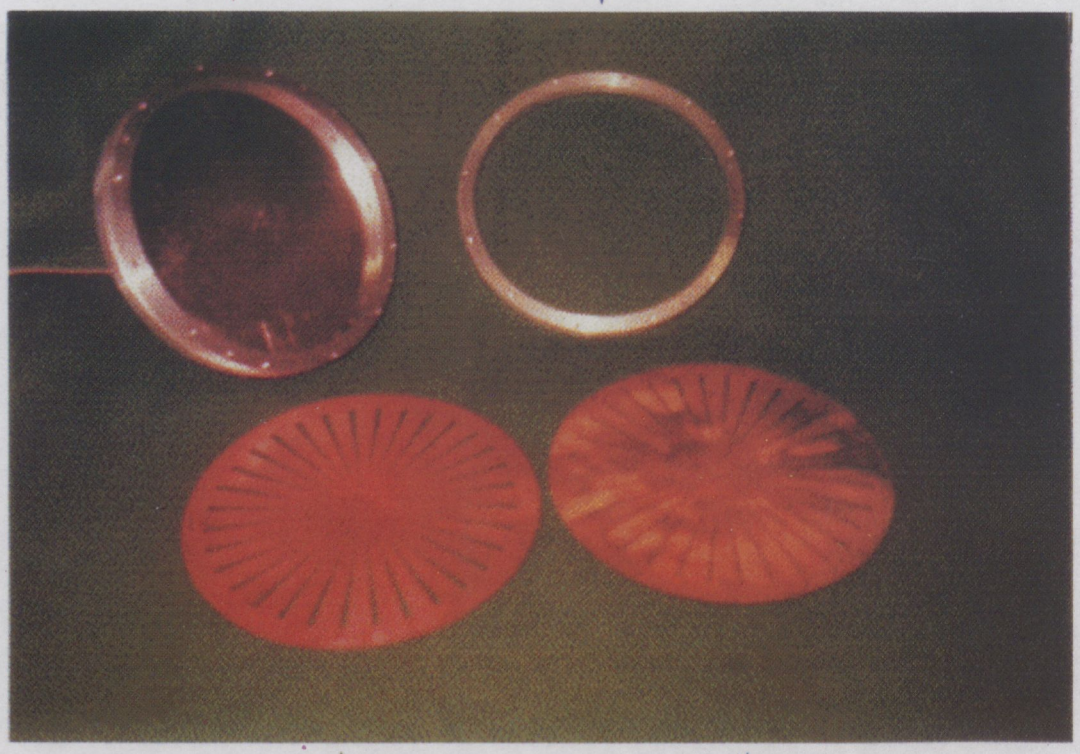

Copper diaphragm with the opening of 3.6° and with the dimensions of ∅ 250 x 0.2 mm

Copper diaphragm with the opening of 1.8°

Fig. 21. Input section of the 15 GHz model of WGM-converter.

Iris with coupling slots 1.8° for 38 GHz MSSA-excited mode converter (metallization is gold)

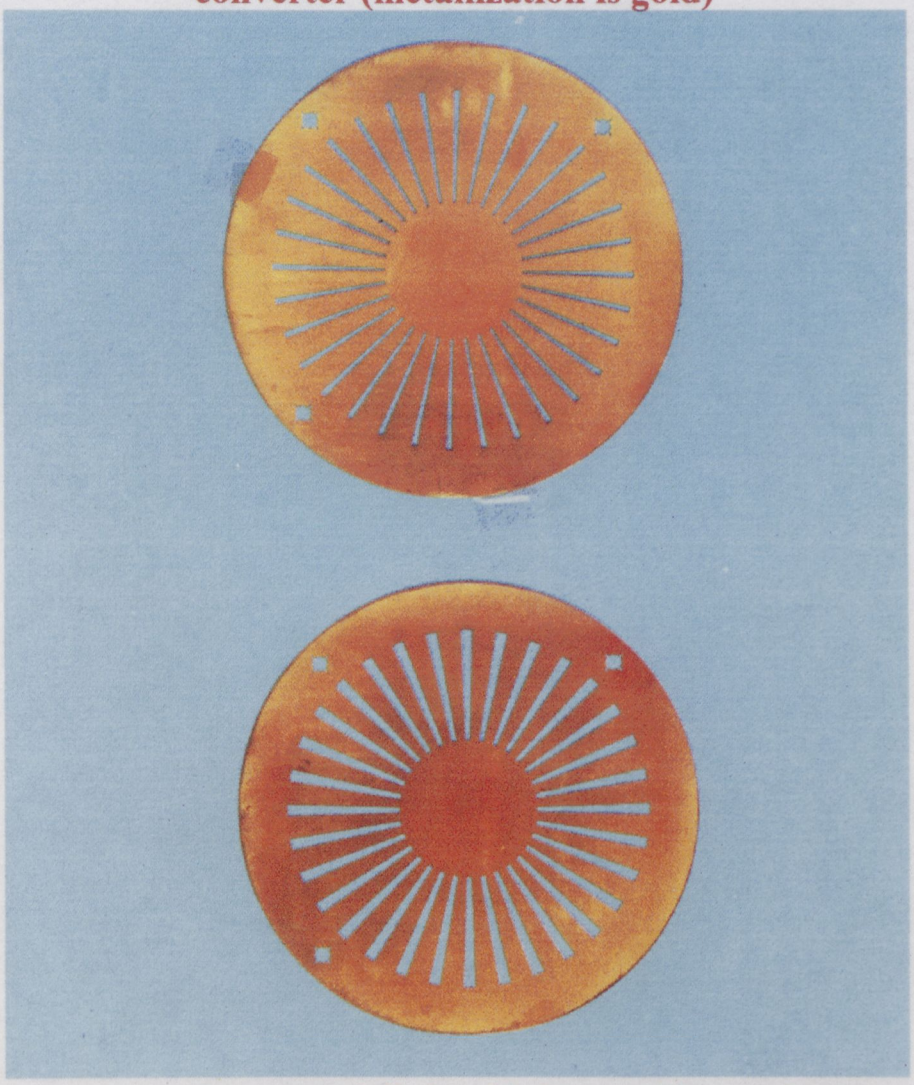

Iris with coupling slots 3.6° for 38 GHz MSSA-excited mode converter (metallization is gold)

Fig. 22. Gold-plated diaphraghmas of the 38 GHz model of MSSA-excited mode converter.

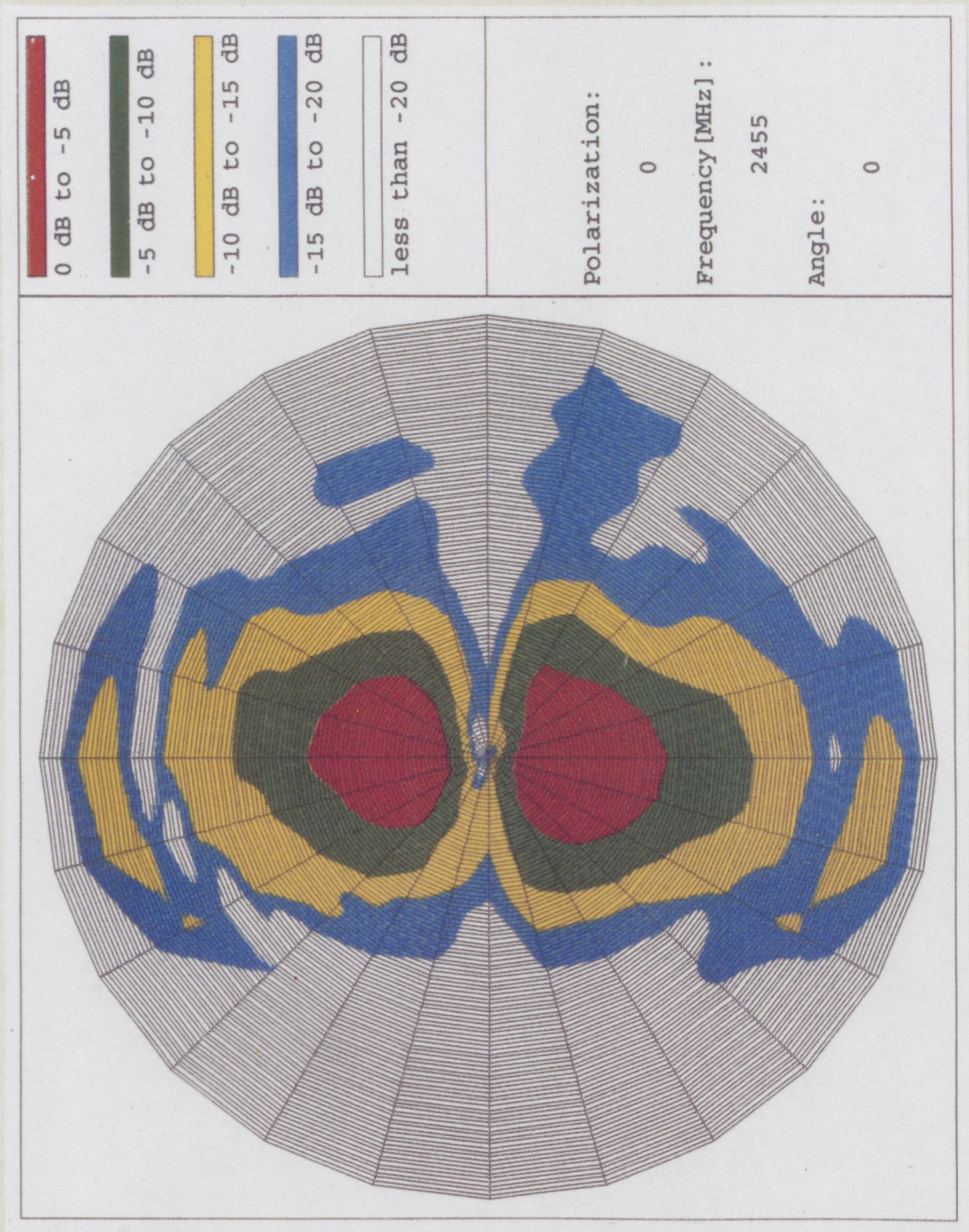

Fig. 8. Measured radiation pattern of Model S.3.

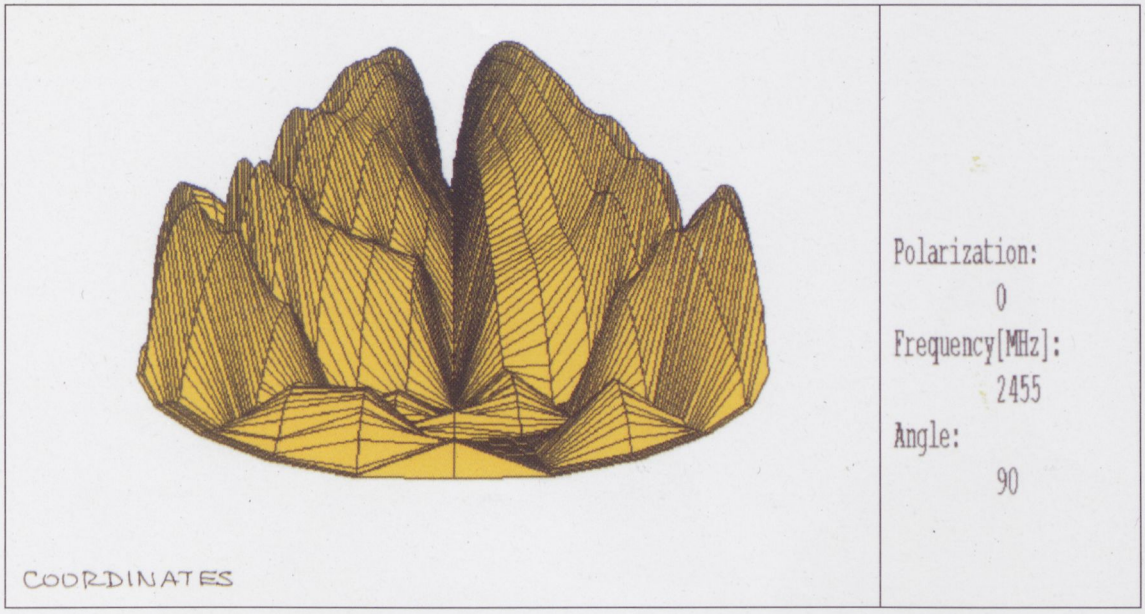

Fig. 13. Stereoscopic radiation of Model S.3, depicted in cyclyndrical coordinates.

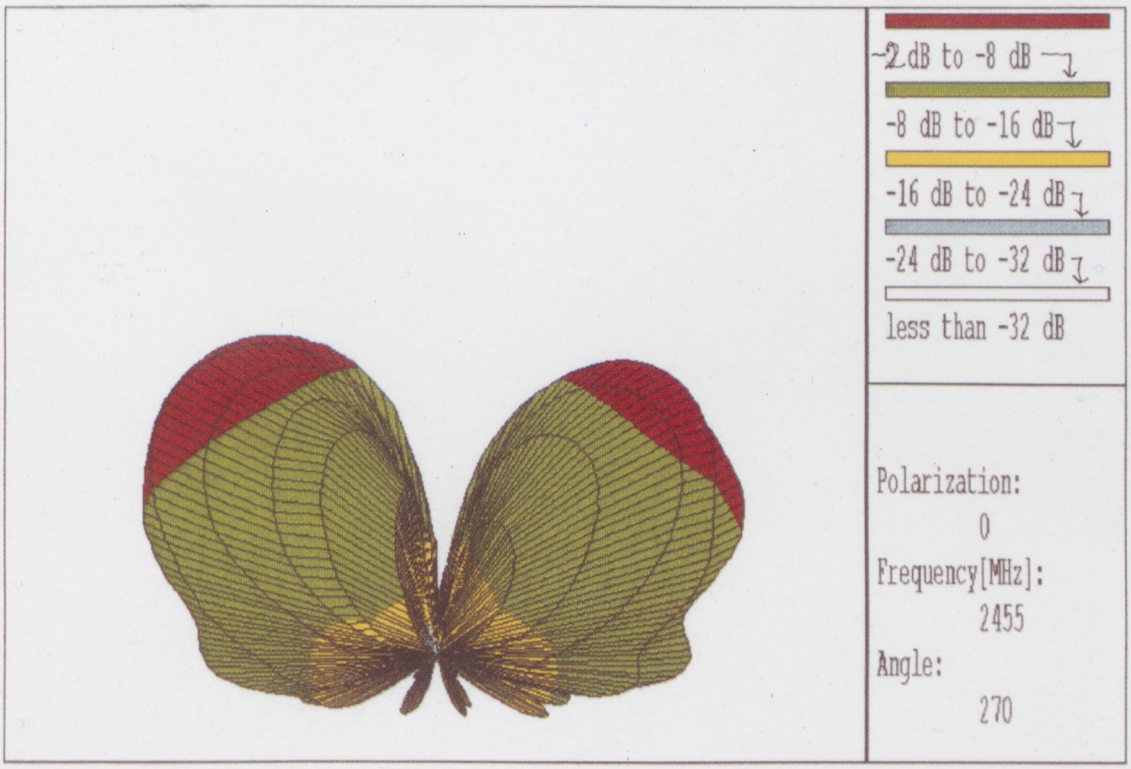

Fig. 14. Stereoscopic radiation of Model S.3, depicted in spherical coordinates.

Fig. 2. A GTEM Chamber with the new cell structure absorber.

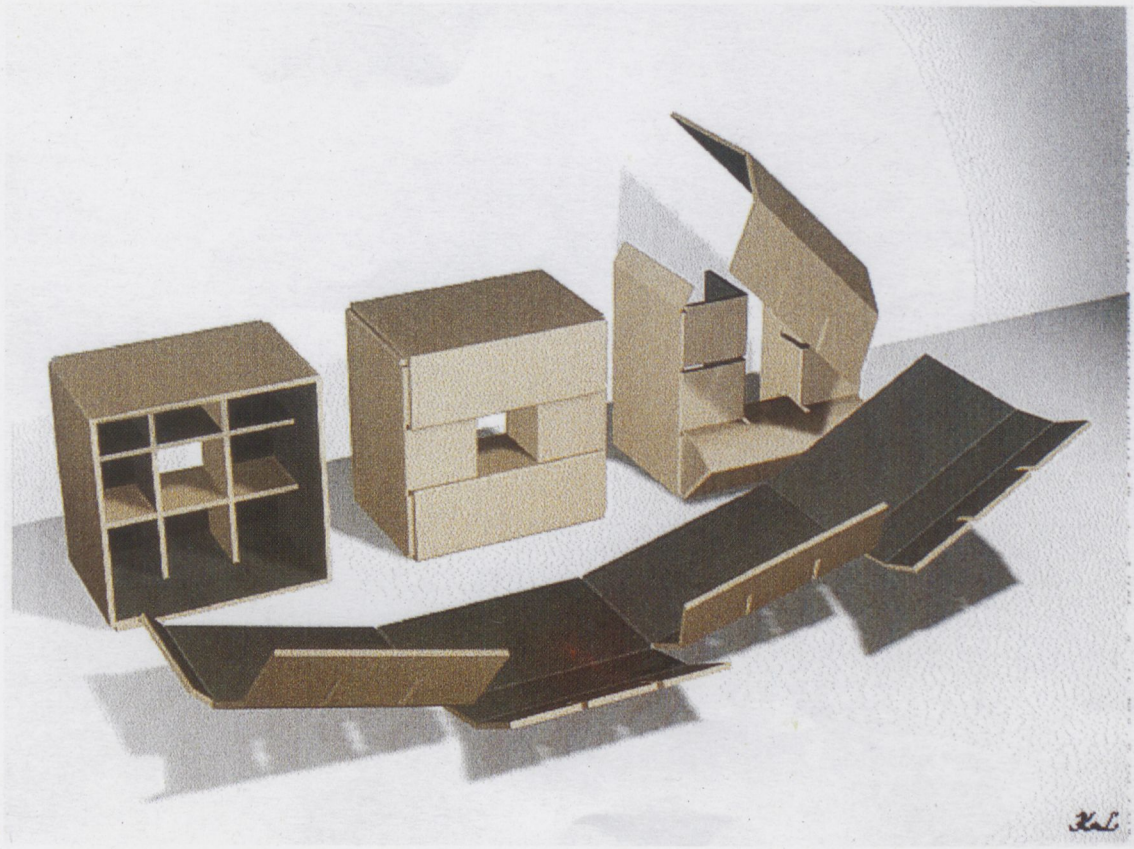

Fig. 3. Construction of an absorber cell.

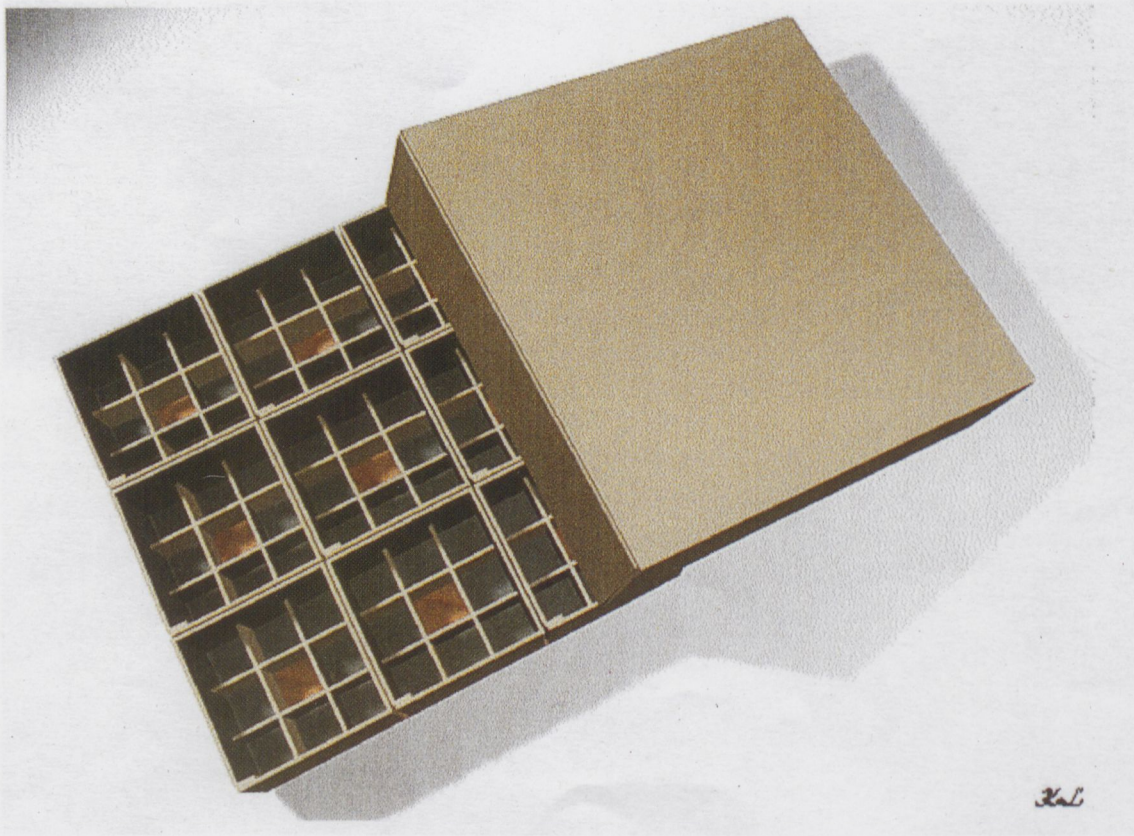

Fig. 4. Construction of the 9-cells absorber.

Fig. 5. Anechoic chamber using our absorbers (suggested for EMC tests in the 80-1000 MHz frequency band)

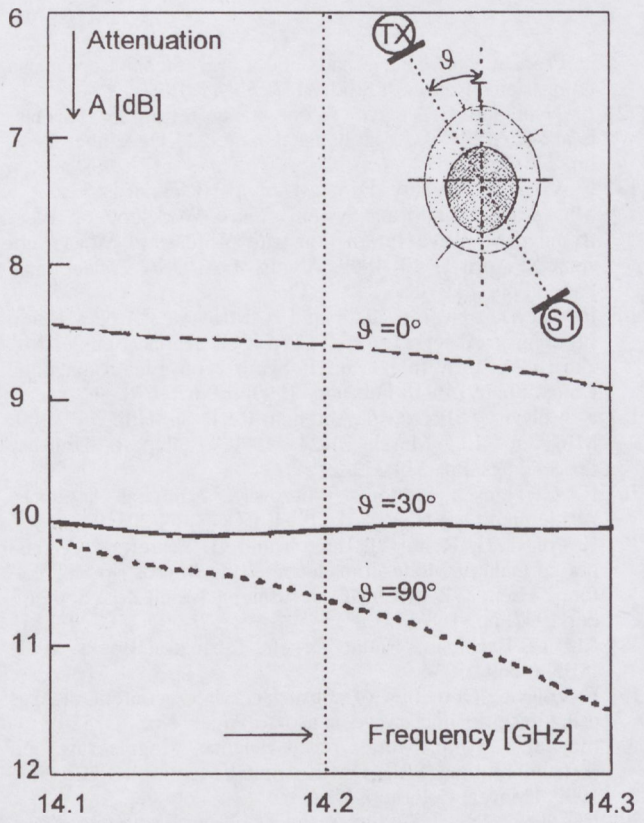

Fig. 16. Measured attenuation of egg versus frequency, where the parameter is the angle of incidence

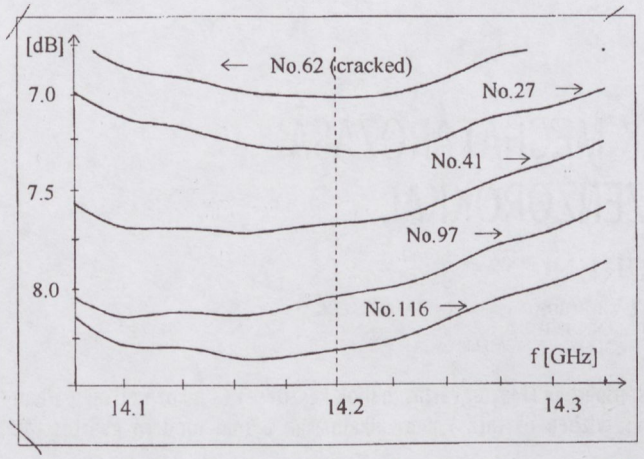

Fig. 17. Measured attenuation versus frequency with zoomed dB scale

The *Fig. 18* shows the recorded attenuation curves obtained with continuously moved (by hand) egg-holder. It can be seen well that the measured attenuation is inversely proportional to the age of eggs passing under the antenna.

The calculated and measured attenuations at the frequency of 14.2 GHz were between 7.5 and 10.5 dB, depending on the dimensions and the ages of eggs. These results show that the very simple attenuation-model seems to be useful.

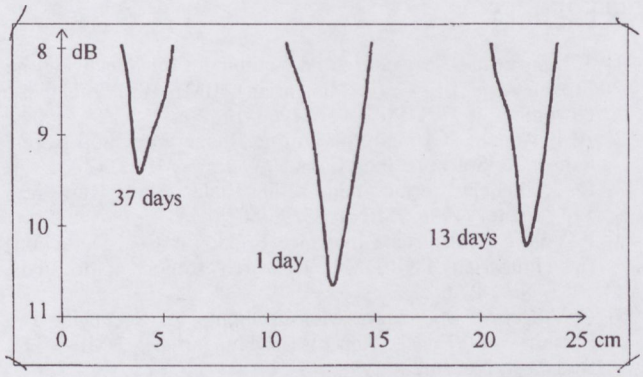

Fig. 18. Recorded attenuation curves versus position, for eggs having the same dimensions, but different ages.

5. CONCLUSIONS

The ability to observe the variations of the egg's water content with age has been verified by microwave sensors operating automatically. They can provide a very useful tool for observing the temporal variations of the subsurface properties of eggs, namely the age of eggs, which is important in food industries and at production of cosmetics.

The results of chemical and physico-chemical measurements of eggs given in the first part of this paper show significant variation with age at ammonia content and viscosity, but the decreasing of water content is the most useful information from the aspect of microwave measurement. At the frequency of 14.2 GHz the measured attenuation for fresh egg is $A = 8 - 10$ dB, the variation with time is dA [dB] $= -0.033T$ [days], so nearly -1 dB/30 days. The uncertainty of the RCS-measurement shows that the direction of egg's bottom has to be avoided. The measured RCS from near to the top of egg shows good accuracy.

We are planning to make further measurements for the change of attenuation of the same egg and for the change of attenuation of many eggs in the mean value with the width of the dispersion.

For the near future we plan to develop a microwave equipment for the automatic selection of old eggs. Using this equipment the quality-control of eggs is very quick ($\sim$ 1 msec/egg) in contrast to the traditional method, where weighing and volume determination e.g. by light gate is performed.

ACKNOWLEDGEMENTS

The author is extremely grateful for the help that he received the chemical laboratory results from Dr. J. Nagy.

REFERENCES

[1] J. Nagy et al.: "Procedure and Equipment for Specifying the Freshness of Eggs " (in Hungarian), BME-BET, Budapest, November 1997, OMFB-05677960416.

[2] A. P. Annan: "Ground Penetrating Radar Workshop Notes" Sensors & Software Inc., Canada, October, 1992, 127 p.

[3] D. J. Daniels: Surface Penetrating Radar, Short Run Press Ltd., Exeter, 1996, ISBN 0 85296 862 0.

[4] F. Völgyi: "Subsurface Interface Radar for Coal-Detection" (in Hungarian),TUB/DMT, Research Report, November, 1987, No. 427.085/87

[5] F. Völgyi: " Microwave Measurements for Specifying the Freshness of Eggs", Report (in Hungarian), BME-MHT, Budapest, November 1998.

[6] F. Völgyi: "Microwave Measurements for Specifying the Freshness of Eggs" Third Workshop on Electromagnetic Wave Interaction with Water and Moist Substances, April 11-13, 1999, Athens, GA, USA pp. 52-56.

[7] F. Völgyi: "Versatile Microwave Moisture Sensor" SBMO'89 Int. Microwave Symp. Brazil, Sao Paulo, 24-27 July 1989. Proc. Vol-II pp. 456-462.

[8] F. Völgyi: "Integrated Microwave Moisture Sensors for Automatic Process Control" Ch. 15. in book: "Microwave Aquametry" (ed. A. Kraszewski), ISBN 0-7803-146-9, IEEE Press, New York, 1996, pp. 223-238.

[9] F. Völgyi et al.: "Treatment and Instrument for Measuring of Substances, Advantageously Applied for Moving, Multilayer Materials" (in Hungarian), Patent, June 1996, MSzH-P 9601630.

[10] Beke J. and F. Völgyi: "Interactions of Kernel Features and Field Parameters in Microwave Drying of Corn" APMC'96 Asia-Pacific Microwave Conference, New Delhi, India, December 17-20, 1996, pp. 383-386.

[11] F. Völgyi: " Polarimetric Measurements of Grain Permittivity in Free Space Using Small- and Large Signal Levels" (in Hungarian), Research Study, TUB/DMT, 1997.

[12] L. Nyúl and F. Völgyi: "Contactless Testing of Particleboards", APMC'98, Yokohama, Japan, 8-11 December 1998, pp. 213-216.

[13] F. Völgyi: "Quality Forecast of Particleboards Using a Microwave Monitoring System" Third Workshop on Electromagnetic Wave Interaction with Water and Moist Substances, April 11-13, 1999, Athens, GA, USA Collection of Papers, pp. 102-106.

[14] F. Völgyi, L. Nyúl, S. Tatár and A. Mrovcza: "A New Radio Frequency Absorber for GTEM Cell Applications" EMC Zurich'99, 13th Int. Zurich Symp. on Electromagnetic Compatibility, 16-18 February 1999, pp. 675-678.

[15] F. Völgyi: "Microstrip Antenna R&D in Hungary" 10th MICROCOLL, March 21-24, 1999, Budapest, Hungary Proceedings, pp. 249-252.

[16] R. C. Hansen (editor): Microwave Scanning Antennas, Academic Press, New York, 1964, CCCN: 64-20319.

[17] F. Völgyi, G. Reiter, T. Berceli and G. Veszely: "A Whispering Gallery Mode Transducer Using Microstrip-Slot Antenna Exciter" 27th EuMC, Jerusalem, Israel, 8-12 September 1997, pp. 168-174.

[18] Ch. G. Bachman: Radar Targets, Lexington Books, 1982, ISBN 0 669 05232 9.

[19] F. Völgyi: "Detection of subsurface water content of eggs using bistatic microwave sensors" Paper No. 3752-08 at the Int. Symp. on Optical Science, Engineering and Instrumentation (SPIE's 44th Annual Meeting), 18-23, July 1999, Denver, Colorado, USA.

[20] F. Völgyi: "Specifying the freshness of eggs using microwave sensors", Subsurface Sensing Technologies and Applications, an International Journal, Vol. I, No. 1, January 2000, Kluwer Academic/Plenum Publishers, New York, USA.

TOJÁSOK MINŐSÉGÉNEK MEGHATÁROZÁSA MIKROHULLÁMÚ SZENZOROKKAL

VÖLGYI FERENC

BUDAPESTI MŰSZAKI EGYETEM, MIKROHULLÁMÚ HÍRADÁSTECHNIKA TANSZÉK
1111 BUDAPEST, GOLDMANN TÉR 3.
TEL.: 36 1 463 1559; FAX: 36 1 463 3289; T-VOLGYI@NOV.MHT.BME.HU

A tyúktojások minőségének, frissességének nagy jelentősége van az élelmiszeriparban (tésztagyártás, habok készítése) és a kozmetikai iparban egyaránt. Az ezek vizsgálatára használt jelenlegi módszerek (átvilágítás, vízben úsztatás) nem alkalmasak a mai modern gyártósorok kiszolgálására.

Érdekes megoldást kínál a roncsolásmentes, érintkezésmentes anyagvizsgálatok köréből a jelen cikkben bemutatott mikrohullámú mérési elrendezés, melynek alapján készítendő ipari berendezés ezredmásodpercek alatt képes egy-egy tojást ellenőrízni és a nem friss tojásokat kiemelni, mielőtt az automatizált gyártósorra kerülnének.

A BME MHT-n kidolgozott, ezen cikkben leírt kísérleti mérőrendszer három kisméretű nyomtatott antenna, egy 14,2 GHz frekvenciájú, mindössze 1 mW teljesítményű oszcillátor és két Schottky-diódás detektor felhasználásával a tojás ún. bisztatikus radar hatásos keresztmetszetét és a rajta áthaladó mikrohullám csillapítását méri. Ezen adatokból következtetni lehet a tojás méretére és korára (frissességére). Előzetesen a BME Biokémiai és Élelmiszer-technológiai Tanszékén végzett fiziko-kémiai vizsgálatok [1] kimutatták, hogy a tojás 30 nap alatt átlagosan 20 %-ot veszít víztartalmából, ez pedig 1 dB csillapítás-csökkenésnek felel meg mikrohullámon.

A fontosabb elméleti összefüggések megadása után a frekvencia, az antennák és a mérési elrendezés kiválasztásának szempontjai, végül a reflexió- és csillapításmérés eredményei kerülnek ismertetésre, számos ábrával illusztrálva.

MSSA-EXCITER USING AS A WHISPERING GALLERY MODE TRANSDUCER*

FERENC VÖLGYI

TECHNICAL UNIVERSITY OF BUDAPEST
DEPT. OF MICROWAVE TELECOMMUNICATIONS
H-1111 BUDAPEST, GOLDMANN TÉR 3, HUNGARY
PHONE: 36 1 463 1559; FAX: 36 1 463 3289; T-VOLGYI@NOV.MHT.BME.HU

A mode transducer is described which generates a whispering gallery mode output with a coaxial TEM mode input. The low-power device will be used for cold-test measurements of a high power gyrotron at 140 GHz. The basic idea, design, experimental model measurement data at 15 GHz, and the design of a new model for 38 GHz are given for the $TE_{16,2}$ transducer using microstrip-slot antenna (MSSA) exciter.

1. INTRODUCTION

It is necessary to operate the high power gyrotrons in high order TE modes (*whispering gallery mode: WGM*) to keep the cavity ohmic losses at an acceptable level, Kreischer et al [1]. A WGM is defined as a TEmn mode with its azimuthal index (m) much greater than its radial index (n). For R&D of gyrotrons, the study of the WGM-fields are sometimes needed (cold-test measurements). Different mode transducers and converters are used for this purposes, Moeller [2], Reiter [3], Völgyi [4] and Völgyi et al [5].

Microstrip antenna arrays draw increasing interest due to their flat profile, low weight, ease of fabrication and low cost. Planar configurations are used for microwave heating at Völgyi [6], in automatic process control at Völgyi [7], and for WLAN-systems at Völgyi [8]. Before the realization of a mm-wave array, scaled models are designed and measured at lower frequencies. Two of these models will be introduced, which are microstrip-slot antenna (MSSA) structures and they are used for exciting of WGM in an overmoded circular waveguide, the first at 15 GHz, and the second at 38 GHz.

The *paper is organized* as follows: the equations of electric field components for $TE_{16,2}$ circular mode are reviewed in the first section, after showing the mechanical structure of the transducer the network model and experimental results for the 15 GHz model are presented in the next section, followed by the design of a new model for 38 GHz and concluding remarks are given in the last section.

2. ELECTRIC FIELD COMPONENTS OF $TE_{16,2}$ CIRCULAR MODE

Assuming a circular-cylindrical coordinate system described by (r, φ, z) then the *transversal electric components of the field of a $TE_{16,2}$ WGM* (neglecting the $\exp(j\omega t)$ time dependence) may be written as:

$$E_\varphi = C_1 J'_{16}(a'_{16,2} r/r_0) \cos(16\varphi) \exp(-j\beta z); \quad (1)$$

$$E_r = C_2 \frac{J'_{16}(a'_{16,2} r/r_0)}{r/r_0} \sin(16\varphi) \exp(-j\beta z), \quad (2)$$

where: C_1 and C_2 are constants, $J_{16}(\,)$ and $J'_{16}(\,)$ are the Bessel function and the derivative of Bessel function, $\beta = 2\pi/\lambda'$ and λ' is the wavelength in $TE_{16,2}$ mode. The value of $a'_{16,2} = 23.264$ is the second root of the $J'_{16}(a'_{16,2}) = 0$ equation. With the cut-off-wavelength of λ'_c, the desired radius of circular-waveguide is:

$$r_0 = a'_{16,2} \frac{\lambda'_c}{2\pi}. \quad (3)$$

Fig. 1 shows the $J_{16}(23.26r/r_0)$ and $J'_{16}(23.26r/r_0)$ Bessel functions versus r/r_0. Using equations (1) and (2), from *Fig. 1* we can establish:

$E_\varphi = 0$ at $r/r_0 = 1$ and $r/r_0 = 0.77$, and $\varphi = \pi/32$ and $3\pi/32$, where E_r have maxima with opposite signs;

$E_r = 0$ at $\varphi = 0;\ \pi/16$ and $\pi/8$,

where E_φ have maxima.

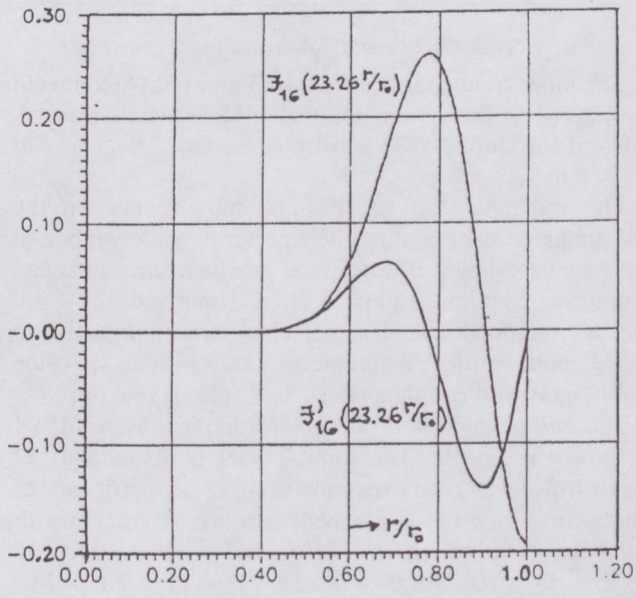

Fig. 1. Bessel functions in eq. (1) and (2).

At last we establish, that we can split the cross-section of circular waveguide to sixteen uniform sectors with the same values of tangential electric components, viz. inside

* This is an extend of the paper presented by F. Völgyi in Jerusalem, Israel at 27th EuMC, 1997 [14].

of a $\pi/8$ sector the relative phases are opposites (positive and negative) in radial (r) direction and in azimuthal (φ) direction, too. This is shown in *Fig. 2.*

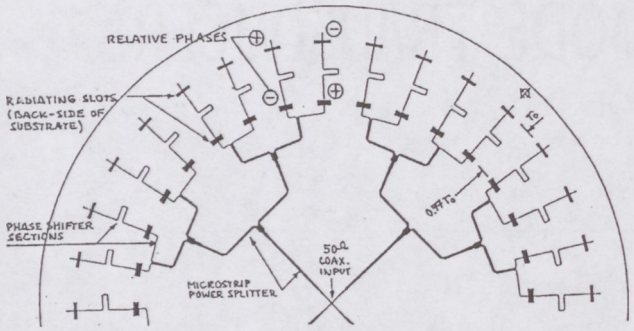

Fig. 2. The half-photomask of the microstrip circuit of MSSA.

3. TEM - $TE_{16,2}$ MODE CONVERTER USING MSSA

The *schematic of the 15 GHz model* of our mode converter is shown in *Fig. 3*, where $\lambda_m (= 15.4$ mm) is the wavelength in the $Z_0 = 140\Omega$ microstrip line, $\lambda_0 (= 20$ mm) is the freespace wavelength and $\lambda' (= 26.85$ mm) is the guided-wavelength in $TE_{16,2}$ circular-waveguide mode with $r_0 = 111$ mm.

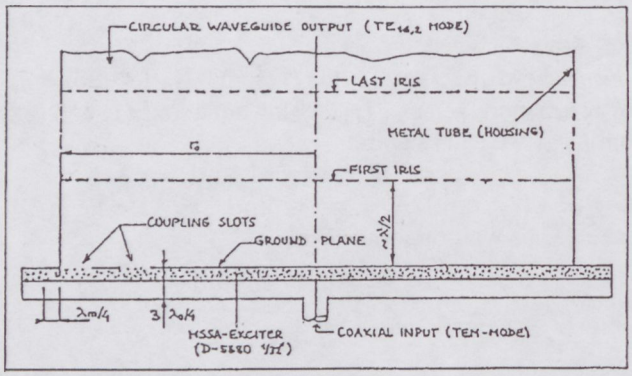

Fig. 3. Schematic of the MSSA-excited mode converter.

The inner conductor of the coaxial-input SMA-connector is soldered to the center point of MSSA-exciter, which is realized on Duroid-5880 substrate, having a thickness of 0.794 mm.

The radiating slots of this antenna are cut on the ground-plane side, exciting the whispering-gallery mode of the circular-cylindrical waveguide in which this mode can propagate. Slot dimensions: 1.4×7.1 mm and 2.5×6.0 mm are, respectively. Transfer characteristic and the so called mode purity requirements are satisfied by using diaphragms with coupling-slots: $1.8°$ (*Fig. 4*) and $3.6°$.

The *half-photomask of the microstrip circuitry of MSSA* is shown in *Fig. 2.* The input power is directed to 32 microstrip-slot antenna sections using a microstrip power splitter, in which the line impedances are (from center to the open circuited end): $157' - 96' - 76 - 63.9' - 45.2' - 38 - 76 - 63.9' - 45.2' - 38 - 76 - 73' - 140$ Ohms, respectively, where the upper mark (') means the transformer section with the length of quarter wavelength $(\lambda_m/4)$.

Appropriate relative phases between slots are set by the designated phase shifters.

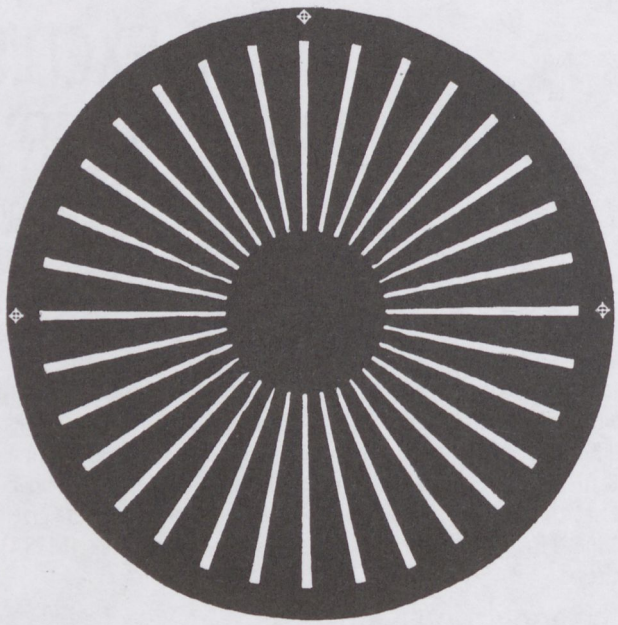

Fig. 4. Iris with the openings of 1.8 degree.

4. THE NETWORK MODEL

Perfect symmetry of the microstrip-slot antenna is supposed, i.e. only the modes of 16k azimuthal mode number (k is odd) will be excited. The waveguide is dimensioned so, that only the modes with the suffices $m = 16$; $n = 1, 2, 3$ can propagate. Using the results of Reiter [9], [10], [11] the network model of the transducer can be constructed (*Fig. 5*). The voltage generator on the left side models the source coupled to the coaxial input. The distributor network symbolizes the mode converter effect of the microstrip-slot antenna: it transforms the voltage into the transmission lines corresponding to the propagating modes and into the lumped reactances corresponding to the cut-off modes respectively. The coupling circuit parts model the mode-coupling effect of the irises. If we use the irises of *Fig. 4*, then according to the orthogonality relations no mode coupling occurs between the modes of the same azimuthal mode suffix. Consequently the upper part of the coupling circuit (belonging to the $TE_{16,2}$ mode) is separated from the lower one.

The transmission lines attached to the other propagating modes can be found in the lower branch, the lengths of these are strongly differ from the half wavelength. The experiences of network calculations show the networks containing transmission lines of lengths differ strongly from the half wavelength are not suitable for signal transmission and their input impedance is pure reactive. Thus through the distributor network the reactances of the lower branch can be drawn into the first two-pole created at the input of the upper branch. Similarly the coupling networks loaded by reactances in the upper branch can be transformed to reactive two-poles. Finally a network is given as the equivalent network of the transducer in which the reactive two-poles are connected to each other by transmission lines attached to the $TE_{16,2}$ mode and of length approximately of half wavelength.

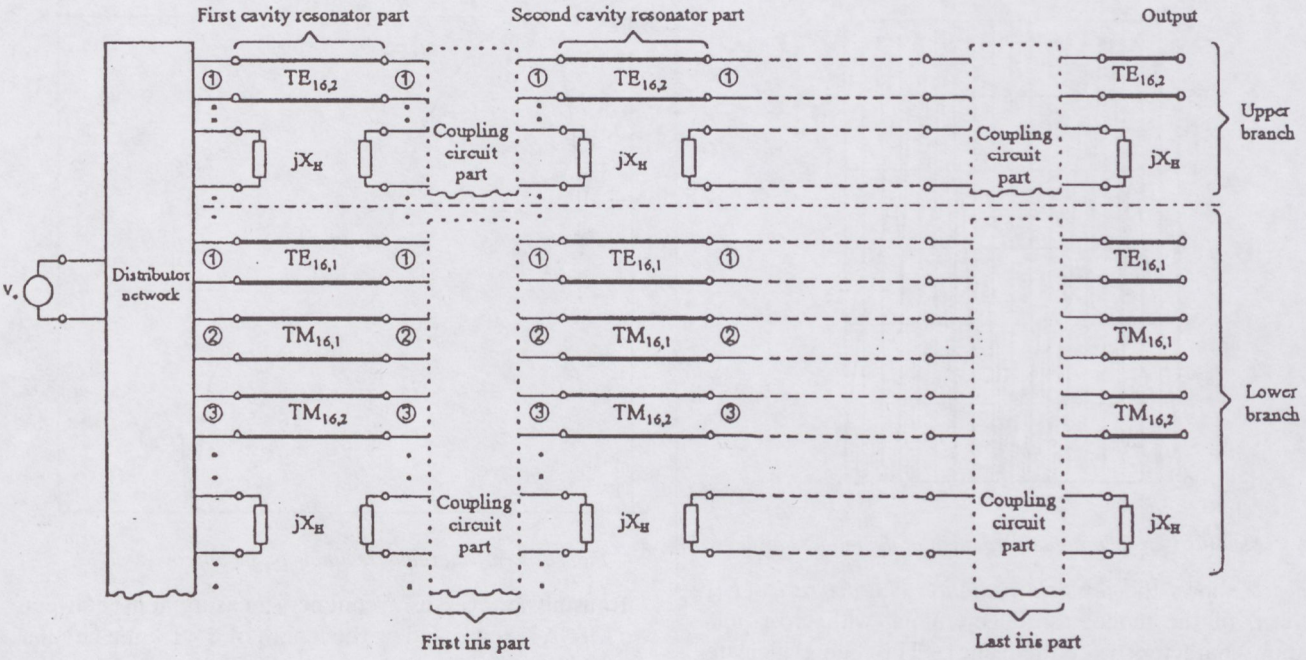

Fig. 5. The network model of the transducer.

If the transmission and reflection measurements are in accordance to this model, then the transducer is mode-pure.

5. EXPERIMENTAL RESULTS

Near-field probing, which is done at distances of millimetres from the MSSA, served as a diagnostic tool in the design and the prototype production stages of the mode converter. Single-element rectangular microstrip patch, miniature dipole with split-coaxial balloon made from semi-rigid cable and a small loop for magnetic-field probing were used for these purposes. Radial and azimuthal scanning of E_r component are shown in *Figs. 6* and *7*. The measured result is in good agreement with the theoretical curve, given in *Fig. 1*. At the radius $r < 55$ mm, the measured value is lower than 22 dB (0.63 %) for the suppressed mode with the index of $n = 1$. Using an absorber phenolic rod less than half the waveguide diameter, this would be vanished, according to the results of Moeller [2].

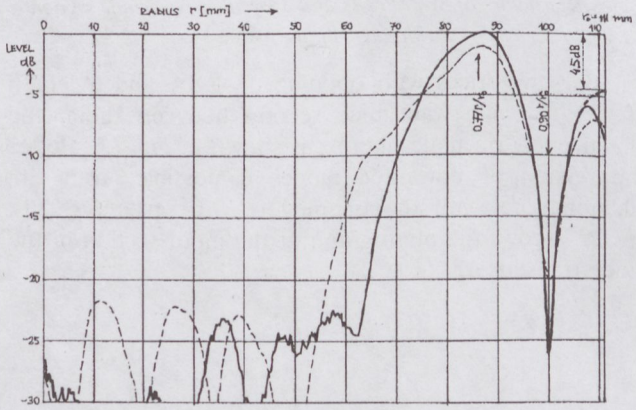

Fig. 6. Radial scanning of the E_r-component.

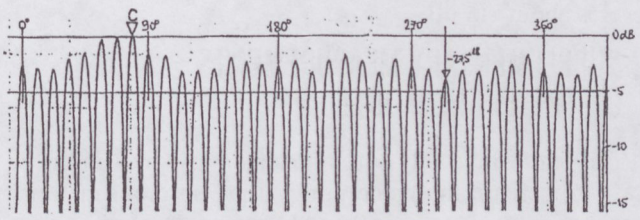

Fig. 7. Azimuthal scanning of the E_r-component.

Fig. 8 shows the *transmission characteristic of closed structure* using two mode-transducers (dotted line) and diaphragms (continuous line). The effectiveness of the mode filtering element is 12 – 20 dB, in the frequency range of 13.5 – 16 GHz.

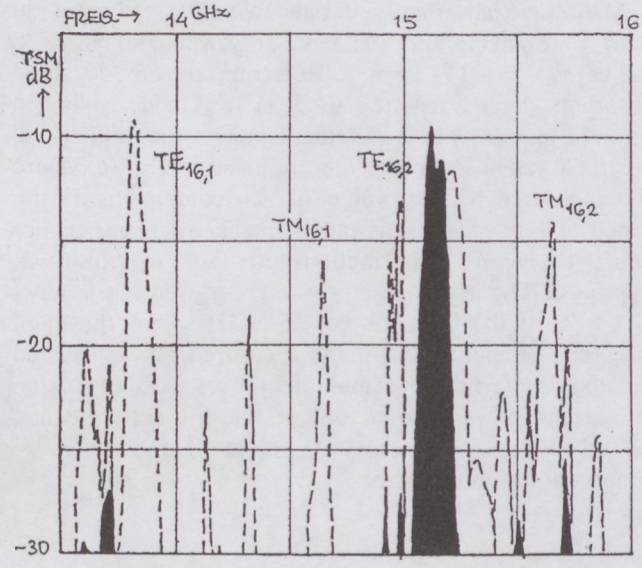

Fig. 8. Measured transmission characteristic of closed structure (black shadowing: using irices).

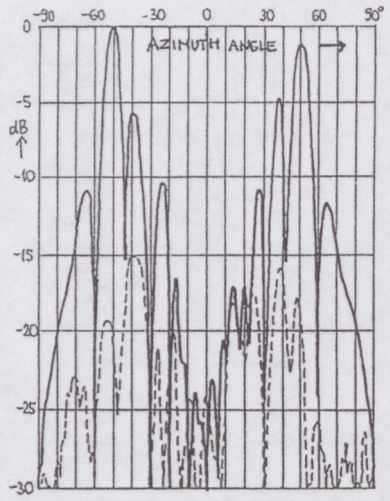

Fig. 9. Measured far-field radiation pattern of the mode transducer.

Fig. 9 shows the *far field radiation characteristic* (E_Θ-pattern) of the mode transducer, along with cross-polarization characteristic (dotted line). This figure indicates the absence of other radial modes having m = 16. In addition, there is evidence of an $m = 1$ component at the -30 (-25) dB level. The measured cross-polarization level is about -15 dB.

6. SUPPLEMENTARY MEASUREMENTS OF THE 15 GHZ MODEL

The motivation of our supplementary measurement was: to increase the mode purity using absorber material (mentioned at Moeller [2]) and making a more correct filter-section according to Reiter [3] using the methods of network theory.

All these experiences were utilized in our new design at 38 GHz. The complete microstrip-slot antenna exciter has been designed with the aid of microwave CADs (MMICAD from Optotek Ltd. and the software of Sainati [12]).

Microwave absorber materials (with the radius of 50 mm) were taken into the circular waveguide having a radius $r_0 = 111$ mm. Referring to *Fig. 1*, these absorbers don't affect the used $TE_{16,2}$ mode, only the parasitic modes with lower mode-indices are influenced. Nearfield radial scanning data are given in *Fig. 10*, where the measured relative value of E_Θ-component at the range of $r < 50$ mm is much smaller than our earlier limit (see *Fig. 6*). The input return loss (L_R) also was improved. The expected improvement in transmission loss is 1.4 dB at the frequency of 15.1 GHz. For the open structure of input MSSA, the measured and calculated radiation patterns show small differences, because of the measurement was carried out in the Fresnel zone and in the reflective laboratory-environment, and there are supposed positioning errors.

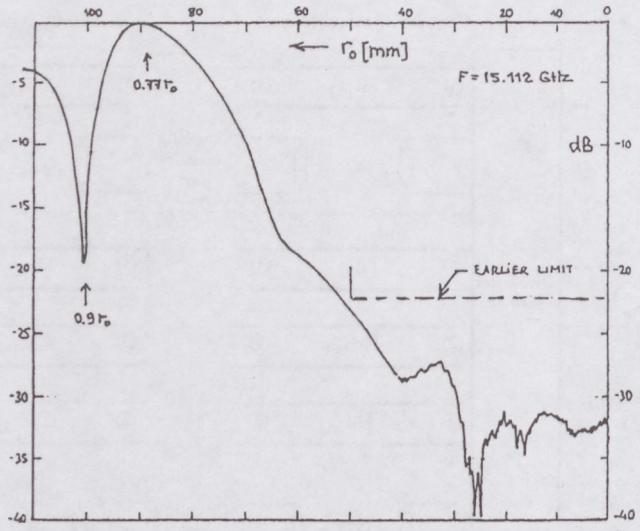

Fig. 10. Nearfield radial scanning of the improved model.

Transmission versus frequency measurement between two MSSA-s, separated by the length of 3×13 mm circular waveguide section is shown in *Fig. 11*. The expected modes are also designated, supposing that ($\lambda g = 26.3$ mm at all frequencies for the different modes. We can conclude: the microstrip-slot antenna type exciter is a relatively broadband structure, having significant coupling not only for the desired $TE_{16,2}$ mode, but at other frequencies for the unwanted $TE_{16,1}$ and $TE_{16,3}$ mode, too.

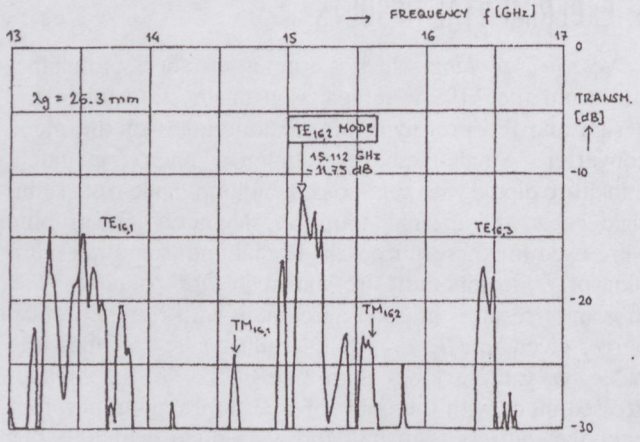

Fig. 11. Measured transmission loss vs. frequency characteristic for closed structure of two MSSAs and a circular waveguide section with a length of 39 mm.

Using two irices with opening of 1.8°, and a length of 3×13 mm waveguide section between them, the effectiveness of mode filtering is shown in *Fig. 12*. Better suppression of unwanted modes is possible, using an additional iris with the opening of 3.6° (see *Fig. 13*). *Fig. 21** shows the photograph of the input section of the mode transducer.

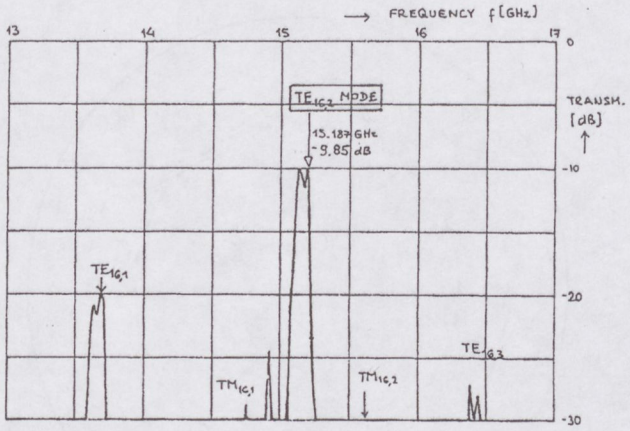

Fig. 12. Mode filtering using 2 × 1.8° irices and a circular waveguide section with a length of 39 mm.

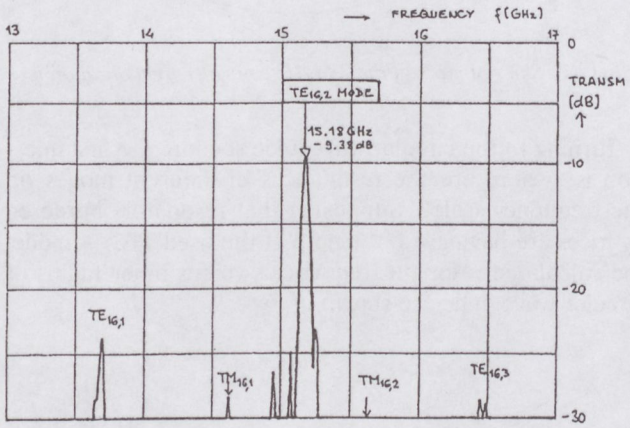

Fig. 13. Mode filtering using irices: $1.8° - 1.8° - 3.6°$

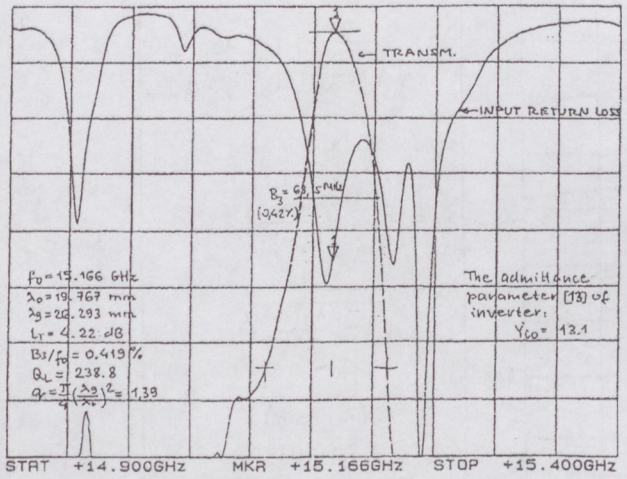

Fig. 14. Input return loss and transmission loss measurements.

To gain equivalent circuit parameters from Reiter [13] of our structure, we have measured transmission characteristics with expanded frequency scale. *Fig. 14* shows the measured diagram for the closed structure of two MSSA-s and one iris (1.8°). The parameters (calculated from measurement) are also given. *Fig. 15* shows the transmission versus frequency characteristic of the closed structure having two MSSA-s, two irices (1.8°) and a waveguide section with the length of 3 × 13 mm. The input return loss measurement set-up is shown on the photograph in *Fig. 20**.

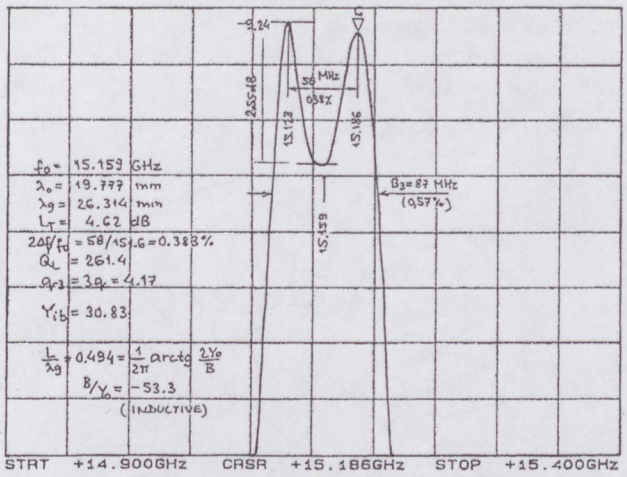

Fig. 15. Measured transmission loss vs. frequency characteristic using $2 \times 1.8°$ *irices.*

7. DESIGN OF A NEW MODEL FOR 38 GHZ

Starting from our basic MSSA-exciter shown in *Fig. 2*, we have changed:

- the impedance level of microstrip lines exciting two slots for $Z_0 = 110\Omega$,
- the length of these lines, shortening them, having the phaseshift of 180° directly between slots, using equation: $3\lambda_m/2 = r_0(1 - 0.77)$, where $r_0 = 39.09$ mm is the radius of our new highly overmoded circular waveguide,
- the input section of the microstrip power-splitter, having impedances of $100°\Omega$, so the input impedance is $100\Omega/4 = 25°\Omega$, which is transformed to $50°\Omega$ inside of the coaxial input section.

In our new design, the impedances from center to the open end:

$$[50 - 35.3' - 25] - 100 - 87.2' - 76 - 53.7' - 76 - 64.7' - 110\Omega$$

are, respectively, where the upper mark (') means the transformer section with the length of quarter wavelength $(\lambda_m/4)$. The selected substrate material was D-5880-10 mil. *Figs. 16* and *17* show the microstrip power-splitter and radiating-slot side of the substrate used for MSSA-exciter at 38 GHz. Slot dimensions: 0.4×2.86 mm and 0.7×2.54 mm are, respectively. The mode purity requirements of the converter is satisfied by using irices with coupling slots 1.8° and 3.6°. To optimize the input section of power splitter a control circuit is designed and will be measured.

The calculated loss (dielectric and copper loss only) versus frequency characteristic is shown in *Fig. 19*. The dotted line shows the calculated values with $\mathrm{tg}\delta = 0.0012$, the continuous line is calculated with a more realistic $\mathrm{tg}\delta = 0.0045$. There are other components of the total loss, too. With approximate values, there are given below:

- extra loss from rough surface of microstrip lines (etching!): $0.8 - 1.2$ dB
- surface waves of substrate: $0.5 - 1$ dB

- radiating loss of discontinuities: ≈ 1 dB
- loss of: input coaxial connector, coaxial-microstrip transition, circular waveguide section, contact at irices, radiating slots, etc. $2.5 - 3$ dB
- calculated loss of the feed network 0.8 dB

So the total loss, to be expected: $\sum L = 5.6 - 7.0\ dB$

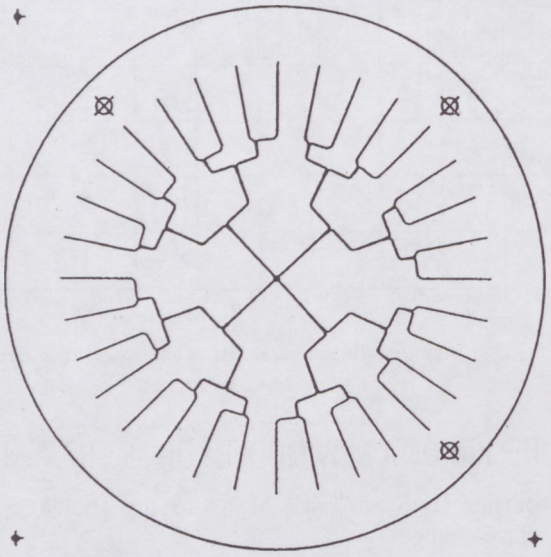

Fig. 16. Microstrip power splitter for MSSA-exciter at 38 GHz (metallization is black).

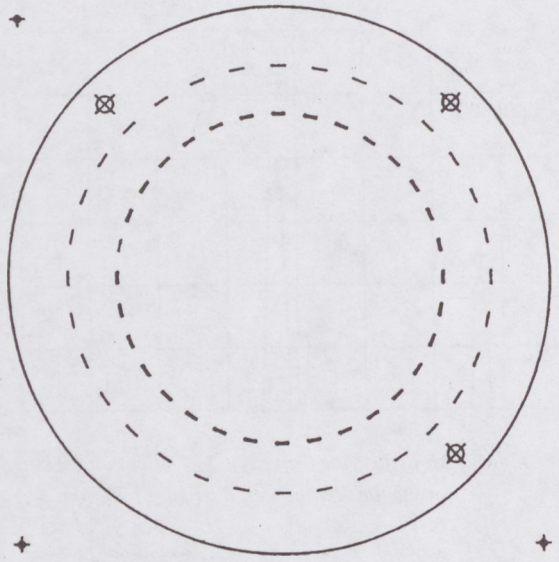

Fig. 17. Slot radiators of the 38 GHz converter (metallization is white).

Turning to the circular waveguide section, the first question is: where are the resonances of different modes on the frequency scale? Supposing that resonators bordered by irices are having $\lambda_g/2$-length at the used $TE_{16,2}$ mode, the calculated resonant frequencies versus inner radius of circular waveguide are shown in *Fig. 18*.

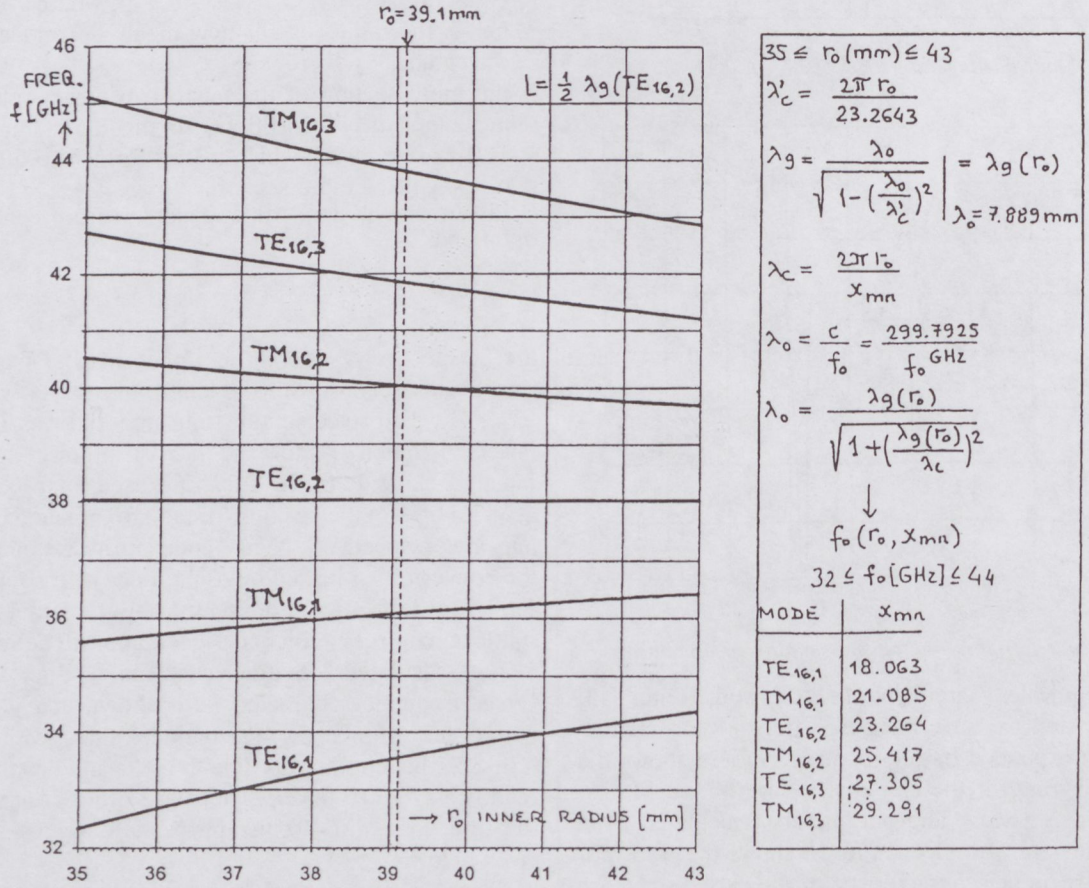

Fig. 18. Calculated resonant frequencies vs. inner radius of circular waveguide.

The used equations are also given in the figure. The photograph of golf-plated diaphraghmas are shown in *Fig. 22**. Calculated radiation pattern of the mode converter and basic equations are given in *Fig. 23.*

*** Coloured pictures cited are shown separately in the colour pages of this issue.**

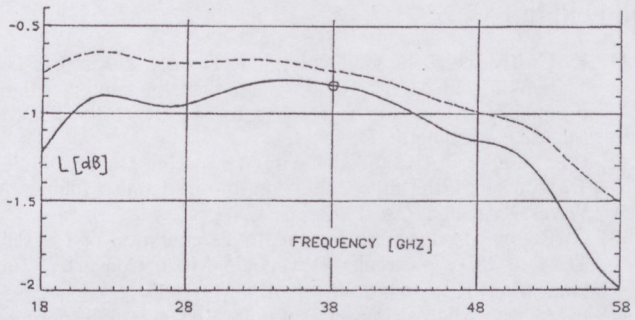

Fig. 19. Calculated loss versus frequency of the feed network.

$$F(\varphi) = 20\log\left(10^{F_{162}(\varphi)/20} + 10^{[F_{11}(\varphi)-25]/20}\right) + 20\log\frac{\sin(0.98\pi\sin\varphi)}{0.98\pi\sin\varphi}$$

$F(TE_{16,2})$ ↑ $F(slot)$

$F(TE_{11})$ ↑

$$F_{162}(\varphi) = \sum_{i=0}^{31}\left[(-1)^i\cos\alpha\cdot e^{j2\pi\frac{d_1}{2}\cos\alpha\cos\varphi} - (-1)^i\cos\alpha\cdot e^{j2\pi\frac{d_2}{2}\cos\alpha\cos\varphi}\right]$$

$0\langle\varphi\langle 180° \quad \alpha = \frac{360°}{32}i$

$f = 38GHz \quad \lambda = 7.889mm$

$d_1 = 9.851\lambda$

$d_2 = 7.580\lambda$

$I_2 = -1.8I_1$

$F_{11} - F_{162} = -25dB$

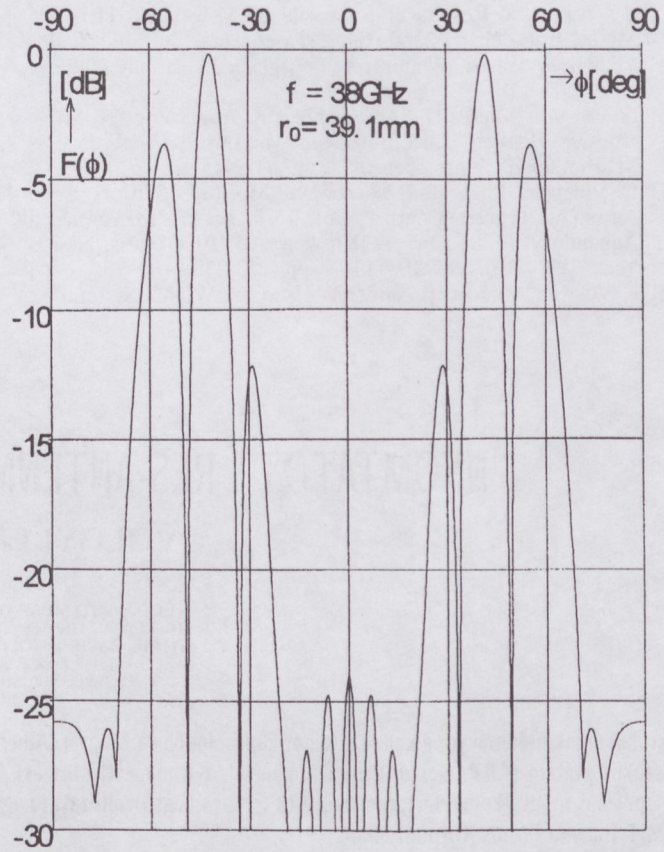

Fig. 23. Calculated radiation pattern of the WGM converter and basic equations.

8. CONCLUSIONS

We have developed the model of a MSSA-type exciter to obtain a TEM to $TE_{16,2}$ converter for the cold-test measurements of a gyrotron at 140 GHz. The basic idea, i.e. to stimulate the field of the useful mode by a MSSA and to filter out the unwanted modes by a circular waveguide-cavity filter is proved to be realizable. *Antenna measurement methods* were applied to control the amplitude and phase distributions of radiating slots, and the far-field characteristic of the open structure. Using the network model, a *network-like measurement* was carried out on the closed device. Design considerations and experimental results of mode converters were given in the paper. In this experiments students were also involved.

The modular design concepts of MSSA and microstrip power splitter can be well exploited in the education and in the laboratory practice of students.

ACKNOWLEDGEMENT

This work was supported by the US-Hungarian Joint Fund. I should like to thank Dr. R. Temkin and Kenneth E. Kreischer of the MIT Plasma Fusion Center, for the useful technical discussions. I wish to acknowledge the helpful consultations with prof. Dr. Tibor Berceli and prof. Dr. Gyula Veszely. The author would like to thank Dr. György Reiter for prividing the network model of the whispering-gallery mode transducer.

REFERENCES

[1] K. E. Kreischer, B. G. Danly, J. P. Hogge, T. Kimura, R. J. Temkin and M. E. Read: "The Development of High Frequency, Megawatt Gyrotrons for ITER" 1995 IEDM Meeting, Washington D. C.

[2] Ch. Moeller: "A Coupled Cavity Whispering Gallery Mode Transducer" 17th Int. Conf. on Infrared and Millimeter Waves, Pasadena, CA, 1992, pp. 42-43.

[3] G. Reiter: "A Proposal for the Implementation of Coaxial TEM to $TE_{16,2}$ Circular Waveguide Mode Converter" (in Hungarian) Research Study, TUB/DMT-1995.

[4] F. Völgyi: "Microstrip-Slot Antenna used as a Whispering-Gallery Mode Converter" Design and Measurement Report, TUB/DMT, May 1996.

[5] F. Völgyi, Gy. Reiter, Gy. Veszely and T. Berceli: "Experimental Results of a Coaxial TEM-Circular $TE_{16,2}$ Mode Transducer" 22nd Int. Conf. on Infrared and Millimeter Waves, Wintergreen, Virginia, USA, July 20-25, 1997.

[6] F. Völgyi: "Microstrip Antenna Array Applicator for Microwave Heating" 23rd European Microwave Conference, Madrid, Spain, September 1993, pp. 412-415.

[7] F. Völgyi: "Integrated Microwave Moisture Sensors for Automatic Process Control" Ch. 15 in book: "Microwave Aquametry" (edited by: A. Kraszewski), IEEE Press, New York, 1996, ISBN 0-7803-1146-9, pp. 223-238.

[8] F. Völgyi: "Microstrip Antennas Used for WLAN Systems" ISAP'96 Int. Symp. on Antennas and Propag. , September 24-27, 1996, Chiba, Japan, Proc. Vol. 3, pp. 837-840.

[9] G. Reiter: "Solution of Field Equations for Strongly Coupled Cavity Systems", Electromagnetic Wave Theory, Proc. of Symposium held in Delft, the Netherlands, Sept 1965. pp. 357-367.

[10] G. Reiter: "Single Mode Coupling Between Cylindrical TE011 Resonators", URSI Int. Symposium on Electromagnetic Theory, August 25-29, Budapest, Hungary, Part B, pp. 500-502.

[11] G. Reiter et al: "A Coaxial TEM-Cirular $TE_{16,2}$ Mode Transducer for Cold Test of Gyrotrons Output Converters", 21st Int. Conf. on Infrared and Millimeter Waves, Berlin, 1996, AT4.

[12] Robert A. Sainati: "CAD of Microstrip Antennas for Wireless Applications" Artech House, Boston-London, 1996, ISBN 0-89006-562-4,

[13] G. Reiter: "A Proposal for the Measurement of Inverter-Admittances Used in Microstrip-Slot Antenna Type Mode Converter" (in Hungarian), Research Study, TUB/DMT, April 1997.

[14] F. Völgyi, G. Reiter, T. Berceli and G. Veszely: "A Whispering Gallery Mode Transducer Using Microstrip-Slot Antenna Exciter" 27th EuMC, Jerusalem, Israel, 8-12 September 1997, pp. 168-174.

NYOMTATOTT RÉS-ANTENNA WGM-ÁTALAKÍTÓHOZ

VÖLGYI FERENC

BUDAPESTI MŰSZAKI EGYETEM
MIKROHULLÁMÚ HÍRADÁSTECHNIKA TANSZÉK
1111 BUDAPEST, GOLDMANN TÉR 3.
TEL.: 36 1 463 1559; FAX: 36 1 463 3289;
T-VOLGYI@NOV.MHT.BME.HU

Mikrohullámok tudományos alkalmazásaihoz kapcsolódóan a Magyar–Amerikai Kutatási Alap támogatásával, együttműködve a Massatsusetts-i Műszaki Egyetem (MIT, Boston) munkatársaival, a Budapesti Műszaki Egyetem Mikrohullámú Híradástechnika Tanszékén kifejlesztettünk egy speciális módus-konvertert, melynek 140 GHz-es végső változatát nagyteljesítményű girotronok ún. hideg-méréséhez kívánták felhaszálni az MIT Plazma Fúziós Központjában.

A szerző feladata a koaxiális TEM-körtápvonal $TE_{16,2}$ WGM (whispering gallery mode) módus konverter 15 és 38 GHz-es modelljeinek kidolgozása volt, nevezetesen a nyomtatott-rés antenna (microstrip-slot antenna, MSSA) mintgerjesztő szerkezet és a módus szűrő íriszeinek és rezonátorainak tervezése, bemérése. Ezen eredmények rövid összefoglalása található ebben a cikkben.

A $TE_{16,2}$ körtápvonal módus téregyenleteinek ismertetése után levonhatók azon következtetések, melyek az MSSA gerjesztő szerkezettel szemben támasztott követelményeket meghatározzák. Az alapötlet és mikrohullámú realizációjhának részletes ismertetése után a hálózati modell kerül megtárgyalásra. A kísérleti eredményeket taglaló rész a 15 GHz-es modell első méréssorozatát, majd a mikrohullám nyelők beépítése utáni kiegészítő méréseket ismerteti. Ezután kerül sor a 38 GHz-es modell tervezésének és mérési eredményeinek bemutatására.

Az alapötlet – vagyis hogy a $TE_{16,2}$ módust egy különleges nyomtatott-rés „antennával" hozzuk létre, és a nem kívánt módusokat a hozzá csatlakozó körkeresztmetszetű csőtápvonal szűrővel nyomjuk el – gyümölcsözőnek bizonyult. A téma külön érdekessége, hogy az „antennás" és „áramköri" szemléletmódra egyaránt szükség volt. Antennamérési módszerekkel (nyitott szerkezet közeltéri letapogatása, valamint távoltéri karakterisztikájának mérése) következtettünk a nyomtatott-gerjesztésű réssugárzók amplitúdó- és fáziseloszlására. Áramköri (hálózati) mérésekkel határoztuk meg a zárt-szerkezet bemeneti illesztését és frekvenciafüggő átvitelét.

A cikk segíti az antenna fogalmának egy tágabb értelmezését és az integrált antennák bevezetését.

*** A színes ábrák ennek az újságnak a színes oldalain találhatók — megfelelő feliratozással.**

MICROWAVE DRYING USING A MICROSTRIP ANTENNA ARRAY APPLICATOR*

FERENC VÖLGYI

TECHNICAL UNIVERSITY OF BUDAPEST
DEPT. OF MICROWAVE TELECOMMUNICATIONS
H-1111 BUDAPEST, GOLDMANN TÉR 3, HUNGARY
PHONE: 36 1 463 1559; FAX: 36 1 463 3289; T-VOLGYI@NOV.MHT.BME.HU

This paper describes the preliminary considerations, design and first experimental results of a 12-element rectangular microstrip antenna array (applicator) used for microwave drying at the frequency of 2.45 GHz with dimensions of $40 \times 30 \times 2.1$ cm^3 and a CW-power of 1 kW. The innovative applicator consists of a planar-array of electrically thick rectangular microstrip antennas and a stripline reactive power splitter with thick copper conductors at the inner strips and filled with a heat conducting insulation in the input section. Although the applicator is used in the radiating near-field, it is possible to design a transmit antenna, e.g. for FM-CW radar applications.

1. INTRODUCTION

Simple radiators, e.g. open-circuit stripline radiator, resonant slotted waveguide, monomode travelling wave radiator or stereomode applicator in [1] are used in the industrial microwave heating systems and in the microwave ovens. Mode stirrers and turntable shelvs are sometimes used, because the electromagnetic field inside the multimode cavity is rather inhomogeneous. Nowadays multiport feeds and near-field applicators are also used in practice. To increase penetration depth and improve control over the radiated field patterns, a new class of focussed electromagnetic hyperthermia applicators (leaky-wave troughguide applicator) have been studied by Rappaport et al [2]. For TEM-mode irradiation of larger volumes, frequently used applicators are the pyramidal horns. In this case, the irradiation chamber is totally enclosed, shielded and lined with anechoic material.

Our task was to develop an applicator for the frequency of 2.45 GHz with a power of 1 kW, which is able to uniformly irradiate A3 sized sheets (297×420 mm^2), or the half or quarter of that (A4, A5), in the radiating near-field. The application areas are: vacuum-drying of books, pictures etc. from the field of antique bibliography. Taking some power-blocks to a vacuum chamber, the low-profile of the applicators was also important. The permitted highest temperature was limited to 60 C°. Quasy-matched conditions were supposed using water-load in the inner plastic container.

We have designed an innovative applicator using the planar array of microstrip antennas, because not any of the above mentioned radiators is applicable to our special case. The advantages of microstrip antennas: low-profile, high efficiency at Völgyi [3], lightweight structure at Völgyi [4], are known. In addition to the applications in telecommunication, industrial applications at Völgyi [5], agricultural applications at Völgyi [6], and automative industry applications (Janus antenna at Mernyei et al [7]) are also frequent. On the other hand, there are only a very limited number of applications in the field of microwave power. For example, we have to mention Tanabe et al [8], where a four-element array of 3.5 turn spiral antennas at the frequency of 915 MHz, with a total power of 26 W were used in local hyperthermia experiments. The surface was cooled by a water pad.

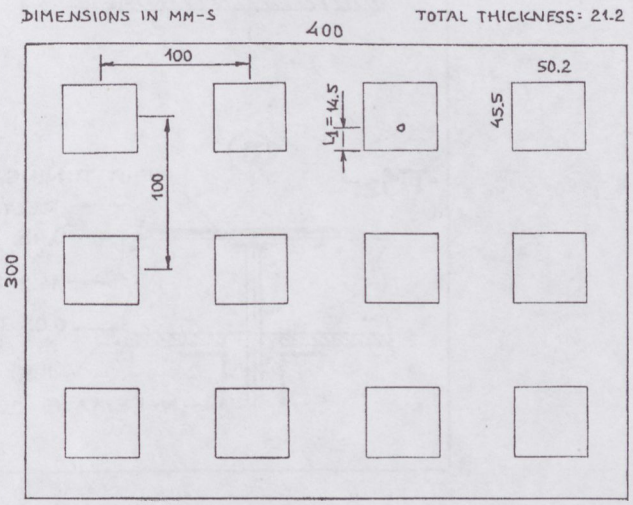

Fig. 1a. Microstrip antenna array applicator for microwave heating

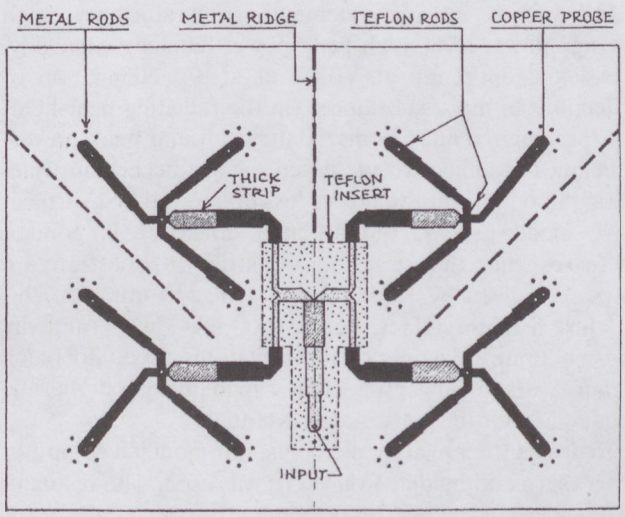

Fig. 1b. Stripline power splitter for microstrip antenna array applicator

* This is a version of the paper presented by F. Völgyi at 23rd EuMC Madrid, Spain in 1993 [13].

The purposes of this paper are to introduce an innovative 12-element microstrip antenna array applicator (see *Fig. 1*) at the frequency of 2.45 GHz with a power of 1 kW, and to show some useful measurement results.

2. MSA-ELEMENTS FOR POWER APPLICATIONS

Power applications of microstrip antenna (MSA) seems to be a contradiction. After all, it is not; it has been proved by our experiments that a nearly 300 W at the frequency of 2.45 GHz for a single MSA-element (see Model-E in *Fig. 7*) is achievable.

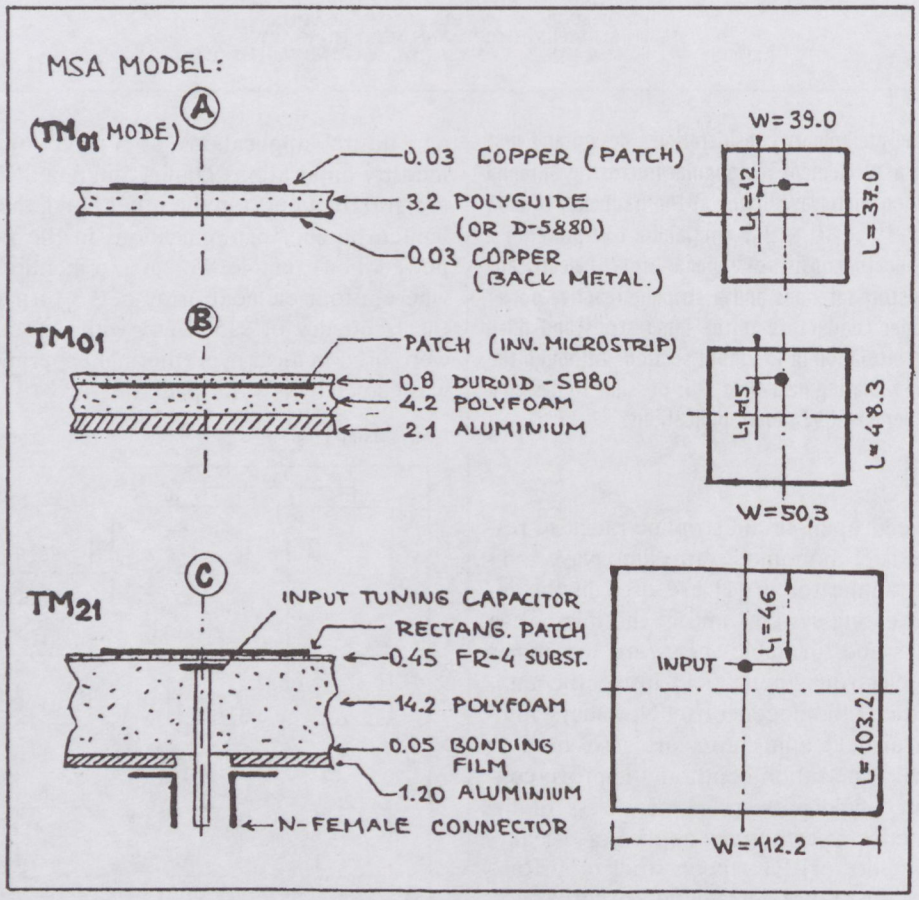

Fig. 2. Experimental microstrip antenna elements

For such a radiating element; good efficiency, high average power level, high peak power handling capability, broadband operation at Völgyi et al [9], elimination of reflections of moist substances (in the radiating near-field) are the major requirements. Bandwidth and peak power-handling capability are increased using thicker substrate. Taking into account the power loss due to the first surface-wave mode (TM_0), the antenna efficiency in general decreases when thickness and permittivity of substrate are increased, given by Roudot et al [10]. In our case this has just a minor effect, because of the low permittivity and moderate thickness of the substrates used. To reach higher average power handling capability, good thermal conductivity of the substrate is essential.

To design the radiating elements, our modified computer program (mentioned at Völgyi [3]) was used. The resonant frequencies of higher order modes of electrically thick rectangular microstrip antennas were calculated using the semi-empirical design equations, given by Garg and Long in [11].

3. NEARLY OPTIMAL ARRAY

A nearly optimal array of 3×4 MSA-elements (Model-E on *Fig. 7*, using Polyfoam and D-5880 substrate, elements are with equal amplitude and constant phase) was selected for the one kW applicator (*Fig. 3*). Each elements radiates a power of 83.3 W and the load of antenna is balanced, not only at full dimension of moist substance, but in the cases of single A4 and A5 sheets too, as can be seen on *Fig. 3* and *Fig. 1b*. Taking into account the losses of radiating microstrip resonators, the calculated rise in temperature of the array-sheet is lower than 2 C°.

4. STRIPLINE POWER SPLITTER

The hardest task in our project was to feed-in the input power of 1 kW and to split it for the MSA-elements. Because of the low profile and low loss requirement, an air-filled stripline power splitter (reactive type) was designed, using thick copper conductors at the inner strips (*Fig. 1b*). The thickness of inner conductor (t) and ground

plane spacing (b) at the input line: 3.0 mm and 12 mm were, respectively, $t/b = 1/8$ was selected at other sections. The characteristic impedances from the input to the radiating element were designed to: $50-41.6*-30-50-70.7*-50-40.9*-28.5*-70-59.2*-50$ Ohm, where the quarter-wave transformer sections are denoted using*.

The inner conductor structure was kept in the symmetry-plane by teflon (PTFE) separation rods (16-pieces), and was fixed to the radiating elements by copper probes (3 mm diameter). Five metal rods were used at each stripline-probe adapters as mode suppressors, since there is an abrupt change in both direction and mode shape. The ground planes were fixed by mounting screws at the edges and at the metal ridges.

Our calculations and the first experiment (using a power of 800 W) showed the temperature rise of the strip conductor at the input line section, because of the bad thermal conductivity of the air-filling. Using PTFE dielectric material at the input section the improvement was 1/5-times in temperature of inner conductor was lower than 60 C°. We will be able to reach additional improvement (2-times) in thermal properties, using heat conducting insulation (written by Hensperger [12]) in the input section and the used 16/7 mm diameter coaxial input connector.

5. EXPERIMENTAL RESULTS

A part of our experimental results are shown on *Figs. 4–13*. Detailed analysis of that (conjunction with the array measurements: thermal-map, etc.) are discussed below.

The measured input return loss versus frequency characteristics of the experimental microstrip antenna elements are shown in *Fig. 4*. Excellent matching and broadband operation are achieved with Model C and B.

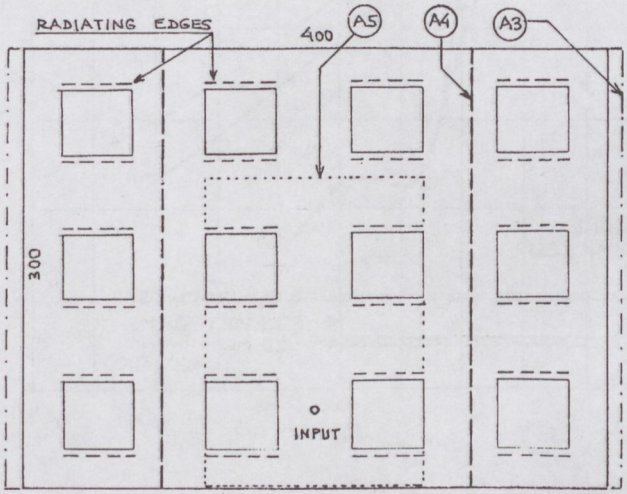

Fig. 3. A nearly optimal array for A3–A5 sized sheets

Fig. 5 shows the construction and the measured input return loss versus frequency diagram of Model-D, using the higher order mode TM_{21} . Excellent input matching ($RL > 30$ dB) and broadband operation ($b = 12.7$ % at $RL = 10$ dB) were the main results. High power handling capability is also expected, because of the thick substrate used.

In *Fig. 6* we have illustrated typical results of input return loss versus frequency measurements for Model-D, where solid curve shows the optimum matching at TM_{21} mode, while the basic mode TM_{01} operation is depicted using dashed line.

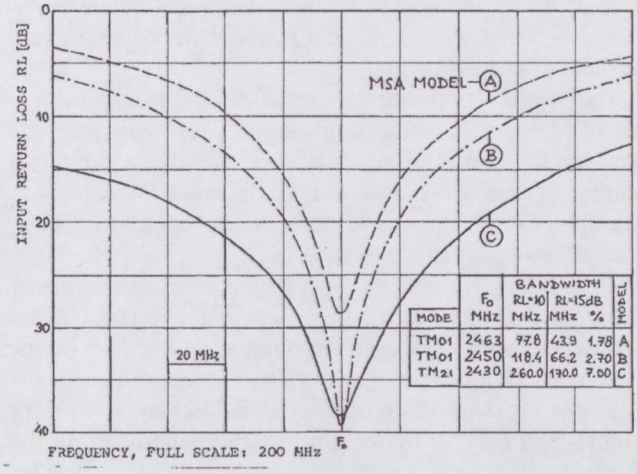

Fig. 4. Measured input return loss versus frequency for MSA-elements

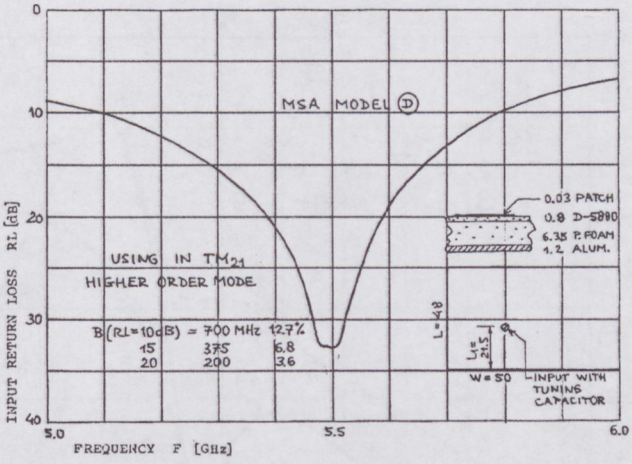

Fig. 5. Input return loss versus frequency for Model-D

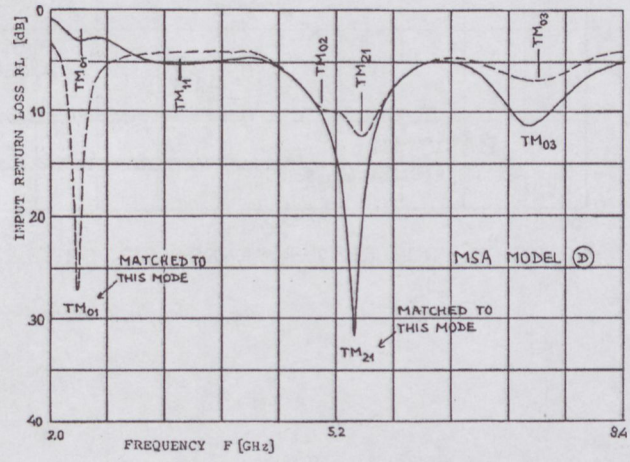

Fig. 6. Input return loss versus frequency for Model-D in TM_{mn} modes

Fig. 7 gives an overview of our near-field experiments for the basic mode TM_{01}, where the construction of Model-E and the positioning of receiving loop-antenna are also shown. The solid curve (1) illustrates that the field varies sinusoidally (absolute value) with maxima at $y = 0$ and $y = L$, where the radiating edges are found for the vertically-polarized rectangular microstrip antenna. On the place of patch the field is nearly constant in direction-x, as shown by curve (2). This field starts changing into quasy far-field of curve (3).

The construction and measured near-field characteristics of Model-F in higher order mode TM_{21} operation are depicted in *Fig. 8*. Dotted line shows, that the field has two minima in direction-x, according to the mode index $m = 2$. The field metamorphosis is illustrated by curves at $z = 1$, $z = 10$ and $z = 60$ mm, respectively.

Fig. 9 also represents the field-metamorphosis for Model-F in TM_{21} mode, but for the $H_x(y)$ component. There is observable an asymmetry in direction-y because of the asymmetry of input point relative to the radiating edges.

This is also illustrated on the far-field characteristic for Model-E in *Fig. 11*, by the shift of the main-beam in the E-plane pattern.

Fig. 10 illustrates how the input return loss versus distance is changing using different wet substances in the nearfield of the broadband microstrip antenna Model-F in higher order mode TM_{21} . Curve (1) is measured with moving absorber, Eccosorb AN 79. The nearest optimum positions at wet substances are nearly $R = 4$ cm with return loss 14 – 19 dB, as shown in curves (3) – (5). Sometimes the moist substance gives greater reflection than the plastic water tank itself [see, curve (6)]. On the other hand, it is possible to obtain "matching" by the dry sample [curve (2) at $R = 5$ cm], which may be useful in certain cases (low-loss reflecting plate or the wall of the dielectric sample holder).

Fig. 11 shows the far-field characteristics of Model-E in basic mode TM_{01} in the H- and E-plane, which can be compared to *Fig. 9*.

In *Fig. 12* the far-field patterns are shown for Model-F in TM_{21} mode in H-plane (dotted line) and E-plane (solid curve), respectively.

Efficient drying results were achieved using the patch-array with a power of 1000 Watts, as shown schematically in *Fig. 13* (the coloured picture is shown separately in the colour pages of this issue.). Right-side of the figure corresponds to the original upward-direction, so the asymmetry is caused by the gravitation. After two minutes the maximum difference between dry and wet areas was lower than 10 %.

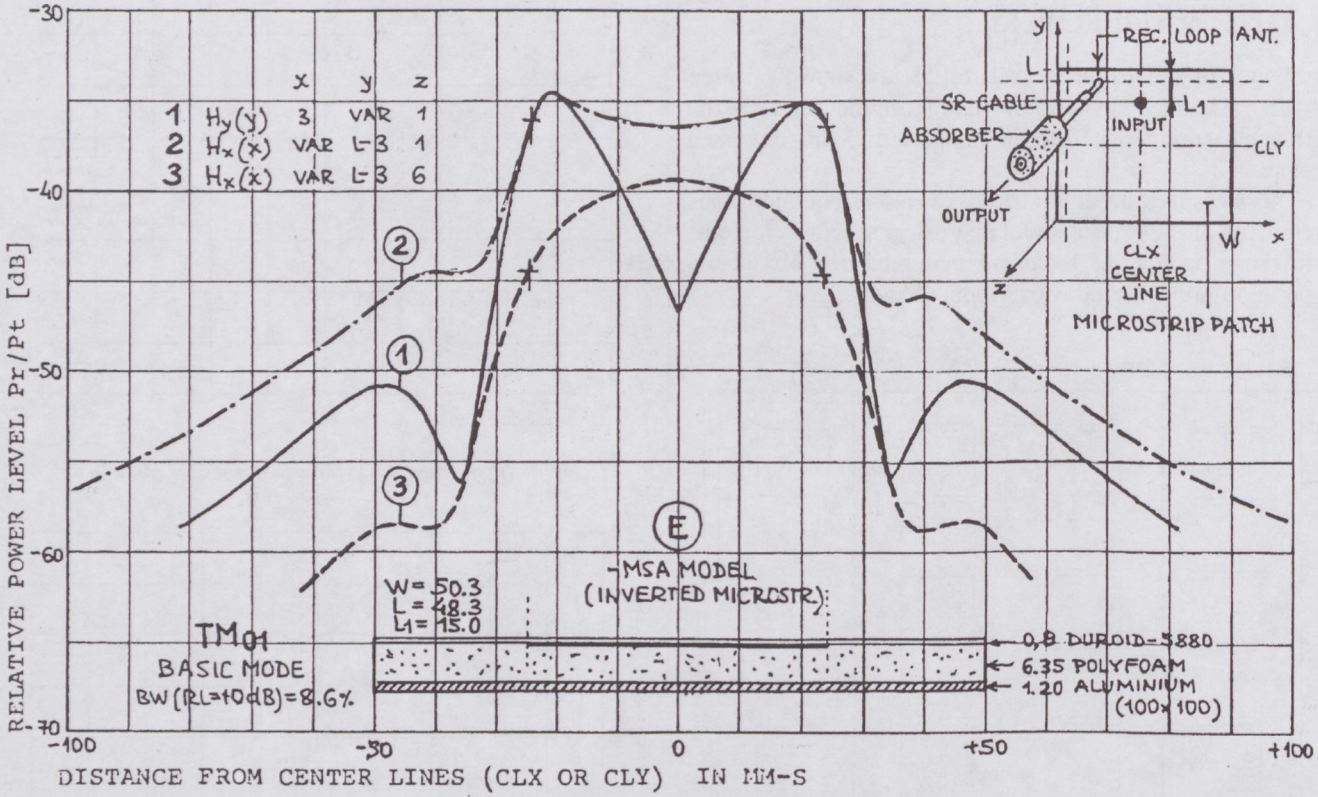

Fig. 7. Near-field characteristic for Model-E in TM_{01} mode

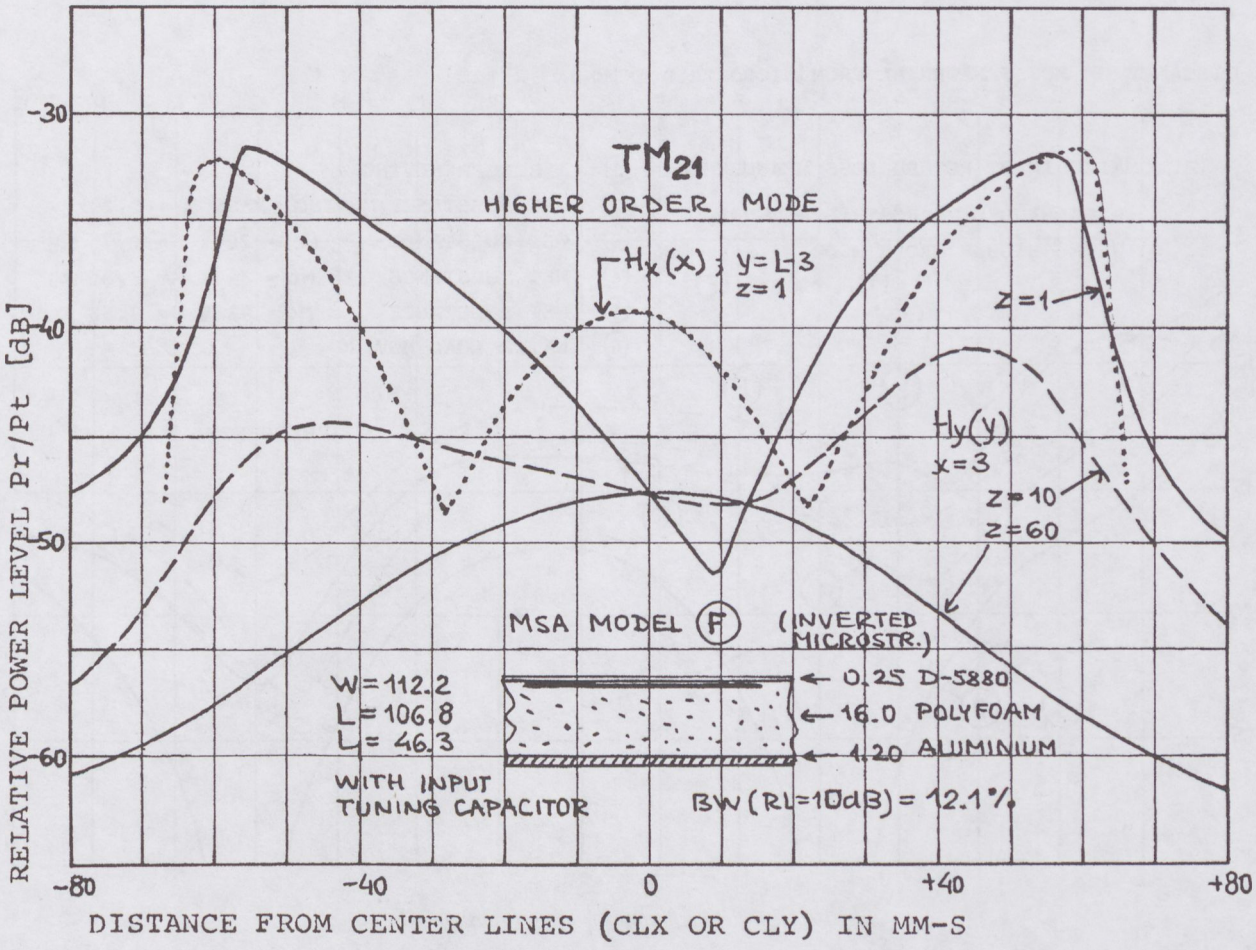

Fig. 8. Near-field characteristic for Model-F in TM_{21} mode

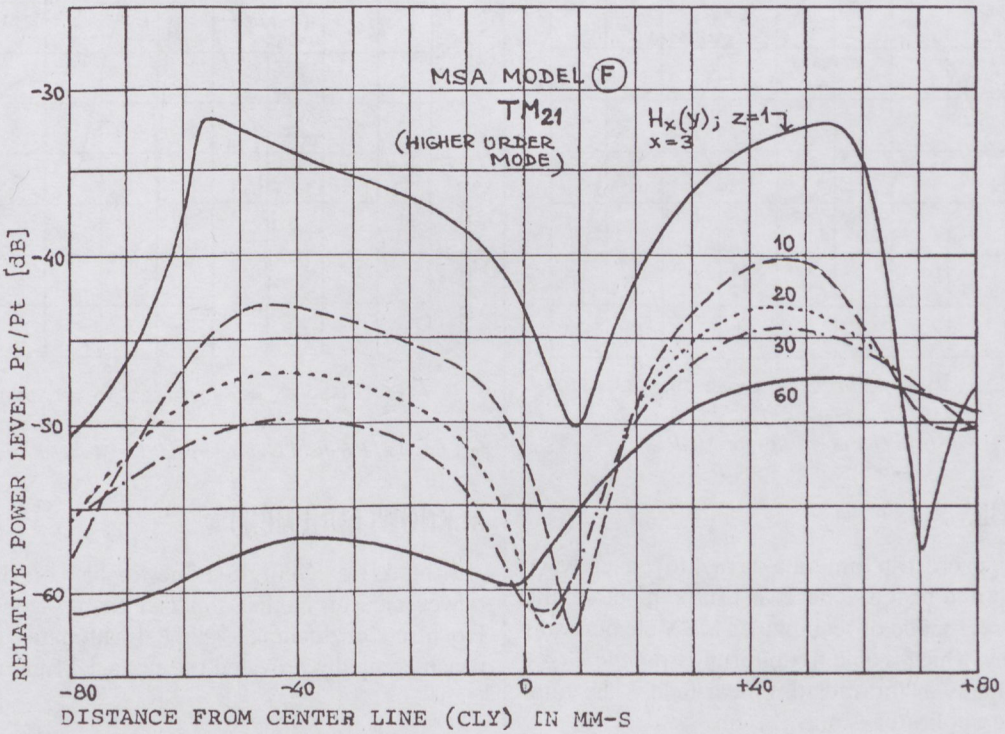

Fig. 9. Field metamorphosis, Model-F in TM_{21} mode

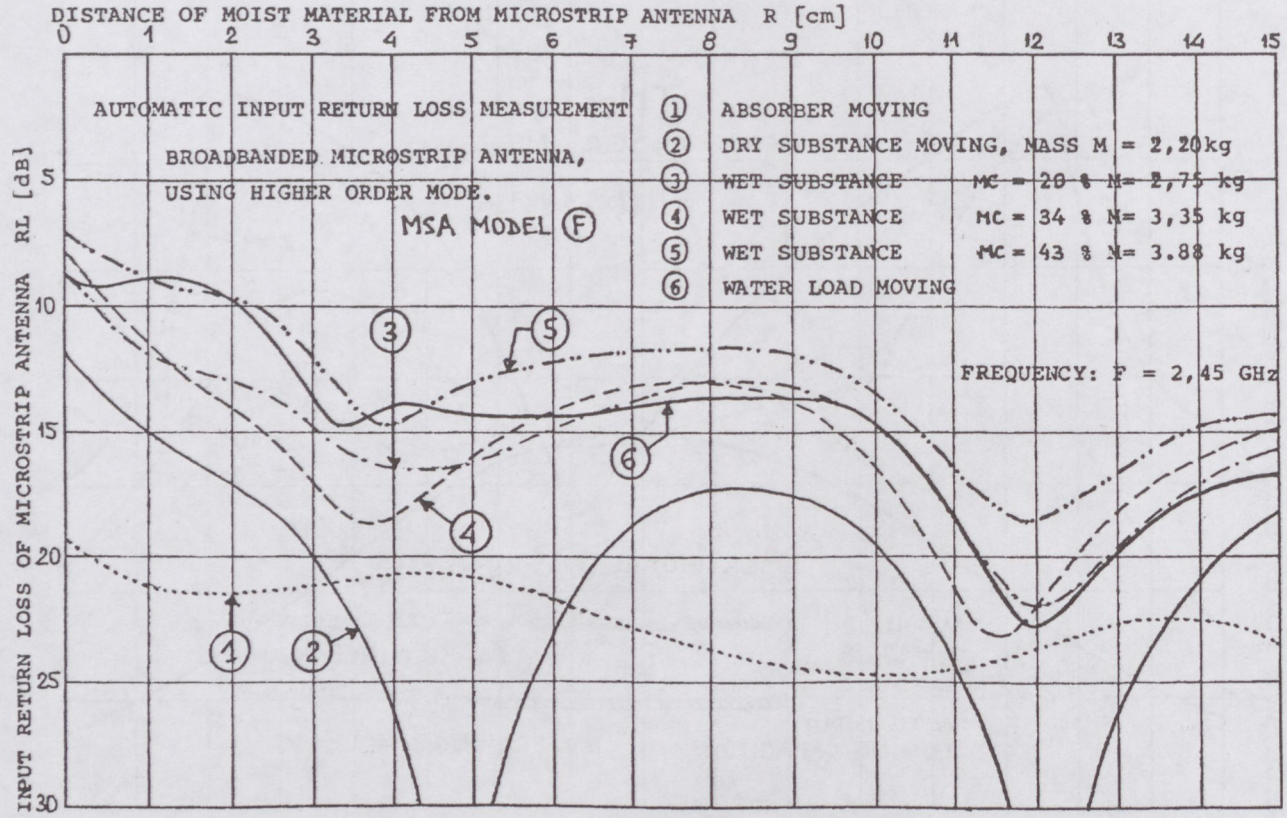

Fig. 10. Near-field reflections from wet substances

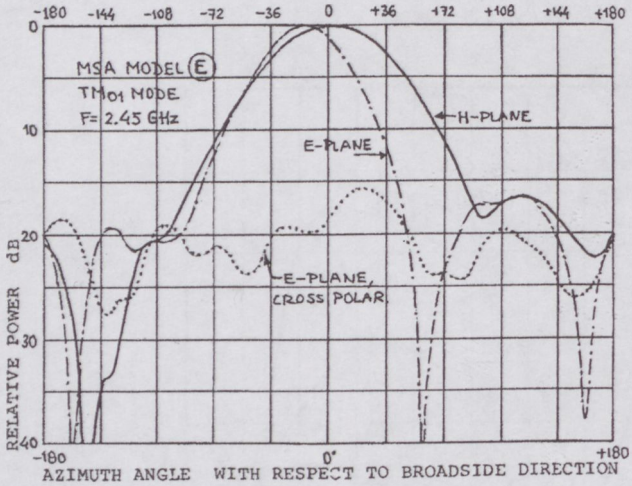

Fig. 11. Far-field characteristics for Model-E

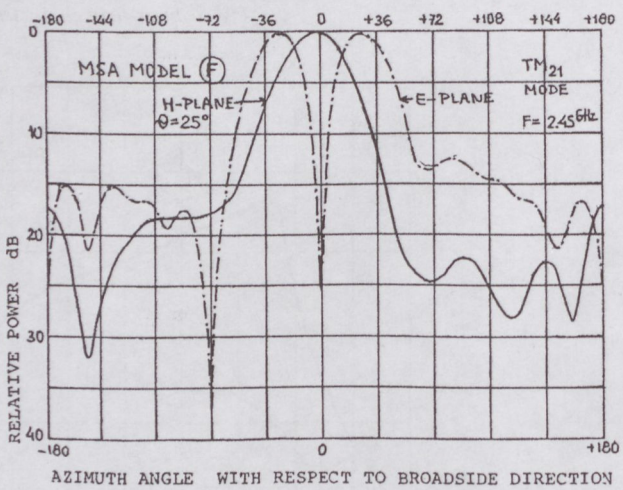

Fig. 12. Far-field characteristics for Model-F in TM_{21} mode

6. CONCLUSIONS

High power microstrip antenna array for microwave drying was built and tested. The $TM_0 1$ basic mode or the TM_{21} higher order mode of rectangular MSA-element was used in the array, which is able to uniformly irradiate larger than 12 dm^2 sheets in the radiating near-field. The total thickness of the applicator is only 2.1 cm.

ACKNOWLEDGEMENT

I thank Dr. Georg Schöne for his contribution in high power measurements. Special thanks goes to the L&S Hochfrequenztechnik GmbH, Lichtenau-Ulm (Germany) which company provided the financial fund for the experiments.

REFERENCES

[1] Catalogue 93-94 of "Microondes Energie Systems" 2 et 4, Avenue de la Cerisaie-Platanes 307, 94266, Fresnes Cedex, France.

[2] Rappaport, C. M., Morgenthaler, F. R and Lele, P. P.: "Experimental Study of the Controllable Microwave Troughguide Applicator" 1987, Journal of Microwave Power, Vol. 22, pp. 71-78.

[3] Völgyi, F.: "High Efficiency Microstrip Antenna Array" 1987, 17th European Microwave Conference, Rome, Italy, Proc. pp. 747-752.

[4] Völgyi, F.: "Flying Decibels – Extremely Lightweight Microstrip Antennas" 1990, ICOMM'90 Int. Conf. on Millimeter Wave and Microwave, Dehradun, India, Proc. pp. 343-348.

[5] Völgyi, F.: "Versatile microwave moisture sensor" in Conf. Rec. SBMO'89, Sao Paulo, Brazil, 1989, Vol. II, pp. 456-462.

[6] Völgyi, F.: "Integrated microwave moisture sensors for automatic process control" Ch. 15 in book: Microwave Aquametry (edited by A. Kraszewski), IEEE Press, New York, 1996, ISBN 0-7803-1146-9, pp. 223-238.

[7] Mernyei, F., Völgyi, F., Heidrich, E., Kehrbeck, J. and Lebherz, M.: "Microstrip Antenna Applications" 1992, Periodica Polytechnica, Budapest, Ser. El. Eng. Vol. 36, No. 1 pp. 273-283.

[8] Tanabe, E., McEuen, A., Vorris, C. S., Fessenden, P. and Samulski, T. V.: "A Multi-Element Microstrip Antenna for Local Hyperthermia" 1983, IEEE MTT-S Digest, pp. 183-185.

[9] Völgyi,F., Somogyi, A., Denk, A., Babits, L. and Tamási, S.: "Broadbanded Microstrip Antenna for Primary Feed Applications" June 30, 1989, Hungarian Patent, No. 205816.

[10] Roudot, B., Mosig, J. R. and Gardiol, F. E.: "Surface Wave Fields and Efficiency of Microstrip Antennas" 1988, 18th European Microwave Conference, Stockholm, Sweden, Proc. pp. 1055-1062.

[11] Garg, R. and Long, S. A.: "Resonant Frequency of electrically Thick Rectangular Microstrip Antennas" 8th October 1987, Electronic Letters, Vol. 23, No. 21, pp. 1149-1150.

[12] Hensperger, E. S.: "Dielectric Material Improves Average Power Ratings" May, 1974, The Microwave Journal, pp. 61-62.

[13] Völgyi, F: "Microstrip Antenna Array Application for Microwave Heating" 23rd European Microwave Conference (EuMC), Madrid, Spain, 6-9 Sept, 1993, pp. 412-415.

MIKROHULLÁMÚ SZÁRÍTÁS NAGYTELJESÍTMÉNYŰ MIKROSZTRIP ANTENNÁVAL

VÖLGYI FERENC

BUDAPESTI MŰSZAKI EGYETEM, MIKROHULLÁMÚ HÍRADÁSTECHNIKA TANSZÉK

A mikrosztrip (nyomtatott, planár) antennák (MSA) előnyös tulajdonságai: jó hatásfok, vékony és könnyű szerkezet, egyszerű gyárthatóság (NYÁK-technológia), aktív elemekkel való integrálhatóság stb. Mikrohullámú adókban és szárítókban való alkalmazásuk azonban igen ritka, a ráadható maximális teljesítmény viszonylag alacsony értéke (20–100 W) miatt.

Az L&S Hochfrequenztechnik GmbH által adott fejlesztési megbízás 1 kW folytonos (CW) teljesítményű mikrosztrip antennára vonatkozott, melyet az antenna közelterében történő speciális vákuumszárítási célokra kívántak felhasználni. Fontos előírás volt egy kb. 30×40 cm^2 nagyságú sík felület egyenletes besugárzása 2,45 GHz frekvencián.

A szerző által kifejlesztett (világviszonylatban is egyedülálló) nagyteljesítményű mikrosztrip antenna (applikátor) egy "elektromosan viszonylag vastag" négyszögletes nyomtatott sugárzókat tartalmazó, 3×4 elemű síkantenna, melyet szalagtápvonalas reaktív teljesítményosztó táplál (antenna + elosztó teljes vastagsága: 2,1 cm). Minimális tápvonal veszteség elérése céjából a szalagvonal légtöltésű, az 1, illetve 3 mm vastag vörösréz belső vezetőt teflon távtartó csapok rögzítik a szimmetria síkban. A nagyteljesítményű bemeneti osztó kisveszteségű és nagy hővezető képességű dielektrikumba ágyazott, a hőleadás növelése miatt.

A lehetséges nagyteljesítményű sugárzó elemek (vastag hordozón felépített MSA, magasabb módusú működtetés) számbavétele után a cikk kísérleti eredményeket ismeretető részében több diagramot találunk a bemeneti illesztés-, közeltéri mérések-,magasabb módusok rezonanciái, sugárzó közeltér–távoltér átmenet téreloszlása-, valamint az alap- és magasabb módusú működés távoltéri iránykarakterisztikáira vonatkozóan.

A cikk jó példája annak, hogy ötletes megoldásokkal kiküszöbölhető a nyomtatott antennák kisteljesítményű működésben jelentkező hátrányos tulajdonsága, a jelen esetben lényeges planár-elrendezés megtartása mellett.

VERSATILE MICROWAVE MOISTURE SENSORS*

FERENC VÖLGYI

TECHNICAL UNIVERSITY OF BUDAPEST
DEPT. OF MICROWAVE TELECOMMUNICATIONS
H-1111, BUDAPEST, GOLDMANN TÉR 3, HUNGARY
PHONE: 36 1 463 1559; FAX: 36 1 463 3289; T-VOLGYI@NOV.MHTBME.HU

An X-band, modularly built, transmission-attenuation type, universal moisture sensor (and meter) applying special microstrip antennas; the measuring results of grains (corn, wheat) textiles and the experiences of industrial applications are discussed.

Keywords: microwaves, moisture measurement, microstrip antennas, microstrip circuits, industrial and agricultural applications

1. INTRODUCTION

There is a rapid progress in the motorization and automatization of agriculture. One of the most important technological processes in Hungary is drying corn up to the moisture content which is specified for storage. For the automatic operation of drying machines the in-line, real-time moisture measurement of grain is a fundamental task [1]. Also, the textile industry uses a great amount of energy for drying textiles. In case of using automatic dryers with microwave moisture sensors [2], 25 % of energy saving is possible [3] together with significant improvement of production quality.

In order to maintain the constant production quality, similar tasks are to be performed in other areas, e.g. rice [4], paper [5], wood, leather or meat industry, mainly in the production of salami. The main requirements of industrial moisture measurement are: non-destructive contactless operation, high speed, reliability and possibly low cost. All these requirements are fulfilled by the presented *microwave moisture sensor* which operates based on the measurement of transmission loss between small-size, flat microstrip antennas (see *Fig. 1*).

The parameters of dielectric materials (ε_r', ε_r'' or $\tan\delta$) directly determine the propagation loss (A) of passing electromagnetic wave, the power dissipated (P_d) in volume (V) and the temperature increase (T_d) during the microwave drying. These parameters are temperature dependent and considering a wide range, frequency dependent as well.

In case of grained agricultural products with different moisture content, the dielectric parameters are strongly dependent on the moisture content (M) and density (ρ) [6]. The main problem is that in the space containing the wet grain, the moisture content should be determined from the dielectric characteristics of the *three-phase mixture* (grain, water, vapory air), by the help of transmission loss measurements. The measurement errors depend on the geometric (g) arrangement, and the microwave (μ) measurement errors in connection with the microwave transmission measurements (reflections, generator instabilities etc.). Ultimately, the information is carried by the U_0 output signal of the moisture sensing and measuring system. Consequently, the problem can be characterized as follows:

$$U_0 = F_0\{A\} \tag{1}$$

$$A = F_1\{\varepsilon_r', \tan\delta, f, g, \mu\} \tag{2}$$

$$\varepsilon_r' = F_2\{M, \rho, T, f\} \tag{3}$$

$$\tan\delta = F_3\{M, \rho, T, f\} \tag{4}$$

The target function is:

$$M = F_4\{U_0\}, \tag{5}$$

where $F_i\{\}$ denotes a functional relation.

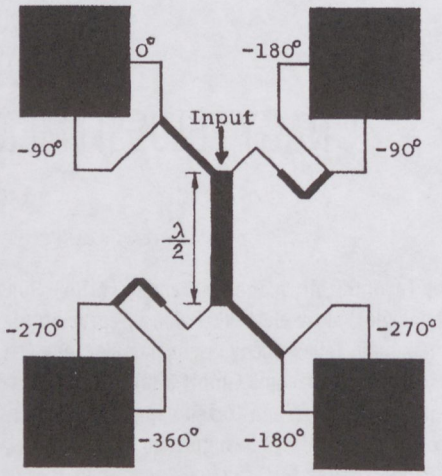

Fig. 1. Circularly Polarized Microstrip Antenna for Textile Moisture Meter [2]. Full scale, thickness: 1.6 mm.

Due to the sophisticated nature of problem, it is very difficult to give F_4 in explicit form.

The usual way is:

- set up of models for multi-phase dielectric mixture [6],
- measurement of ε_r', ε_r'' or $\tan\delta$ dielectric parameters on a large number of samples with different fixed measurement parameters [7],
- regression analysis of measurement results (diagrams) [1],
- cleaning up and analysis of special errors [8],
- definition of F_4 in diagram or expression, which under given circumstances and within a specified range of parameters the error is below a specified value.

2. DESIGN OF MICROWAVE MOISTURE SENSORS

2.1. Preliminary Measurements

Before designing the moisture sensors for different purposes, preliminary measurements were conducted on lots of granulated materials and grains to obtain reference attenuation data [1]. With given density and temperature of

* This is a reprint of the revised paper [13].

sampled materials, the microwave attenuation is characteristic to the moisture content, if the constant thickness of sample is maintained e.g., with a proper container [8].

The reference measurement setup intended for microwave moisture measurement (MMM) was built around a Hewlett-Packard Frequency Response Test Set [9] and it is shown in *Fig. 2.* With the dual-channel amplitude analyzer the attenuation of the moist material and the reflection of the antenna can be simultaneously analyzed as a function of frequency. The dynamic range of system is around 55 – 60 dB. The output of sweep oscillator is connected to the transmit antenna trough a directional coupler or Reflecto-Meter Bridge, depending on the attenuation to be measured. The measured characteristics are output to a plotter. Typical measured data are shown in *Fig. 3.* Based on measured data in the X-band, it can be concluded that in the typical moisture range the characteristic attenuation values are: 2 – 20 dB for wheat, 1 – 50 dB for corn, 0.5 – 12 dB for textile, 2 – 20 dB for leather, etc.

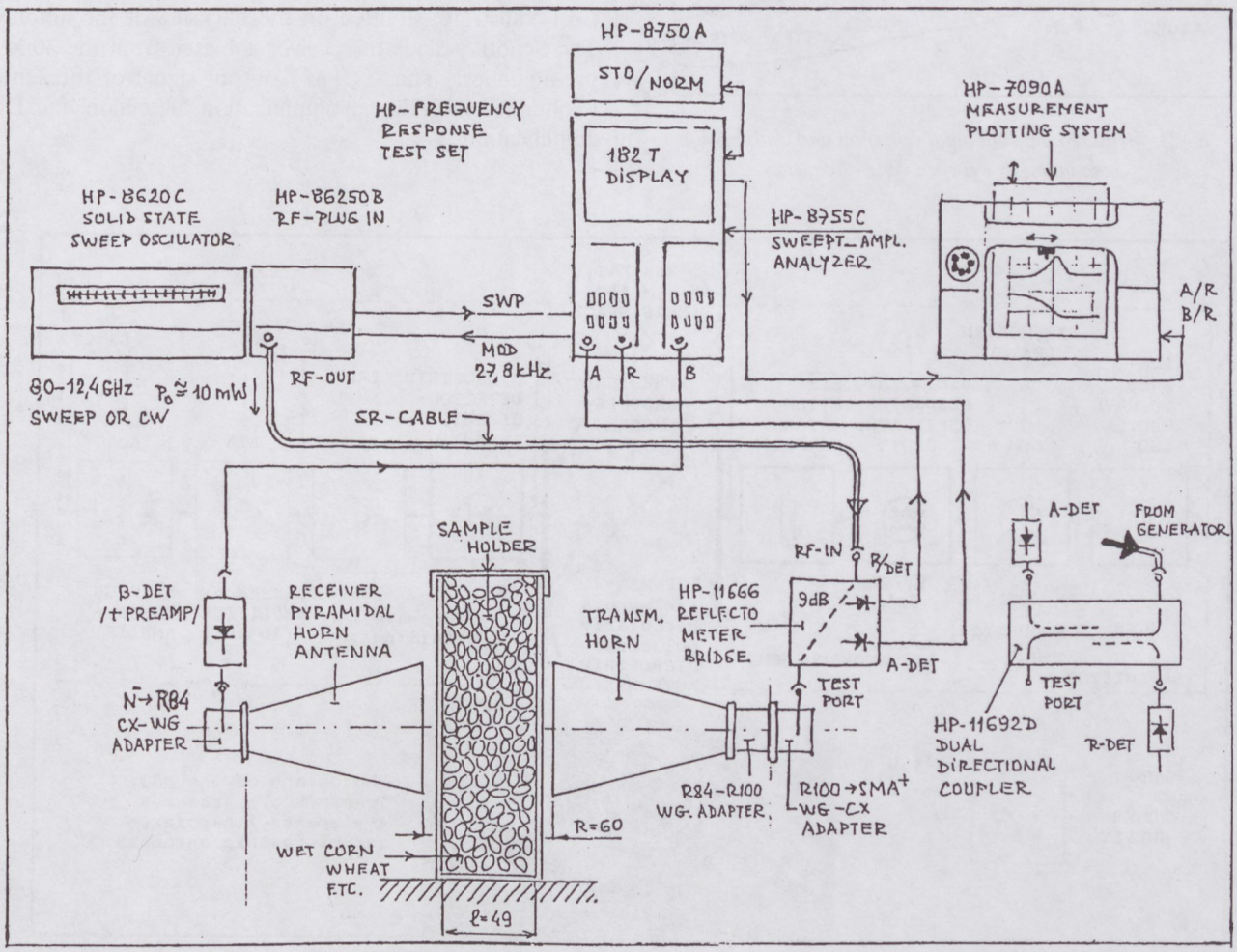

Fig. 2. Reference test setup for microwave moisture measurement

2.2. Design Considerations

Since besides of the aforementioned applications the microwave moisture sensors are used in other systems (e.g., in different applications of microwave energy [10]) as well, the major requirements are; simplicity, small size and low cost. Instead of the two-parameter (attenuation and phase) measurements which are accurate and well suitable for laboratory conditions [8], we measure only the attenuation (it simplifies the receiver) and the errors are decreased by other means.

As a new solution, the attenuation of moist material is measured between microstrip antennas which are optimized in number of elements, polarization and arrangement. Similarly to that in [9], a square-wave modulated system (30 kHz) was developed, thus a reduced oscillator noise and simplified signal processing on the receiver side can be achieved. In the receiver, instead of the costly mixer and local oscillator arrangement, a simple microstrip detector is used integrated onto the receive antenna. There are good methods for calibration and temperature correction of diode power detectors [11]. It was aimed, that the system should be expandable with further modules, and connections are to be provided to allow the calibrations, frequency response and reflection measurements with existing measuring systems (e.g., with the aforementioned HP-FRTS [9]).

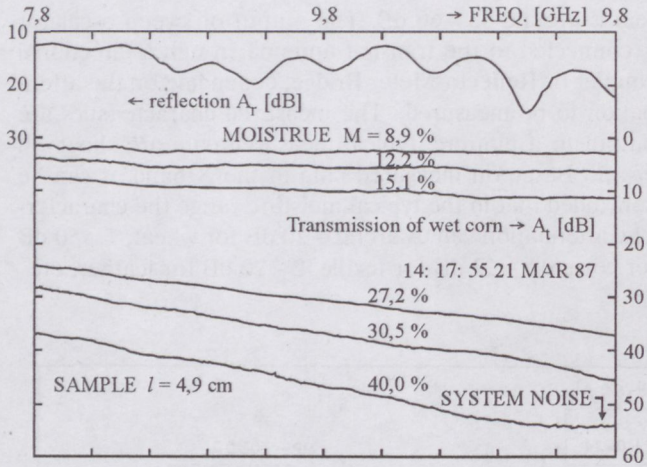

Fig. 3. Measured antenna input reflection and transmission attenuation of wet corn versus frequency

2.3. Microwave Moisture Sensor for Textile

The block scheme is shown in *Fig. 4*, where the <No> sign denotes the connection points of different modules. The photo shows the transmitter, receiver, radomes and the four-element microstrip antennas with linear polarization (similar to *Fig. 2* of [12]). Later these were replaced with those shown in *Fig. 1* on this paper. The master oscillator of transmitter is a FET-oscillator stabilized with dielectric resonator, with simple on-off modulation. The load-pull effect is reduced by the fixed attenuator. These circuits were realized on a Duroid-5880 (Rogers Co.) substrate, situated on the backside of the antenna. The Schottky-diode of receiver is biased from the 30 kHz pre-amplifier. The U_0 (M) output signal of the sensor is obtained after linear amplification, detection and DC-amplification.

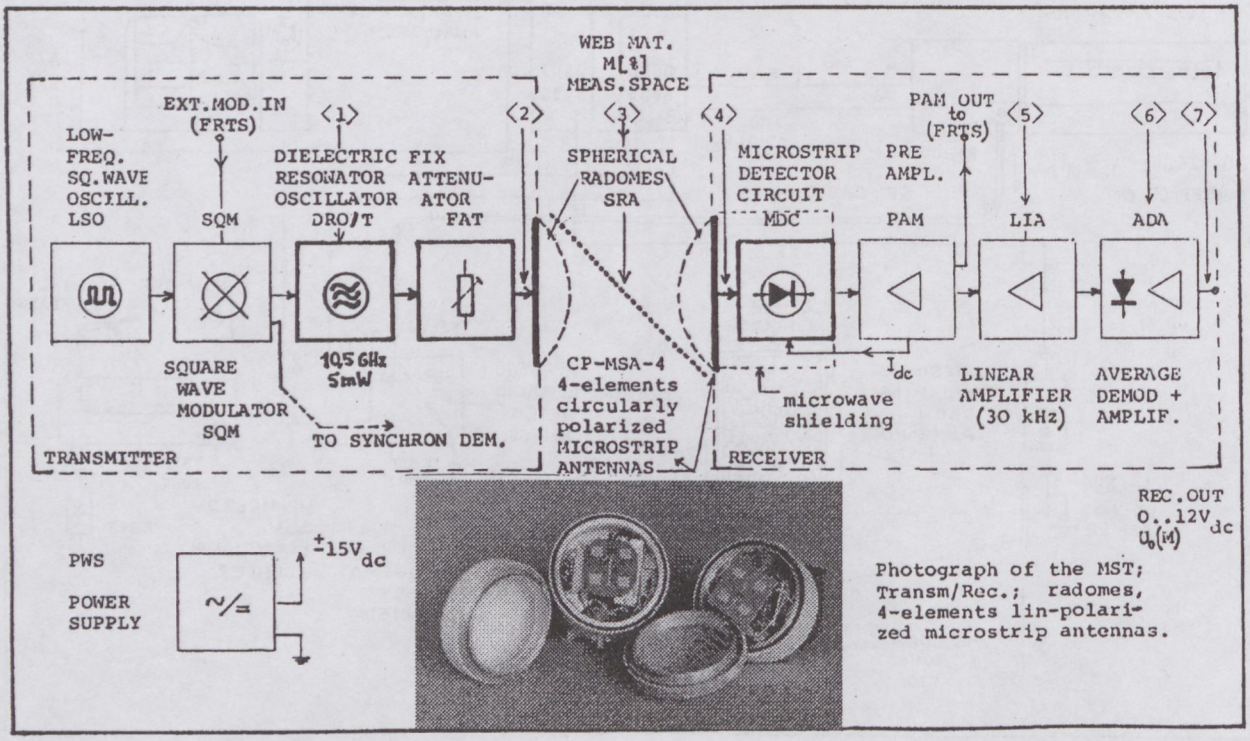

Fig. 4. Block scheme and photograph of the microwave moisture sensor for textile (MST)

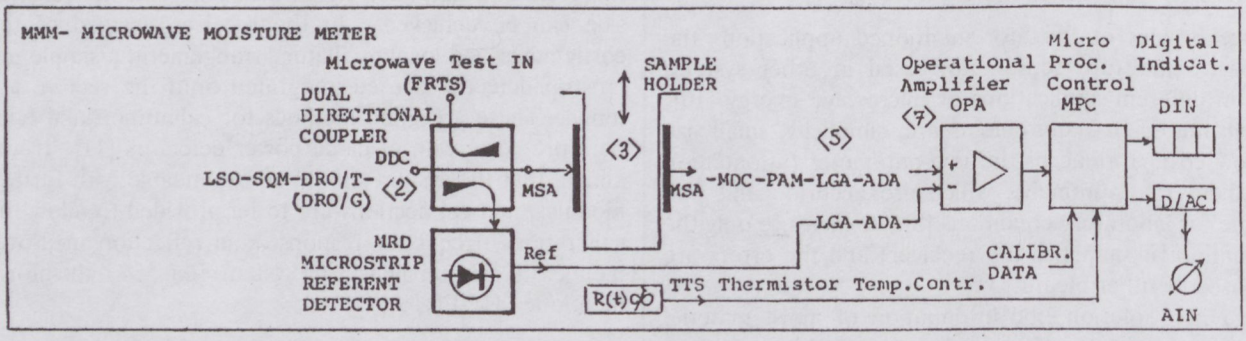

Fig. 5. Block scheme of the microwave moisture meter (MMM)

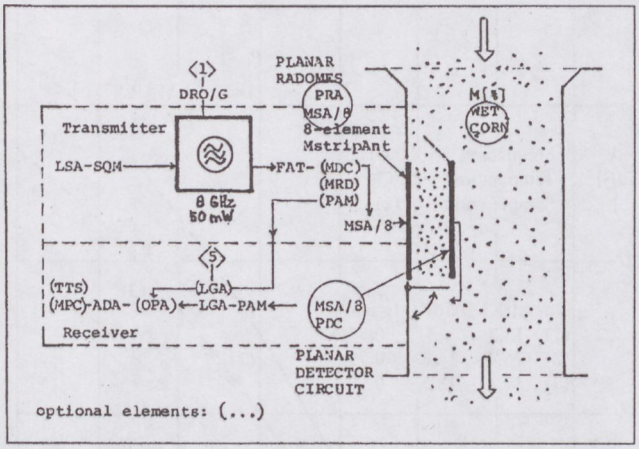

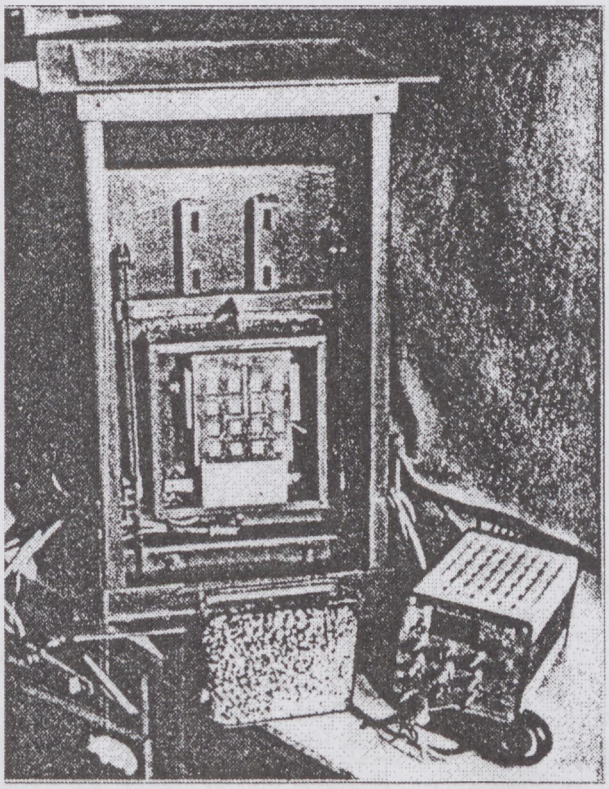

Fig. 6. Block scheme and photograph of the microwave moisture sensor for grain (MSG)

By using the above-mentioned principles, we were developing also Microwave Moisture Meter (MMM, see *Fig. 5*) and Microwave Moisture Sensor for: Grain (MSG, see *Fig. 6*), for Leather (MSL, see *Fig. 7*), for Salami (MSS, with focussed conformal microstrip antennas). Shortenings and designations on *Figs. 4–7* are given below:

ADA average demodulator
AIN analog indicator
DAC Digital/analog converter

DDC dual directional coupler
DIN digital indicator
DRO dielectric resonator oscillator
FAT fix attenuator
FRTS frequency response test set
LGA logarithmic amplifier
LIA linear amplifier
LSO low-frequency square-wave oscillator
MBF microstrip bandpass filter
MDC microstrip detector circuit
MMM microwave moisture meter
MRD microstrip referent detector
MPC microprocessor control
MSA microstrip antenna
MSG microwave moisture sensor for grains
MSL microwave moisture sensor for leather
MSS microwave moisture sensor for salami
MST microwave moisture sensor for textile
OPA operational amplifier
PAM pre-amplifier
PDC planar detector circuit
PRA planar radome
PWS power supply
SRA spherical radome
TTS thermistor temperature sensor

3. EXPERIMENTAL RESULTS

The characteristics, obtained in the reference-measuring set-up are shown in *Fig. 3*. The results of corn measurements in the frequency range of 7.8–9.8 GHz show that for extreme high moisture content and at upper end of frequency range the received signal is in the order of system noise, therefore in the later measurements lower frequencies (8 GHz) were used. The curves clearly show that the attenuation linearly varies with frequency. The reflection attenuation varied between 13 and 25 dB. *Fig. 8* shows the microwave attenuation of wet corn as a function of moisture content, the average density value taken from the literature and the loss factor calculated from the measurements together with its regression expression. *Fig. 9* shows the measurement results of soft autumn wheat. The measured microwave attenuation values from wet textiles are shown in *Fig. 10*, the derived empirical expressions are also given.

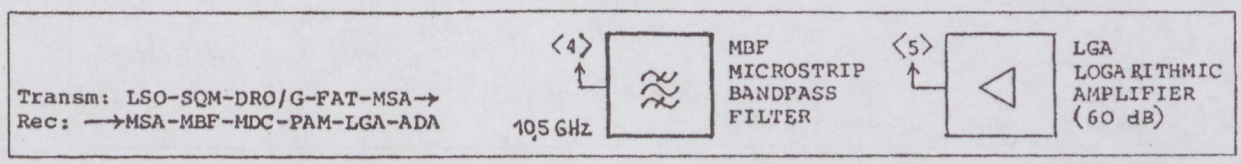

Fig. 7. Basic elements of the microwave moisture sensor for leather (MSL)

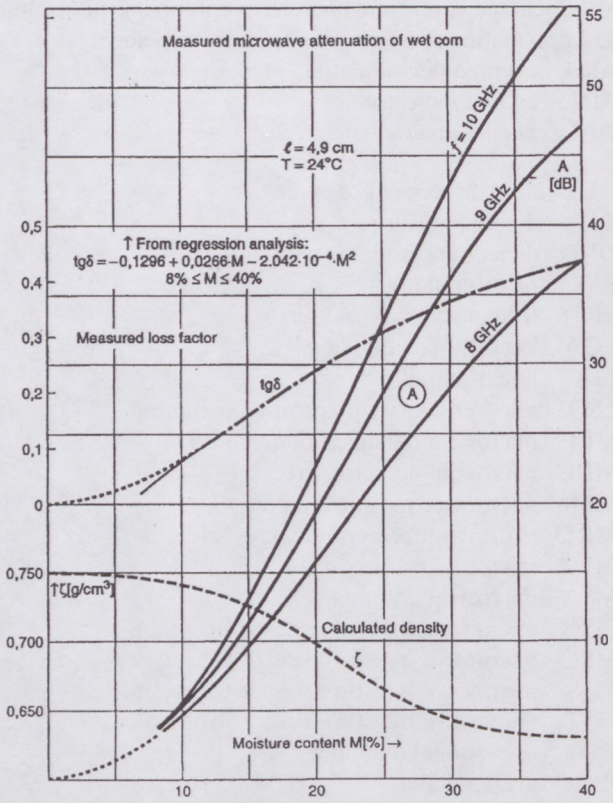

Fig. 8. Measured microwave attenuation of wet corn versus moisture content

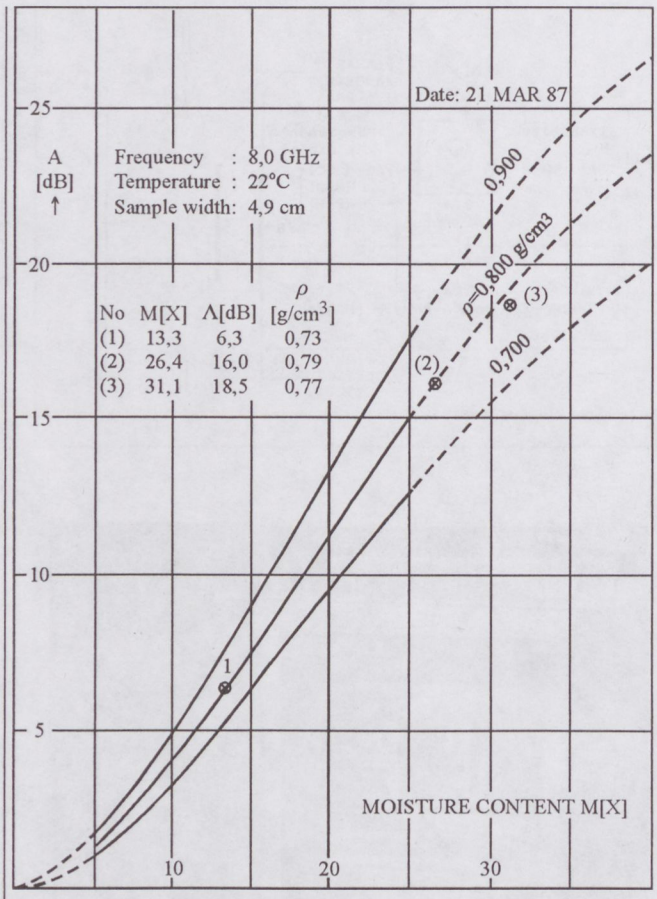

Fig. 9. Measured microwave attenuation of soft autumn wheat versus moisture content

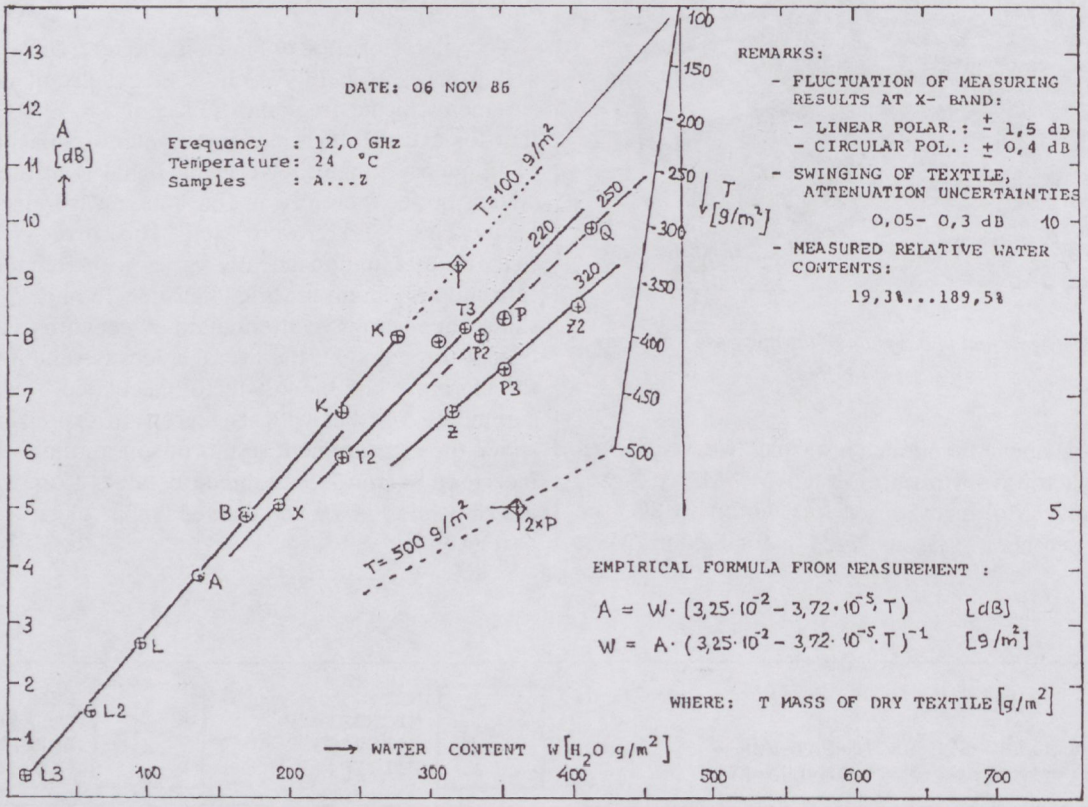

Fig. 10. Measured microwave attenuation of wet textiles versus water content

4. EXPERIENCES OF INDUSTRIAL APPLICATIONS

For the calibration of the *sensors of agricultural drying equipment* a Burrows Model-700 Digital Moisture Counter was used. Already during the laboratory tests it was revealed that the operation of planar detector and antenna (mounted originally on a plastic sheet within the vertically downward – moving corn) was disturbed bystatic charges. This was eliminated by replacing the plastic sheet with metallic one. The microwave moisture sensors were mounted at the input and output of a corn dryer with 80 tons of capacity and 15–20 tons per hour drying speed. The low variation of corn density in the sample space was provided in a mechanical way by directing sheets, the temperature correction of the output signal was maintained with a microprocessor control. An optimum control was found based on 1 sample/minute with moving averaging. The automatic equipment is in regular use with good results. The following experiences have been collected with our *moisture sensor in the textile industry*:

- vertically moving textile is bettering terms of sensor contamination,
- the effect of the swinging of textile on the measured values can be decreased by using circularly polarized microstrip antennas and by tilted $\sim 45°$ sensors relative to the direction of incidence,
- there is no specific need for temperature compensation, at most, only the Winter and Summer operations should be differently handled,
- there are different calibration curves for the materials with different dry density [g/m^2]. These can be included in the microprocessor control,
- a significant reduction of power consumption, and improved, stabilized product quality has been achieved by controlling the output air flow and material speed based on the output microwave moisture measurement.

5. CONCLUSIONS

One problem with the existing moisture sensors working by microwave transmission attenuation measurement is that due to their relatively large dimensions it is difficult to place the widely used horn antennas along or inside of the belt carrying the wet material. Owing to their small dimensions and low profile the *microstrip antennas* are excellent candidates for this purpose, too. It was experienced that in terms of propagation loss and near-field reflections, there is an *optimum size* (or element number) of antenna. Good results were achieved with circular polarization in cases of measuring anizotropic materials or at places with significant reflections from closely spaced metallic objects.

It is possible to develop a *series of* versatile microwave moisture *sensors* built from simple microstrip circuits, where the degree of sophistication can be optimally set to the precision and cost requirements of users. The active microstrip circuits can be *integrated* onto the microstrip antenna, and in mass production monolithic integrated approach would also be feasible further reducing cost and size and increasing reliability. This would help the widespread use of microwave moisture sensors.

REFERENCES

[1] F. Völgyi: "Microwave Moisture Measuring Instrument for Agricultural Applications"(in Hungarian), Research Report, BME/MHT-1987.

[2] F. Völgyi: "Circularly Polarized Microstrip Antenna in a Microwave Moisture Sensor for Textile" (in Hungarian), Research Report, BME/MHT-1986.

[3] H. Pleva: "Primarenergie-Einsparung bei Trocknung" VDI-Berichte, Nr. 345/1979, pp. 105-109.

[4] Y. Miyai: "A New Microwave Moisture Meter for Grains" Journal of Microwave Power, 13(2), 1978, pp. 163-166.

[5] M. Fisher, P. Vainikainen, E. Nyfors, M. Kara: "Fast Moisture Profile Mapping of a Wet Paper with a Dual-Mode Resonator Array" Proc. of the 18th European Microwave Conference, Stockholm, Sweden, 1988, pp. 607-612.

[6] S. O. Nelson: "Density Dependence of the Dielectric Properties of Wheat and Whole-Wheat Flour" Journal of Microwave Power, 19(1), 1984, pp. 55-64.

[7] S. O. Nelson: "Electrical Properties of Agricultural Products – A Critical Review" Transactions of the ASAE, 1973, pp. 384-400.

[8] A. Kraszewski: "Microwave Aquametry in Grain" SBMO'87 International Microwave Symposium, Brazil, 1987, pp. 145-150.

[9] H. Vifian, F. K. David, W. L. Frederick: "A Voltmeter for the Microwave Engineer" (HP-Model 8755 Frequency Response Test Set) Hewlett-Packard Journal, November, 1972, Vol. 24, No.3.

[10] S. O. Nelson and R. B. Russel: "Potential RF and Microwave Energy Applications in Agriculture" SBMO'87 International Microwave Symposium, Brazil, 1987, pp. 129-137.

[11] B. A. Herscher and R. H. Britton: "An Automatic Calibration System for Diode Power Detectors" SBMO'87 International Microwave Symposium, Brazil, 1987, pp. 1137-1144.

[12] F. Völgyi: "High Efficiency Microstrip Antenna Array" Proc. of the 17th European Microwave Conference, Rome, Italy, 1987, pp. 747-752.

[13] F. Völgyi: "Versatile Microwave Moisture Sensor" SBMO'89 International Microwave Symposium, Sao Paulo, Brazil, 1987, Symp. Proc., Vol. II, pp. 457-462.

MIKROHULLÁMÚ NEDVESSÉGÉRZÉKELŐK SOKOLDALÚ FELHASZNÁLÁSRA

Nedves dielektromos közegek mikrohullámú frekvenciákon mutatott csillapítása alapján sokféle nedvességérzékelőt fejlesztettünk ki, melyeket eredményesen használtak a textiliparban, mezőgazdaságban, élelmiszeriparban. Az általános követelmények és a mérési probléma matematikai megfogalmazása után a cikk részletesen ismerteti az előzetesen elvégzendő tájékozódó méréseket, a tervezéssel kapcsolatos megfontolásokat és a különféle mikrohullámú nedvességérzékelők blokksémáit. A kísérleti eredményekkel foglalkozó fejezetben a szerző által elvégzett mérések kalibrációs és mérési diagramjait találjuk különféle textilanyagokra, kukoricára és lágy őszi búzára vonatkozóan. Az üzemi kísérletek tapasztalatai szerint igen jelentős (25 %) energiamegtakarítás volt elérhető textilipari szárító berendezések mikrohullámú nedvességérzékelők beépítésével történő automaizálásával. Hasonlóan kiváló eredményeket kaptunk a Bábolnán gyártott szemestermény-szárító berendezéseknél való alkalmazás során is. Ezen sikerekhez nagyban hozzájárultak a nyomtatott antennák terén szerzett tapasztalataink.

MINIATURE ANTENNAS USED FOR WLAN SYSTEMS*

FERENC VÖLGYI

TECHNICAL UNIVERSITY OF BUDAPEST
DEPT. OF MICROWAVE TELECOMMUNICATIONS
H-1111 BUDAPEST, GOLDMANN TÉR 3, HUNGARY
PHONE: 36 1 463 1559; FAX: 36 1 463 3289; T-VOLGYI@NOV.MHT.BME.HU

With reference to the literature, after reciting the different types of microstrip antennas (MSAs) for WLANs, this paper describes the design considerations and experimental work performed on miniature MSAs for fixed stations and passive detector/backscatterers, which have been introduced into an electronic shelf label project and a complex permittivity monitoring system. Radiation pattern data and estimates of received signal strength are given for various kinds of arrangements. Experimental results are consistent with theoretical calculations.

1. INTRODUCTION

A new concept is frequently used at microwave WLAN systems: there are passive terminal stations (e.g. IC-cards in [1]), acting as transponders in which no microwave power is generated, and there are *fixed stations* (FXS) where most of the microwave active functions are executed or transferred to a central station e.g. by means of a fiber optic link [2]. The latter case allows the microwave hardware in FXS to be very simple. From microwave point of view, only a single Schottky-diode is used at the passive terminal station, acting as a *passive detector/backscatterer* (PDB), and using the modulated backscatter technology. Since a system normally has only a few FXSs but many PDBs, the most severe design constraints are on the PDB (portability, small size, long life and low cost).

The above mentioned technology offers inexpensive solutions for building low data rate wireless links, such as RF tag, Smart Card, radio frequency identification (RF/ID), electronic shelf label (ESL), electronic retail system (ERS), automatic vehicle identifier (AVI), road transport information (RTI) system, etc. Different types of *microstrip antennas* (MSAs) are used in these applications. A small-size *dual-port slot antenna* was designed to a wireless IC-card in [1], where the transmitter-receiver equipment was provided with a *shaped beam* circularly polarized *patch array*. A capacitively tuned thick patch radiator or a *higher order mode* rectangular MSA (introduced in [3]) is suggested to FXS, for broadband operation. For diversity experiments, a modified *inverted-F antenna* was used, as a built-in MSA [4].

Circularly polarized microstrip antennas are used in WLAN-systems [8] and e.g. in microwave moisture sensors [5], eliminating the disturbing effect of the reflected waves from the near-environment. The *directional terminal antennas* used in mm-wave indoor radio networks, suppress the outside cell interference, resulting in a significant capacity improvement [6]. The application of *dual-polarized MSAs* for polarization shift keying resulted 3dB improvement in signal-to-noise ratio in a microwave transponder [7]. The computer-aided design of a PDB-module at 5.8 GHz was described in [9]. The PDB consists of a specially formed *rectangular patch antenna* and a Schottky barrier diode. The realization of FXS and PDB-s in the industrial-scientific-medical (ISM) frequency bands are supported by low cost monolithic microwave integrated circuits (MMIC), [10]. *Modified microstrip circular patch* antennas are introduced in [11], where coplanar feed line and a parasitic slot are used to improve the matching and to control the desired mode of operation. A four-element *array of circular MSAs* with circular polarization (see *Fig. 1*) is used in FXS at 5.8 GHz [12], producing a shaped beam with a 3dB beam width of 22° and 82°. The bandwidth and gain of the array 130 MHz and 12.5 dB are, respectively. The two-layer structure consists of a power splitter and hybrids with dimensions of 0.8x45x105mm and a radiating-layer with dimensions of 1.6x25x105 mm. The thick substrate at radiators results in wideband operation and high efficiency. Via-hole groundings are made at the center of circular patches, suppressing higher-order modes.

This paper describes the design considerations and experimental work performed on microstrip antennas for FXS and PDB-s, which has been introduced into an electronic shelf label (ESL) project and a complex permittivity monitoring system.

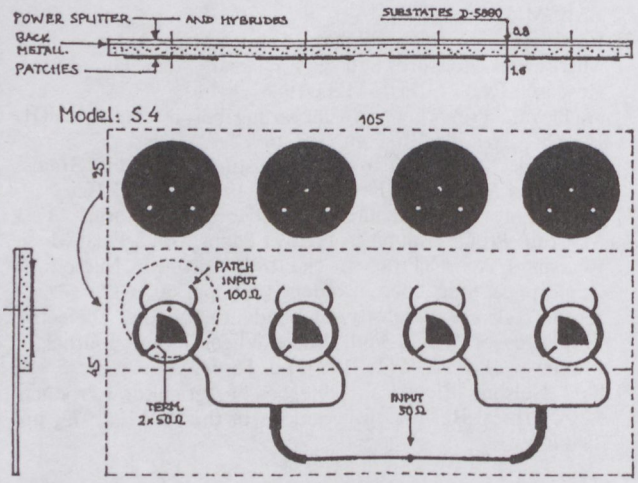

Fig. 1. RHCP-array for FXS at 5.8 GHz

2. DESIGN CONSIDERATIONS AND REALIZATIONS

The basic arrangement of an electronic shelf label system for super stores is shown in *Fig. 2.* In order to comply with FCC 15.247 (licence free operation), the FXS utilize direct sequence spread spectrum (DSSS) principle

* This is an extend of the paper presented by F. Völgyi in Chiba, Japan in September, 1996 [13].

for the uplink and downlink communication with the PDB. The effective isotropic radiated power (EIRP) of the FXS is +36 dBm. The PDBs, having individual codes, are interrogated (Downlink) successively by the 2.45 GHz transmitter using on-off keying (OOK) modulation.

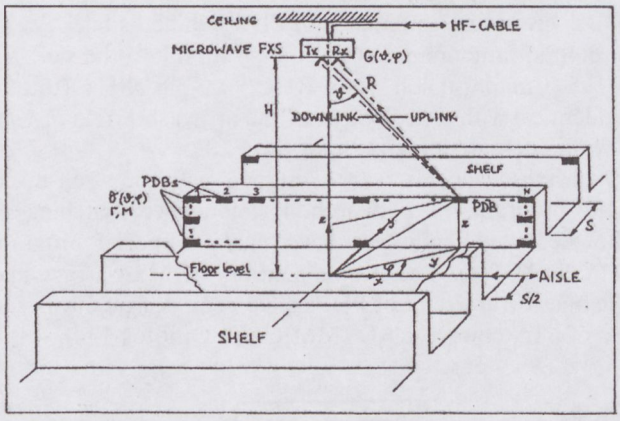

Fig. 2. Basic arrangement of an ESL-system

The Schottky diode detector of the PDB demodulates the signal and transfers the data to the digital circuits of PDB. The radar cross section (RCS or σ) of the PDB is changed by 10.7 MHz, so that the incoming CW-signal will be backscattered (Uplink) and binary-phase-shift-keying (BPSK) modulated and ultimately detected by the receiver of FXS. The single diode microwave circuit of the PDB offers simplicity, low cost and small dimensions. The HF-cable of FXS is suited to IF-RF communication between FXS and the other blocks of the system (multi cell controller, Ethernet-LAN, control PC).

To estimate the received power (P_r), set off the radar equation, using the designation of *Fig. 2*,

$$P_r = \frac{P_t}{(4\pi)^3 R^4}[\lambda_0^2 \sigma(\theta,\phi) G^2(\theta,\phi)\Gamma^2 M] \quad (1)$$

$$R = \sqrt{x^2 + y^2 + (H-z)^2} \quad (2)$$

$$\phi = \mathrm{tg}^{-1}(y/x) \quad (3)$$

$$\theta = \mathrm{tg}^{-1}\left[\sqrt{x^2+y^2}/(H-z)\right] \quad (4)$$

where P_t is the transmitted power, P_r is the received power, λ_0 is the free-space wavelength, $\sigma\ (\theta,\phi)$ is the radar cross section of the PDB, $G\ (\theta,\phi)$ is the gain of Tx and Rx antennas, Γ is the reflection coefficient of RF-diode circuit in PDB, M is the BPSK modulation rate. Calculated values of P_r versus x, y, z position of the PDB are shown in *Fig. 3*, neglecting θ and ϕ-dependence of σ. Three models of FXS antennas are taken into account in calculation. Well equalized characteristics, and relatively high received signal-levels are resulted at distances $x > 3$ m, using the dual-beam MSA-array (model S.3, shown in *Fig. 4*).

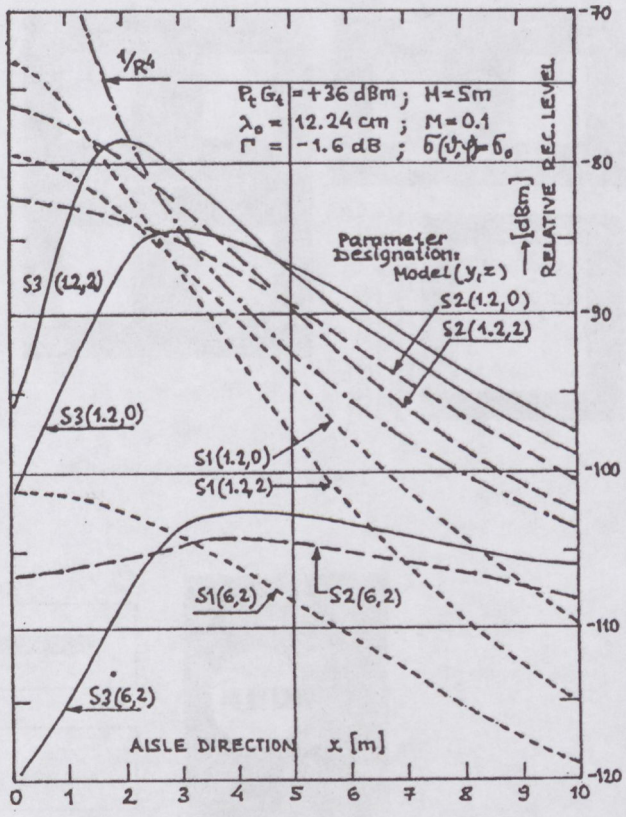

Fig. 3. Calculated Pr levels versus distance in aisle direction

The *design criteria for FXS-antennas* are:

- appropriate radiation characterics, depending on the cell-structure of the WLAN system, sufficiently high gain (but this is determined by the radiation patterns),
- linear or circular polarization (LP or CP), depending on the system design,
- possibility of diversity reception,
- high isolation between Tx/Rx-MSAs,
- integration with Tx/Rx equipment, etc.

To fulfill these challenges, we have designed, realized and measured the *next models* (see *Fig. 4*):

- S.1 A higher gain, 2.45 GHz single element MSA on a relatively thick substrate, which is suggested to WLAN systems with hexagonal ("flower") cell structure.
- S.2 Dual-element MSA, to deploy the FXS-antennas in a straight line which may simplify installation considerably.
- S.3 Dual-beam MSA-array (with four elements), reducing the radiation under FXS, expanding the connection in aisle direction.
- S.4 Shaped-beam CP-MSA array, used in our complex permittivity monitoring system [12] at the frequency of 5.8 GHz (see *Fig. 1*).

The *design criteria for PDB-antennas* are:

- extremely small dimensions,
- polarization is the same as which was selected to FXS,
- broad-beam radiation in both main-plane,
- higher gain models at critical(shadowed) places,
- many kinds of models are needed, partially compensating the variation of received signal, integration with Schottky-diode and its matching circuit, etc.

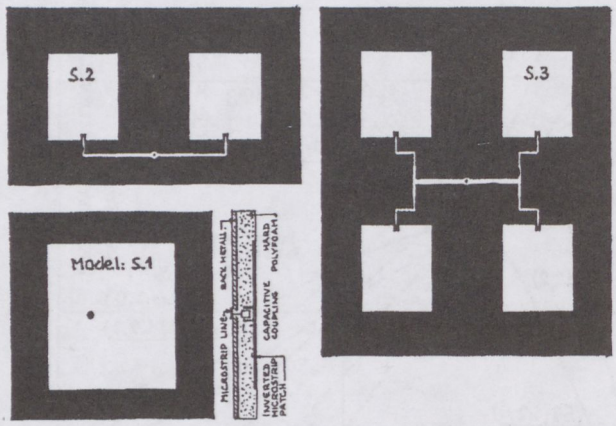

Fig. 4. Microstrip antenna models for FXS

We have designed, realized and measured the *next models* (see *Fig. 5*):

- B.1 Lightened rectangular patch antenna for 2.5 GHz with monolithic integration of the PDB.
- B.2 Printed dipole for 2.45 GHz. The Schottky diode PDB is integrated to the backside of the dipole.
- B.3 Inverted F-antenna with PDB behind its back.
- B.4 Slot antenna with PDB integration into the slot.
- B.5 Circular-patch with RHCP at 5.8 GHz (this is identical with one element of the array, shown in *Fig. 1*), with backside integration of the PDB.

All these models were designed with our self-made MSA-program. For hyperbolic impedance matching of the measured diode, we have made a special program (HYPMATCH). The power splitters of MSA-arrays and the microstrip circuit of PDBs have been designed with the aid of a microwave CAD (MMICAD, Optotek Ltd).

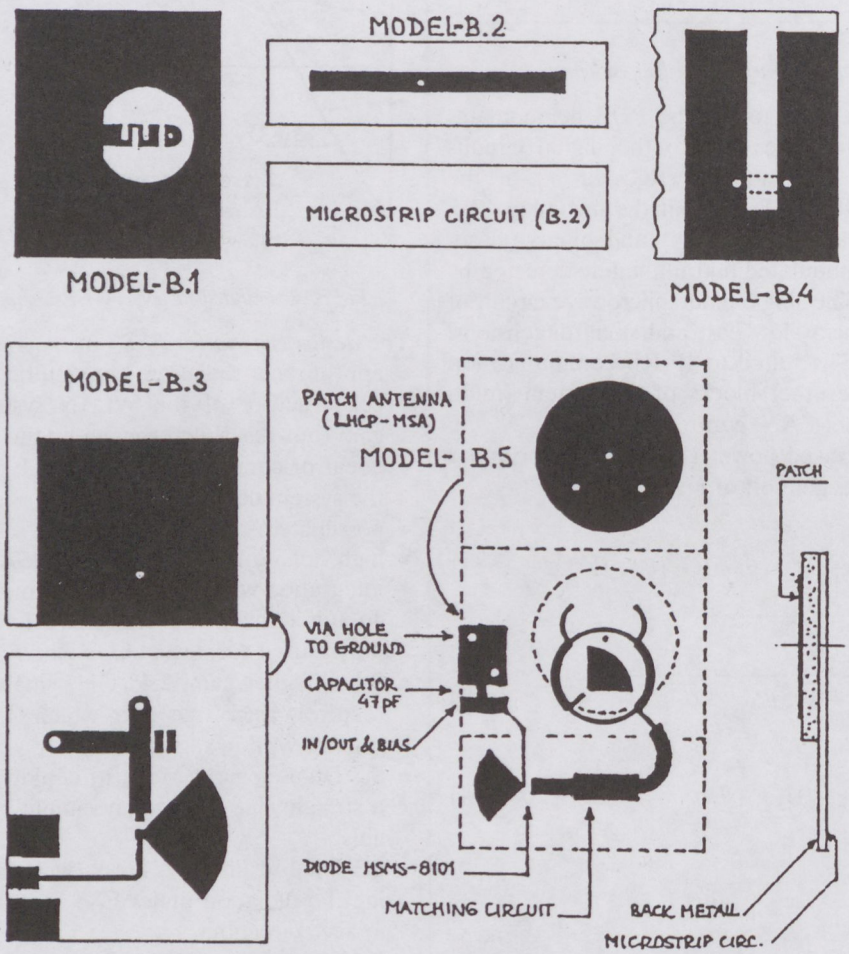

Fig. 5. Miniature PDB-antennas with integrated detector/backscatterer

We have to make *some comments on the selected models*. To reach a relatively high gain and broadband operation, low permittivity thick substrate (e.g. hard polyfoam with a thickness of 6.4 mm at model *S.1*) was chosen. The inductive reactance of the coaxial feedthrough was compensated by a built-in series capacitor. The substrate material of some other models is the higher permittivity ($\varepsilon_r \sim 4$) low cost FR-4 laminate, with the thickness of 1.4 mm. Using this substrate, the radiation pattern was broadened in the E-plane at model *S.2*, while the gain-specification was accomplished by the dual-element configuration. The antiphase excitation of patches in E-plane at model *S.3* results the dual-beam operation. At minimal field direction (perpendicularly to the antenna sheet) the radiation level can be increased by changing the input power rate of the patches in E-plane. Low loss

substrate (D-5880) was used at the higher frequency ISM band (5.8 GHz) at model *S.4*.

A simple monolithic integration with PDB is realised at model *B.1*, where the meander-line is used as an optimal matching element of the diode. Model *B.2* is the smallest one (0.8 cm^3). The inverted F-antenna *B.3* is a more effective radiator. Slot antenna *B.4* has the largest bandwidth. The circular patch *B.5* with right hand circular polarization (RHCP) is useful in reflective environment.

3. EXPERIMENTAL RESULTS

The measured results of the realized MSA-models are summarized in *Table 1*. The radiation patterns of model *B.1* are shown in *Fig. 6*. A main-beam shift of 11° is observable, because of the asymmetry of patch in E-plane. *Fig. 7* shows the received and preamplified (gain: 38 dB) DSSS signal versus frequency characteristic.

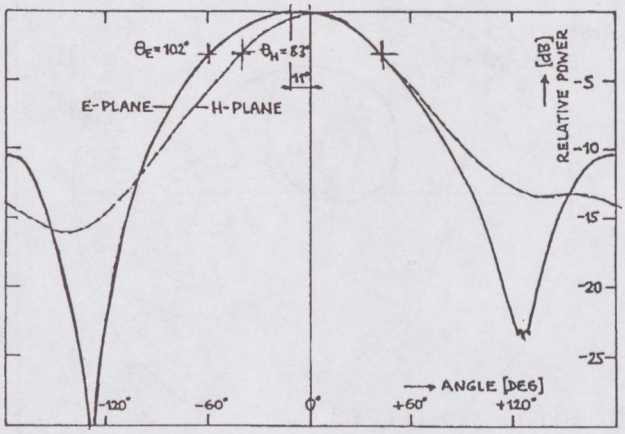

Fig. 6. Measured far-field characteristics of Model B.1

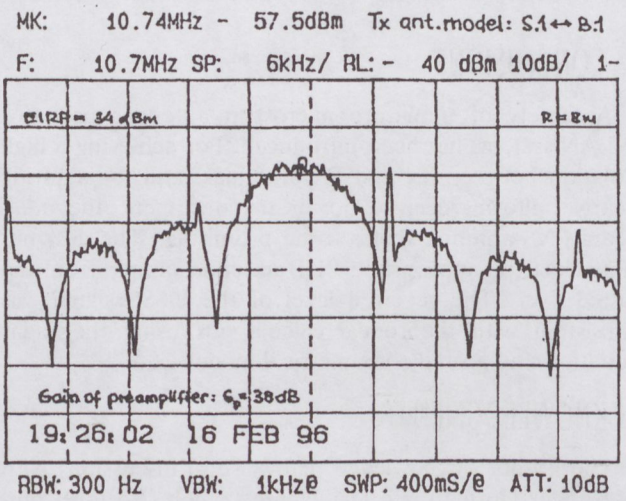

Fig. 7. Received power level versus frequency

Informative diagrams are shown in *Figs. 8–14*. The measured radiation pattern of model S.3 is shown in Fig. 8 (in colours*). This is a special projection of the stereoscopic radiation, where Θ-angle is radially scaled and azimuth angle Φ is scaled on periphery. The ranges of relative power levels are picted with colored areas.

A quarter of this measured diagram with more contour-lines is shown in *Fig. 9*. The relative values of pattern at directions characterized by $x = 0 \ldots 10$ m, (y, z) of coordinates are also given using continuous lines and broken lines. These values were used at calculations making diagrams in Fig. 3.

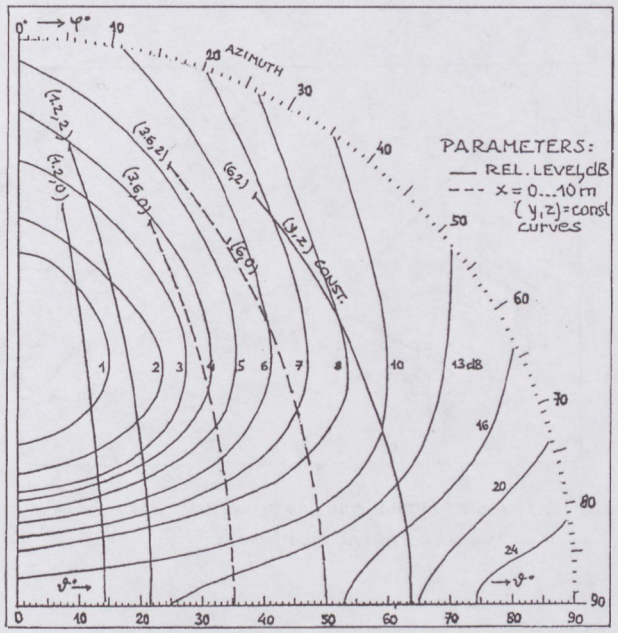

Fig. 9. Extrapolated pattern from measurement (shown in Fig. 8). These results are used to create S.3 values in Fig. 3.

The mutual coupling between transmitting- and receiving-model S.1 antennas is better than 46 dB, if the distance D between antennas is larger than 33 cm, as can be seen in the measured diagram of *Fig. 10*.

The input return loss versus frequency characteristic of model S.1 is given in *Fig. 11*, where the $RL = 10$ dB bandwidth is also written, i.e. 233 MHz (9.5 %), which can be achieved only by this capacitively broadbanded structure shown in *Fig. 4*.

The coupled radiating-resonator effect is also depicted in *Fig. 12* (loop-type impedance curve). The spatial radiation of model S.3 antennas is also illustrated in *Figs. 13* and *14* (in colours*), in cylindrical coordinates and spherical coordinates, respectively.

Table 1. Measured results of the realized microstrip antenna models

MSA models for FXS and PDBs	Type:	S.1	S.2	S.3	S.4	B.1	B.2	B.3	B.4	B.5
Center frequency	f_0 [GHz]	2.45	2.45	2.45	5.80	2.45	2.45	2.45	2.45	5.80
Gain (to isotropic)	G [dBi]	9.0	6.0	7.5	12.5	3.5	0	3.8	-0.6	6.8
Monostatic radar cross section	σ [cm^2]	753	-	-	-	60	12	68	9	49
Bandwidth ($RL = 10$ dB)	B [MHz]	233	60	140	130	56	40	134	200	130
Relative bandwidth	$b = 100B/f_0$ [%]	9.5	2.5	5.7	2.2	2.3	1.6	5.5	8.2	2.2
Beamwidth, 3 dB, E-plane	Θ_E [deg]	64	122	2x52	82	102	100	120	86	82
Beamwidth, 3 dB, H-plane	Θ_H [deg]	68	65	56	22	83	119	82	130	82
Figure of Merit	$M = 10^{-4}G\Theta_E\Theta_H$	3.5	3.2	3.3	3.2	1.9	1.2	2.4	1.0	3.2
Antenna Volume	V [cm^3]	32.3	8.4	16.8	8.0	1.6	0.8	5.0	0.8	2.3

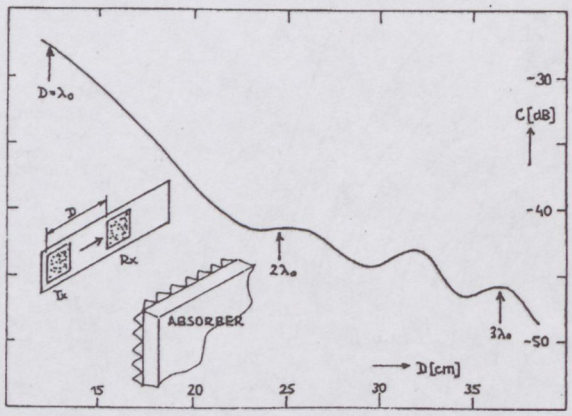

Fig. 10. Measured mutual coupling between S.1 antennas with horizontal polarization

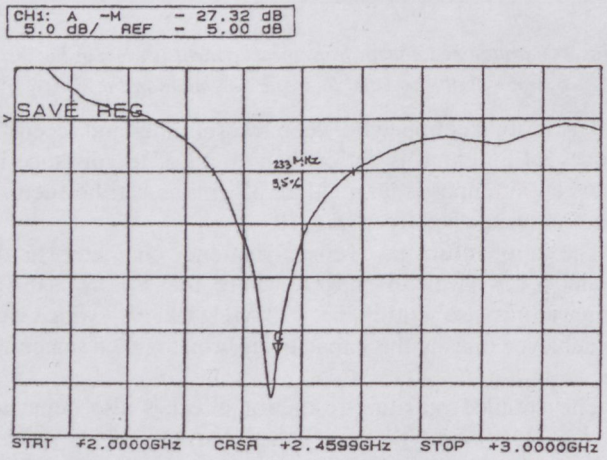

Fig. 11. Measured input return loss versus frequency for FXS antenna Model S.1

*** Coloured pictures cited are shown separately in the colour pages of this issue.**

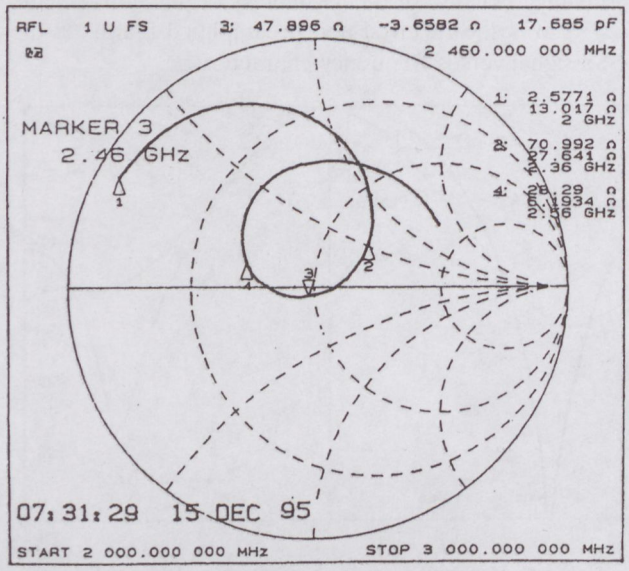

Fig. 12. Measured input impedance of the FXS antenna Model S.1

4. CONCLUSIONS

A variety of miniature microstrip antennas used for WLAN systems has been introduced. For achieving a high isolation between Tx and Rx antennas, and for assuring nearly uniform received power to consumers, the dual-beam FXS-antenna seems to be promising. The designer can select the appropriate PDB-antenna sample from the tested five. The received level of the DSSS signal was consistent with theoretical calculations using the radar equation and a simple geometrical model.

ACKNOWLEDGMENTS

The author acknowledge many useful discussions with Alexander Herman and Dr. Noam Livneh (Boston Communication Networks), and the help by Tom Cheatham (BCN, USA) and Prof. Dr. Csaba Szabó (BCN, Budapest) in creating the ESL-System.

The author would like to thank his colleagues Dr. Ferenc Lénárt (research associates) and Tamás Marozsák (PhD-student) for the spatial radiation-patterns used in this paper.

REFERENCES

[1] K. Konno, H. Wada and K. Matsukawa: "A 2.45 GHz Wireless IC Card System for Automatic Gates" 1993 IEEE MTT-S, Atlanta, USA, Digest pp. 797-800.

[2] S. Meyer, J. Guena, J. C. Leost, E. Penard and M. Goloubkoff: "A New Concept of LANs: Passive Microwave Links Hooked Onto a Fiber Optic Backbone" 1993 IEEE MTT-S, Atlanta, USA, Digest, pp. 1549-1552.

[3] Völgyi, F.: "Microstrip Antenna Array Application for Microwave Heating" 23rd European Microwave Conference (EuMC), Madrid, Spain, 6-9 Sept, 1993, pp. 412-415.

[4] Ogawa, K. and Uwano, T.: "A Diversity Antenna for Very Small 800 MHz Band Portable Telephones" IEEE Trans on AP, Vol. 42, No. 9, Sept. 1994, pp. 1342-1345.

[5] Völgyi, F.: "Integrated Microwave Moisture Sensors for Automatic Process Control" 1993 IEEE MTT-S, Atlanta, USA, WSMJ-Workshop, Proc. pp. 39-44.

[6] Kajiwara, A.: "Effects of Cell Size, Directional Antennas, Diversity and Shadowing on Indor Radio CDMA Capacity" PIMRC'94 Personal, Indor and Mobile Radio Communications Conf., September 18-22, 1994, Holland, pp. 60-64.

[7] Smith, D. and Jefferson, R. L.: "Dual Polarized Microstrip Antenna Design for Polarization Shift Keying Microwave Transponder" 19th EuMC, London, 1989, pp. 149-154.

[8] Chan, T. K. and Korolkiewicz, E.: "Design of the Microwave Transponder for Automatic Debiting Systems" 24th EuMC, Cannes, France, September 5-8, 1994, pp. 1025-1029.

[9] N. V. Schneider, C. Tran and R. Trambarulo: "Computer-Aided Design of Modulated Backscatter Microwave Modules" 24th EuMC, Cannes, France, 1994, pp. 1745-1749.

[10] M. Camiade, V. Serru, J. Ph. Brandeau and M. Parisot: "Low-Cost GaAs MMICs for 5.8 GHz Short Range Communications" MM'94 Conf., London, 1994, pp. 147-150.

[11] S. Mellah, M. Drissi and J. Citerne: "Novel Microstrip Circular Patch Antennas" 24th EuMc, Cannes, France, September 5-8, 1994, pp. 1750-1755.

[12] Völgyi, F. and Zombori, B.: "A New Application of WLAN-Concept: Complex Permittivity Monitoring of Large Sized Composite Boards" 1996 IEEE MTT-S Workshop, June 17, 1996, San Fransisco, USA, pp. 119-122.

[13] Völgyi, F.: "Microstrip Antennas used for WLAN Systems" ISAP'96 Int. Symp. on Antennas and Propagation, 24-27 September, 1996, Chiba, Japan, Proc. Vol. 3, pp. 837-840.

WLAN-RENDSZEREKBEN HASZNÁLT MINIATŰR ANTENNÁK

VÖLGYI FERENC

BUDAPESTI MŰSZAKI EGYETEM
MIKROHULLÁMÚ HÍRADÁSTECHNIKA TANSZÉK
TEL.: 36 1 463 1559; FAX: 36 1 463 3289; T-VOLGYI@NOV.MHT.BME.HU

Kis adatsebességű, vezetéknélküli lokális hálózatok (személyazonosítók, beléptető rendszerek, elektronikus jármű-azonosítók, áruházak elektronikus árucímkéző és raktározó rendszerei, közúti szállítási információs rendszerek stb.) esetében gyakori igény, hogy a mikrohullámú szempontból általában passzív végállomások antennái hordozhatók, kisméretűek, integráltak, olcsók legyenek. Ezen antennák ismertetésére vállalkozott a szerző ebben az írásban.

A WLAN-rendszerekben használt nyomtatott antennákra vonatkozó irodalom áttekintése után a cikk a bázisállomások és végállomások (passzív detektorok/visszaverők) antennáinak tervezési megfontolásait és a kísérleti munka fázisait ismerteti. Részletesen foglalkozik egy áruházi címkéző (raktározó) kommunikációs rendszer, és egy komplex permittivitást monitorozó szórt-spektrumú mérőrendszer antennáival. Egyszerű, a lokátor egyenletből kiinduló modell- és térbeli antenna iránykarakterisztika mérések alapján meghatározza a vételi jelszintet különféle elrendezésekre. Az elméleti számítások a gyakorlatban jól használható, kísérletileg alátámasztott eredményeket adtak.

A cikk nagyban segíti a tervezők munkáját a Mikrohullámú Híradástechnika Tanszéken kifejlesztett sokféle integrált antenna bemutatásával és főbb jellemzőinek táblázatos összefoglalásával.

SIMPLE METHODS FOR TESTING THE TEMPERATURE DEPENDENCE OF MICROSTRIP ANTENNA ARRAYS*

FERENC VÖLGYI

TECHNICAL UNIVERSITY OF BUDAPEST
DEPT. OF MICROWAVE TELECOMMUNICATIONS
H-1111, BUDAPEST, GOLDMANN TÉR 3, HUNGARY
PHONE: 36 1 463 1559
FAX: 36 1 463 3289
T-VOLGYI@NOV.MHT.BME.HU

This paper presents methods that can be used to determine the temperature dependence of microstrip antennas (MSA). The input reflection of the MSA array and the Radar Cross Section (RCS) was measured without special equipment in laboratory conditions. These experiments showed the change in resonant frequency (f_r) and antenna gain (G) versus temperature. Using the measured data, the temperature dependence of the dielectric constant of the substratum can be calculated by computer modelling.

1. INTRODUCTION

Though methods for compensating the temperature dependence of MSA are available [1] and there are special substrates with low temperature dependence [2], the technical literature of this field usually gives calculated values [3] , while measurement results are rarely at hand [4].

RCS measurements carried out on a constant temperature are getting more and more frequent. Such measurements on planar patch antennas we have designed were performed in Karlsruhe – by way of a cooperation between the Technical University of Budapest (Hungary) and the University Karlsruhe (Germany) [5].

Testing the temperature dependence of microwave circuits and antennas can be performed in climatic chambers. The near field of multi-element, high gain antenna arrays is greater than the size of these equipments. However it is obvious that the objects in the near field cause measurement errors.

The methods described here have been carried out without climatic chamber. Two antennas have been tested in input reflection, one on 3M CuClad-217 substratum designed for 4.41 GHz with 64 elements [6] (No. 1.), the other for 8.14 GHz on RT-Duroid 5880 with 256 elements [7] (No. 2.). A quarter of our 1024-element MSA array – designed for 12.7 GHz – has been tested by RCS measurement. We have achieved variations in temperature by local heating/cooling using Peltier elements – which were used at our previous circuits [8] successfully – at the input reflection test and using infrared lamps at the RCS measurements.

* This is an extended version of paper [14].

2. TEMPERATURE DEPENDENCE OF MSA IMPEDANCES

The temperature dependence of the feeding network and of the radiating elements are different from each other in case of high gain MSA-s [7], as their parameters depend on the geometrical sizes and substratum parameters in different ways. It is important to stress that the bandwidth of the antenna elements is smaller ($1-5$ %) than that of the feeding network.

While the variation in the characteristic impedance of the feeding network can be negligible as a function of temperature, the most important factor is the change in resonance frequency (f_r) of the radiating elements, caused by the temperature dependent length of the patch $L(T)$ and dielectric constant $\varepsilon_r(T)$. At the same time the input impedance of the radiating elements hardly changes.

As comes of all the above, the return loss $A_r(f)$ of the antenna elements will shift on the frequency axis as a change in temperature occurs. While this shift is within the bandwidth of the feeding network, this is the most significant change as a function of temperature concerning the whole multi-element antenna array. This fact has been used in our measurement method.

3. TEMPERATURE DEPENDENT INPUT IMPEDANCE MEASUREMENTS

A 2×2 element module has been used at the measurement of the 64-element (No. 1.), and a 4×4-element module with the 256-element one (No. 2.), each with a size of 100×100 mm. The modules were thermally insulated. A material having low loss and low permittivity has been used in front of the antenna, in the radiating field. The antennas were mounted on two (thermally serially connected) Peltier elements, which were mounted on a cooling rib, diving into melting ice (*Fig. 1*). This way the temperature of the cooling rib was stabilized around $0°C$. With the two separately controlled Peltier elements we have managed to achieve a $40°C$ difference in temperature. While heating the antennas we took the melting ice away gaining a $20°$ rib temperature. So the available measurement range was $-40 \ldots +60°C$. The module, prepared this way was connected to a network analyzer to measure the return loss versus the frequency $A_r(f)$ continously. When a sig-

nificant change occurred we plotted the $A_r(f)$ curve and recorded the temperature.

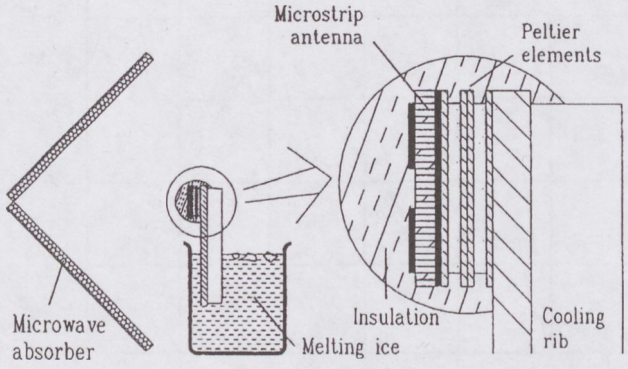

Fig. 1. The scheme for temperature dependent input impedance measurement of MSA-modules.

4. TEMPERATURE DEPENDENT RCS MEASUREMENTS

In the measurement of the temperature dependent gain of the MSA arrays two major problems emerge: we have to use too great measurement distances and ensure uniform heating of the antenna. In order to decrease measurement distances, we used the MSA array (to be measured) as a reflecting antenna, terminated with an open end. This way we have calculated the gain of the antenna on the basis of the measured bistatic RCS [9]. The antenna was heated by infrared lamps from behind, thus the antenna temperature could be easily varied between $+20°C$ and $+50°C$ in standard laboratory conditions.

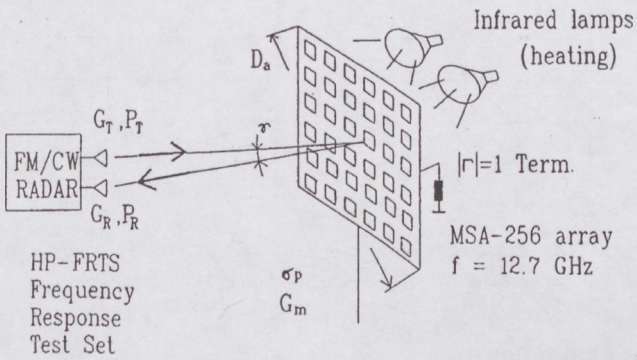

Fig. 2. Temperature dependent RCS-measurements of MSA-arrays.

To calculate the measurement distance we have used our function fit on the data from Kell and Hendrick's results [9]. In case we renounce the fine structure of the RCS it results in $R_c = 3.1$ m minimal distance to measure a square MSA with $D_a = 50$ cm diagonal at 12.7 GHz. On the other hand, based on the formula $2D_a^2/\lambda$ (from the plane wave condition), the distance would have been 20.8 m. Due to the small distance, measurement equipments with low dynamic range are suitable, and the background reflections – caused by the standard laboratory conditions – have a minor effect on the measurement accuracy. Using a small-size transmitter and receiver antenna, we have got $\gamma \leq 1°$ bistatic angle from R_c distance. It can be considered a monostatic RCS measurement. Based on the radar equation the effective radar cross section of the reflecting antenna – using the notation of *Fig. 2* – results in:

$$\sigma_p[\mathrm{dBm}^2] = 11 + 40\log R[\mathrm{m}] - \\ - 10\log(P_T/P_R) - 20\log(G\lambda[\mathrm{m}]/4\pi \quad (1)$$

and the measured antenna gain is:

$$G_M[\mathrm{dBm}] = 5.5 + \sigma_p[\mathrm{dBm}^2] - 10\log(\lambda[\mathrm{m}]) \quad (2)$$

5. EXPERIMENTAL RESULTS

By the end of the input impedance measurement we have got different $A_r(f)$ curves for each variation of temperature (*Fig. 3*). As can well be seen the curves shifted as was previously expected.

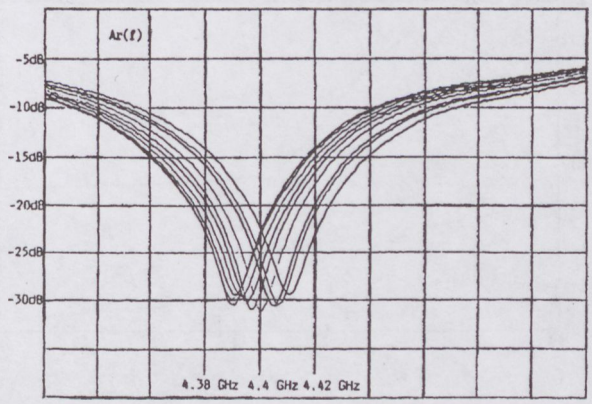

Fig. 3. Measured temperature dependent input return loss versus frequency characteristics.

Describing the change in resonant frequency versus temperature we have got *Fig. 4*, which is the most characteristic feature of temperature dependence. The nonlinearity of the curves is due to the nonlinear $\varepsilon_r(T)$ function, which is a typical behavior of PTFE (teflon) substrates near $20°C$. These functions – which are missing parameters of the substrates – can be calculated from the thermal expansion data [10], [12] and from the measured resonance frequency. We have used our previously developed CAD program for the calculations, which analyzes the MSA as a function of geometry and substrate parameters.

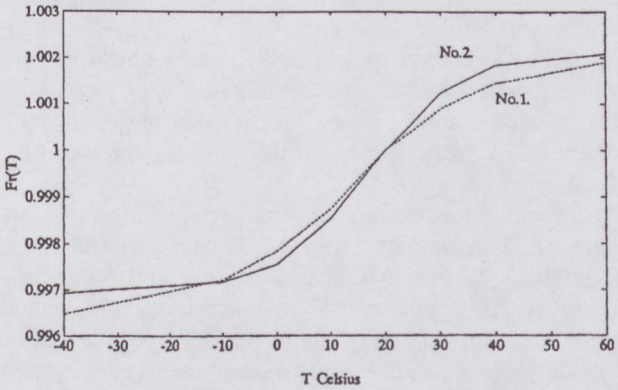

Fig. 4. Measured relative resonance frequency as a function of temperature.

The $\varepsilon_r(T)$ functions (*Fig. 5*) gained this way are in accordance with the data published in [11] where -96 ppm/°K was the thermal coefficient of 3M-CuClad DX-060-045, while the data we have got for antenna No. 1. and No. 2. based on our measurements and calculations can be seen in *Table 1* (thermal coefficient of ε_r in ppm/°K at different temperature ranges for the two antennas, with extrapolated data at 100°C).

Table 1.

Temp. °C	$-5\ldots+25$	$-10\ldots+30$	$-40\ldots+60$	$0\ldots+100$
No. 1.	-207	-161	-124	-92
No. 2.	-455	-386	-240	-154

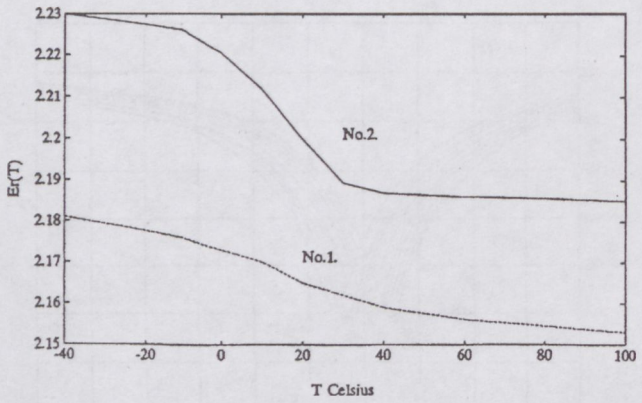

Fig. 5. Dielectric constant as a function of temperature (calculated from measurements).

Because data in *Table 1* also depend on their thermal expansion data – which are not the same at the different data sheets – they are valid only with [10] and [12].

Fig. 6 describes the RCS measurement results, showing the relative received power as a function or frequency at two different temperatures. It brings about the following statements:

- we can sense about ± 0.5 dB fluctuation resulting from -25 dB relative background reflections [9], which seems to be acceptable in standard laboratory conditions,
- due to the variation of the return loss – caused by the modification of the resonance frequency (*Fig. 3*) – the curve of the relative received power shifts upwards in frequency, so does the RCS curve of the reflecting antenna in return,
- the relative received power decreases by about 0.4 dB which means a 0.2 dB decrease in gain, owing to a 28°C rise in temperature. Therefore the thermal coefficient of the MSA array gain is -0.007 dB/°K, which can be negligible in practice.

The temperature-dependent input impedance can be compensated by varactor tuning. Because of the thermal coefficients of varactor-capacitance and substrate-permittivity are opposites, this compensation may be automatic, selecting an appropriate bias voltage of the varactor diode. The measured relative resonant frequency versus temperature characteristic [13] of the varactor-tuned MSA-array is shown in *Fig. 7*. An excellent frequency-compensation is measured at reverse-bias of 1 V.

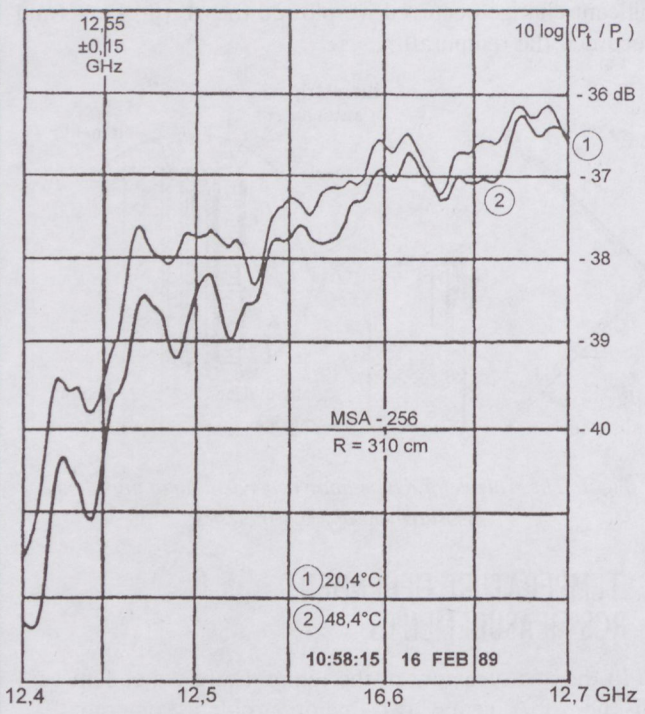

Fig. 6. Measured relative received power as a function of frequency at two different temperatures.

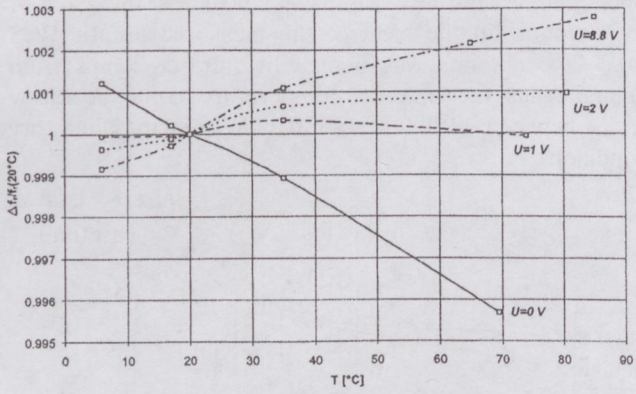

Fig. 7. The measured relative resonant frequency versus temperature characteristic of the varactor-tuned MSA-array.

6. CONCLUSIONS

The methods described here show simple tests of important antenna parameters versus temperature, where only a few additional equipment is needed to complete the normal microwave laboratory test sets. The measurements have made it clear that a smaller module test is enough for the temperature test of the multi-element antenna arrays, moreover that the temperature should be registered if measurements are made on MSA-s of small bandwidth.

The RCS-measurements have resulted in the fact that the change in gain as a function of temperature is determined by the change in $A_r(f)$, the effect of other losses can be negligible. It can be considered as a further important result that $\varepsilon_r(T)$ functions could be determined by the result of our measurements and computer simulations.

As the control and measurement of temperature was carried out electronically, the whole process could have been fully automated using computer control.

7. ACKNOWLEDGMENT

The author wish to acknowledge Ferenc Mernyei for many informative discussions, for his assistance in experiments and for his help in the preparation of the earlier version of this paper.

REFERENCES

[1] M. A. Weiss and R. E. Munson: "Temperature Compensated Radio Frequency Antenna and Methods Related Thereto" US. Patent No. 4366484 (1981).
[2] G. R. Traut: "Clad Laminates of PTFE Composites for Microwave Antennas" Microwave Journal, November, 1980.
[3] J. R. James, P. S. Hall and C. Wood: "Microstrip Antenna-Theory and Design" Peter Peregrinus Ltd., Stevenage, UK, 1981.
[4] G. R. Traut: "Electrical Test Methods for Microwave PCB's" Microwave Journal, Dec. 1981.
[5] E. Heidrich and W. Wiesbeck: "Features of Advanced Polarimetric RCS-Antenna Measurements" IEEE AP-S Int. Symp. and URSI Meeting, San Jose, June 1989.
[6] F. Völgyi and F. Mernyei: "MACORD Trans./Rec. Microstrip Antenna" Know-How Documentation, TUB/DMT, Budapest, 1987.
[7] F. Völgyi: "High Efficiency Microstrip Antenna Array" Proc. of the 17th EuMC, 7-11 September 1987, Rome, Italy, pp. 747-752.
[8] F. Völgyi: "Parametric Amplifiers on Plastic Substrates" XX. Int. Coll. TH-Ilmenau, 1975.
[9] C. G. Bachman: "Radar Targets" Lexington Books D. C. Heath and Company, 1982, ISBN: 0-669-05232-9.
[10]3M Cu-Clad 217, Bulletin No. EL-CCB (90.8) JR.
[11]3M Microwave Tech. Topics, Bulletin No. EL-MTT/2 (20.15) II.
[12]RT/Duroid-5880 Data Sheet, Rogers Ref. Book 1165: 2-14, T. R. 1391, J449C12E.
[13]Z. Varga: "Theoretical and Experimental Study of MSAs" Diploma Thesis, TUB/MHT, 1997, Supervisor: F. Völgyi.
[14]F. Mernyei and F. Völgyi : "Simple Methods for Testing the Temperature Dependence of Microstrip Antenna Arrays" 20th EuMc, Budapest, Hungary, September 10-13, 1990, Proc. pp. 365-370.

EGYSZERŰ ELJÁRÁSOK NYOMTATOTT ANTENNÁK HŐMÉRSÉKLETFÜGGÉSÉNEK VIZSGÁLATÁRA

VÖLGYI FERENC

BUDAPESTI MŰSZAKI EGYETEM
MIKROHULLÁMÚ HÍRADÁSTECHNIKA TANSZÉK
TEL.: 36 1 463 1559; FAX: 36 1 463 3289; T-VOLGYI@NOV.MHT.BME.HU

Az eső okozta csillapítás, valamint a jegesedés hatását antennákra régóta ismerik, míg a hőmérsékletváltozás okozta deformációkat és antenna paraméter változásokat csak a műholdakra szerelt antennáknál kezdték először vizsgálni. A nyomtatott antennáknál (MSA) ez alapvető követelmény, hiszen a rezonáns elemekből felépített planár-antennák sávszélessége általában kicsi, így a hőmérsékletváltozás okozta rezonancia frekvencia változás, mely főleg a szubsztrátumtól függ, nem elhanyagolható.

Számítással ezen hatások bizonyos mértékig leírhatók, azonban az antennák hőmérsékleti vizsgálata során nagyméretű, költséges klímaberendezésekre van szükség. A cikk újdonsága, hogy az MSA-k hőfokfüggő vizsgálatára egyszerű módszereket ajánl, melyek a mikrohullámú laboratóriumokban megtalálható szokásos mérőműszerekkel elvégezhetők.

Elemi nyomtatott antennáknál vagy kisebb elemszámú antenna moduloknál a legjelentősebb hőmérsékleti hatás a rezonancia frekvencia elcsúszásában jelentkezik. Ennek mérésére a szerző Peltier-hűtőelemekre szerelt MSA-k reflexiómentesített közel-környezetben való bemeneti reflexió vizsgálatát javasolja. A másik lehetséges hatás az antenna nyereség hőmérsékleti változása. Mivel a nyereség a távoltéri iránykarakterisztikával van kapcsolatban, nagyméretű MSAk-nál 10 GHz-nél nagyobb frekvenciákon igen nagy mérőtávolságok adódnak, melyeknél a klíma-követelmények nem teljesíthetők. Ebből a szempontból a cikk újdonsága az, hogy a nyereség hőfokfüggésének ellenőrzését radar hatásos keresztmetszet (RCS) mérésre vezeti vissza, mely kis mérő-távolságok esetén is elfogadható pontosságú eredményeket szolgáltat.

A cikkben részletezett mérési eredmények a vizsgált 4-elemes moduloknál 0.5 % körüli rezonancia frekvencia változást adtak a kritikus $-10 \ldots + 40°C$ hőmérséklet tartományban. A részletes mérési eredményekből egyébként a dielektromos hordozó hőmérsékletfüggése is visszaszámolható volt a Tanszéken kifejlesztett MSA-program inverz alkalmazásával. A hőmérsékletfüggő RCS-mérésből meghatározott nyereségváltozás elhanyagolható mértékű volt, melyben csupán a rezonancia frekvencia eltolódásából adódó reflexiós csillapításváltozás hatása volt kimutatható. Összefoglalóan megállapíthatjuk, hogy ez a cikk a nyomtatott antennáknál egy igen lényeges hatásra hívja fel a figyelmet, az ellenőrzésre konkrét javaslatokat tesz, s azokat kísérleti módszerekkel vizsgálja.

RF – ABSORBERS FOR GTEM-CELL APPLICATIONS*

FERENC VÖLGYI

TECHNICAL UNIVERSITY OF BUDAPEST
DEPT. OF MICROWAVE TELECOMMUNICATIONS
H-1111, BUDAPEST, GOLDMANN TÉR 3, HUNGARY
PHONE: 36 1 463 1559; FAX: 36 1 463 3289; T-VOLGYI@NOV.MHT.BME.HU

SÁNDOR TATÁR

TKI – INNOVATION COMPANY FOR TELECOMMUNICATION
H-1142 BUDAPEST, UNGVÁR U. 64-66.

Different types of EMC testing sites (TEM, GTEM Cells) and various materials and structures used as radio frequency absorbers are summarised. Then a new type cellular structure radio frequency absorber is presented which has several advantages compared to the usual large, expensive pyramid absorbers. Some measurement results (reflection versus frequency characteristic) and a short description of an experimental GTEM chamber with this new absorber are also given.

1. INTRODUCTION

The European Economic Community EMC Directive introduced step-by-step the need for various electronic products to respond the severe EMC criteria for reliability. *A good EMC test method is*: reproducible between sites, repeatable between measurements, simple (implementable, fast, efficient, inexpensive). Because no single method is clearly ideal, a *variety of test environments for EMC immunity and emission measurements* are used in practice. A brief discussion of this is given in [1], starting with the description of open area test site (OATS).

1.1. TEM Cells

For simulations operating in the electromagnetic pulse mode, such as *large EMP Simulators*, parallel plate structures are used, tapered at each end to mate with standard coaxial line (see e.g. [2]). An alternative to the simple parallel plate line is a coaxial line with rectangular cross section, an outer rectangle with a wide flat inner conductor. Such TEM cells are closed and not coupled to the outside, but they form a cavity and thus can have strong field resonances at higher frequencies.

A TEM cell with a *space saving planar terminator* is described in paper [3], where the limiting frequency caused by the radiation of the planar terminal was expanded from 50 to 250 MHz, using a constriction of the inner conductor. A new conical active absorber was considered at [4], terminating a TEM cell. "Activity" means that both sides of the cell were provided with equal waves using a high precision power splitter. For low cost electromagnetic immunity test setup, a *Triple-TEM cell* was described in paper [5]. The advantage of this method is that an equipment under test (EUT) can be irradiated with differently polarised fields without rearranging the test setup.

1.2. GTEM Cells

The so called GTEM Cell (GHz TEM Cell) is a tapered asymmetric TEM cell which was developed at ABB in Switzerland [6]. This is one of the most useful device for emission and immunity testing [7], in which an overall field uniformity (with position and frequency) of 4 dB within the recommended test volume is achievable [8] due to combine a lumped resistive load with an absorber (typically cone or pyramid) wall at the cell termination.

These combined loads were analytically examined together in [9] and [10] by using a transmission line model for low frequencies and a local mode expansion for higher frequencies. In the GTEM Cell a slightly spherical TEM wave is propagating from the source (apex) through a flared 50Ω rectangular coaxial transmission line section into the distributed hybrid termination. As the opening angle of the waveguide is small this spherical wave approximates a plane wave. Loading effects, excitation and scattering were extensively studied [11], [12]. The GTEM Cell is providing a useful tool for characterising the electromagnetic scattering of objects under laboratory conditions, too [13]. The article [14] reports on the design and construction of a new GTEM configuration that allows two degrees of motion between the EUT and GTEM. This configuration allows for fast and accurate testing, as the EUT does not require special fixturing for each test. Due to the asymmetry of GTEM Cell, it presents interesting and peculiar EM-pulse propagation characteristics, but completely predictable by the model of [15].

1.3. Microstrip antennas in sophisticated systems

The problems of weight are essential for the space technologies, so the microstrip antenna (MSA) being light [16] and not bulky, could be used to replace the conventional aerials in the future. Our MSA-s are applied for microwave heaters [17], in moisture sensors [18] and in WLAN-systems [19], too. *The susceptibility of MSA-s to EMP interferences* was studied in [20].

Sometimes the immunity of the simple electronic system is not large enough relative to the EMC-pollution (radiation of microwave ovens, high power dryers in industrial environment, etc.). In these cases more sophisticated systems are used to suppress the unwanted interferences (e.g. spread spectrum systems in [21] and [22] or adaptive DSSS-system in [23]).

2. RADIO FREQUENCY ABSORBERS

EMC standards commonly prescribe radiative EMI measurements to be made in the 30–1000 MHz frequency range (OATS or its alternatives). Carbon loaded foam tapered in the form of pyramid is the generally used RF absorber in anechoic chambers having low reflections. To characterise the reflectivity of large pyramids an experi-

* This is an extend of the paper presented by F. Völgyi in Zurich, Switzerland at EMC' Zurich Symp. 1999 [31].

ment with flared waveguide was described in [24]. For standard absorber with dimensions of $0.61 \times 0.61 \times 0.92$ m^3, at the frequency 100 MHz and 300 MHz the measured reflectivities -12 dB and -35 dB were, respectively. Analysis and measurements of electromagnetic scattering by these pyramidal absorbers are given in [25]. Evaluation of various absorber materials (foam, polystyrene, ferrite) in the frequency range of 30-300 MHz, and a lumped element network representation of the absorber is described in [26]. Reference [27] reports the results of an experimental test program using TEM cell ($1.22 \times 1.22 \times 2.44$ m^3) with RF absorbing materials on the inside walls. It was tested to see how suppression of resonances affects the field distribution within the cell. A detailed comparison of *urethane pyramids, twisted-pyramids, wedges, as well as ferrite tiles, ferrite grids, and hybrid combinations of urethanes and ferrites* is given in [28]. At last we must mention composite materials such as graphite/epoxy (G/E) fiber-reinforced composites, which have been widely used as substitutes for metals in modern aircraft systems due to their superior mechanical properties. From EMC point of view these periodic laminated composite structures are modelled and characterised (0.1 MHz – 100 GHz) in [29].

3. DESCRIPTION OF THE NEW TYPE CELLULAR STRUCTURE ABSORBER

A new type *cellular structure absorber has been invented.* It has a modular trellis-work structure, which is composed of *dielectric plates covered with graphite*. Between the separating walls there are additional smaller cell-walls as seen on *Fig. 1.*

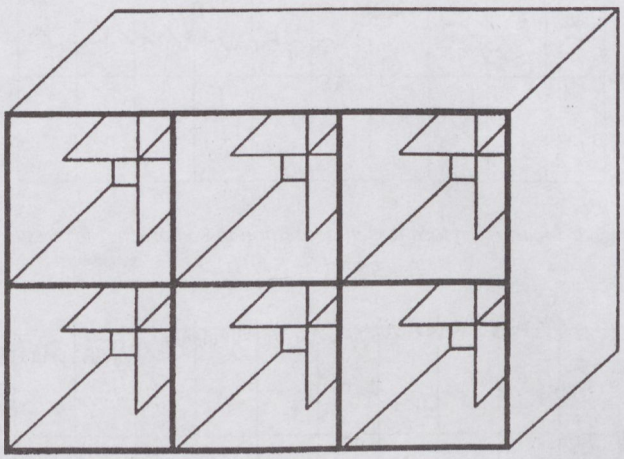

Fig. 1. Some absorbing modules.

These walls can be repeated with decreasing dimensions if necessary. Longest walls have a length of a fraction of the quarter wavelength (e.g. 1/40 wavelength) at the lower cut-off frequency. Plane cell-walls are perpendicular to each other, so they absorb radio frequency signals arriving from the cell aperture efficiently, independently of the signals' polarisation. Electrical field strength (E) can be distributed into two components parallel to the graphite-covered walls' planes and each wall attenuates the appropriate parallel field component. To decrease the reflection caused by the edges of the walls a smaller wall can be inserted into each cell. If the distance between the edges of higher and the lower wall is a quarter wavelength at a certain frequency, the reflection coefficient will have a minimum at this point, because the two reflected wave having a phase difference of 180 degrees cancel each other. Choosing proper wall heights a flat, equalised reflection characteristic in a wide frequency range can be achieved which is not exceeding a given level (e.g. -20 dB). Resistance of the graphite layers depends on their thickness. A square resistance of 377Ω (free-space wave impedance) could be a good choice for our purposes.

3.1. Advantages of the structure

,

- simple construction (modular, on demand expandable structure),
- has excellent reflection properties,
- a much larger test volume is available, relative to the large pyramidal absorber,
- large surface enables extremely high power dissipation,
- therefore formation of smoke caused by overheating is unlikely,
- cheap, environmentally friendly materials can be used as substrate of the graphite layer (e.g. fibreboard, composite board or corrugated cardboard),
- absorbing graphite can be painted in aqueous silicate solution (silicated board), which also acts as flame protection (non-combustible absorber),
- in this case smoke gases formed at extreme overcharge do not contain any poisonous or environment-damaging materials,
- rounding off edges is not necessary because of the reflection-cancelling mentioned above, so the cell structure can support heavy-weighted loads,
- low-cost transportation (in disassembled state uses negligible volume).

The base element of the absorber wall is a box-like module specially folded from corrugated cardboard (see *Fig. 3* in colours*). It is painted internally with resistive ink and has inner cells. To make them dust resistant, absorber blocks – containing 2×2, 3×3, $4 \times 4, \ldots$ modules – are covered. This is shown in *Fig. 4* in colours*, for the 3×3 modules absorber. This covered blocks absorber can be bonded to the wall or to the ceiling of a shielded room like tiles using rapid epoxy adhesive. The absorber wall can carry heavy load, therefore the covered blocks are suitable to lay directly under the floor. Although this is designed for indoor application, the cover can be hermetic for request. Absorber wall tiled with these blocks provide attractive view (*Fig. 5* in colours*). Using the room shown in the picture for radiated emission EMC tests in 80–1000 MHz band, 300 mm deep cell structure absorber is sufficient.

This double cell structure of the absorber module, the proper size of the box walls and the resistance of the carbon layer ensure competitive broadband performances.

The operational principle is similar to the multi-layer absorber solutions, but the frequency characteristic can be tuned for customer request (i.e. quarter wave resonance can be set).

4. AN EXPERIMENTAL GTEM CHAMBER

Using the presented cell structure absorber a new type GTEM chamber has been developed. Because of the small dimensions of the absorber it is possible to stand the pyramidal chamber on its basement also in a living room. A simple drawing shows the arrangement (*Fig. 2* in colours*).

5. MEASUREMENT RESULTS

Testing of absorbers were done in GTEM Cell models (see *Table 1*).

Table 1. GTEM Chamber Models

Pyramid – base×height (mm^3)	245x125x250	420x420x720
Equipment under test (mm^3)	80x80x40	250x120x150
Field strength deviation (100 MHz–4 GHz)	±5 dB	±6 dB
Reflection loss (100 MHz–4 GHz)	–20 dB	–20 dB

The return loss characteristic of 100 mm deep modules measured in GTEM Cell demonstrates the one of the main advantages of the cell structure absorber (see *Fig. 6*).

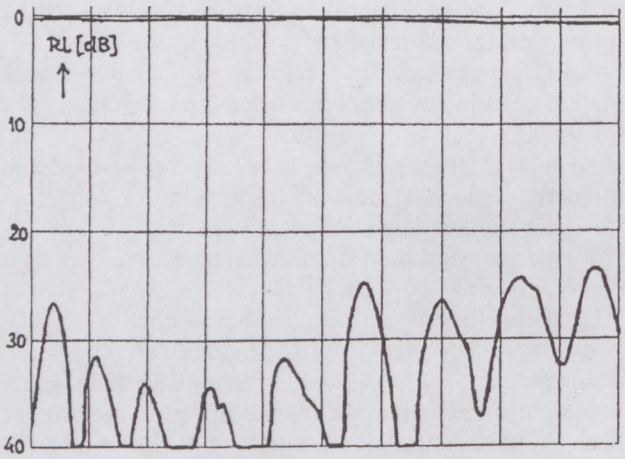

Fig. 6. Measured return loss characteristic versus frequency (DC-2 GHz).

The result – that 100 mm deep absorber is equal to a 500–600 mm high conventional pyramid – is perhaps surprising, but it can be explained by the coupling between the cell walls and the 50 Ohm distributed load of the internal conductor (septum plate) of the GTEM Cell. This measure of coupling can not be achieved by the usual foam pyramids.

During the GTEM Cell measurements disconnecting the 50 Ohm load of the septum plate, we got an acceptable better than 15 dB return loss value at 0.5 GHz.

The high frequency characteristics of a covered block are shown in *Figs. 7–10*. Return loss (continuous line) and insertion loss (dotted line) curves of absorber wall built up from 100 mm deep cell structure absorber modules (vertical scale: 10 dB/div., angle: +15°) are shown in the figures. Foam pyramids of the same size, have better performances over 5 GHz, but worse below 3 GHz [30]. According to our test results, roughly one-third deep/high cell structure absorber replaces the very expensive pyramids in both GTEM Cell and anechoic room applications, saving significant space.

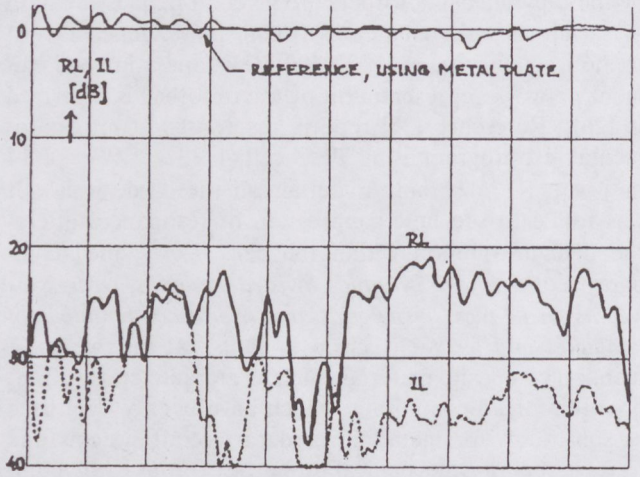

Fig. 7. Measured return loss and insertion loss characteristic versus frequency (2–4 GHz).

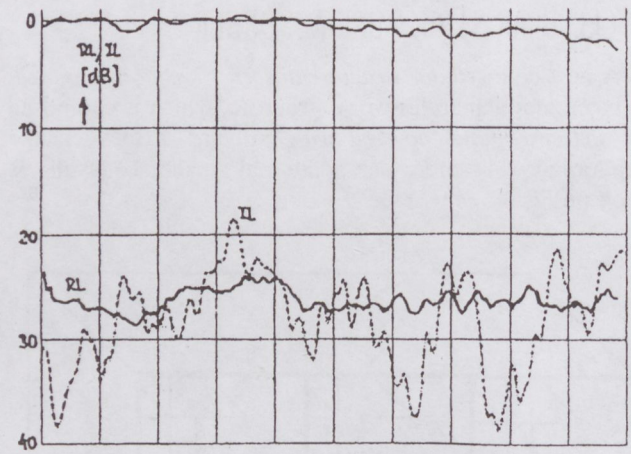

Fig. 8. Measured return loss and insertion loss characteristic versus frequency (4–8 GHz).

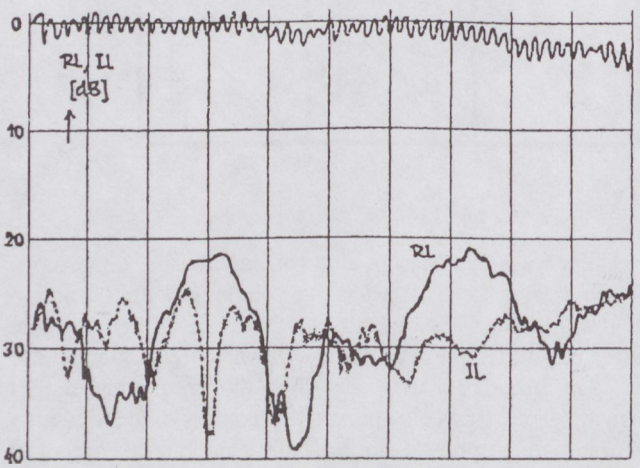

Fig. 9. Measured return loss and insertion loss characteristic versus frequency (8–12 GHz).

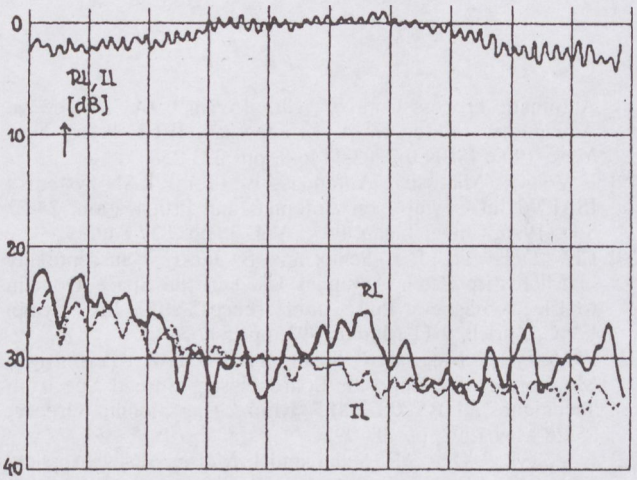

Fig. 10. Measured return loss and insertion loss characteristic versus frequency (12–18 GHz).

The results of reflection-loss measurements for the 300 mm deep cell structure absorber (CSA-300) and for the combination of CSA-300 and AEH-12 pyramidal absorber (Advanced ElectroMagnetics, Inc., a subsidiary of ORBIT/FR, Inc., USA) are shown in *Figs. 11* and *12*. The loading-effect of CSA-300 is also shown in *Fig. 12*.

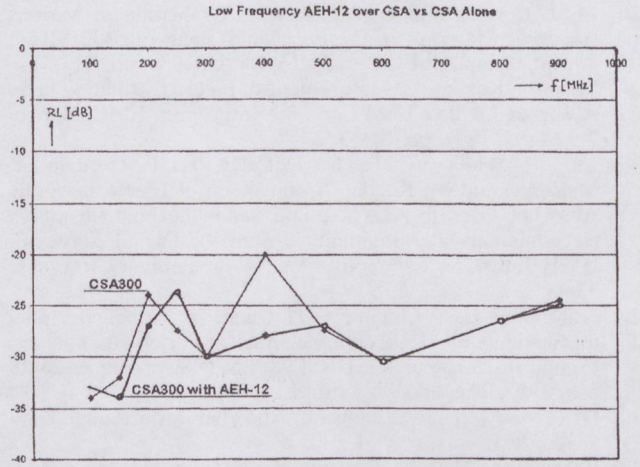

Fig. 11. Measured reflection loss versus frequency of CSA-300 alone and AEH-12 pyramid over CSA-300 absorbers.

The oblique angle performances of our new cell structure absorber and a standard one were measured, using our Particleboard Monitoring System [32]. The results are given in *Table 3* of paper titled "A Microwave Monitoring System used for Prediction of the Quality of Particleboards", written in this Journal. We can establish, that the CSA-100 absorber at oblique angles $\geq 30°$ (measured from perpendicular direction) overfulfils the standard absorber with a thickness of 110 mm.

Simultaneously with these experiments we have started the finite element simulation of our GTEM chamber model with cell-structure absorber. The results are computed by the High Frequency Structure Simulator (HFSS) from Hewlett Packard. HFSS creates an initial mesh that fills the geometric structure and defines the points that contribute to the solution. For each adaptive pass the mesh is refined providing greater detail in the regions where electromagnetic field intensities are greatest. The complexity of this simulation is reduced using the vertical symmetry plane of our structure analysed by HFSS.

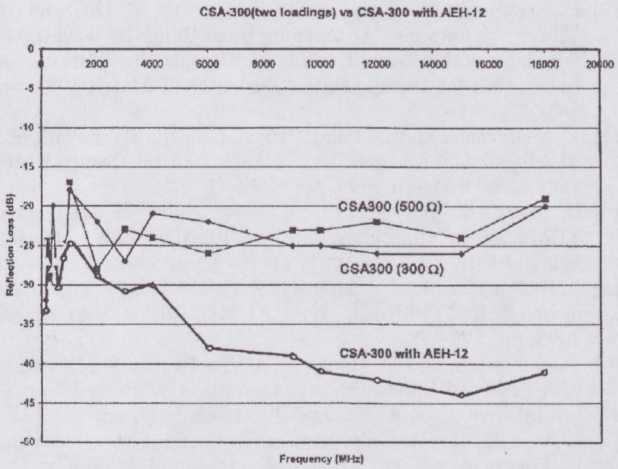

Fig. 12. Measured reflection loss versus frequency of CSA-300 (two loadings) and AEH-12 pyramid over CSA-300 absorbers.

6. CONCLUSIONS

In this paper a variety of test environments for EMC measurements and RF absorbers have been briefly reviewed using the results of some references. A new type RF absorber was introduced having cell structure. The new cell structure absorber made of inexpensive materials developed for replacement of costly pyramidal foam absorbers saves space, reducing drastically the building cost of GTEM Cells and anechoic rooms.

7. ACKNOWLEDGMENTS

The development of the cellular structure absorber was carried out in TKI Innovation Company for Telecommunication, Budapest, Hungary.

The authors would like to acknowledge Jeff Polan (ORBIT/FR, Horsham, PA, USA) and Gabe Sanchez (AEMI, San Diego, CA, USA) for organizing the control measurements and tests. They also thank Árpád Mrovcza (TKI), István Seres and Imre Király (MEEI) for their assistance in experiments. The authors would like to extend their appreciation Lajos Kocsis (TKI) for making the computer-artwork and László Nyúl (TUB/DMT) for his help in the preparation of the earlier version of this paper.

*** Coloured pictures cited are shown separately in the colour pages of this issue.**

REFERENCES

[1] P. Wilson: "Alternatives to Open Area Test Sites", 11th Int. Symp. EMC, Zurich, 7-9 March 1995, pp. 579-582.

[2] F. Arreghini, M. Ianoz, P. Zweiacker, D. V. Giri and A. Tehori: "Semiramis: An Asymmetrical Bounded Wave EMP Simulator with a Good Confinement Inside the Transmission Line", 10th Int. Symp. EMC, Zurich, 9-11 March 1993, pp. 583-588.

[3] L. Jendernalik and D. Peier: "Expanding the Bandwidth of a TEM-Cell with a Planar Terminator", 10th Int. Symp. EMC, Zurich, 9-11 March 1993, pp. 579-582.

[4] G. Moenich: "A New Conical Active Absorber Terminated TEM-Cell for Time-Harmonic and Transient Use", 11th Int. Symp. EMC, Zurich, 7-9 March 1995, pp. 599-602.

[5] F. B. J. Leferink: "A Triple-TEM Cell: Three Polarisations in one Setup", 10th Int. Symp. EMC, Zurich, 9-11 March 1993, pp. 573-578.

[6] D. Königstein and D. Hansen: "A New Family of TEM-Cells with Enlarged Bandwidth and Optimized Working Volume", 7th Int. Symp. on EMC, Zurich, March 1987, pp. 127-132.

[7] F. Attardo, C. Tarantola, M. Cappio Borlino, M. Giunta and L. Lavezzaro: "GHz TEM Cell: Radiated Immunity Test Performance", 10th Int. Symp. EMC, Zurich, 9-11 March 1993, pp. 589-593.

[8] D. Hansen, P. Wilson, D. Koenigstein and H. Garbe: "Emission and Susceptibility Testing in a Tapered TEM Cell", 8th Int. Symp. EMC, Zurich, 7-9 March 1989, pp. 227-232.

[9] R. De Leo, L. Pierantoni, T. Rozzi and L. Zappelli: "Wideband Analytical Model of the GTEM Cell Termination", 11th Int. Symp. EMC, Zurich, 7-9 March 1995, pp. 607-612.

[10] R. De Leo, T. Rozzi, C. Svara and L. Zappelli: "Local Mode Analysis of GTM Cell", 20th EuMC, 10-13 Sep. 1990, Budapest, Hungary, pp. 1346-1350.

[11] P. Wilson, F. Gassmann and H. Garbe: "Theoretical and Practical Investigation of the Field Distribution Inside a Loaded/Unloaded GTEM Cell", 10th Int. Symp. EMC, Zurich, 9-11 March 1993, pp. 595-598.

[12] R. De Leo, L. Pierantoni, T. Rozzi and L. Zappelli: "Excitation and Scattering in GTEM Cells", 10th Int. Symp. EMC, Zurich, 9-11 March 1993, pp. 599-604.

[13] T. Rozzi, R. De Leo, L. Pierantoni and L. Zappelli: "Fundamental Mode Propagation in GTEM Cell and Scattering by Conducting Cubes", 23rd EuMC, Madrid, 6-9 Sep. 1993, pp. 929-932.

[14] H. S. Berger: "A Variable Position, Gravity Down G-TEM Configuration", 11th Int. Symp. EMC, Zurich, 7-9 March 1995, pp. 465-470.

[15] L. Pierantoni and T. Rozzi: "E. M. Pulse Propagation in GTEM Cell" 11th Int. Symp. EMC, Zurich, 7-9 March 1995, pp. 603-606.

[16] F. Völgyi: "Flying Decibels – Extremely Lightweight Microstrip Antennas" ICOMM'90 Int. Conf. on Millimeter Wave and Microwave, Dehra Dun, India, December 1990, pp. 343-348.

[17] F. Völgyi: "Microstrip Antenna Array Applicator for Microwave Heating", 23rd EuMC, Madrid, 6-9 Sep. 1993, pp. 412-415.

[18] F. Völgyi: "Integrated Microwave Moisture Sensors for Automatic Process Control", Ch. 15. in book "Microwave Aquametry" (edited by A. Kraszewski), IEEE Press, New York, 1996, ISBN 0-7803-1146-9, pp. 223-238.

[19] F. Völgyi: "Microstrip Antennas Used for WLAN Systems", ISAP'96 Int. Symp. on Antennas and Propagation, 24-27 Sep. 1996, Chiba, Japan, Proc. Vol. 3. pp. 837-840.

[20] Ch. Delaveud, J. P. Seaux and B. Jecko: "Susceptibility of Microstrip Patch Antennas Used in the Space Domain to Electromagnetic Pulse Interferences", 10th Int. Symp. EMC, Zurich, 9-11 March 1993, pp. 509-514.

[21] F. Völgyi, I. Mojzes, R. Seller and P. Olasz: "Permittivity Monitoring of Composite Boards Using Spread Spectrum Techniques", URSI'98 EMT Symp., Thessaloniki, Greece, 25-28 May 1998, pp. 97-99.

[22] F. Völgyi, P. Olasz, R. Seller and I. Mojzes: "New Application of WLAN Concept; Modulated Backscatter- and Spread Spectrum Techniques", PIERS'98, Progress in Electromagnetic Research Symposium, Nantes, France, 13-17 July 1998.

[23] C. P. Tou: "Interference Suppressions Using Adaptive Spread-Spectrum Techniques", 8th Int. Symp. EMC, Zurich, 7-9 March 1989, pp. 593-596.

[24] H. Pues: "Electromagnetic Absorber Measurement in a Large Waveguide", 8th Int. Symp. EMC, Zurich, 7-9 March 1989, pp. 253-258.

[25] N. Ari, D. Hansen and H. Garbe: "Analysis and Measurements of Electromagnetic Scattering by Pyramidal Absorbers", 8th Int. Symp. EMC, Zurich, 7-9 March 1989, pp. 301-304.

[26] M. J. Coenen and L. P. Janssen: "Evaluation of Various Absorber Materials in the Frequency Range 30-300 MHz", 8th Int. Symp. EMC, Zurich, 7-9 March 1989, pp. 315-318.

[27] Vasantha Kumara: "Measurement of Field Distribution in an Absorber-Loaded TEM Cell", 8th Int. Symp. EMC, Zurich, 7-9 March 1989, pp. 319-322.

[28] Ch. L. Holloway, R. R. DeLyser, R. F. German, P. McKenna and M. Kanda: "Comparison of Electromagnetic Absorber Used in Anechoic and Semi-Anechoic Chambers for Emissions and Immunity Testing of Digital Services", IEEE Trans. on EMC, Vol. 39, No. 1, February 1997, pp. 33-45.

[29] H. K. Chiu, H. C. Chu and C. H. Chen: "A Simplified Model for Shielding and Reflection Analyses of Periodic Laminated Composite Structures", URSI'98 EMT Symposium, 25-28 May 1998, Thessaloniki, Greece, pp. 736-738.

[30] GEC – Marconi Broadband Absorber, AF Range Data Sheet 1995.

[31] F. Völgyi, L. Nyúl, S. Tatár and A. Mrovcza: "A New Radio Frequency Absorber for GTEM -Cell Applications" EMC' Zurich, 13th International Zurich Symposium and Tech. Exhibition on Electromagnetic Compatibility, February 16-18, 1999, pp. 675-678.

[32] F. Völgyi: "Monitoring of Particleboard Production using Microwave Sensors" Ch. 10, pp. 249-274, in book: Sensors Update, Vol. 7 (Editors: H. Baltes, W. Göpel, J. Hesse, Guest Editors: K. Kupfer, A. Kraszewski, R. Knöchel), WILEY-VCH Verlag GmbH, D-69469 Winheim, GE, 2000, ISBN 3-527-29821-5, pp. 249-274.

RÁDIÓFREKVENCIÁS NYELŐANYAGOK GTEM-CELLÁKHOZ

Magyarországon 1999. szeptember 9-én lépett életbe a 31/1999 GM-KHVM sz. együttes rendelet az elektromágneses összeférhetőségről (EMC), amely rendelet az EU-direktívák hazai jogrendbe való bevezetését irányozza elő. A korszerű nagyfrekvenciás emissziós és immunitási méréseket nagyrészt GTEM (GHz TEM) cellákban végzik, amelyek egyik végükön rádiófrekvenciás (RF) nyelőkkel borítottak. Nagy mennyiségben használják ezen költséges anyagokat (grafitot vagy kormot tartalmazó poliuretán gúlák, csavart gúlák, ékalakú nyelőanyagok, ferrit csempék, ferrit rácsok és ezek hibrid kombinációi, grafit/epoxi szálerősített anyagok, valamint többrétegű szerkezetek) reflexió-mentes mérőszobák kialakítására. A szerzők találmányuk tárgyát képező, új típusú, olcsó, cella szerkezetű abszorbert (CSA) ismertetnek, amelynek csökkentett méretű poliuretán gúlákkal való hibrid kombinációjával kiváló reflexiós tulajdonságok érhetők el a 0.1–18 GHz frekvenciasávban. A cikk részletesen ismerteti a GTEM-kamrában végzett reflexiómérések, valamint a szabadtéri reflexió- és árnyékolóhatás mérések eredményeit.

COMING SOON:2000/1-5

PIRELLI

Key Stages in Photonics Road Map: Stage 5

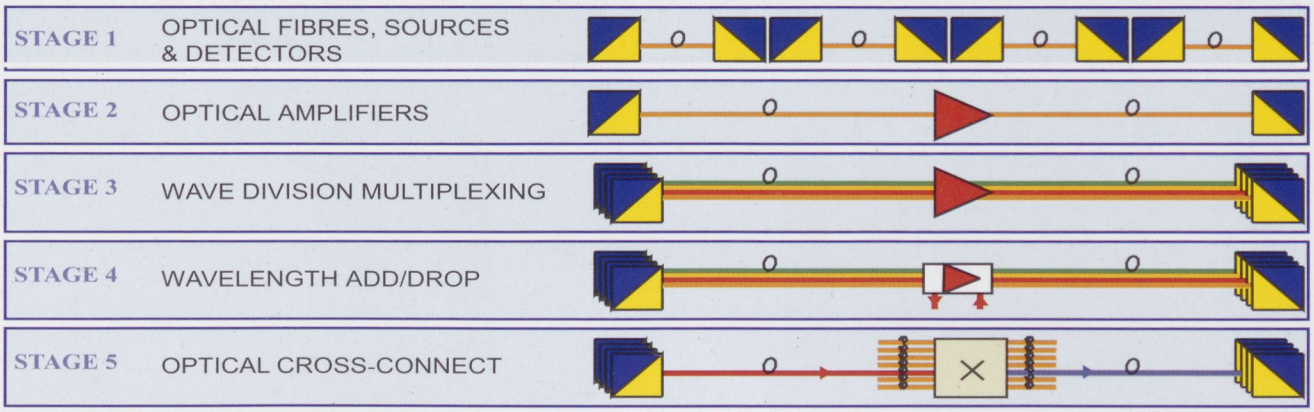

Anticipated OXC capability

•512x512 wavelengths, non-blocking, fast protection

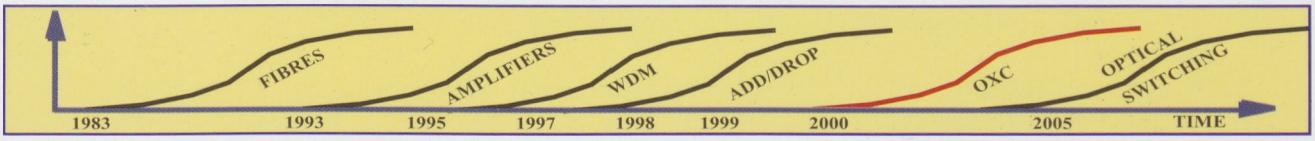

Key Stages in Photonics Road Map: Stage4 C65

PIRELLI

Key Stages in Photonics Road Map: Stage 6

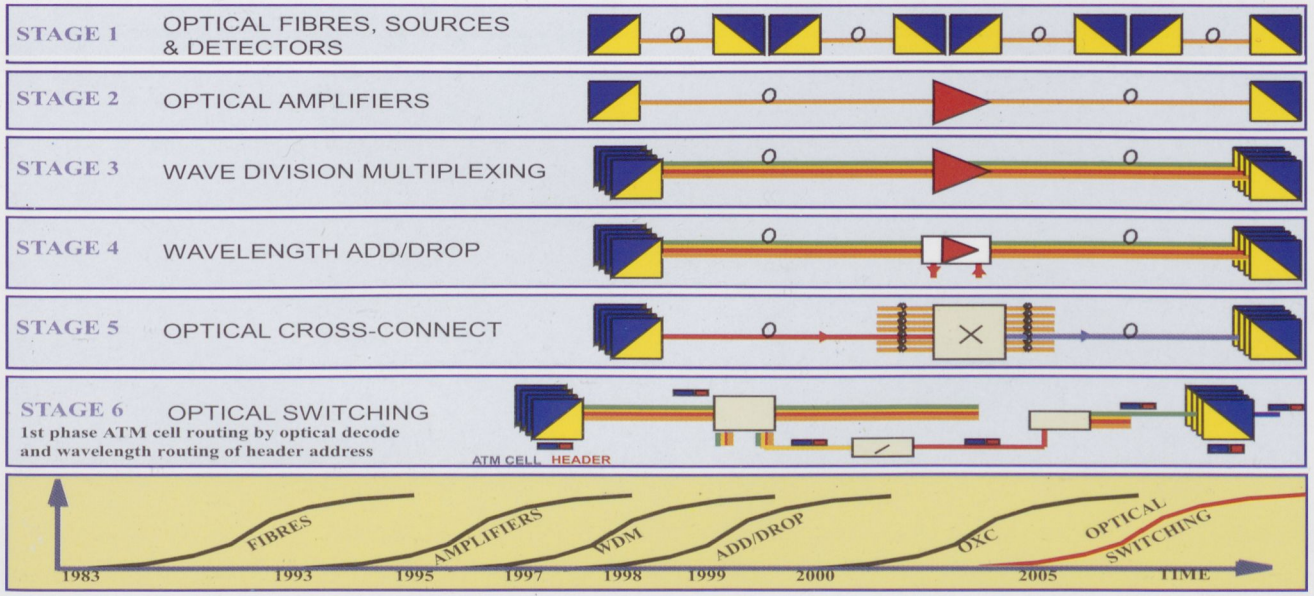

THE FIRST WDM WORKSHOP IN HUNGARY

COMING SOON:2000/1-5

WDM link robustness

- Degradation of the optical levels in the link

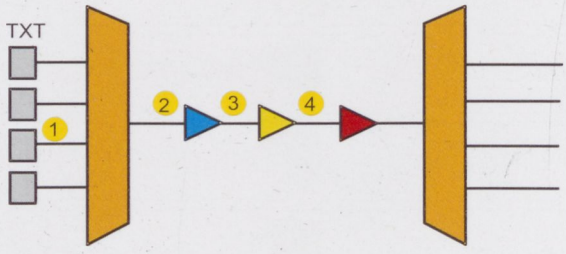

- Definition of the penalty
  - » Penalty = Shift in dB of the BER curves with degraded conditions compared to the BER curves in nominal conditions

Double degradation in Paris - Rouen link

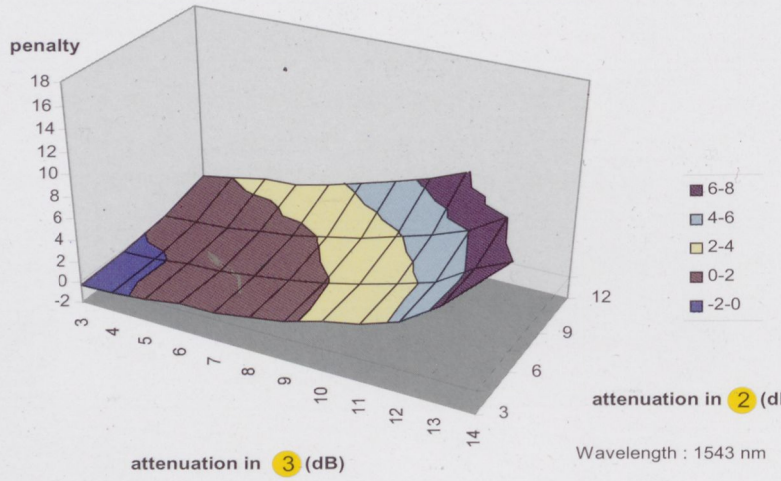

At 9 dB attenuation in 2 and 10 dB in preamplifier 3 input power is 0.3 dB lower than nominal condition ones

Wavelength : 1543 nm

THE FIRST WDM WORKSHOP IN HUNGARY

COMING SOON:2000/1-5

Technical options

- STM 64 :
  ADM's availability ; Cost of new technology
  - » Fibre limitation (Chromatic Dispersion, PMD)
- WDM :
  - » Up to 16X STM-16 Channels commercially available
  - » MUX and de-MUX passive elements
  - » Use of transponders
  - » Flexibility of increasing the number of channels in operation in the installed wavelength multiplex
  - » Gain flatness of optical amplifiers to be considered for long links
- The FT choice today is WDM :
  - » Maturity of the technology compared to STM-64 new generation equipment

The long distance network

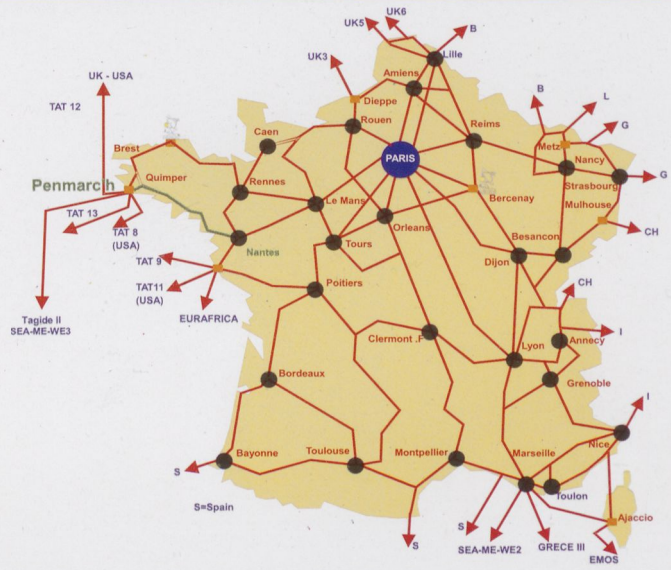

THE FIRST WDM WORKSHOP IN HUNGARY

COMING SOON:2000/1-5

S

SIEMENS TransXpress WDM Portfolio:
Leadership in Span Performance

TransXpress Infinity
MULTIWAVELENGTH TRANSPORT SYSTEM

Ultra-high capacity 320 Gbit/s

Ultra-long haul 600 km

TransWave™ WL

longest span
non regenerated
1200 km

TransXpress Infinity WLS

longest unrepeated
span 370 km

TransXpress WaveLine

Gigabit Services for
Metropolitan Area

3

J. Kovats
ICN TR VT1, 03/99

S

SIEMENS TransXpress WDM Portfolio:
Leadership in Span Performance

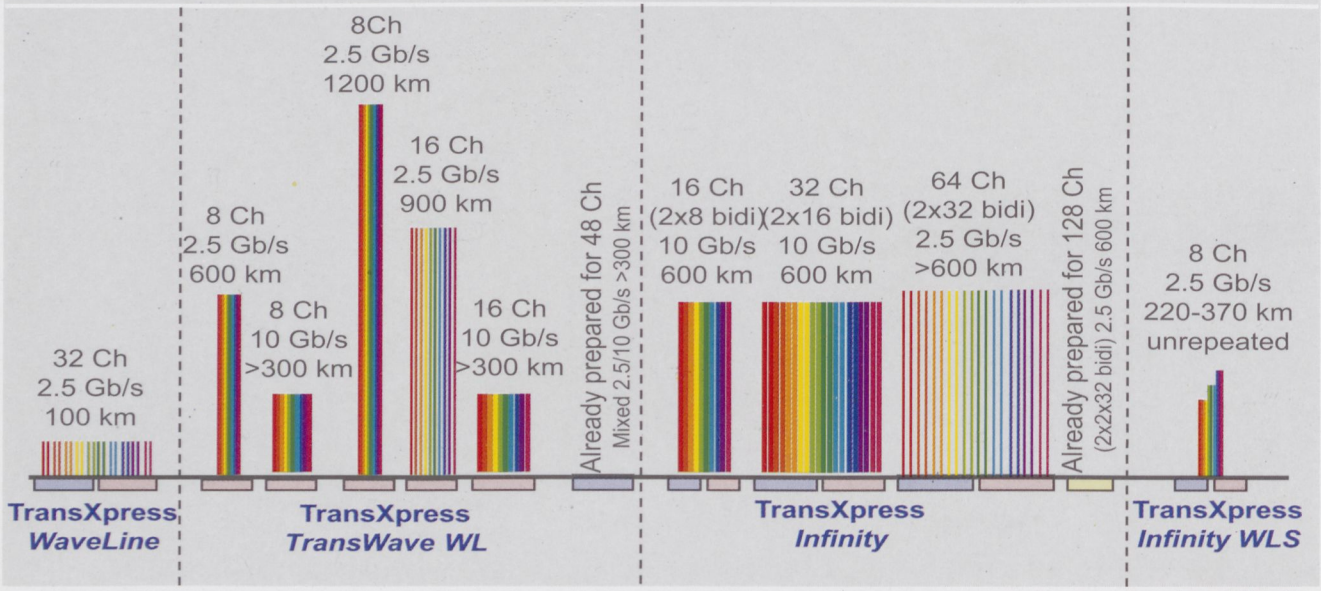

4

J. Kovats
ICN TR VT1, 03/99

THE FIRST WDM WORKSHOP IN HUNGARY

A kezében van a helyzet megoldása

Az új Nokia TETRA professzionális mobil rádió megsokszorozza a gyorsaság, a higgadtság, a döntésképesség, a csapatmunka erejét.

A Nokia TETRA rendelkezik az Európai Távközlési Szabványügyi Intézet (ETSI) által specifikált új digitális technológia minden lényeges elemével. Számos helyzetben jó szolgálatot tesz a rövid hívásfelépülési idő, a hang- és adatátviteli lehetőség, a megosztható felhasználás, a hatékony frekvenciakihasználás, a prioritási szintek beállításának lehetősége.

A Nokia a teljes rendszerek szállítása és a rádiós berendezések területén szerzett rendkívüli tapasztalatával és nemzetközi ügyfélszolgálati hálózatával segíti az Ön munkáját.

Nokia TETRA. Megbízható technológia egy megbízható cégtől.

NOKIA
CONNECTING PEOPLE

D24&25

COMING SOON:2000/1-5

EURESCOM

1st Hungarian WDM Workshop, 23 March 1999, Budapest

swisscom

Traffic Layering Today

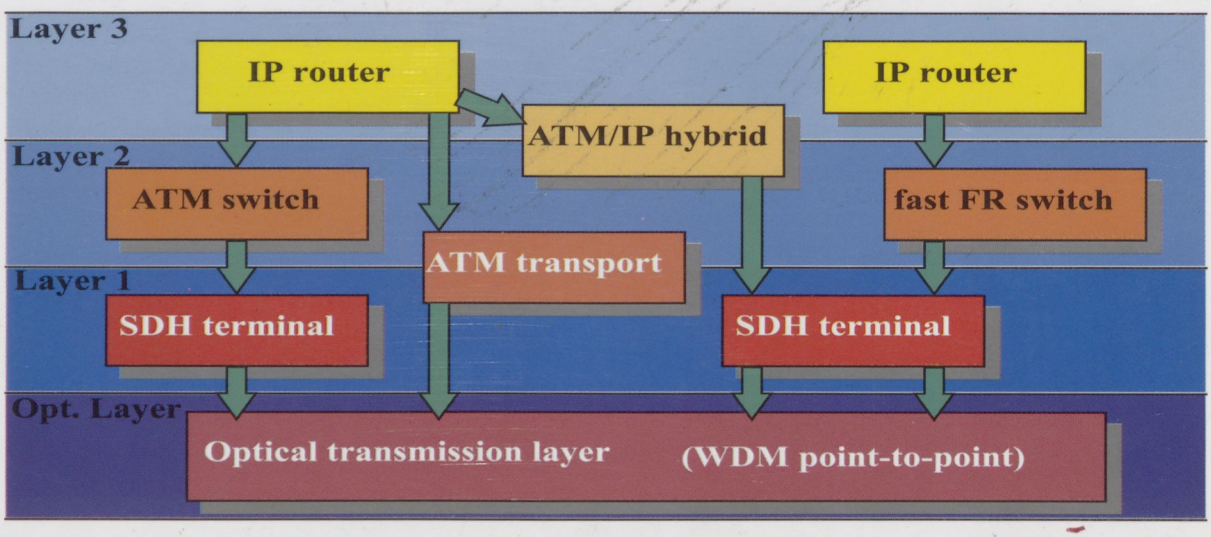

EURESCOM

1st Hungarian WDM Workshop, 23 March 1999, Budapest

swisscom

Traffic Layering Tomorrow

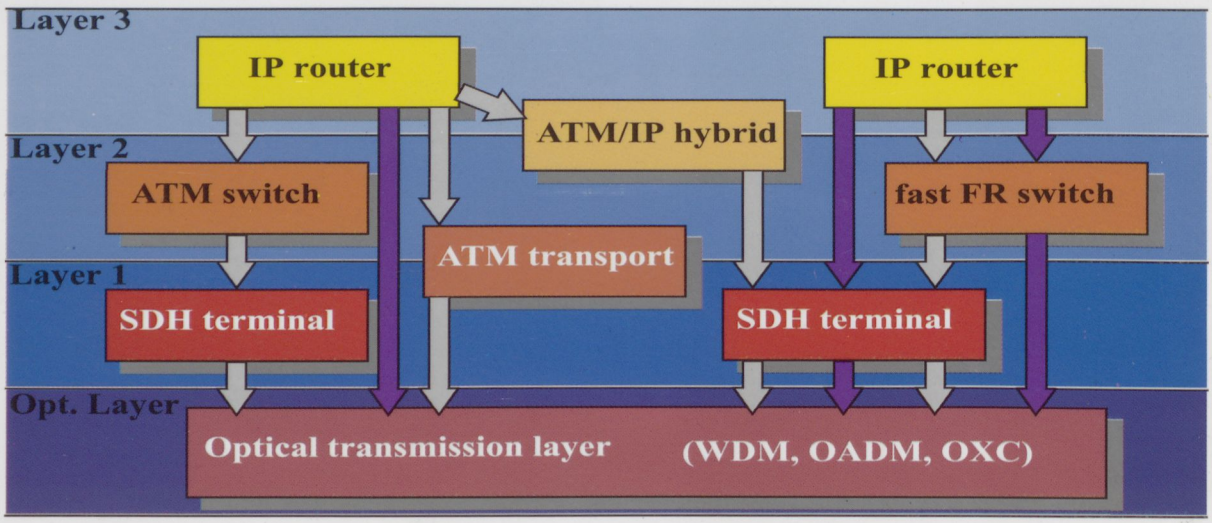

THE FIRST WDM WORKSHOP IN HUNGARY